FrozenNature – The palynological contribution to reconstruct paleo fire, vegetation, land use, and pollution dynamics from high-alpine ice cores

Inauguraldissertation
der Philosophisch-naturwissenschaftlichen Fakultät
der Universität Bern

vorgelegt von
Sandra Olivia Brügger
von Kandergrund BE

Leiter der Arbeit:
Prof. Dr. Willy Tinner
Institut für Pflanzenwissenschaften
und Oeschger Zentrum für Klimaforschung
Universität Bern

FrozenNature – The palynological contribution to reconstruct paleo fire, vegetation, land use, and pollution dynamics from high-alpine ice cores

Inauguraldissertation
der Philosophisch-naturwissenschaftlichen Fakultät
der Universität Bern

vorgelegt von
Sandra Olivia Brügger
von Kandergrund BE

Leiter der Arbeit:
Prof. Dr. Willy Tinner
Institut für Pflanzenwissenschaften
und Oeschger Zentrum für Klimaforschung
Universität Bern

Von der Philosophisch-naturwissenschaftlichen Fakultät angenommen.

Bern, 18. Dezember 2018 Der Dekan:

Prof. Dr. Zoltan Balogh

Contents

Introduction

Current as well as past fire-climate relationships are complex and differ between biomes and with variable degrees of anthropogenic modifications (Bond et al. 2005, Bowman et al. 2009, Marlon et al. 2016, Lasslop and Kloster 2017). On a global scale, fires affect the Earth climate directly by releasing aerosols, CO_2, and other greenhouse gases to the atmosphere and indirectly through disruption of vegetation compositions and structure, soil carbon releases, and modification of the surface albedo (Page et al. 2002, Randerson et al. 2006, Bowman et al. 2009, Andela et al. 2017).

For the period since 1850 AD, previous charcoal compilations proposed a decoupling of fire activity from climate and population density that was ascribed to increasing landscape fragmentation and fire management (called “broken fire hockey stick”-hypothesis, Marlon et al. 2008, van der Werf et al. 2013). The proposed fire decline remains highly ambiguous due to large dating uncertainties of most sediment records especially during the 20th century, a strong geographical bias of observations towards Europe and North America (Marlon et al. 2016), and lacking supporting data (e.g. Mischler et al. 2009). These ambiguities suggest that the underlying processes are not entirely understood. For instance, long-term vegetation dynamics, fuel availability and its flammability may likewise play an important and complex role for fire distribution and frequencies, which is not well constrained (Kloster et al. 2012, Andela et al. 2017). However, recent uncontrolled and destructive wildfires on all vegetated continents caused enormous ecological and societal costs, and combined with these uncertainties raise major public and scientific concerns about future fire management strategies under predicted climate change (Kehrwald et al. 2013, Moritz et al. 2014, Syphard et al. 2017, Wendel et al. 2017, Young et al. 2017).

Glaciers can deliver valuable insights into long-term fire, vegetation, land use, and pollution dynamics and their relationship with changing climate (e.g. Eichler et al. 2011, Arienzo et al 2017). They preserve microfossils over millennia and usually provide high-resolution records and excellent age-depth models, especially for the most recent 200 years, where glacier chronologies can rely on annual layer counting and reference horizons as for instance volcanic ash layers (e.g. Eichler et al. 2011, Herren et al. 2013, Konrad et al. 2013, Uglietti et al. 2016). Multiple climate and environmental proxies from the same cores as for instance temperature reconstructions or chemical fire tracers as black carbon (Eichler et al. 2011, Osmont et al. 2018, Sigl et al. 2018) contribute to assess numerous dimensions of past environmental dynamics. Despite the high potential of ice archives, most of the previous palynological studies remained largely restricted to changing wind-directions and pollen source areas or pollen-based seasonality as an additional dating method (e.g. Hicks and Isaksson 2006, Festi et al. 2015), hence their ecological potential was not fully exploited.

The goal of this thesis is to explore the timing and different interactions between long-term fire, vegetation, land use, climate, and pollution dynamics that occur in various biomes for the first time based on palynological records from ice cores. This goal is achieved with comparable methods and globally distributed ice cores that provide excellent chronologies (Blunier et al. 1993, Sigl et al. 2009, Kellerhals et al. 2010, Herren et al. 2013), particularly after 1800 AD to present, the period that experienced important climatic changes and an increasing globalization of human activities. The ice records derive from regions that are or will be highly threatened by climate change and land use pressure and/or provide recent high-quality data for direct comparison and proxy calibration. Combined, the investigated ice records cover the tropical (Illimani), the subtropical-temperate (Colle Gnifetti), the steppic-boreal (Tsambagarav), and the arctic biome (Summit; Figure 1).

The palynological methods in this thesis comprise pollen and spores to infer vegetation composition and land use activity, microscopic charcoal for fire activity from biomass burning (e.g. Finsinger and Tinner 2005, Eichler et al. 2011), and spheroidal carbonaceous particles (SCP) for industrial pollution from high-temperature combustion of fossil fuel (Hicks and Isaksson 2006, Rose 2015). The optical discrimination of microscopic charcoal and SCP provides a huge benefit to define burning sources (biomass vs. fossil fuel) and can contribute to separate sources of less specific burning tracers that were analyzed on the same ice cores i.e. black carbon (Sigl et al. 2018).

Microfossil concentrations in remote ice archives are comparably low and maximum extraction of items is crucial. Although comparable methods are a fundamental requirement to achieve reliable environmental reconstructions and to obtain comparable results among different records, a quantitative comparison of the existing microfossil extraction approaches was missing, and no standard palynological extraction method was proposed for ice samples. The aim of **Manuscript 1** is to provide a quantitative comparison of available extraction approaches and to propose an improved method for microfossil extraction from ice archives.

Europe offers high-quality data on past fire, vegetation, and land use dynamics including numerous high-quality sedimentary paleoecological records (e.g. Vannière et al. 2016) and written sources for the past centuries (e.g. Pfister et al. 2015). The focus of **Manuscript 2** is the generation of a palynological ice record from the Swiss Alps (Colle Gnifetti), in the Center of the densely populated European continent spanning the past 1000 years. We aim at investigating the impact of industrialization and globalization on past vegetation, fire, landuse, and pollution dynamics across biomes in comparison to pre-industrial conditions and at linking the large-scale ice core evidence to historical sources.

Boreal forest-steppe dynamics in remote southern Siberia are largely controlled by climate variations (Bonan 2008) and projected future climate change in combination with changing land use may greatly increase boreal forest fire risks and release massive carbon emissions to the atmosphere (IPCC 2014). Tsambagarav glacier in the Mongolian Altai is located close to the boreal forest-steppe ecotone and currently surrounded by widespread steppe vegetation. In **Manuscript 3** we present a novel palynological record from Tsambagarav glacier spanning the past 5500 years and compare it to a previously investigated ice record in the densely forested Russian Altai 320 km northwest (Belukha, Eichler et al. 2011). The study aim is to examine past vegetation and fire responses to climate variability in the Mongolian Altai and to use these past response dynamics to anticipate future boreal forest responses to climate change in the Russian Altai and other Central Asian areas.

Neotropical ecosystems are precious biodiversity hotspots with a high degree of endemism and considered among the most threatened ecosystems by modern anthropogenic disruptions and climate change (Olson and Dinerstein 2002, Ibisch and Mérida 2004). Pre-Columbian societies are assumed to have influenced these environments since millennia but the scale of their impacts on ecosystems and fire activity remains unclear (e.g. Levis et al. 2017, McMichael et al. 2017). **Manuscript 4** investigates a continuous Holocene-long record from the Central Andean Illimani glacier. Its proximity to Lake Titicaca, a core region of pre-Columbian activities is ideal to study the extent and magnitude of ecosystem alterations by pre-Columbian societies, compared to Colonial and modern land-use impacts and ultimately, to derive natural baseline conditions for planning of ecosystem conservation.

The Arctic region is experiencing fast climate change that rapidly transforms sensitive arctic plant communities (Pearson et al. 2013, Büntgen et al. 2015). Although North American boreal forests are likely the dominant source for the biomass-burning signal in Central Greenland (Bauer et al. 2013), current observations of fires in thawing permafrost areas along the Greenland coast suggest that Arctic fire activity may become more important in the future (Wendel et al. 2017). Moreover, growing deposition of black particles from burning (e.g. microscopic charcoal, SCP) on snow may increase melting processes and further accelerate climate change. In **Manuscript 5**, we assess the potential of palynology in Central Greenland ice. A short ice record (1730–1989 AD) from Summit Eurocore '89 is used to investigate large-scale vegetation, fire, and pollution dynamics and their interaction with changing climate in the Arctic region.

Although most microscopic charcoal particles in natural archive derive from regional fires ca. 40 km around a site (Adolf et al. 2017), some particles may be transported over large distances. For instance, the devastating Portugal fires in June 2017 produced an ash plume that crossed Western Europe and deposited a surprising amount of black carbon and microscopic charcoal particles on the Jungfraujoch in the Swiss Alps ca. 1500 km westwards (Figure 2). Especially for remote archives as the glaciers in this thesis, more knowledge about long-distance transport mechanisms may contribute to a better understanding of how various sources contribute to the microfossil signal. The aim of **Manuscript 6** is to implement for the first-time microscopic charcoal particles into a global climate-aerosol model (ECHAM6-HAM) and to simulate their atmospheric transport and interactions with other aerosols, clouds, and radiation. The model simulations are validated with modern microscopic charcoal influx from the ice cores in this thesis and sedimentary archives (Adolf et al. 2017, ALPADABA database Bern).

Ultimately, the presented thesis contributes to the overarching goal of the SNF-Sinergia project *Paleo fires from high-alpine ice cores*, which is an integrated research framework, aiming to test the “broken fire hockey stick”-hypothesis with multiproxy fire reconstructions from ice cores.

Figure 1 Distribution of the investigated ice archives for this thesis overlaid on a global vegetation map. Vegetation classes modified from the biome classification in Olson et al. (2001).

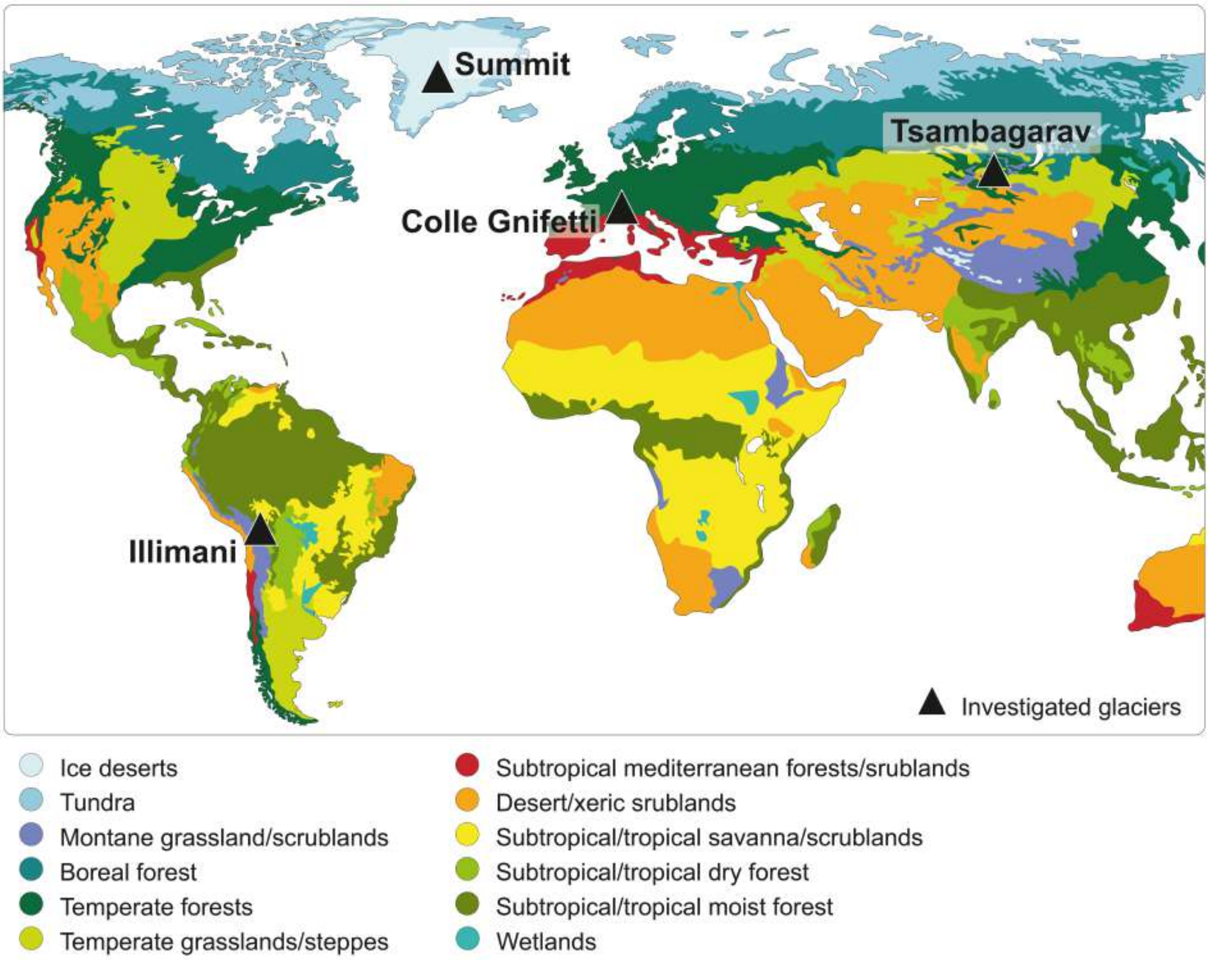

Figure 2 A comparison of microscopic charcoal and black carbon concentrations in a snow profile at Jungfraujoch (Swiss Alps) spanning June 2017 (black carbon analysis: Dimitri Osmont). Dating of the snow pit is derived from estimates of snow accumulation rates based on precipitation measurements at the nearby Lauterbrunnen meteorological station. Concentrations of both fire tracers increased significantly after 22nd June 2018, when the atmospheric ash plume from Portugal reached the Jungfraujoch station. Its origin was confirmed by calculations of back trajectories for the air masses (Osmont et al. in preparation).

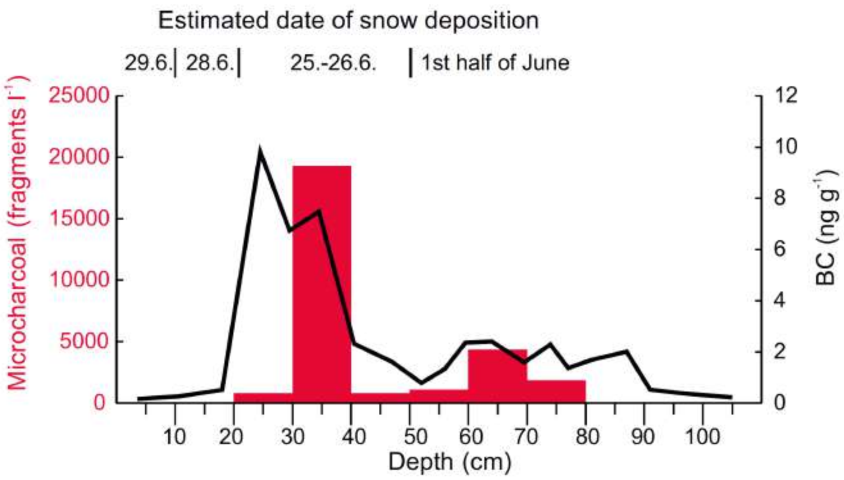

References

Adolf C, Wunderle S, Colombaroli D, Weber H, Gobet E et al. (2018) The sedimentary and remote-sensing reflection of biomass burning in Europe. *Global Ecology and Biogeography* 27(2) 199-212

Andela N, Morton DC, Giglio L, Chen Y, Van Der Werf GR et al. (2017) A human-driven decline in global burned area. *Science* 356(6345) 1356-1362

Arienzo MM, McConnell JR, Murphy LN, Chellman N, Das S et al. (2017) Holocene black carbon in Antarctica paralleled Southern Hemisphere climate. *Journal of Geophysical Research: Atmospheres* 122(13) 6713-6728

Bauer SE, Bausch A, Nazarenko L, Tsigaridis K, Xu B et al. (2013) Historical and future black carbon deposition on the three ice caps: Ice core measurements and model simulations from 1850 to 2100. *Journal of Geophysical Research: Atmospheres* 118(14) 7948-7961

Blunier T, Chappellaz JA, Schwander J, Barnola JM, Desperts T et al. (1993) Atmospheric methane, record from a Greenland ice core over the last 1000 year. *Geophysical Research Letters* 20(20) 2219-2222

Bonan GB (2008) Forests and climate change: forcings, feedbacks, and the climate benefits of forests. *Science* 320(5882) 1444-1449

Bond WJ, Woodward FI, Midgley GF (2005) The global distribution of ecosystems in a world without fire. *New Phytologist* 165(2) 525-538

Bowman DMJS, Balch JK, Artaxo P, Bond WJ, Carlson JM et al. (2009) Fire in the Earth system. *Science* 324(5926) 481-484

Büntgen U, Hellmann L, Tegel W, Normand S, Myers-Smith I et al. (2015) Temperature-induced recruitment pulses of Arctic dwarf shrub communities. *Journal of Ecology* 103(2) 489-501

Eichler A, Tinner W, Brütsch S, Olivier S, Papina T, Schwikowski M (2011) An ice-core based history of Siberian forest fires since AD 1250. *Quaternary Science Reviews* 30(9) 1027-1034

Festi D, Kofler W, Bucher E, Carturan L, Mair V et al. (2015) A novel pollen-based method to detect seasonality in ice cores: a case study from the Ortles glacier, South Tyrol, Italy. *Journal of Glaciology* 61(229) 815-824

Finsinger W, Tinner W (2005) Minimum count sums for charcoal concentration estimates in pollen slides: accuracy and potential errors. *The Holocene* 15(2) 293-297

Herren P A, Eichler A, Machguth H, Papina T, Tobler L et al. (2013) The onset of Neoglaciation 6000 years ago in western Mongolia revealed by an ice core from the Tsambagarav mountain range. *Quaternary Science Reviews* 69 59-68

Hicks S, Isaksson E (2006) Assessing source areas of pollutants from studies of fly ash, charcoal, and pollen from Svalbard snow and ice. *Journal of Geophysical Research: Atmospheres* 111(D2)

Ibisch PL, Mérida G (2004) Biodiversity: the richness of Bolivia: state of knowledge and conservation. *Editorial FAN*

IPCC (2014) Climate Change 2014: Synthesis Report. Contribution of Working Groups I, II and III to the Fifth Assessment Report of the Intergovernmental Panel on Climate Change. IPCC, Geneva

Kehrwald NM, Whitlock C, Barbante C, Brovkin V, Daniau AL et al. (2013) Fire Research: Linking Past, Present, and Future Data. *Eos, T*ransactions *American Geophysical Union* 94(46) 421-422

Kellerhals T, Tobler L, Brütsch S, Sigl M, Wacker L et al. (2010) Thallium as a tracer for preindustrial volcanic eruptions in an ice core record from Illimani, Bolivia. *Environmental Science & Technology* 44(3) 888-893

Kloster S, Mahowald NM, Randerson JT, Lawrence PJ (2012) The impacts of climate, land use, and demography on fires during the 21st century simulated by CLM-CN. *Biogeosciences* 9(1) 509-525

Konrad H, Bohleber P, Wagenbach D, Vincent C and Eisen O (2013) Determining the age distribution of Colle Gnifetti, Monte Rosa, Swiss Alps, by combining ice cores, ground-penetrating radar and a simple flow model. *Journal of Glaciology* 59(213) 179-189

Lasslop G, Kloster S (2017) Human impact on wildfires varies between regions and with vegetation productivity. *Environmental Research Letters* 12(11) 115011

Levis C, Costa FR, Bongers F, Peña-Claros M, Clement CR (2017) Persistent effects of pre-Columbian plant domestication on Amazonian forest composition. *Science* 355(6328) 925-931

Marlon JR, Bartlein PJ, Carcaillet C, Gavin DG, Harrison SP et al. (2008) Climate and human influences on global biomass burning over the past two millennia. *Nature Geoscience* 1(10) 697

Marlon JR, Kelly R, Daniau AL, Vannière B, Power MJ (2016) Reconstructions of biomass burning from sediment charcoal records to improve data-model comparisons. *Biogeosciences* 13 3225-3244

McMichael CH, Feeley KJ, Dick CW, Piperno DR, Bush MB (2017) Comment on “Persistent effects of pre-Columbian plant domestication on Amazonian forest composition”. *Science* 358(6361) eaan8347

Mischler JA, Sowers TA, Alley RB, Battle M, McConnell JR et al. (2009) Carbon and hydrogen isotopic composition of methane over the last 1000 years. *Global Biogeochemical Cycles* 23(4)

Moritz MA, Batllori E, Bradstock RA, Gill AM, Handmer J et al. (2014) Learning to coexist with wildfire. *Nature* 515(7525) 58-66

Olson DM, Dinerstein E (2002) The Global 200: Priority ecoregions for global conservation. *Annals of the Missouri Botanical garden* 199-224

Olson DM, Dinerstein E, Wikramanayake ED, Burgess ND, Powell GV et al. (2001) Terrestrial Ecoregions of the World: A New Map of Life on EarthA new global map of terrestrial ecoregions provides an innovative tool for conserving biodiversity. *BioScience* 51(11) 933-938

Osmont D, Wendl IA, Schmidely L, Sigl M, Vega CP et al. (2018) An 800-year high-resolution black carbon ice core record from Lomonosovfonna, Svalbard. *Atmospheric Chemistry and Physics* 18(17) 12777-12795

Osmont D, Brugger SO, Weber H, Gilgen A, Sigl M et al. (in preparation) Biomass burning emissions observed at Jungfraujoch: a case study.

Page SE, Siegert F, Rieley JO, Boehm HDV, Jaya A, Limin S (2002) The amount of carbon released from peat and forest fires in Indonesia during 1997. *Nature* 420(6911) 61

Pearson RG, Phillips SJ, Loranty MM, Beck PS, Damoulas T et al. (2013) Shifts in Arctic vegetation and associated feedbacks under climate change. *Nature climate change* 3(7) 673

Pfister C, Wetter O, Brázdil R, Dobrovolný P, Glaser R et al. (2015) Tree-rings and people–different views on the 1540 Megadrought. Reply to Büntgen et al. 2015. *Climatic Change* 131(2) 191-198

Randerson JT, Liu H, Flanner MG, Chambers SD, Jin Y et al. (2006) The impact of boreal forest fire on climate warming. *Science* 314(5802) 1130-1132

Rose NL (2015) Spheroidal carbonaceous fly ash particles provide a globally synchronous stratigraphic marker for the Anthropocene. *Environmental science & technology* 49(7) 4155-4162

Sigl M, Abram NJ, Gabrieli J, Jenk TM, Osmont D, Schwikowski M (2018) No role for industrial black carbon in forcing 19th century glacier retreat in the Alps. *The Cryosphere Discuss*

Sigl M, Jenk TM, Kellerhals T, Szidat S, Gäggeler HW et al. (2009) Towards radiocarbon dating of ice cores. *Journal of Glaciology* 55(194) 985-996

Syphard AD, Keeley JE, Pfaff AH, Ferschweiler K (2017) Human presence diminishes the importance of climate in driving fire activity across the United States. *Proceedings of the National Academy of Sciences* 201713885.

Uglietti C, Zapf A, Jenk TM, Sigl M, Szidat S et al. (2016) Radiocarbon dating of glacier ice: overview, optimisation, validation and potential. *The Cryosphere* 10(6) 3091-3105

Van der Werf GR, Peters W, van Leeuwen TT, Giglio L (2013) What could have caused pre-industrial biomass burning emissions to exceed current rates?. *Climate of the Past* 9(1) 289-306

Vannière B, Blarquez O, Rius D, Doyen E, Brücher T et al. (2016) 7000-year human legacy of elevation-dependent European fire regimes. *Quaternary Science Reviews* 132 206-212

Wendel J (2017) Greenland fires ignite climate change fears. *Eos* 98

Young AM, Higuera PE, Duffy PA, Hu FS (2017) Climatic thresholds shape northern high-latitude fire regimes and imply vulnerability to future climate change. *Ecography* 40(5) 606-617.

Manuscript 1

A quantitative comparison of microfossil extraction methods from ice cores

Sandra O. Brugger[1,2,*], Erika Gobet[1,2], Federica R. Schanz[1], Oliver Heiri[1,2], Christoph Schwörer[1,2], Michael Sigl[2,3], Margit Schwikowski[2,3,4], Willy Tinner[1,2]

[1]Institute of Plant Sciences, University of Bern, Switzerland
[2]Oeschger Center for Climate Change Research, University of Bern, Switzerland
[3]Paul Scherrer Institute, Villigen, Switzerland
[4]Department for Chemistry and Biochemistry, University of Bern, Switzerland

[*]Corresponding author: Sandra O. Brugger

Keywords: Ice biology – Paleoclimate – *Eucalyptus* marker – Glacier – *Lycopodium* marker – Palynology – Pollen

Journal of Glaciology 64(245) 432-442

Journal of Glaciology (2018), **64**(245) 432–442 doi: 10.1017/jog.2018.31

A quantitative comparison of microfossil extraction methods from ice cores

SANDRA O. BRUGGER,[1,2] E. GOBET,[1,2] F. R. SCHANZ,[1] O. HEIRI,[1,2] C. SCHWÖRER,[1,2] M. SIGL,[2,3] M. SCHWIKOWSKI,[2,3,4] W. TINNER[1,2]

[1]*Institute of Plant Sciences, University of Bern, Switzerland*
[2]*Oeschger Center for Climate Change Research, University of Bern, Switzerland*
[3]*Paul Scherrer Institute, Villigen, Switzerland*
[4]*Department for Chemistry and Biochemistry, University of Bern, Switzerland*
Correspondence: Sandra O. Brugger <sandra.bruegger@ips.unibe.ch>

ABSTRACT. Microfossil records from ice archives allow vegetation, fire and land-use activity reconstructions on broad spatial scales. Samples typically contain low microfossil concentrations. Therefore, large ice volumes are often needed for palynology. Hence, it is crucial to extract maximum microfossil numbers through appropriate physical-chemical treatments. We compare six methods covering the main water reduction procedures: evaporation, filtration and centrifugation with snow samples. Adding a known number of *Lycopodium* marker spores prior to sample treatment and a second marker (*Eucalyptus*) after laboratory processing allows a quantitative microfossil loss assessment during pollen extraction. We applied the best-performing method (average loss of 22%) to high-alpine firn cores from Colle Gnifetti glacier for validation with a natural archive containing extremely low microfossil concentrations. We conclude that samples processed with different microfossil extraction protocols may give different results for pollen concentrations, percentages and ratios between different pollen types, especially if vesiculate conifer pollen is an important pollen assemblage component. We recommend a new evaporation-based method which delivers the smallest and least variable losses among the tested approaches. Since microfossil losses are inevitable during laboratory procedure, adding markers prior to sample processing is mandatory to achieve reliable microfossil concentration and influx estimates.

KEYWORDS: ice biology, paleoclimate, *Eucalyptus* marker, glacier, *Lycopodium* marker, palynology, pollen

1. INTRODUCTION

Only a handful of microfossil records from ice cores and surface snow samples are available at present (overview in Table 1), probably because the records are difficult to retrieve and the concentrations of the target material are low. In contrast to the more traditional archives of palynology (e.g. lakes and peat bogs), ice archives have specific advantages. For instance, they are well suited to address vegetation dynamics and land-use activities at subcontinental scales (Liu and others, 1998), since drilling sites on high-alpine glaciers are remote from microfossil sources and undesired local biases are absent. Further, they do not suffer from fine-scale disturbances that may affect lakes or peatlands such as soil erosion and related reworking issues. Ice cores usually provide excellent chronologies and high temporal resolution records, especially for the most recent 200 years where age-depth models can rely on absolutely-dated reference horizons (e.g. volcanic layers) and annual layer counting (e.g. Preunkert and others, 2003; Olivier and others, 2006; Jenk and others, 2009; Sigl and others, 2009; Herren and others, 2013; Konrad and others, 2013). Multiproxy climate and environmental evidence from the same cores (e.g. temperature reconstructions or chemical tracers for environmental variables; Eichler and others, 2011) contribute to assess past ecosystem dynamics.

Glaciers contain extremely low microfossil concentrations compared with lake and mire sediments, hence large ice volumes are needed for quantitative microfossil analyses. Furthermore, given the difficulty of accessing the often remote drilling sites, ice core material is usually very limited and therefore it is crucial to extract a maximum of microfossils for analysis. This provides a major challenge for sample processing. Different methods have been used in the past to concentrate and extract pollen from ice or snow samples with three main water elimination approaches described in the literature: evaporation, centrifuging followed by decanting of the supernatant liquid and filtering methods (see Table 1 for an overview of the available methods). No qualitative or quantitative comparison of the different extraction methods is available so far. Differences among the approaches may impede comparison of microfossil ice core results, but this potential source of uncertainty is unexplored. Thus, the situation is very different than for pollen analysis in lake and mire sediments with well-recognized preparation procedures and protocols (Faegri and Iversen, 1989; Moore and others, 1991; Lang, 1994).

Marker spike application is a long-established and reliable method to estimate microfossil concentrations and influx (Benninghoff, 1962; Stockmarr, 1971; Peck, 1974; Birks and Birks, 1980; Maher, 1981; Birks and Gordon, 1985; Moore and others, 1991). Its use additionally allows to check for microfossil losses during sample preparation (Stockmarr, 1971). Most of the previous microfossil records

Table 1. Methods for microfossil extraction from ice, grouped according to the main water elimination procedure with an indication of marker use

Centrifugation	***Filtration***
Eichler and others (2011)* (EICHLER method)	*Dissolving filter*
Festi and others (2015)[†] (FESTI method)	Andreev and others (1997)[‡]
Vareschi (1934)[‡]; Ambach and others (1966)[‡]	Hicks and Isaksson (2006)*
Fredskild and Wagner (1974)[‡]	Koerner and others (1988)[‡]
Feurdean and others (2011)[‡]	McAndrews (1984)[‡]
	Short and Holdsworth (1985)* (SHORT method)
Evaporation	*Rinsing filter*
Liu and others (1998; 2005; 2007)* (LIU method),	Papina and others (2013)[‡]
Reese and Liu (2002; 2005)*,	*Counting on filter*
Reese and others (2003)*	Nakazawa and others (2004, 2005, 2006, 2011)[‡]
Yang and others (2008)* (YANG method)	Uetake and others (2006)[‡]
	Santibañez and others (2008)[‡]
	Bourgeois (1990; 2000), Bourgeois and others (2000; 2001)*

Approaches used for the method comparison in this paper with method-name in brackets. Filtration-based approaches are divided in methods that chemically dissolve the filter, rinse the microfossils with water from the filter surface or methods where microfossils are directly counted on the filter.
* Marker added, †No marker added, ‡No information available.

from ice cores rely on marker application (e.g. Liu and others, 1998; Eichler and others, 2011; see Table 1 for an extensive list). Exceptionally, its use has been neglected in recent ice studies (Festi and others, 2015) because the utility of this standard palynological approach has been questioned (Festi and others, 2016). Here we address existing knowledge gaps and open questions in respect to the effects of sample preparation methods on pollen assemblages from ice core records with the following aims: (1) to compare different palynological extraction methods for snow, firn and ice core records; (2) to assess the risk of microfossil losses during the extraction procedure and thus the utility of markers in ice core samples; and (3) to propose an improved extraction protocol to gain reliable, accurate and comparable microfossil results from snow and ice samples with a minimum of loss during extraction.

2. MATERIALS AND METHODS

2.1. Marker tablets

To quantify the losses during the different extraction procedures, we added two different markers to the samples, one before and another after the physical and chemical treatments. We used *Lycopodium clavatum* (Batch number 3862 with 9666 spores per tablet ± 671 Std dev.) and *Eucalyptus* marker tablets (Batch number 106720 with 13500 pollen grains ± 210) provided by University of Lund (Maher, 1981). Before proceeding with microfossil extraction, we tested the reliability of the marker tablets by mixing one tablet of *Lycopodium* marker and one tablet of *Eucalyptus* marker. Ten of these marker tablet pairs were dissolved in 10% HCl following standard procedures for palynology (e.g. Moore and others, 1991). The marker suspensions were mounted on microscopic slides. We counted a sum of 1000 grains (*Lycopodium* + *Eucalyptus*) to estimate the accuracy of the expected marker ratio between *Lycopodium* and *Eucalyptus* grains.

2.2. Microfossil extraction methods

2.2.1. Snow replicate samples

To compare the different microfossil extraction methods from snow and ice, we collected 10 surface snow samples (uppermost 30 cm) of ~4 kg at Jungfraujoch (Swiss Alps, 46° 32′ 54.6″ N, 7° 58′ 58.8″ E, 3400 m a.s.l.) in July 2016 after conifers flowered in late spring (Lauber and Wagner, 2012). The 10 samples (Jung-1 – Jung-10) were transported frozen to the laboratory and separated in small pieces in the freezing chamber at −17°C to avoid melting. The pieces were homogenized well before dividing them into six replicate subsamples, resulting in a total of 60 test samples. Each of the six replicate samples weighed between 370 and 400 g (corresponding to a volume of 370–400 mL). The microfossil extraction followed five methods from the literature covering the main physical water reduction procedures of evaporation (Liu and others, 1998; Yang and others, 2008), centrifuging and decanting (Eichler and others, 2011; Festi and others, 2015), and filtration (Short and Holdsworth, 1985; Fig. 1), followed by a chemical treatment involving several centrifuging steps. For simplicity, we labeled the applied methods using the first author's name in the publications (e.g. LIU method for the method described in Liu and others, 1998; and accordingly, YANG, EICHLER, FESTI and SHORT method; Table 1). The evaporation-based methods LIU and YANG differ in a HF treatment included in the latter method, which requires additional steps for the laboratory protocol. The EICHLER and FESTI methods follow a comparable protocol except for the addition of *Lycopodium* tablets and an alcohol treatment to lower the water surface tension in the samples used by FESTI. Microfossil concentration methods based on filtration, with direct counts of microfossils on the filter, were not considered in this study due to the strong limitations in the taxonomic resolution that can be achieved (Nakazawa and others, 2005).

We tested a new extraction method, which we refer to as BRUGGER method (Fig. 1). This method starts with evaporation in a drying cabinet (1 week at 70°C for 400 mL sample volume) to reduce the water content to ~20 mL. The samples are then transferred to 50 mL tubes including

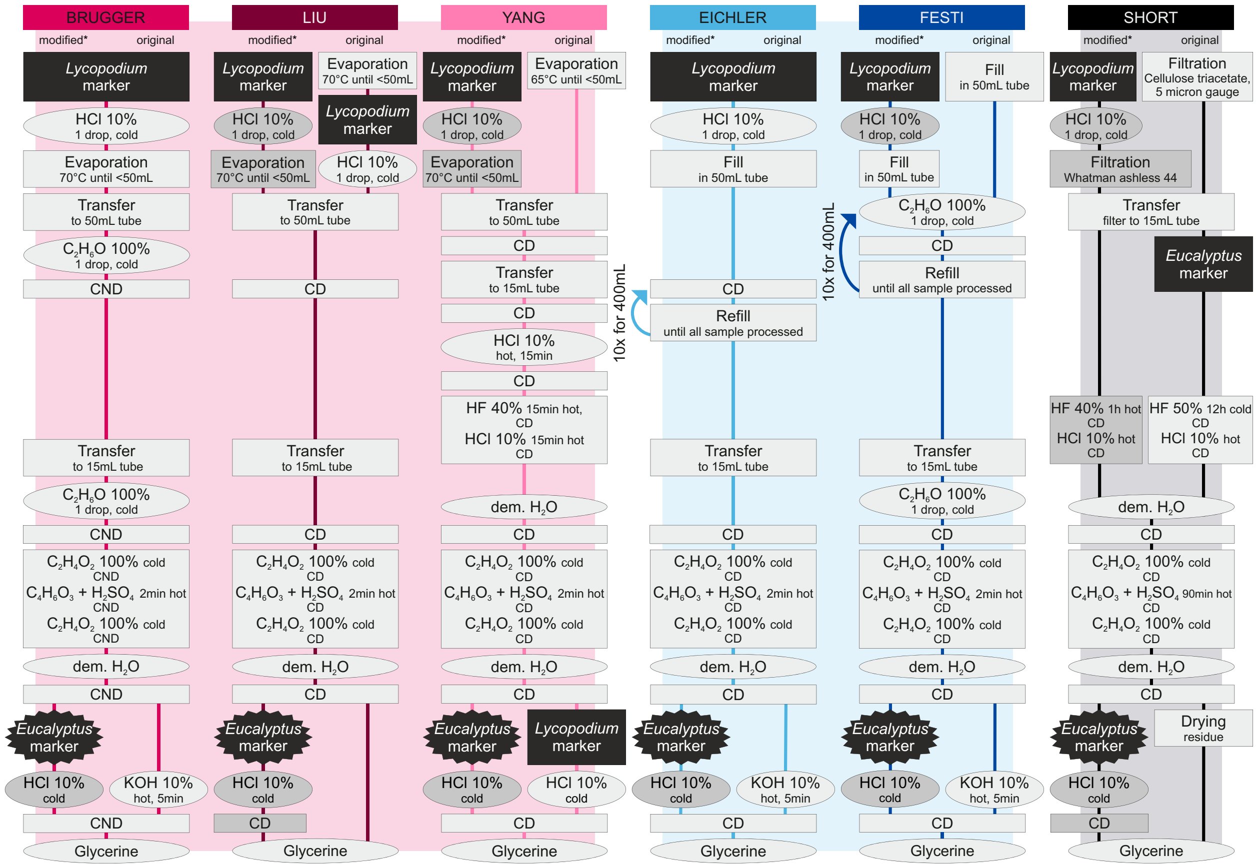

* Left column for each extraction method shows needed modification of original lab protocols for the standardized comparison in this study with a double treatment of exotic markers.

Fig. 1. Flowcharts for ice and snow sample extraction methods: BRUGGER = this study, LIU = Liu and others (1998), YANG = Yang and others (2008), EICHLER = Eichler and others (2011), FESTI = Festi and others (2015), SHORT = Short and Holdsworth (1985). Right column for each method indicates original method description. Left column (shaded in dark grey) indicates required steps to add a second marker (*Eucalyptus*) and the deviation from the original protocol for the standardized method comparison of this paper with two markers. CND = centrifuging, shock-freezing in liquid nitrogen, decanting, CD = centrifuging, decanting. C_2H_6O = ethanol, $C_2H_4O_2$ = glacial acetic acid, $C_2H_6O_3$ = acetic anhydride, H_2SO_4 = sulphuric acid, dem. H_2O = demineralized water.

careful rinsing of the original containers. After each centrifugation step, we shock-freeze the bottom liquid of the tubes, which contains the sunken microfossils, with liquid nitrogen and decant the remaining water. Subsequently, the samples are transferred to 15 mL tubes. Acetolysis and a 10% KOH treatment follow before mounting the samples in glycerine (for details on acetolysis see Moore and others, 1991). The protocol is comparable with the method described in Liu and others (1998) but it includes the step of shock-freezing the bottom liquid after each centrifugation step to avoid material losses. Additionally, we add a drop of ethanol (C_2H_6O) to the centrifuge tubes before centrifuging for all protocol steps with water to reduce floating of microfossils due to water surface tension effects (Dietrich, 1923). Finally, to test for microfossil losses during the physical and chemical procedure we added one *Lycopodium* tablet to each snow replicate sample prior to sample processing (Stockmarr, 1971). After sample processing, we added one *Eucalyptus* marker tablet and we applied once more 10% HCl to dissolve the tablet before the last centrifugation step (Fig. 1). *Lycopodium* spores and *Eucalyptus* pollen are nonvesiculate grains and have a diameter of ~25 and 20 μm, respectively.

2.2.2. High-alpine ice core samples

To further evaluate our new method, we applied it to high-alpine ice core samples from Colle Gnifetti glacier. This glacier saddle forms part of the Monte Rosa massive in the Swiss Alps (45°55′50″N, 7°52′33″E, 4450 m a.s.l.). The ice core was drilled in September 2015 and stored frozen at the Paul Scherrer Institute in Villigen. In total 18 samples from adjacent core segments of varying length (Samples Colle-1 – Colle-18) spanning 2015–01 AD were cut in the freezing chamber. We included one additional replicate sample (Colle-15 replicate) from core segment 15 to examine the reproducibility of the results. Each sample contained between 230 and 870 g of ice. The samples were processed identically to the Jungfraujoch snow samples following the BRUGGER method, involving the same protocol modification for the second marker treatment (Fig. 1).

2.3. Pollen analysis

A pollen sum of 500 grains per sample was counted except for the high-alpine ice samples from Colle Gnifetti for which we reached a pollen sum of 350 due to low pollen concentrations. Pollen identification was conducted under a light microscope at 400× magnification following Beug (2004) and the reference collection of the Institute of Plant Sciences at University of Bern. Pollen percentage calculations are based on the terrestrial pollen sum, and concentrations were standardized to one liter of water. *Lycopodium* and *Eucalyptus* markers were counted alongside pollen and we obtained a minimum sum of 1000 marker grains for each sample.

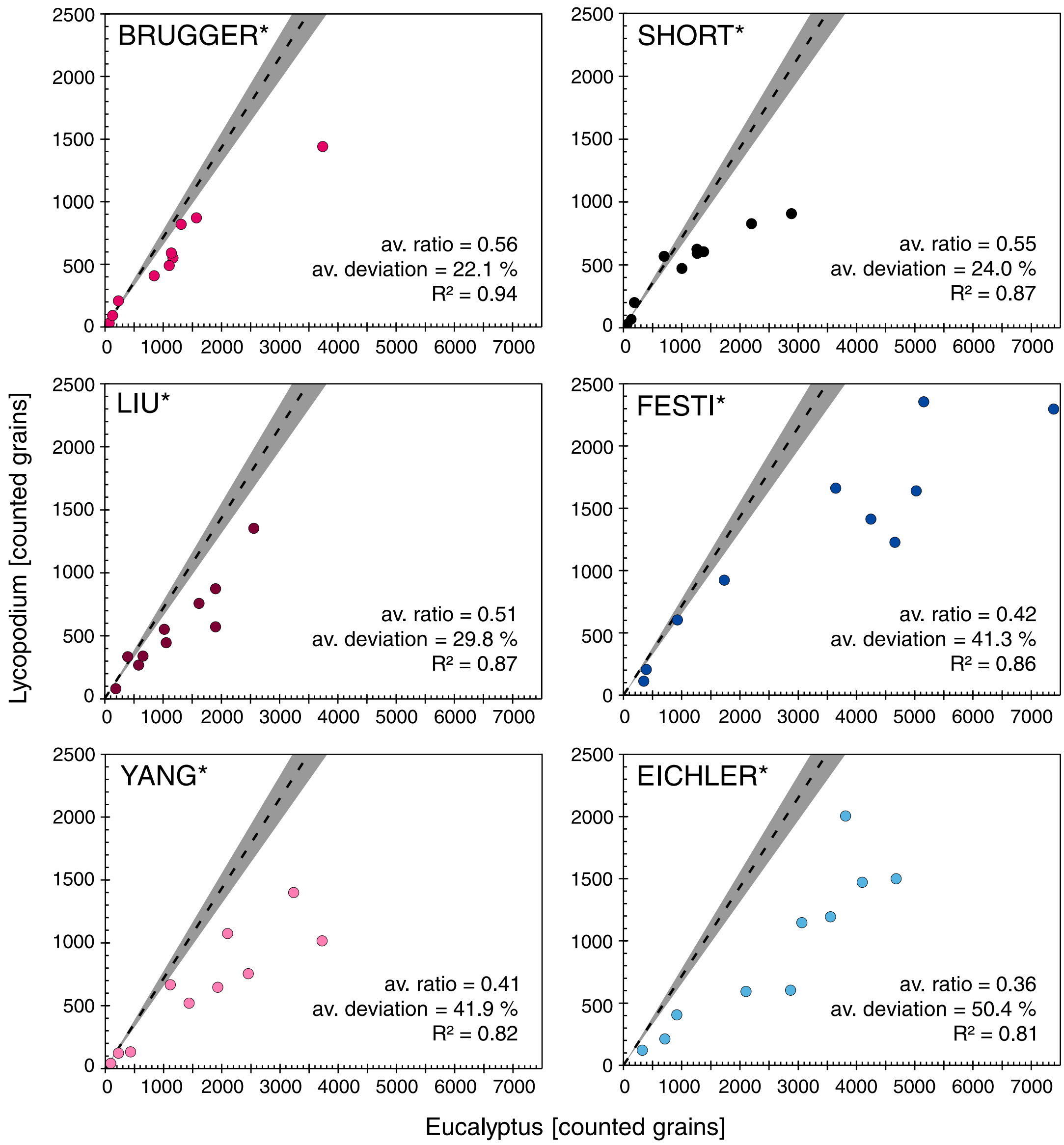

Fig. 2. Marker ratio of *Lycopodium* (added prior to sample processing) to *Eucalyptus* (added before mounting in glycerine) for standard snow replicate samples from Jungfraujoch (Jung-1 to Jung-10). Sample preparation according to flowcharts in Figure 1 (modified for the standardized method comparison with two markers). Ideal marker relationship (dashed lines) with confidence intervals for marker tablet uncertainties based on standard deviations of tablet content (grey). Marker ratio and average deviation of markers from ideal marker ratio (% of 0.72) indicating average sample loss during processing with R^2 as a measure of correlation strength indicating loss variability.

2.4. Numerical analysis

We estimated average deviation of marker loss in percentages from the ideal marker ratio *Lycopodium* : *Eucalyptus* (0.72) based on the mean content of one marker tablet with one standard deviation of each marker to indicate the range of the ratio uncertainty for the tablets (0.66–0.78). We calculated coefficients of determination (R^2) for the marker ratios for each extraction method of the snow replicate samples and for the marker ratio of the high-alpine ice core samples as well as for pollen percentages of the two Colle Gnifetti replicate samples of segment Colle-15, with all pollen types >1%, including and excluding vesiculate pollen taxa. To test statistically potential differences between the effects of the extraction methods, we conducted one-way ANOVA followed by a Tukey-Kramer post-hoc test for the marker ratios and the vesiculate pollen percentages for all 60 snow samples grouped by extraction methods.

We performed ordination analyses to visualize the distance between the pollen assemblages of the 60 snow samples. The short length of the first axis (1.48 Std dev. units) of a detrended correspondence analysis (DCA, by segments) for the pollen percentage dataset of the snow replicate samples justifies using linear ordination methods (ter Braak and Prentice, 1988). Principal component analysis (PCA, ter Braak and Šmilauer, 2002) was performed based on a correlation matrix for pollen percentages (all taxa >1%), which is the standard unit to present pollen data (Maher, 1981; Faegri and Iversen, 1989). Additionally, we conducted PCA with the same explanatory variable based on a covariance matrix for pollen concentrations (grains l^{-1}) standardized by norm to assess potential absolute differences of single pollen types independently from each other (data not shown). Ordinations were carried out using CANOCO version 4.5 (ter Braak and Šmilauer, 2002).

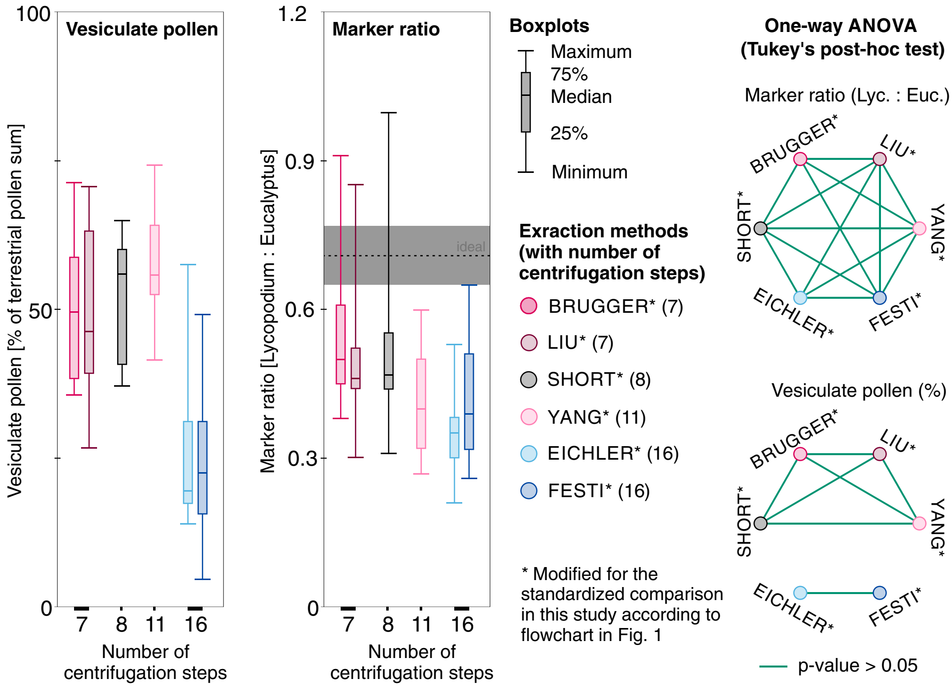

Fig. 3. Left: Boxplots for vesiculate pollen (as percentages of the terrestrial pollen sum, left side) and the counted marker ratio (*Lycopodium* : *Eucalyptus* with indication of the ideal marker ratio and one standard deviation uncertainty in grey, right side) for the different extraction methods sorted according to number of involved centrifugation steps including the physical and chemical treatment for 400 mL water (see numbers on the x-axis and in brackets in the method description) applied to standard snow replicate samples from Jungfraujoch. Right: One-way ANOVA followed by Tukey-Kramer post-hoc test results of marker ratios (top) and vesiculate pollen percentages among the different extraction methods. Circles joined by green lines indicate samples for which the tests did not provide evidence for statistical differences at the p= 0.05 level. All protocols modified from original lab protocols for the standardized comparison with a second marker (see flowchart in Fig. 1).

3. RESULTS AND INTERPRETATION

3.1. Marker tablet reliability

Given that the tablets completely dissolved in HCl, the added marker did not alter the quality of the samples. Instead, we assume that the marker spores and pollen increase the quality by adding more mass to the samples, thus contributing mass to and strengthening the organic pellet formed at the base of the centrifuge tubes (Moore and others, 1991). The tablets contained only the declared spores and pollen and the screening of the entire microscopic slides yielded no foreign materials (e.g. other pollen, charcoal) as potentially deriving from contamination during the tablet production process (see Festi and others, 2016). The ratio of *Lycopodium/Eucalyptus* grains was in all 10 samples of the marker reliability test within the expected ratio (0.66–0.78 *Lycopodium/Eucalyptus*) confirming that the marker tablets are reliable to use for our quantitative investigations.

3.2. Comparison of microfossil extraction methods with standard snow samples

All 60 samples yielded countable microfossil slides. The average marker ratio *Lycopodium/Eucalyptus* in the replicate snow samples processed with the BRUGGER method is 0.56 (22.1% average deviation from the ideal marker ratio i.e. 0.72). The number of counted *Lycopodium* spores is strongly correlated with the counted *Eucalyptus* pollen (R^2 of 0.94; Figs 2 and 3), suggesting that this pollen loss resulted in a systematic (and thus predictable) shift in the estimated pollen concentrations. Slightly higher marker deviation with 24% (average ratio = 0.55) is reached with the filtration-based SHORT method and 29.8% deviation (average ratio = 0.51) with the related LIU method, while the R^2 of 0.87 reached in both methods is somewhat reduced compared with the BRUGGER method (R^2 of 0.94, Fig. 2). Extraction methods which involve many centrifugation steps without bottom freezing (EICHLER, FESTI, YANG) result in higher average marker deviation and lower R^2 (Figs 2 and 3, marker ratio = 0.36–0.42, 41–50% deviation, R^2 = 0.81–0.86) suggesting that, on average, considerable numbers of *Lycopodium* spores (and thus of the targeted microfossils) are lost during water removal and chemical treatment and that the loss variability is larger with these extraction methods. However, ANOVA for the marker ratio differences between the extraction methods (Fig. 3) suggests that only the best performing BRUGGER and the least performing EICHLER method yield statistically significant differences in the mean marker ratios.

The pollen assemblages in all samples are dominated by *Picea abies*, *Pinus sylvestris*-type (both vesiculate = pollen with air bladders), *Alnus* and Poaceae with lower amounts of *Betula*, *Plantago lanceolata*-type, Cyperaceae and small pollen grains of *Castanea* and *Urtica* (Fig. 4). *Picea abies* and *Pinus sylvestris*-type pollen percentages and concentrations are generally higher in samples processed with evaporation- (BRUGGER, LIU, YANG) or filtration-based (SHORT) methods compared with samples processed with solely centrifugation-based methods (EICHLER, FESTI), suggesting that centrifugation may reduce vesiculate pollen grains compared with nonvesiculate pollen grains (Fig. 4). The large and relatively constant amount of *Urtica* (grain diameter ~10–15 µm, 15–20% abundance in all replicates from Jung-2) and *Alnus*, Poaceae and *Betula* (grain diameter 20–30 µm) in all replicate samples indicates that the six tested methods do not induce biases related to pollen grain size in the small to medium size range. Assessing differences in the amount of

Fig. 4. Pollen percentage diagram of all pollen types more common than 5% in any one sample based on the terrestrial pollen sum and concentrations [grains^{-1}] of vesiculate and nonvesiculate pollen for standard snow samples from Jungfraujoch. Each sample (Jung 1–10) was divided into replicate samples that were processed with six extraction methods (Modified from original protocols for a standardized comparison with a second marker, see flowchart in Fig. 1). Hollow bars = 10× exaggeration.

large nonvesiculate pollen (>50 μm, e.g. *Larix)* was not possible as these pollen types were too rare in our snow samples. The pollen concentrations in the snow replicate samples vary between 12000 and 65000 grains l^{-1} (average 26000 grains l^{-1}) except samples Jung-4 and Jung-10 which contain five to 10 times higher pollen concentrations (Figs 3 and 4). Nonvesiculate pollen shows only small variability among snow replicate samples while vesiculate pollen concentrations show a much larger variability confirming that vesiculate pollen is mainly responsible for the differences in the percentages of the replicate samples, and therefore also of the main pollen percentage diagram for trees, shrubs and herbs.

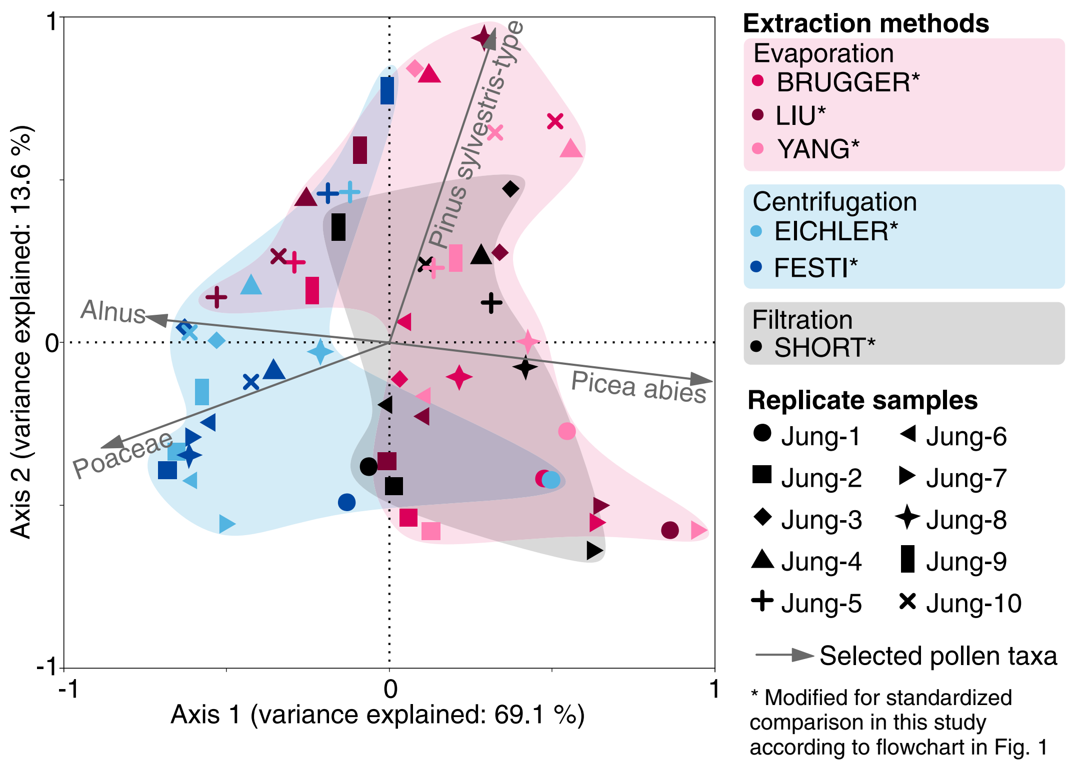

Fig. 5. Principal component analysis of pollen assemblages (percentages of the terrestrial pollen sum) for standard snow replicate samples from Jungfraujoch processed with six different microfossil extraction methods modified from original lab protocols for a standardized comparison with a second marker; see flowchart in Fig. 1. Colors refer to extraction methods grouped according to the main water elimination procedures: evaporation, centrifugation and filtration. Symbols refer to replicate samples.

The first PCA axis for the pollen percentages of the snow replicate samples explains 69.1% of the variance, and separates samples that used evaporation (BRUGGER, LIU and YANG) and filtration (SHORT) from samples that underwent many centrifugation steps without bottom freezing (EICHLER and FESTI methods). These latter samples contain generally lower amounts of *Picea abies* pollen (Fig. 5). The second axis explains 13.6% of the variance, and possibly reflects *Pinus sylvestris*-type abundance in the samples. Thus, the high cumulative variance explained by the two axes (82.7%) suggests that the vesiculate pollen abundance in the pollen assemblages may be strongly affected by the microfossil extraction procedure. Analyses with absolute values (pollen concentrations in grains l^{-1}) yield comparable results confirming the ordination results of the percentage dataset (data not shown).

The boxplots (Fig. 3) for vesiculate pollen percentages grouped by methods also indicate a selective vesiculate pollen loss with centrifugation-based methods without bottom freezing (EICHLER and FESTI by ~25%). It also seems that pollen composition among samples is characterized by a slightly higher variability compared with the evaporation and filtration-based methods. ANOVA for vesiculate pollen percentages grouped by extraction methods (Fig. 3) provides no evidence for statistically significant differences between samples processed with evaporation and filtration-based methods (BRUGGER, LIU, SHORT and YANG). For the centrifugation-based methods EICHLER and FESTI, ANOVA also provides no evidence for statistically significant differences in vesiculate pollen percentages. However, the analyses indicate statistically significant differences between these samples and those processed with the four other methods. Both ANOVA and visual examination of the data, therefore, suggest a distinct difference between evaporation- or filtration-based methods and solely centrifugation-based methods in respect to the percentage of vesiculate pollen, with a clearly larger loss of vesiculate pollen in the EICHLER and FESTI methods. In contrast, the influence of different extraction methods on the marker ratio is less distinct (Fig. 3). This suggests a disproportionate effect of the solely centrifugation-based methods on vesiculate pollen (i.e. EICHLER and FESTI methods involving 16 centrifugation steps for 400 mL water, Fig. 3).

3.3. Validation of the BRUGGER method with high-alpine glacier ice samples

We applied the BRUGGER method to ice samples from the high-alpine Colle Gnifetti glacier because it yielded the smallest loss among all approaches used in our comparison with snow replicates from Jungfraujoch. The average marker ratio (0.57, 20.2% deviation from ideal ratio) in the high-alpine ice samples is very similar to the average marker ratio in the snow replicate samples processed with the same method (0.56, 22.1%), suggesting minor losses of *Lycopodium* and thus microfossils. The slightly lower correlation between *Lycopodium* spores and *Eucalyptus* pollen ($R^2 = 0.78$, Fig. 6a), when compared with snow samples (Fig. 6a), may be explained by properties inherent to these specific samples, for example low concentrations of insoluble organic and inorganic particles leading to smaller pellets during the concentration process. Indeed the microscopic slides from ice contained fewer dust particles than those from snow.

Pollen concentrations in the high-alpine ice core samples from Colle Gnifetti are low when compared with the snow

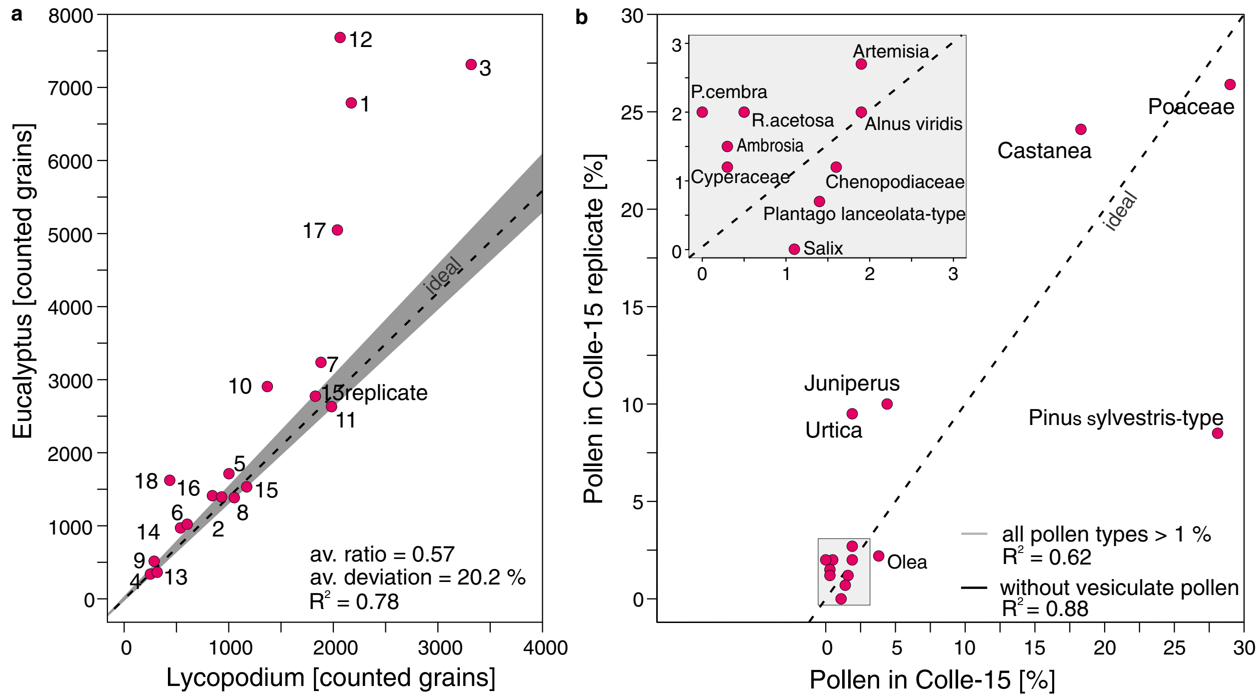

Fig. 6. Application of the BRUGGER method to Colle Gnifetti ice samples. Protocol with second marker application (see flowchart in Fig. 1). a) Marker ratio of *Lycopodium* spores (added prior to sample processing) and *Eucalyptus* pollen (added before mounting in glycerine) for 18 ice samples and one replicate of sample 15 from Colle Gnifetti glacier. Ideal marker relationship (9666 *Lycopodium* spores : 13500 *Eucalyptus* pollen = 0.72; dashed line) with tablet uncertainty (grey). b) Pollen assemblage comparison of sample 15 and its replicate (15 replicate) with all taxa presented as percentages of the terrestrial pollen sum. All pollen types >1 % in one of the samples are shown. Dashed black line indicates ideal 1:1 pollen percentage ratio. *P. cembra* = *Pinus cembra*, *R. acetosa* = *Rumex acetosa-type*. Insert box: Magnification for pollen types with percentages between 1 and 3.

samples from Jungfraujoch, ranging between 310 and 18300 grains l^{-1} (mean of 6600 grains l^{-1}) vs. 12000–400000 grains l^{-1} (115000 grains l^{-1}), respectively. This finding may reflect the altitudinal difference of 1000 m between Colle Gnifetti (4450 m a.s.l.) and Jungfraujoch (3400 m a.s.l.), which markedly increases the distance to the vegetation at lower altitudes (colline to alpine belts between ~200 and 3000 m a. s.l.; Ellenberg, 1996) that produces the palynological signal. Pollen percentages for taxa >1% in the two replicate samples of Colle-15 are very similar resulting in a high R^2 between pollen percentages of different taxa in these two samples (0.88 for pollen >1% occurrence without vesiculate). The exception is *Pinus sylvestris*-type which occurs at 27% in Colle-15 and 10% in the Colle-15 replicate resulting in a much lower R^2 (0.62, Fig. 6b), if the vesiculate pollen taxa are included in the dataset (Fig. 6b). This suggests a high reproducibility of most pollen taxa (e.g. Poaceae and *Castanea*). The vesiculate morphology of *Pinus sylvestris*-type may influence the reproducibility of its abundance compared with other pollen taxa with a nonvesiculate morphology, while *Pinus cembra* values (2% vs. 0%, respectively) are too low to be assessed. Even though the statistical power of two high-alpine ice core replicates is limited, these results strongly support the outcome of the snow replicates as discussed in Section 3.2.

4. DISCUSSION

4.1. The necessity of marker application

Adding microfossil markers to palynological sediment samples has been a standard in palynology since the early 1970s (e.g. Stockmarr, 1971; Moore and others, 1991; Dark and Allen, 2005; Finsinger and Tinner, 2005; Maher and others, 2012; Brugger and others, 2016; Campbell and others, 2016; Rey and others, 2017). This allows quantitative pollen concentration and influx estimates (Stockmarr, 1971; Birks and Gordon, 1985), which cannot be achieved otherwise unless the entire sample is counted (von Post, 1916; Welten, 1944; Moore and others, 1991). Adding markers also helps to estimate losses during pollen extraction. Some recent studies tend to avoid adding markers to the palynological samples because of the costs, the additional labor or presumed contamination issues (Festi and others, 2016). Based on our results presented here, we can reject these speculations about contamination issues when using commercially available, standardized and quality checked marker tablets (e.g. *Lycopodium* tablets provided by the University of Lund; Maher, 1981).

Our results clearly show that microfossil loss during pollen extraction from ice samples is inevitable (i.e. >20% of the *Lycopodium* marker is lost). This loss occurs while initially reducing the water content (e.g. evaporation, filtration, centrifuging followed by decanting), during the chemical treatment involving inevitable centrifuging steps in all tested methods and after sample processing. The very low amount of pollen in ice and snow samples is not easy to extract from the centrifuge tubes, to be fixed without losses on the slide and partly becomes covered under the microscopic cover slip margins. These losses strongly affect any absolute microfossil counts (e.g. pollen, charcoal particles in ice core samples) that do not add markers. Thus, marker application is imperative to estimate realistic absolute values (concentrations, influx) and as a control for total sample loss

(Stockmarr, 1971; Peck, 1974; Finsinger and Tinner, 2005), particularly for ice samples.

4.2. Influence of specific ice sample properties on pollen extraction

Ice samples have specific properties that may explain differences in the microfossil behavior during laboratory processing compared with sedimentary samples. The microfossil deposition on glaciers is different than the deposition in lake and mire sediment archives. Fresh pollen, spores and other microfossils (e.g. charcoal) get directly covered with snow after deposition on the surface and incorporated into the ice. This is unlike pollen deposited in lake sediments, which only settles to the lake bottom when it is saturated with water and dense enough to sink (Faegri and Iversen, 1989; Dark and Allen, 2005). A special behavior of vesiculate pollen compared with nonvesiculate pollen was demonstrated in transect studies in lakes, with shore sediments enriched in vesiculate pollen compared with sediments from the lake center. This pattern is explained by the fact that vesiculate pollen floats for a long time and is thus transported to the shore where it accumulates (Ammann and Tobolski, 1983). The different behavior of vesiculate and nonvesiculate pollen was also observed in floating pollen traps in lakes (Giesecke and Fontana, 2008). Early controlled laboratory experiments on the pollen floating behavior confirmed that the majority of vesiculate pollen (e.g. *Pinus* sp.) floated on the water surface in still standing glass beakers for hours while most fresh nonvesiculate pollen (e.g. 95–100% *Corylus*, *Quercus, Juniperus* and *Larix*) sank within the first 5 minutes after the experiment started (Hopkins, 1950). We thus assume that pollen of vesiculate pollen floated on the water surface after thawing of the ice samples and was preferentially lost during the subsequent decanting of the centrifuge tubes. A major difference between ice and sediment samples is that while pollen is frozen in ice, sediment pollen is soaked in water over years to millennia, potentially reducing its floating capacity. The high floating capacity of well-preserved vesiculate pollen in ice may explain the larger variability of vesiculate compared with nonvesiculate pollen (Fig. 4). This finding is important because it implies a negative bias on vesiculate pollen concentration estimates from ice core records. Peck (1972), Davis and Brubaker (1973) and Holmes (1990) reported differences of settling time among nonvesiculate pollen depending on the size. However, based on our results we cannot confirm a larger variability of pollen grains with small diameters and lower densities compared with larger grains (e.g. *Urtica* and *Castanea* vs. *Alnus* and Poaceae).

While the morphology of vesiculate pollen is an evolutionary advantage for wind and water pollination (the latter because buoyancy aids floating upwards in a liquid drop into the ovules; Owens and others, 1998; Runions and others, 1999), it is a clear disadvantage for laboratory processing of palynological samples. This implies that thawed ice samples should stand around some days to extend the water saturation and sinking time for pollen before applying centrifugation steps. This waiting time is inherent to evaporation-based methods (BRUGGER; LIU; YANG) where the pollen stays in the water for several days during the initial evaporation. Similarly, filtration-based methods (SHORT; or the method in Nakazawa and others, 2005) circumvent the problem of floating pollen in the first water reducing step. However, centrifuging samples may also help vesiculate pollen to sink from a water surface by filling the air bladders with water (Hopkins, 1950) implying that increasing the centrifugation time in each centrifuging step may help to increase the number of sunken vesiculate pollen.

Microfossils from ice samples are not incorporated in a matrix as is typical for sediment samples from lakes or mires. We assume that this causes higher and more variable pollen loss during the pollen extraction from ice samples, especially during decanting of centrifuge tubes. Indeed, pollen assemblage differences were smaller in sediment samples as evidenced by a tentative comparison with replicate sediment samples from Moossee, Switzerland (unpublished results). Similarly, snow replicate samples from Jungfraujoch with most likely higher dust concentrations have a lower pollen loss variability than the high-alpine ice samples from Colle Gnifetti glacier, presumably since they form a more stable pellet at the bottom of centrifugation tubes after centrifugation. Our solution to this problem is to minimize pollen losses in ice samples by mimicking a matrix through shock-freezing of the tube bottom always after centrifuging and before decanting. The pollen quality was not affected by the shock-freezing procedure. However, our observations suggest that the low concentrations of suspended particles in the high-alpine ice core samples compared with samples with a sediment matrix may influence the sinking behavior during centrifugation. Comparing samples that are processed with identical laboratory protocols except for an alcohol treatment before centrifuging to lower the surface tension (EICHLER and FESTI methods) points to smaller pollen loss with an alcohol treatment (FESTI), although marker ratios are not significantly lower according to the comparison statistics (Fig. 3).

Our data indicate that losses increase with the number of increasing centrifuging steps (Fig. 3) suggesting that the number of centrifuging steps is crucial for microfossil losses. Remote archives at high altitudes (e.g. high alpine glaciers in the Andes above 6000 m a.s.l.; Liu and others) or high latitudes (e.g. Arctic sites, Short and Holdsworth, 1985; Hicks and Isaksson, 2006) usually demand high ice volumes (e.g. >400 mL) because of low pollen concentrations. Microfossil concentrations may also be more diluted in archives with high snow accumulation rates common in some mountain ranges (e.g. Neff and others, 2012; Schwikowski and others, 2013; Mariani and others, 2014). Given that the required sample volume for reliable analysis is much larger (i.e. several liters) in such extreme archives, evaporation methods appear best suited to reduce undesired pollen losses.

5. CONCLUSIONS

The BRUGGER extraction method is developed from existing evaporation-based water reducing methods (e.g. LIU protocol; Liu and others, 1998) with a newly invented step of freezing the tube bottom after centrifugation during the chemical treatment. Based on our results, the BRUGGER protocol can minimize microfossil loss if compared with the other approaches. However, the differences are statistically not pronounced. Our study highlights that pollen assemblages from ice cores processed with different microfossil extraction protocols challenge the reproducibility between records from different study sites. This is especially valid for sites where vesiculate pollen grains from conifers are an important component of pollen assemblages. Remote ice archives at extreme altitudes, high latitudes, or with high snow accumulation rates and consequently extremely low microfossil concentrations, need a special focus when processing samples for palynological analysis. We show that significant losses are inevitable during processing of samples. Therefore, applying high-quality marker tablets prior to microfossil extraction from ice records is crucial if the goal is to produce absolute counts and not only percentages. Speculations about marker contaminations or other negative effects on the pollen assemblage quality can definitely be rejected. To conclude, we recommend following a strictly standardized protocol that includes high-quality marker tablets to obtain reliable concentration and influx estimates. Applying the new BRUGGER approach may contribute to minimizing microfossil losses and gaining reproducible results.

SUPPLEMENTARY MATERIAL

The supplementary material for this article can be found at https://doi.org/10.1017/jog.2018.31

ACKNOWLEDGEMENTS

We are grateful to Ruth Drescher-Schneider for providing *Eucalyptus* tablets, to Florencia Oberli for technical assistance with developing the new extraction method, to Daniela Festi, Klaus Oeggl and their colleagues from Innsbruck University for stimulating discussions, to Dimitri Osmont and Denis Alija for their help with sampling in the freezing room and at the Jungfraujoch station. We thank H.J.B. Birks and an anonymous reviewer for their constructive remarks, which substantially improved the manuscript. We acknowledge the SINERGIA project *Paleo fires from high-alpine ice cores* funded by the Swiss National Science Foundation (SNF grant 154450).

AUTHORS CONTRIBUTIONS

SO Brugger and E Gobet contributed equally.

REFERENCES

Ambach W, Bortenschlager S and Eisner H (1966) Pollen-analysis investigation of a 20 m. Firn Pit on the Kesselwandferner (Ötztal Alps). *J. Glaciol.*, **6**(44), 233–236 (doi: 10.3189/S0022143000019249)

Ammann B and Tobolski K (1983) Vegetational development during the late-Würm at Lobsigensee (Swiss Plateau) (studies in the late quaternary at Lobsigensee 1). *Rev. Paleobiol.*, **2**, 163–180

Andreev AA, Nikolaev VI, Bolíshiyanov DY and Petrov VN (1997) Pollen and isotope investigations of an ice core from Vavilov ice cap, October Revolution Island, Severnaya Zemlya Archipelago, Russia. *Geogr. Phys. Quat.*, **51**(3), 379–389 (doi: 10.7202/033137ar)

Benninghoff WS (1962) Calculation of pollen and spore density in sediments by addition of exotic pollen in known quantities. *Pollen Spores.*, **4**, 332–333

Beug H-J (2004) *Leitfaden der Pollenbestimmung für Mitteleuropa und angrenzende Gebiete*. Pfeil, München

Birks HJB and Birks HH (1980) *Quaternary palaeoecology*. Edward Arnold, London

Birks HJB and Gordon AD (1985) *Numerical methods in quaternary pollen analysis*. Academic Press, London

Bourgeois JC (1990) A modern pollen spectrum from Dye 3, south Greenland ice sheet. *J. Glaciol.*, **36**(124), 340–342 (doi: 10.3189/002214390793701363)

Bourgeois JC (2000) Seasonal and interannual pollen variability in snow layers of Arctic ice caps. *Rev. Palaeobot. Palynol.*, **108**, 17–36 (doi: 10.1016/S0034-6667(99)00031-7)

Bourgeois JC, Koerner RM, Gajewski K and Fisher DA (2000) A holocene ice-core pollen record from Ellesmere Island, Nunavut, Canada. *Quat. Res,*. **54**, 275–283 (doi: 10.1006/qres.2000.2156)

Bourgeois JC, Gajewski K and Koerner RM (2001) Spatial patterns of pollen deposition in arctic snow. *J. Geophys. Res. Atmos.*, **106** (D6), 5255–5265 (doi: 10.1029/2000JD900708)

Brugger SO and 13 others (2016) Long-term man–environment interactions in the Bolivian Amazon: 8000 years of vegetation dynamics. *Quat. Sci. Rev.*, **132**, 114–128 (doi: 10.1016/j.quascirev.2015.11.001)

Campbell JFE, Fletcher WJ, Hughes PD and Shuttleworth EL (2016) A comparison of pollen extraction methods confirms dense-media separation as a reliable method of pollen preparation. *J. Quat. Sci.*, **31**(6), 631–640 (doi: 10.1002/jqs.2886)

Dark P and Allen JRL (2005) Seasonal deposition of Holocene banded sediments in the Severn Estuary Levels (southwest Britain): palynological and sedimentological evidence. *Quat. Sci. Rev.*, **24**(1), 11–33 (doi: 10.1016/j.quascirev.2004.08.001)

Davis MB and Brubaker LB (1973) Differential sedimentation of pollen grains in lakes. *Limnol. Oceanogr.*, **18**(4), 635–646 (doi: 10.4319/lo.1973.18.4.0635)

Dietrich W (1923) Die Erscheinungen an den Grenzflächen. In *Einführung in die Physikalische Chemie für Biochemiker, Mediziner, Pharmazeuten und Naturwissenschaftler*. Springer, Berlin Heidelberg, 1–105

Eichler A and 5 others (2011) An ice-core based history of Siberian forest fires since AD 1250. *Quat. Sci. Rev.*, **30**(9), 1027–1034 (doi: 10.1016/j.quascirev.2011.02.007)

Ellenberg H (1996) *Vegetation Mitteleuropas mit den Alpen in ökologischer, dynamischer und historischer Sicht*. 5th edn. Ulmer, Stuttgart

Faegri K and Iversen J (1989) *Textbook of pollen analysis*. 4th edn. Wiley, Winchester

Festi D and 6 others (2015) A novel pollen-based method to detect seasonality in ice cores: a case study from the Ortles glacier, South Tyrol, Italy. *J. Glaciol.*, **61**(229), 815–824 (doi: 10.3189/2015JoG14J236)

Festi D, Hoffmann DL and Luetscher M (2016) Pollen from accurately dated speleothems supports alpine glacier low-stands during the early Holocene. *Quat. Res.*, **86**(1), 45–53 (doi: 10.1016/j.yqres.2016.05.003)

Feurdean A, Perşoiu A, Pazdur A and Onac BP (2011) Evaluating the palaeoecological potential of pollen recovered from ice in caves: a case study from Scărişoara Ice Cave, Romania. *Rev. Palaeobot. Palynol.*, **165**(1), 1–10 (doi: 10.1016/j.revpalbo. 2011.01.007)

Finsinger W and Tinner W (2005) Minimum count sums for charcoal concentration estimates in pollen slides: accuracy and potential errors. *Holocene*, **15**(2), 293–297 (doi: 10.1191/0959683605hl808rr)

Fredskild B and Wagner P (1974) Pollen and fragments of plant tissue in core samples from the Greenland ice cap. *Boreas*, **3** (3), 105–108 (doi: 10.1111/j.1502-3885.1974.tb00668.x)

Giesecke T and Fontana SL (2008) Revisiting pollen accumulation rates from Swedish lake sediments. *Holocene*, **18**(2), 293–305 (doi: 10.1177/0959683607086767)

Herren PA and 6 others (2013) The onset of Neoglaciation 6000 years ago in western Mongolia revealed by an ice core from the Tsambagarav mountain range. *Quat. Sci. Rev.*, **69**, 59–68 (doi: 10.1016/j.quascirev.2013.02.025)

Hicks S and Isaksson E (2006) Assessing source areas of pollutants from studies of fly ash, charcoal, and pollen from Svalbard snow and ice. *J. Geophys. Res. Atmos.*, **111**(D2), D02113 (doi: 10.1029/2005JD006167)

Holmes PL (1990) Differential transport of spores and pollen: a laboratory study. *Rev. Palaeobot. Palynol.*, **64**(1-4), 289–296 (doi: 10.1016/0034-6667(90)90144-8)

Hopkins JS (1950) Differential flotation and deposition of coniferous and deciduous tree pollen. *Ecology*, **31**(4), 633–641 (doi: 10.2307/1931580)

Jenk TM and 9 others (2009) A novel radiocarbon dating technique applied to an ice core from the Alps indicating late Pleistocene ages. *J. Geophys. Res. Atmos.*, **114**(D14), D14305 (doi: 10.1029/2009JD011860)

Koerner RM, Bourgeois JC and Fisher DA (1988) Pollen analysis and discussion of time-scales in Canadian ice cores. *Ann. Glaciol.*, **10**, 85–91 (doi: 10.1017/S0260305500004225)

Konrad H, Bohleber P, Wagenbach D, Vincent C and Eisen O (2013) Determining the age distribution of Colle Gnifetti, Monte Rosa, Swiss Alps, by combining ice cores, ground-penetrating radar and a simple flow model. *J. Glaciol.*, **59**(213), 179–189 (doi: 10.3189/2013JoG12J072)

Lang G (1994) *Quartäre Vegetationsgeschichte Europas: Methoden und Ergebnisse*. Gustav Fischer, Jena

Lauber K and Wagner G (2012) *Flora helvetica*. 5th edn. Haupt, Bern

Liu KB, Yao Z and Thompson LG (1998) A pollen record of Holocene climatic changes from the Dunde ice cap, Qinghai-Tibetan Plateau. *Geology*, **26**(2), 135–138 (doi: 10.1130/0091-7613(1998)026<0135:APROHC>2.3.CO;2)

Liu KB, Reese CA and Thompson LG (2005) Ice-core pollen record of climatic changes in the central Andes during the last 400 yr. *Quat. Res.*, **64**(2), 272–278 (doi: 10.1016/j.yqres.2005.06.001)

Liu KB, Reese CA and Thompson LG (2007) A potential pollen proxy for ENSO derived from the Sajama ice core. *Geophys. Res. Let.*, **34**(9), L09504 (doi: 10.1029/2006GL029018)

Maher LJ (1981) Statistics for microfossil concentration measurements employing samples spiked with marker grains. *Rev. Palaeobot. Palynol.*, **32**(2–3), 153–191 (doi: 10.1016/0034-6667(81)90002-6)

Maher LJ, Heiri O and Lotter AF (2012) Assessment of uncertainties associated with palaeolimnological laboratory methods and microfossil analysis. In Birks H, Lotter A, Juggins S and Smol J, eds. *Tracking environmental change using lake sediments*. Springer, Dordrecht, 143–166 (doi: 10.1007/978-94-007-2745-8_6)

Mariani I and 6 others (2014) Temperature and precipitation signal in two Alpine ice cores over the period 1961-2001. *Clim. Past*, **10**(3), 1093 (doi: 10.5194/cp-10-1093-2014)

McAndrews JH (1984) Pollen analysis of the 1973 ice core from Devon Island Glacier, Canada. *Quat. Res.*, **22**(1), 68–76 (doi: 10.1016/0033-5894(84)90007-3)

Moore PD, Webb JA and Collison ME (1991) *Pollen analysis*. Blackwell Scientific Publications, Oxford

Nakazawa F and Fujita K (2006) Use of ice cores from glaciers with melting for reconstructing mean summer temperature variations. *Ann. Glaciol.*, **43**(1), 167–171 (doi: 10.3189/172756406781812302)

Nakazawa F, Fujita K, Uetake J, Kohno M, Fujiki T, Arkhipov SM, Kameda T, Suzuki K and Fujii Y (2004) Application of pollen analysis to dating of ice cores from lower-latitude glaciers. *J. Geophys. Res. Earth. Surf.*, **109**(F4), F04001 (doi: 10.1029/2004JF000125)

Nakazawa F and 6 others (2005) Dating of seasonal snow/firn accumulation layers using pollen analysis. *J. Glaciol.*, **51**(174), 483–490 (doi: 10.3189/172756505781829179)

Nakazawa F and 7 others (2011) Establishing the timing of chemical deposition events on Belukha glacier, Altai Mountains, Russia, using pollen analysis. *Arct. Antarc. Alp. Res.*, **43**(1), 66–72 (doi: 10.1657/1938-4246-43.1.66)

Neff PD and 5 others (2012) Ice-core net snow accumulation and seasonal snow chemistry at a temperate-glacier site: Mount Waddington, southwest British Columbia, Canada. *J. Glaciol.*, **58**(212), 1165–1175 (doi: 10.3189/2012JoG12J078)

Olivier S, and 8 others (2006) Temporal variations of mineral dust, biogenic tracers, and anthropogenic species during the past two centuries from Belukha ice core, Siberian Altai. *J. Geophys. Res. Atmos.*, **111**(D5), D05309 (doi: 10.1029/2005JD005830)

Owens JN, Takaso T and Runions CJ (1998) Pollination in conifers. *Trends Plant Sci.*, **3**(12), 479–F04485 (doi: 10.1016/S1360-1385(98)01337-5)

Papina T and 5 others (2013) Biological proxies recorded in a Belukha ice core, Russian Altai. *Clim. Past*, **9**(5), 2399–2411 (doi: 10.5194/cp-9-2399-2013)

Peck RM (1972) Efficiency tests on the Tauber trap used as a pollen sampler in turbulent water flow. *New Phytol.*, **71**(1), 187–198 (doi: 10.1111/j.1469-8137.1972.tb04827.x)

Peck RM (1974) A comparison of four absolute pollen preparation techniques. *New Phytol.*, **73**(3), 567–587 (doi: 10.1111/j.1469-8137.1974.tb02133.x)

Preunkert S, Wagenbach D and Legrand M (2003) A seasonally resolved alpine ice core record of nitrate: comparison with anthropogenic inventories and estimation of preindustrial emissions of NO in Europe. *J. Geophys. Res. Atmos.*, **108**(D21), 10 (doi: 10.1029/2003JD003475)

Reese CA and Liu KB (2002) Pollen dispersal and deposition on the Quelccaya Ice Cap, Peru. *Phys. Geogr.*, **23**(1), 44–58 (doi: 10.2747/0272-3646.23.1.44)

Reese CA and Liu KB (2005) Interannual variability in pollen dispersal and deposition on the tropical Quelccaya Ice Cap. *Prof. Geogr.*, **57**(2), 185–197 (doi: 10.1111/j.0033-0124.2005.00471.x)

Reese CA, Liu KB and Mountain KR (2003) Pollen dispersal and deposition on the ice cap of Volcán Parinacota, southwestern Bolivia. *Arct. Antar. Alp. Res.*, **35**(4), 469–474

Rey F and 10 others (2017) Vegetational and agricultural dynamics at Burgäschisee (Swiss Plateau) recorded for 18,700 years by multi-proxy evidence from partly varved sediments. *Veget. Hist. Archaeobot.*, **26**(6), 571–586 (doi: 10.1007/s00334-017-0635-x)

Runions CJ, Rensing KH, Takaso T and Owens JN (1999) Pollination of Picea orientalis (Pinaceae): saccus morphology governs pollen buoyancy. *Am. J. Bot.*, **86**(2), 190–197 (doi: 10.2307/2656936)

Santibañez P and 8 others (2008) Glacier mass balance interpreted from biological analysis of firn cores in the Chilean lake district. *J. Glaciol.*, **54**(186), 452–462 (doi: 10.3189/002214308785837101)

Schwikowski M, Schläppi M, Santibañez P, Rivera A and Casassa G (2013) Net accumulation rates derived from ice core stable isotope records of Pío XI glacier, Southern Patagonia Icefield. *Cryosphere*, **7**(5), 1635–1644 (doi: 10.5194/tc-7-1635-2013)

Short SK and Holdsworth G (1985) Pollen, oxygen isotope content and seasonally in an ice core from the penny Ice Cap, Baffin Island. *Arctic*, **38**(3), 214–218 (doi: 10.14430/arctic2136)

Sigl M, and 10 others (2009) Towards radiocarbon dating of ice cores. *J. Glaciol.*, **55**(194), 985–996 (doi: 10.3189/002214309790794922)

Stockmarr J (1971) Tablets with spores used in absolute pollen analysis. *Pollen Spores*, **XIII**(4), 615–621

Ter Braak CJF and Prentice IC (1988) A theory of gradient analysis. *Adv Ecol Res* **18**, 271-317 (doi: 10.1016/S0065-2504(03)34003-6)

Ter Braak CJF and Šmilauer P (2002) *Canoco for windows version 4.5*. Biometris–Plant Research International, Wageningen

Uetake J and 7 others (2006) Biological ice-core analysis of Sofiyskiy glacier in the Russian Altai. *Ann. Glaciol.*, **43**(1), 70–78 (doi: 10.3189/172756406781811925)

Vareschi V (1934) Pollenanalysen aus Gletschereis. *Ber. Geobot. Inst. Eidgenöss. Tech. Hochsch. Stift. Rübel*, **1934**, 81–99

von Post L (1916) Einige südschwedischen Quellmoore. *Bull. Geol. Inst. Univ. Upsala*, **15**, 219–278

Welten M (1944) *Pollenanalytische, stratigraphische und geochronologische Untersuchungen aus dem Faulenseemoos bei Spiez* (Vol. 21). Huber, Zürich

Yang B, Tang L, Bräuning A, Davis ME, Shao J and Jingjing L (2008) Summer temperature reconstruction on the central Tibetan Plateau during 1860–2002 derived from annually resolved ice core pollen. *J. Geophys. Res. Atmos.*, **113**(D24), D24102 (doi: 10.1029/2008JD010142)

MS received 25 November 2017 and accepted in revised form 8 March 2018; first published online 18 April 2018

Supplementary material

Table S1 Results of one-way ANOVA with Tukey-Kramer post-hoc test for vesiculate pollen percentages among the different extraction methods.

One-way ANOVA	Sum of squares	df	Mean square	F	p(same)
Between groups	9838.16	5	1967.63	11.99	7.89
Within groups	8859.28	54	164.06		
Total	18697.40	59			

Tukey-Kramer post-hoc test		Extraction method						
		BRUGGER	LIU	YANG	EICHLER	FESTI	SHORT	
Extraction method	BRUGGER		1	0.76	<0.01	<0.01	1.00	p(same)
	LIU	0.17		0.69	<0.01	<0.01	1.00	
	YANG	1.91	2.07		<0.01	<0.01	0.89	
	EICHLER	5.79	5.62	7.70		1.00	<0.01	
	FESTI	6.23	6.08	8.15	0.46		<0.01	
	SHORT	0.39	0.55	1.52	6.18	6.63		
		Q statistics						

Table S2 Results of one-way ANOVA with Tukey-Kramer post-hoc test for marker ratios among the different extraction methods.

One-way ANOVA	Sum of squares	df	Mean square	F	p(same)
Between groups	0.33	5	0.07	2.90	0.02
Within groups	1.21	54	0.02		
Total	1.54	59			

Tukey-Kramer post-hoc test		Extraction method						
		BRUGGER	LIU	YANG	EICHLER	FESTI	SHORT	
Extraction method	BRUGGER		0.96	0.30	0.04	0.33	1.00	p(same)
	LIU	1.17		0.80	0.26	0.83	0.99	
	YANG	2.98	1.81		0.94	1.00	0.41	
	EICHLER	4.26	3.10	1.29		0.92	0.07	
	FESTI	2.88	1.72	0.09	1.38		0.45	
	SHORT	0.28	0.89	2.70	3.99	2.61		
		Q statistics						

Manuscript 2

Ice record reveals industrial footprint in European vegetation

Sandra O. Brugger[1,2,*], Erika Gobet[1,2], Christian Rohr[2,3], Federica R. Schanz[1], Fabian Rey[4], Christoph Schwörer[1,2], Michael Sigl[2,5], Margit Schwikowski[2,5,6], Willy Tinner[1,2]

[1]Institute of Plant Sciences, University of Bern, Switzerland
[2]Oeschger Center for Climate Change Research, University of Bern, Switzerland
[3]Institute of History, University of Bern, Switzerland
[4]Department for Environmental Sciences, University of Basel, Switzerland
[5]Paul Scherrer Institute, Villigen, Switzerland
[6]Department for Chemistry and Biochemistry, University of Bern, Switzerland

[*]Corresponding author: Sandra O. Brugger

Keywords: Colle Gnifetti ice core – Microscopic charcoal –Palynology – Pollen – SCP (Pollution) – *Zea mays* (maize)

Prepared for *Vegetation History and Archaeobotany*

Abstract

Land use and rapid climate change are threatening ecosystems across Europe, increasing environmental risks and hazards e.g. through the spread of pathogens or invasions of alien species. Paleoecological studies from natural archives provide valuable information on long-term environmental dynamics and thus may reveal novel potentials for future ecosystem conservation. Nevertheless, natural archives are rarely used to investigate the long-term impact of industrialization and globalization on continental-scale vegetation. To fill this gap, we present a unique palynological record from the high-alpine glacier Colle Gnifetti on Monte Rosa in the Alps spanning the past millennium with exceptional temporal resolution and precision. Our ice archive is located at the interface between Western, Central, and Southern Europe, and thus has the potential to integrate fire, land use, and pollution dynamics across important European biomes. We combine ice core evidence with historical sources to provide novel insights into industrial impacts on land use, fire regime, and vegetation dynamics. Preindustrial land use depended mainly on photosynthesis and thus solar energy. Hence, solar societies heavily affected natural vegetation already before the medieval climate optimum when our record begins. Our multiproxy-data suggest that in Europe the transformation to fossil fuel-based industrial land use (e.g. shift to large scale maize production and massive fire increase) started shortly after 1750 AD together with first signs of large-scale atmospheric pollution. The pronounced shift around 1750 AD challenges 1750–1850 AD as a pre-industrial reference period suggesting that 1650–1750 AD might be more suited to define European preindustrial conditions. We conclude that lowland vegetation suffered from progressive globalization of economies that intensified industrialized production on fertile lowland soils. While these formerly forested areas are further disrupted, industrialized agriculture may provide novel opportunities for the recovery of quasi-natural plant communities in mountain forests, riparian wetlands, and alpine grasslands.

1 Introduction

Progressive land-use pressure combined with rapid climate warming is increasingly raising public and scientific concern about the fate of quasi-natural ecosystems in heavily populated and industrialized Europe. Despite their high potential to solve conservation and mitigation issues (Lamentowicz et al. 2015), natural archives are seldom used to study the long-term impact of industrialization and globalization on continental-scale vegetation (Seddon et al. 2014). This scantiness of data comes from low temporal resolution and dating uncertainties of most sediment records, which challenge the comparison with written sources and the assessment of large-scale industrialization and globalization impacts (e.g. Wehrli et al. 2010; Giesecke et al. 2014; Mauri et al. 2015; Seppä et al. 2015; Pérez-Díaz et al. 2016; Kaplan et al. 2017). Indeed, most paleoecological studies were designed to assess local to regional vegetation changes and either focus on prehistoric periods or the most recent decades for modern calibrations (e.g. Ammann and Lotter 1989; Lotter 1999; Giesecke et al. 2014; Seppä et al. 2004, Bjune et al. 2010; Seppä et al. 2015; Birks et al. 2014; Felde et al. 2016; Poraj-Górska et al. 2017; Rey et al. 2017; Adolf et al. 2018a, 2018b). Despite the unique potential of high-alpine glaciers to study large-scale vegetation, fire, and pollution dynamics (e.g. Eichler et al. 2011, Brugger et al. 2018a), no long-term palynological records from high-alpine ice archives in Europe are available. This lack of data hampers the understanding of processes that may allow identifying future potentials of plants under changing land use and climatic conditions. Using ice cores would allow filling this gap and in addition it would contribute to circumvent the ^{14}C-plateau after 1600 AD that prevents precise dating of sedimentary records during the early industrialization period (Guilderson et al. 2005; Hua 2009), unless varved sediments are used (e.g. Haltia-Hovi 2007; Rey et al. 2018).

Colle Gnifetti glacier is located on the Monte Rosa massif at the border between Western, Central, and Southern Europe (Sigl et al. 2018). The location in the center of Europe together with its very high elevation > 4,000 m a.s.l. allows ice accumulation over long periods and results in a wide catchment covering important sections of the continent (Wagenbach and Geis 1989; Thevenon et al. 2009, Sigl et al. 2018). These special characteristics combined with an exceptional temporal resolution and precision, especially for the period of increased globalization (recent 250 years), may permit to answer how globalization and industrialization impacted biomes across Europe. Here we aim at 1) reconstructing large-scale vegetation, land use, fire, and industrial pollution dynamics at the interface between Western, Central, and Southern Europe with an exceptional temporal resolution and precision, (2) discussing the retrieved vegetation information in the light of historical sources, and (3) assessing the ecosystem responses to land use, fire, industrialization, climate change, and increasing globalization. A better understanding of past ecosystem responses to industrial impacts may contribute to refine conservation strategies for mitigating ecosystem degradation under global change conditions.

2 Study site

The high-alpine glacier Colle Gnifetti is located on the Monte Rosa massif in the Swiss Alps close to the Italian border (Fig. 1A). It is the highest glacier saddle of the Alps and a so-called cold glacier (Wagenbach and Geis 1989) that allows the formation of a long-term ice archive with relatively low annual snow accumulation rates (ca. 0.33 m $year^{-1}$) due to preferential erosion of dry winter snow (Jenk et al. 2009; Thevenon et al. 2009). Being located on the border between Southern, Western, and Central Europe it provides the unique opportunity to investigate large-scale environmental dynamics across different European biomes.

Europe is characterized by strong climatic gradients from a moister oceanic climate in the west to an increasingly dry continental climate in the east combined with strong latitudinal temperature increases from cold subarctic Northern Europe towards the subtropical Mediterranean (Lang 1994). The predominant wind direction is the Westerlies. The continent is under intense anthropogenic influence since millennia including humanization of vegetation in vast agricultural areas (Stoate et al. 2001). The Alps as a natural barrier divide southern European (subtropical mediterranean) from western (oceanic temperate) and central European (subcontinental temperate) vegetation (Fig. 1, Lang 1994). The modern altitudinal vegetation belts in the Alps are controlled by temperature. The permanent snow line is at around 3,000 m a.s.l. (Ellenberg 1996), while the tree line reaches uppermost elevations of 2,400 m a.s.l. that are occupied by *Larix decidua* and *Pinus cembra* (Tinner and Theurillat, 2003). The forests in the montane belt are dominated by *Picea abies*, *Abies alba,* with increasing importance of *Fagus sylvatica* below 1,400 m a.s.l. Temperate mixed *Fagus* and *Quercus* communities dominate the forests in the lowlands north and south of the Alps (Ellenberg 1996). South of the Alps, *Castanea sativa* is an important submediterranean forest component of the colline belt (Ellenberg 1996). Towards the Mediterranean Sea subtropical evergreen broadleaved trees and shrubs such as *Quercus ilex*, *Pistacia,* and *Olea* become increasingly important (Lang 1994).

3 Material and Methods

We analyzed samples from two ice cores (CG03B and CG15) of Colle Gnifetti glacier. The glacier saddle was drilled in September 2003 AD for CG03B at an altitude of 4,450 m a.s.l. (45°55’55’’N, 7°52’34’’E). The drilling reached bedrock with a total ice core length of 82 m and a diameter of 8.2 cm. In September 2015 AD an additional shallow core (CG15 covering 2002–2015 AD; Sigl et al. 2018) was drilled to update CG03B to the recent period. Frozen core segments of ca. 70 cm were transported to the Paul Scherrer Institute (PSI) for sample processing.

202 continuous samples spanning the period 1050 AD to 2015 AD (56.5–0 m weq of CG03B and 6–0 m weq of CG15; weq = water equivalent, corrected for varying density) were dedicated to palynological analysis. The exponential depth-age relationship (Fig. 2) results in varying annual layer thickness along the ice record. Thus, the temporal sampling resolution in the younger part was much higher compared to the older part where the ice had thinned substantially. This results in a changing microfossil detection threshold with growing core depth. The resulting sample resolution is 10–20 years (1050–1500 AD) and 5–10 years (1500–1900 AD). Samples covering 1900–2015 AD reached extremely high-resolution (less than one year per sample), therefore they were merged to five years after microfossil analysis using the existing chronology (Jenk et al. 2009; Sigl et al. 2009; Fig. 2). Each sample contained 110–1,000 g ice (average = 400 g). The microfossil extraction followed the protocol for ice sample preparation developed in Brugger et al. (2018b), which involves initial evaporation to reduce the water content, followed by acetolysis and KOH treatment before mounting in glycerine.

We use pollen and spores to infer vegetation dynamics and the coprophilous fungal spore *Sporormiella* for herbivore-grazing activity (Cugny et al. 2010). Pollen sums varied largely along the record (average pollen sum = 427 grains) with a minimum of 101 and a maximum of 2,300 grains in the uppermost part (1900–2015 AD) where samples were merged after analysis. Pollen and spore identification under a light microscope at 400x magnification followed Beug (2004) and the reference collection in Bern, Switzerland. We present pollen and spore data as percentages of the terrestrial pollen sum with summary curves for primary and secondary cultural indicators (complete taxa list and assignment to summary curves in supplementary table S1; Lang 1994).

Optimal sum-of-squares partitioning was applied for zonation of the pollen data including all taxa >5 % (= 27 taxa; Birks and Gordon 1985). Subsequently, we inferred statistically significant local pollen assemblage zones (LPAZ) with the broken stick approach (Bennett 1996). We applied principal component analysis (PCA) to summarize the pollen percentage data since the short gradient length of the first axis (= 1.734) of a detrended correspondence analysis (DCA, detrended by segments) justifies using linear ordination methods (ter Braak and Prentice 1988).

Microscopic charcoal >10 µm is used to infer fire activity (e.g. MacDonald et al. 1991; Conedera et al. 2009; Brugger et al. 2018a). We counted a minimum sum of 200 items (charcoal fragments and *Lycopodium* grains; Tinner and Hu 2003; Finsinger and Tinner 2005) and, if needed due to low charcoal concentrations, we continued until a minimum of 20 charcoal fragments was reached. Subsequently, we calculated the >90-percentile (10 % upper charcoal concentration values over the entire record = 7,350 particles l^{-1}) to infer regional fire activity peaks. SCP (= spheroidal carbonaceous particles) with a diameter >10 µm and clear features were counted along pollen and spores to reconstruct industrial air pollution (Rose 2015). All microfossil concentrations were standardized to one liter.

4 Results and Interpretation

4.1 Glacier ice pollen signal and its interpretation

More than 180 different pollen and spore types (Supplementary table S1) were determined. The modern pollen concentration of ca. 4,920 grains l^{-1} corresponds to a total influx of 230 grains cm^{-2} $year^{-1}$. This is similar to other high-alpine glacier records with comparable preparation methods (e.g. Brugger et al. 2018a) but extremely low compared to influx values from Alpine treeline pollen traps or sedimentary sites (e.g. at Gouillé Rion ca. 3,000 grains cm^{-2} $year^{-1}$; Tinner et al. 1996; van der Knaap et al. 2001).

The largest amount derives from arboreal pollen (AP; = 71 %) with high portions of mediterranean taxa as e.g. *Olea europaea* (6 %; Fig. 3). The record also contains high shares of wind-pollinated summer-flourishing taxa as *Castanea*, while the late-winter to early-spring flourishing taxon *Corylus* is underrepresented compared to sedimentary studies possibly due to wind-erosion of dry winter snow at Colle Gnifetti (Lauber and Wagner 1996; Thevenon et al. 2009). Poaceae and other nonarboreal (NAP) secondary cultural indicators (12 % and 15 %, respectively) are abundant and possibly derive from (sub)-alpine meadows. Primary cultural indicators are rare (1 %), indicating low pollen dispersal of modern industrially managed crop fields. Occasional pollen of *Lygeum spartum* that grows in North Africa along the record correlates with visible red dust layers in the ice record. Red dust layers were recorded during sampling and indicate air masses from the Sahara.

The palynological record suggests no strong long-term shift in and between biomes during the past millennium. Short-term pollen composition changes between samples might be related to the nature of the archive (Fig. 4). Our palynological record is a mixture of different altitudinal belts and vegetation regions, thus it is not suited for a conventional local to regional vegetation reconstruction but can be used to assess vegetation composition and land use dynamics on a subcontinental to continental scale, covering the boreal, temperate, mediterranean, and steppic biomes.

4.2 Large scale vegetation changes

Two statistically significant local pollen assemblage zones (LPAZ) were identified along the palynological record (CG-1 and CG-2; Fig. 4). We additionally divided LPAZ CG-1 in three non-significant subzones (CG-1a–c). Results are presented as pollen percentages and pollen concentrations, on an average reaching 3,000 pollen grains l^{-1} along the record.

Pollen data in zone CG-1a (1050–1300 AD, Fig. 4) consist of ca. 60 % AP at the beginning, then values drop to 40 % for temperate and boreal trees. Important arboreal taxa include *Pinus sylvestris*-type, *Quercus robur-pubescens*-type, *Q. ilex*-type, *Alnus glutinosa*-type, *A. viridis, Juniperus*, and up to 5 % *Castanea*. NAP consist mainly of Poaceae and other secondary cultural indicators that reach highest shares (see supplementary table S1) as well as primary cultural indicators as e.g. *Cannabis*-type or *Secale*. In combination with high *Sporormiella* percentages, this may indicate intensification of arable and pastoral farming activities in and around the Alps. A first peak of *Cannabis*-type percentage together with *Urtica* occurs around 1150–1200 AD, which is in line with sedimentary records from north and south of the Alps, suggesting a period of increased hemp production (van der Knaap et al. 2000).

After 1300 AD at the beginning of zone CG-1b (Fig. 4), AP increases to 70 % suggesting expansions of trees and shrubs. Primary cultural indicators decrease around 1350 AD and again after 1450 AD pointing to periods with reduced land use. Subsequently, the peak of *Beta*-type around 1500 AD together with a second increase in *Cannabis*-type possibly hints to intensified land use. After 1600 AD increasing *Olea europaea* percentages point to olive plantations more than spontaneous afforestation dynamics since other mediterranean trees as e.g. *Quercus ilex*-type, *Ostrya*-type and shrubs such as *Pistacia* remain low. First *Zea mays* pollen and frequent occurrence of *Platanus* pollen after 1750 AD suggest the introduction of maize agriculture and the plantation of ornamental and wind-protecting trees e.g. along roads and in parks.

The period 1820–1890 AD (LPAZ CG-1c, Fig. 4) is characterized by tree pollen decreasing to 30 %. Reductions comprised boreal (e.g. *Pinus sylvestris*-type, *Larix*), temperate (e.g. *Fagus*, *Quercus robur-pubescens*-type) as well as mediterranean taxa (e.g. *Ostrya*-type). Together with the contemporaneous increase of heliophilous and disturbance-adapted *Juniperus* this vegetational change points to large-scale deforestation (Fig. 4). Some primary cultural indicators increase (e.g. Cerealia type, *Beta*-type and *Zea mays*), while *Secale* and *Cannabis*-type decrease, suggesting general expansions of arable land but substantial reductions of rye and hemp cultivation.

After 1890 AD (zone CG-2, Fig. 4), *Larix, Abies, Pinus sylvestris*-type, *Alnus glutinosa*-type, *Ostrya*-type, and *Fraxinus ornus* increase, while *Juniperus* decreases, together indicating forest expansion and shrubland reduction. This results in a general increase of tree pollen to ca. 60 % during the 20th century. *Castanea* pollen percentages show low values around 1940 AD, and start to increase after 1960 AD with a major rise after 1990 AD. The systematic appearance of neophyte pollen originating from varying biomes (e.g. *Eucalyptus*, *Nothofagus*, *Parthenocissus quinquefolia*, *Fallopia*, *Pterocarya*, and *Heliotropium*) after 1910 AD implies the introduction or expansion of alien species. At the same time, the disappearance of *Vitis* pollen suggests vineyard decreases during the 20th century.

The first two axes of the PCA explain 20.9 % and 15.7 % of the total variance, respectively. The sample distribution on these axes shows a large LPAZ overlap suggesting only minor biome shifts over the past millennium (Fig. 5A). The PCA groups boreal AP taxa (e.g. subalpine *Picea*, *Larix, Alnus viridis*-type), temperate AP taxa (e.g. *Fagus*, *Corylus*), dry adapted mediterranean (e.g. *Olea*, *Quercus ilex*-type, *Phyllirea, Pistacia*) or steppic taxa (*Ephedra fragilis*-type), as well as land use indicators (e.g. Poacaea, *Urtica*, *Cannabis*-type, *Castanea* or *Vitis*, Fig. 5B). Thus, the ordination groups the taxa according to their occurrence in the natural biome, concurrently dividing natural plants from field crops, weeds and fruit trees. In summary, the PCA results support that intensified land-use phases occurred synchronously across biomes.

4.3 Fire and industrial pollution history

The average charcoal concentration in the recent part (ca. 8,540 particles l^{-1} for the period 2000–2015 AD) corresponds to a microscopic charcoal influx of ca. 390 particles cm^{-2} $year^{-1}$ or 0.16 mm^2 cm^{-2} $year^{-1}$ (Tinner and Hu 2003). This is similar to other high-alpine glacier records that used analogue preparation methods (e.g. 200 particles cm^{-2} $year^{-1}$ at

Tsambagarav; Brugger et al. 2018a) but very low compared to sedimentary time-series (e.g. Tinner et al. 1998; Adolf et al. 2018a; Rey et al. 2017).

Charcoal concentrations are low (average ca. 2,500 particles l^{-1}) and show no peak values (>90-percentile) before 1750 AD, implying no major fire activity (Fig. 4, 6). Charcoal concentrations sharply increase after 1750 AD, revealing a major fire regime change with increased fire activity (probably frequency, Conedera et al. 2009). This fire-regime shift coincided with the first pollen-inferred *Zea mays* cultivation. Major charcoal peaks (> 90-percentile) are concentrated in the period 1750–1820 AD and during the 20th century with a maximum peak in 1970 AD. Conversely, charcoal concentrations are lower 1820–1890 AD (average ca. 2,500 particles l^{-1} and no peaks >90-percentile), suggesting minimum fire activity, which coincided with maximum NAP-inferred openland abundance.

Frequent SCP finds occur after 1770 AD and delimit the onset of atmospheric pollution, likely as a result of fossil fuel burning (Fig. 4). Most strikingly, initial atmospheric pollution occurred contemporaneously with the onset of *Zea mays* cultivation and the sharp increase of fire activity after 1750 AD. SCP concentrations raise during the 20th century suggesting reinforced fossil fuel burning that reached extremes around 1970 AD (ca. 900 particles l^{-1}). SCP concentrations decrease again after 1980 AD to values comparable to the early 20th century, most probably as a consequence of technical advances and environmental regulations (Fig. 6). Indeed, after excessive levels 1970–1980 AD, by 2000–2015 AD charcoal and SCP levels had fallen to 19th century levels.

5 Discussion

5.1 Pre-Industrial land-use

The Medieval climate optimum (ca. 1000-1300 AD) in Europe is widely recognized as a period of propitious climatic conditions for agriculture (Ruddiman 2003). Population grew rapidly and further space was needed for crops, husbandry and settlements (Jones 2003). New agricultural innovations increased the crop yields (e.g. in tons per hectare through three-field-crop-rotation system) and expanded the area that could be managed by each farmer (e.g. heavy plow technology or shift from oxen to horse-pulled plows; Cipolla 2004). These innovations are mirrored in the Colle Gnifetti record with increased cultivation and maximum landscape openness. The openness pattern before 1300 AD is also recorded at sedimentary sites (e.g. Rösch et al. 1992; Tinner et al. 2003; Gobet and Tinner 2012) and in historical data (e.g. Bätzing 2015). Timber was cut for house construction, used as heating fuel, and furthermore for iron smelting e.g. in the lowlands of the Southern Alps (Pini 2002; Colombaroli et al. 2010). Additionally, subalpine forests were cleared for pasture, hay meadow areas, and crop cultivation (e.g. Gobet et al. 2003). In particular, when the Walser people left the Canton of Valais from the 13th century onwards, they settled close to the treeline (and even beyond) in the Swiss Cantons of Uri and the Grisons, as well as in western Austria. They cut forests to create new pastures and thereby increased the risk of avalanches (Renner 2013 for the Ursern Valley).

Crop cultivation and pasture activities were markedly reduced at the end of the medieval climate optimum ca. 1300 AD according to our glacier record, when climate became cooler and famines and Black Death reduced population (Rösch et al. 1992; Ruddiman 2003; Campbell 2016, 2018). Subsequently, shrublands and forests expanded in the pollen catchment of our ice record, a process also recorded in sedimentary sites north and south of the Alps (e.g. Tinner et al. 1999; Gobet and Tinner 2012). The period of unfavorable conditions lasted until the end of the Little Ice Age (LIA) cold period ca. 1850 AD (Holzhauser et al. 2005). Somewhat surprisingly, no centennial-scale LIA effects are recorded at Colle Gnifetti. However, particularly cold phases of the LIA (e.g. 1600–1650 AD, 1675–1715 AD, 1790–1840 AD; Luterbacher et al. 2001; Masson-Delmotte et al. 2013; CH2014-

Impacts 2014) coincide with reduced agricultural activity (e.g. primary cultural indicators reduced at 1650 AD, 1670 AD, 1720 AD, 1830 AD, 1900 AD; see figure 4 and Bracher 2016 for Upper Valais pasture areas). Our record suggests two further very pronounced short-term periods of reduced cultivation (no finds of primary cultural indicators) around 1350 AD and 1450 AD that correlate with historical events. The Black Death of 1347–1352 AD largely reduced population across Europe and the related agricultural activities (Aberth 2005; Hoffmann 2014; Campbell 2016, 2018). A hundred years later, the Kuwae volcanic eruption of 1453 AD significantly affected the climate, accelerating the LIA cooling trend that had intensified after 1430 AD (Camenisch et al. 2016; Esper et al. 2017). The following three cold decades (Esper et al. 2017) strongly reduced crop yields, causing famines and other societal problems. The problem were not only the numerous wet summers with poor harvests, but the extended rain in autumn furthermore hampered the sowing of winter grain. Additionally, it led to the stored grain being more vulnerable to the spread of the grain weevil, other insects, infections, and fungi (Campbell 2016; Camenisch 2018; Camenisch and Rohr 2018). In contrast, the Tambora eruption (1815 AD) left no visible impact in the Colle Gnifetti record in regard to subsequent agricultural yields, despite the historically documented crop failures (Krämer 2015). This lacking sensibility of our record is explicable by the unfortunate pollen sampling that bridges the Tambora eruption (recorded with an ash layer in the ice; see Fig. 2) with an insufficient sample resolution of ten years, which impedes a thorough assessment of the short-term climatic effects (ca. 1-3 years).

1540 AD is historically widely documented as a “Megadrought” year in Europe, lasting from spring to autumn and covering most parts of Europe from the southern British Isles to southern Italy and from the Iberian Peninsula to Poland. More than 300 independent documentary sources give evidence about extremely low river flows and lakes, crop failure and Europe-wide forest and settlement fires (Pfister et al. 2015). Trees and vines suffered from severe drought stress. Surprisingly, previous highly resolved natural archives (e.g. tree ring records) failed to detect this drastic event (Wetter et al. 2014; Büntgen et al. 2015; Pfister et al. 2015), while in our time series wide-scale burning over Europe is unambiguously recorded (charcoal peak dated at 1538 AD; fig. 4). Other minor charcoal-inferred fire episodes from the Colle Gnifetti record may correspond to historically important dry periods, which increased the fire risk in Europe markedly (e.g. 1473 AD, 1718-1719 AD; Wetter et al. 2014; Camenisch et al. in review). Combining our pre-industrial ice core evidence with historical sources suggests that large-scale agricultural dynamics depended on both, climate and societal crises. Thus, small-scale subsistence systems that were characteristic for preindustrial societies show a high sensitivity to large-scale drivers of ecosystem change (Tinner et al. 2003; Hoffmann 2014).

5.2 Onset of European Industrialization and Globalization around 1750 AD

Our Colle Gnifetti record suggests a pronounced shift in land-use, fire, and pollution history around 1750 AD. Historically the 18th century was characterized by huge scientific progresses of the enlightenment (the Century of Philosophy; Israel 2002) that released rapid population growth and agrarian innovations, which started the transformation from subsistence economy to industrialized machine-age production. During the LIA (especially during the Maunder minimum ca. 1675–1715 AD), crop storage over winter was extremely difficult. This facilitated the invention of novel crops that were less susceptible to rain or hail and less complicated for winter storage (Pfister 1979, 1984; Montanari 1996; Luterbacher et al. 2001; Xoplaki et al. 2011; Sereni 2014). Maize was introduced in Europe after Columbus and became the first edible plant from America that was widely accepted (Montanari 1996; Bätzing 2015). The high productivity of maize compared to traditional European crops (e.g. *Triticum*, *Panicum*, *Setaria*, *Hordeum*) opened new income possibilities with high margins and nutrition at low cost in southern Europe. This promoted the shift from garden-cultivation of maize to large-scale production on agricultural fields after the 16th century (Montanari 1996). By the mid-18th century, maize production expanded rapidly in northern Italy and after the crisis in 1740/41 AD in the Balkan region, where it replaced millet and barley as the major crop within decades (Montanari 1996; Sereni 2014). Soon the diet of Mediterranean peasants was based on maize to a degree that the novel malnutrition disease Pellagra appeared in 1730 AD. The new disease was closely associated with the almost exclusive maize diet that eventually caused skin maladies and dementia (Montanari 1996; Hegyi 2004).

With industrial food production and population growth, energy needs increased (Jones 2003; Wrigley 2013; Malanima 2016). Around 1750 AD, timber and charcoal were the main fuels for e.g. energy-demanding salt extraction in Austria as well as for mining, metallurgy, and smelting in Piemont and Lombardy (Hürlimann 2008; Mathieu 2015). Timber and charcoal were exported from forested subalpine regions in immense quantities (Hürlimann 2008). The drastic shift of the fire regime documented in the Colle Gnifetti record may reflect a change in land use activity connected to the introduction of new crops such as maize (e.g. burning of crop residuals after harvest) or increasing forest burning. For instance, historically, forest fires in the Engadin region and in the Canton of Valais were connected to accidents during charcoal production as well as fires in wooden-built villages (Flückiger-Seiler 2006; Rohr 2011). Indeed, frequent fires and shortage of timber in the southern Alps caused a shift in architecture towards stone buildings or at least a decrease of wooden shingle roofs. However, in some cases the local people did not fight large forest fires such in the case of Nendaz (1821 AD), because the ash seemed more useful than the timber itself (Rohr 2011). The fire event in Nendaz, only ca. 30 km away from Colle Gnifetti glacier, correlates clearly with a fire peak in the ice record.

The lacking response in forest cover change (AP remains unchanged) may primarily indicate that young forests or timber was collected or affected, producing no marked pollen signal

(Conedera et al. 2004). In the ice record the effects of the so-called "timber era" (large-scale forest disruption; Sombart 1919; Stuber 2008) are recorded after 1820 AD, with marked AP declines (von Gunten et al. 2008). Natural wood resources only recovered with the transition to fossil energy consumption (black or stone coal; Stuber 2008; Radkau 2012; Wrigley 2013; Malanima 2016). However, new forest protection paradigms also contributed to forest recovery (Mathieu 2015). Indeed, negative consequences of the deforested landscapes (e.g. erosion, frequent flood events, avalanches) were so massive that they triggered the creation of first mountain forest protection laws (1876 AD in Switzerland and 1877 AD in Italy; Pfister and Brändli 1999; Summermatter 2012).

The onset of SCP deposition deriving from fossil fuel burnings is dated at ca. 1770 AD in the Monte Rosa ice core. In lake sediments, SCPs are regularly recorded after 1850 AD, when fossil energy, mainly as black or brown coal, was already widely consumed on the European continent (Rose 2015; Mathieu 2015; Malanima 2016). SCPs often serve as a temporal marker (onset = 1850 AD) to refine lake sediment chronologies (Kamenik et al. 2009; Rose 2015). Various archeological sites in Europe document the use of black coal from small outcrops already since the Roman period (Harris 1946; Dearne and Branigan 1995). In fact, the first large-scale burnings of black coal are documented from Great Britain in the 17th and 18th century, where energy demands exceeded timber availability much earlier than on the still to some extent forested European continent. For instance, 650,000 tons of black coal were shipped from Tyneside to Wearside each year by 1750 AD (Wrigley 1967; Wrigley 2013; Malanima 2016). Wherever people mined for black coal, the problem of transport remained until the breakthrough of steam-powered ships and railways in the mid-19th century. Hence, black coal was only used for steam engines close to the coal deposits. The search for black coal deposits in Switzerland began in the 16th century and was intensified during the 18th century, but most of the deposits in Switzerland were relatively small and therefore exploited after some years or decades. After 1850 AD, black coal became important also for Swiss industries and transport. It was mostly imported from Germany (Saarland district), Belgium and eastern France (Loire basin near Saint-Etienne; Pelet 2008). Our precise chronology from Colle Gnifetti ice record suggests that first SCP-derived fossil fuel pollution reached the Alps shortly after 1750 AD (Jenk et al. 2009; Sigl et al. 2009), possibly related to the easiness of recognition in clean ice compared to dark sediments and/or the larger SCP-catchment for the ice record (Rose 2015). The subsequent SCP-derived increase of fossil fuel pollution 1770–1850 AD correlates well with the black carbon pattern from Colle Gnifetti, which was, however, mainly attributed to forest fire activity (Malanima 2016; Sigl et al. 2018). Indeed, SCP is a more specific tracer for industrial burning than black carbon. Specifically, it allows the detection of small fossil fuel burning portions that cannot be distinguished from wood burning with less specific chemical tracers (Sigl et al. 2018).

The shift to fossil energy in Europe also facilitated the transportation of people and goods tremendously as e.g. the decline of *Cannabis* cultivation in the 19th century is connected to the replacement of hemp and flax by imported cotton that initiated the successful Swiss textile industry (van der Knaap et al. 2000). Fossil fuel-operated steamboats suddenly allowed a rapid exchange between continents e.g. crossing of the Atlantic Ocean in <14 days (Dumpleton 2002). Henceforth, European colonialists in the 19th century could not only bring seeds or bulbs from their travels but imported entire new plant species for botanical gardens (Mack and Lonsdale 2001; McAleer, 2016). Some of these exotic plants spread to an extent that they become detectable in the Colle Gnifetti record already at the beginning of the 20th century (e.g. *Eucalyptus*, *Fallopia*). The increasing exchange of plants between continents brought also new plant pathogens as e.g. the grape *Phylloxera* that was introduced with American wine species in Europe after 1860 AD and spread quickly from France to neighboring countries. In the late 19th century, the "grape pest" reached Germany and the very west of Switzerland, whereas vineyards in the Bielersee region on the Swiss Plateau and in Northern Switzerland were only slightly affected in the 1910s (Schneider-Orelli 1923; Aebischer 2018; Deppeler 2018). Swiss vineyards were adjusted by selection of resistant varieties, but were reduced in general since the 1880s due to a lower demand for Swiss wines, among other reasons caused by the anti-alcohol campaigns in Switzerland (Auderset and Moser 2016). This overall (southern) European reduction is visible to an extent that *Vitis* pollen vanishes in the Colle Gnifetti record despite the growing likelihood to discover *Vitis* pollen grains because of increasing sampling resolution during the 20th century.

5.3 Responses of humanized vegetation to industrial agriculture

Temperate mixed beech or oak forests are the predominant lowland forest vegetation on fertile soils in Western and Central Europe. Forests were heavily disrupted since millennia and their species composition changed markedly in response to land use (Conedera et al. 2017; Whitlock et al. 2018; Rey et al. 2017). Industrial agriculture with fossil-based heavy machineries concentrated on lowland areas, which are most profitable for large-scale production. Our Colle Gnifetti record suggests that lowland forest disruption continued until 2015 AD, which is in agreement with sedimentary time series from central areas (Tinner et al. 2005; Colombaroli et al. 2007; Vannière et al. 2008; Tinner et al. 2009; Kaltenrieder et al. 2010; Rey et al. 2017). Cereal production in the lowlands further increased during the 20th century with growing population. The cereal pollen decrease during the past decades in the Colle Gnifetti record may be related to the collapse of cereal production on terraces in and around the Alps or less likely to new varieties and/or cereal elaboration developed in the last decades that may have affected pollen dispersal (Stoate et al. 2001).

Increasing fossil-fuel-powered cultivation and the use of fertilizers as well as pesticides facilitated more agricultural biomass on shrinking field areas (Erb et al. 2008). This centralization triggered the abandonment of subsistence cultivation on less favorable grounds for large-scale agricultural production as e.g. on mountain terraces that could not be managed profitably with heavy machines (Zoller et al. 1996; MacDonald et al. 2000; Erb et al. 2008; Mathieu 2015). Over this “historical pastoralization” many unprofitable subsistence crop fields were either converted to pasture areas or completely abandoned in and around the Alps (Bätzing 2015), as e.g. documented after 1800 AD at Colle Gnifetti. In agreement, shrinking *Secale* and *Cannabis* cultivation was recorded at Gouillé Rion in the Central Swiss Alps (Tinner et al. 1996, van der Knaap et al. 2001). The desertion of less favorable vineyards in the Alpine region after 1900 AD provides another example for reduced cultivation activity in marginal areas (Aebischer 2018; Deppeler 2018). This land use-decline allowed subalpine and montane forest recoveries, which is mirrored in the Colle Gnifetti as e.g. *Pinus sylvestris, Abies alba,* and *Larix decidua* expanded in the most recent period. Forest recoveries were also reconstructed at lake sites in the Alps and the Iberian mountains and were attributed to land abandonment partly in combination with ongoing climate warming (Desprat et al. 2003; Gobet et al. 2003; Gehrig-Fasel et al. 2007; Schwörer et al. 2014a; Schwörer et al. 2014b; Morales-Molino et al. 2018). Most strikingly, our high-alpine glacier archive perfectly mirrors the forest and chestnut cultivation fluctuations in the colline belt of the southern Alps during the last century (Tinner et al. 1998).

Land-use pressure decline in marginal areas with little agricultural value favored submediterranean woodland communities dominated by *Ostrya carpinifolia* and *Fraxinus ornus*, which form pioneer vegetation on carbonate rock slopes south of the Alps and expanded in the Colle Gnifetti record and elsewhere south of the Alps during the past decades (Poldini 1982; Gobet et al. 2000). In general, forests expanded across many landscapes in and around Alps, as in the Northern and Central Alps the forest areas increased by 27–50 % between 1880 AD and 2000 AD and in the Southern Alps by 100 % (Poyatos et al. 2003; Ginzler et al. 2011; Mathieu 2015). Interestingly, shrublands did not expand at the large scale covered by our record, as expected for pioneer vegetation types after abandonment of land use. For instance, *Alnus viridis* thickets often spread as initial succession after abandonment of subalpine meadows (Gobet et al. 2003; Bühlmann et al. 2014), but this species did not increase in our record.

Fluvial wetland areas provide fertile soils for profitable agriculture, limited by recurrent floods that may harm crop yields (Blume et al. 2016). During the 19th and 20th century, many rivers were straightened to drain additional wetland areas for production and to prevent flood events as e.g. the Po-plain-wetlands in Northern Italy, the Rhone, Linth, and Jura water corrections (Vischer 1986, 2003; Simeoni and Corbau; 2009; Summermatter 2012). On the other hand, riparian forests in the remaining wetlands could recover since small-scale production in these marginal areas was reduced. In agreement, the riparian taxa *Alnus glutinosa* and *Pinus sylvestris* expanded in the Colle Gnifetti record or in records from remote peatland areas (e.g. Gałka et al. 2017) during the past century. Land abandonment and forest successions in the past decades and near future will further increase dead biomass, which may potentially enhance fire risks in the Southern Alps and the Mediterranean, counteracting public efforts of fire prevention (Tinner et al. 1998, 2000, 2005; Conedera and Tinner 2010; Daniau et al. 2012).

6 Conclusions

For the first time, we directly combine palynological ice core data with historical sources to provide novel insights into industrialized and globalized land-use impacts on fire regime and vegetation dynamics across European biomes. Preindustrial land use was mainly based on solar energy i.e. timber regrowth, field harvests, animal power depend directly or indirectly on photosynthesis. Solar societies heavily affected natural vegetation since the onset of agriculture, and hence since millennia before the medieval climate optimum when our record begins. The transformation to fossil fuel-based industrial land use started soon after 1750 AD together with first signs of large-scale atmospheric pollution, which challenges 1750–1850 AD as a pre-industrial reference period (Sigl et al. 2018). Therefore, an earlier reference period e.g. 1650–1750 AD might be used as a baseline to infer pre-industrial conditions for e.g. atmospheric modeling approaches. Today, industrialized production is concentrated in central areas, where ecosystems are heavily exploited, including the conversion of formerly forested areas in industrial, urban, and farmland space. While lowland vegetation suffers from progressive globalization of economies, industrialized agriculture may provide novel opportunities for the recovery of quasi-natural plant communities in marginal areas. However, current rapid climate warming, the introduction of new invasive species, and pathogens might counteract potential vegetation recoveries.

7 Acknowledgments

We thank J.F.N. van Leeuwen for support with rare pollen type analysis, D. Osmont for assistance in the cold room, and the field crews for the drilling campaigns at Colle Gnifetti in 2003 and 2015. We acknowledge the Sinergia project Paleo fires from high-alpine ice cores funded by the Swiss National Science Foundation (SNF grant 154450).

8 References

Aberth J (2005) The Black Death: the great mortality of 1348-1350: a brief history with documents. Palgrave Macmillan, New York

Adolf C, Doyon F, Klimmek F, Tinner W (2018b) Validating a continental European charcoal calibration dataset. Holocene in press

Adolf C, Wunderle S, Colombaroli D, Weber H, Gobet E et al. (2018a) The sedimentary and remote-sensing reflection of biomass burning in Europe. Global Ecol Biogeo 27(2): 199-212.

Aebischer S (2018) Die Reblauskrise am Bielersee. Eine historische Untersuchung zum

Rebbaugebiet im Kanton Bern (Berner Studien zur Geschichte 2/1). Historisches Institut, Bern

Ammann B, Lotter AF (1989) Late-Glacial radiocarbon-and palynostratigraphy on the Swiss Plateau. Boreas 18(2): 109-126

Auderset J, Moser P (2016) Rausch & Ordnung. Eine illustrierte Geschichte der Alkoholfrage, der schweizerischen Alkoholpolitik und der Eidgenössischen Alkoholverwaltung (1887-2015). Eidgenössische Alkoholverwaltung, Bern

Bätzing W (2015) Die Alpen: Geschichte und Zukunft einer europäischen Kulturlandschaft. CH Beck, Munich

Bennett KD (1996) Determination of the number of zones in a biostratigraphical sequence. New Phytol 132(1): 155-170

Beug HJ (2004) Leitfaden der Pollenbestimmung für Mitteleuropa und angrenzende Gebiete. Pfeil, Munich

Birks HJB, Gordon A (1985) Numerical Methods in Quaternary Pollen Analysis. Academic Press, London

Birks HH, Aarnes I, Bjune AE, Brooks SJ, Bakke J et al. (2014) Lateglacial and early-Holocene climate variability reconstructed from multi-proxy records on Andøya, northern Norway. Quat Sci Rev 89: 108-122

Bjune AE, Birks HJB, Peglar SM, Odland A (2010) Developing a modern pollen–climate calibration data set for Norway. Boreas 39(4): 674-688

Blume HP, Brümmer GW, Horn R, Kandeler E, Kögel-Knabner I et al. (2016) Scheffer/Schachtschabel: Lehrbuch der Bodenkunde. Springer, Berlin Heidelberg

Bracher C (2016) Die vorindustrielle Alpwirtschaft im Oberwallis aus klima- und wirtschaftshistorischer Perspektive. Eine Fallstudie aus dem Binntal und dem Simplongebiet 1770-1835. Blätter aus der Walliser Geschichte 48: 1-83

Brugger SO, Gobet E, Schanz FR, Heiri O, Schwörer C et al. (2018b) A quantitative comparison of microfossil extraction methods from ice cores. J Glaciol 64(245): 432–442

Brugger SO, Gobet E, Sigl M, Osmont D, Papina T et al. (2018a) Ice records provide new insights into climatic vulnerability of Central Asian forest and steppe communities. Global Planet Change

Bühlmann T, Hiltbrunner E, Körner C (2014) Alnus viridis expansion contributes to excess reactive nitrogen release, reduces biodiversity and constrains forest succession in the Alps. Alpine Bot 124(2): 187-191

Büntgen U, Tegel W, Carrer M, Krusic PJ, Hayes M, Esper J (2015) Commentary to Wetter et al. (2014): Limited tree-ring evidence for a 1540 European 'Megadrought'. Climatic Change 131(2): 183-190

Camenisch C, Keller KM, Salvisberg M, Amann B, Bauch M et al. (2016) The 1430s: A cold period of extraordinary internal climate variability during the early Spörer Minimum with social and economic impacts in Northwestern and Central Europe. Clim Past 12: 2107-2126

Camenisch C (2018) Two Decades of Crisis: Famine and Dearth During the 1480s and 1490s in Western and Central Europe. In: Famines During the ‘Little Ice Age’ (1300–1800). Socionatural Entanglements in Premodern Societies. Springer, Cham, pp. 69-90

Camenisch C, Rohr C (2018) When the Weather Turned Bad. The Research of Climate Impacts on Society and Economy during the Little Ice Age in Europe. An Overview. Cuadernos de Investigación Geográfica 44(1): 99-114

Camenisch C, Wetter O, Kiss A, Rohr C, Retsö D et al. (in review), Wildfires, desiccated fountains and locusts in Europe: Heat and drought in the first half of the 1470s. Regional Environmental Change

Campbell BMS (2016) The great transition: Climate, disease and society in the late-medieval world. Cambridge University Press, Cambridge

Campbell BMS (2018) The European Mortality Crises of 1346–52 and Advent of the Little Ice Age. In: During the ‘Little Ice Age’ (1300–1800). Socionatural Entanglements in Premodern Societies. Springer, Cham, pp. 19-41

CH2014-Impacts (2014) Toward Quantitative Scenarios of Climate Change Impacts in Switzerland. OCCR, FOEN, MeteoSwiss, C2SM, Agroscope, ProClim, Bern

Cipolla CM (2004) Before the industrial revolution: European society and economy 1000-1700. Routledge, London

Colombaroli D, Henne PD, Kaltenrieder P, Gobet E, Tinner W (2010) Species responses to fire, climate and human impact at tree line in the Alps as evidenced by palaeo-environmental records and a dynamic simulation model. J Ecol 98(6): 1346-1357

Colombaroli D, Marchetto A, Tinner W (2007) Long-term interactions between Mediterranean climate, vegetation and fire regime at Lago di Massaciuccoli (Tuscany, Italy). J Ecol 95(4): 755-770

Conedera M, Tinner W (2010) Langzeit-Feuerökologie der Schweiz. Schweiz Z fur Forstwes 161(11): 424-432

Conedera M, Colombaroli D, Tinner W, Krebs P, Whitlock C (2017) Insights about past forest dynamics as a tool for present and future forest management in Switzerland. Forest Ecology Management 388: 100-112

Conedera M, Krebs P, Tinner W, Pradella M, Torriani D (2004) The cultivation of Castanea sativa (Mill.) in Europe, from its origin to its diffusion on a continental scale. Veg Hist Archaeobot 13(3): 161-179

Conedera M, Tinner W, Neff C, Meurer M, Dickens AF, Krebs P (2009) Reconstructing past fire regimes: methods, applications, and relevance to fire management and conservation. Quat Sci Rev 28(5): 555-576

Cugny C, Mazier F, Galop D (2010) Modern and fossil non-pollen palynomorphs from the Basque mountains (western Pyrenees, France): the use of coprophilous fungi to reconstruct pastoral activity. Veg Hist Archaeobot 19(5-6): 391-408

Daniau AL, Bartlein PJ, Harrison SP, Prentice IC, Brewer S, (2012) Predictability of biomass burning in response to climate changes. Global Biogeochemical Cycles 26(4).

Dearne MJ, Branigan K (1995) The use of coal in Roman Britain. Antiq J 75: 71-105

Deppeler F (2018) Die Reblausplage und ihre Auswirkungen in den Kantonen Aargau und Zürich (Berner Studien zur Geschichte 2/2). Historisches Institut, Bern

Desprat S, Goñi MFS, Loutre MF (2003) Revealing climatic variability of the last three millennia in northwestern Iberia using pollen influx data. Earth Planet Sc Lett 213(1-2): 63-78

Dumpleton B (2002) Story of the paddle Steamer. Intellect Books

Eichler A, Tinner W, Brütsch S, Olivier S, Papina T, Schwikowski M (2011) An ice-core based history of Siberian forest fires since AD 1250. Quat Sci Rev 30(9-10): 1027-1034

Ellenberg H (1996) Vegetation Mitteleuropas mit den Alpen in ökologischer, dynamischer und historischer Sicht. Ulmer, Stuttgart

Erb KH, Gingrich S, Krausmann F, Haberl H (2008) Industrialization, fossil fuels, and the transformation of land use: An Integrated Analysis of Carbon Flows in Austria 1830–2000. J Ind Ecol 12(5-6): 686-703

Esper J, Büntgen U, Hartl-Meier C, Oppenheimer C, Schneider L (2017) Northern Hemisphere temperature anomalies during the 1450s period of ambiguous volcanic forcing. Bull Volcanol 79(41): 3-9

Felde VA, Peglar SM, Bjune AE, Grytnes JA, Birks HJB (2016) Modern pollen–plant richness and diversity relationships exist along a vegetational gradient in southern Norway. Holocene 26(2): 163-175

Finsinger W, Tinner W (2005) Minimum count sums for charcoal concentration estimates in pollen slides: accuracy and potential errors. Holocene 15(2): 293-297

Flückiger-Seiler R (2006) Dorfbrände im Oberwallis. Blätter aus der Walliser Geschichte 38: 1-63

Gałka M, Tobolski K, Górska A, Lamentowicz M (2017) Resilience of plant and testate amoeba communities after climatic and anthropogenic disturbances in a Baltic bog in Northern Poland: implications for ecological restoration. Holocene 27(1): 130-141

Gehrig-Fasel J, Guisan A, Zimmermann NE (2007) Tree line shifts in the Swiss Alps: climate change or land abandonment?. J Veg Sci 18(4): 571-582

Giesecke T, Ammann B, Brande A (2014) Palynological richness and evenness: insights from the taxa accumulation curve. Veg Hist Archaeobot 23(3): 217-228

Ginzler C, Brändli UB, Hägeli M (2011) Waldflächenentwicklung der letzten 120 Jahre in der Schweiz. Schweiz Z fur Forstwes 162(9): 337-343

Gobet E, Tinner W (2012) Von der Ur- zur Kulturlandschaft. In: Geschichte des Kantons Schwyz, Band 1: Zeiten und Räume - Frühzeit bis 1350. Chronos, Zürich, pp. 39-60

Gobet E, Tinner W, Hochuli PA, van Leeuwen JFN, Ammann B (2003) Middle to Late Holocene vegetation history of the Upper Engadine (Swiss Alps): the role of man and fire. Veg Hist Archaeobot 12(3): 143-163

Gobet E, Tinner W, Hubschmid P, Jansen I, Wehrli M et al. (2000) Influence of human impact and bedrock differences on the vegetational history of the Insubrian Southern Alps. Veg Hist Archaeobot 9(3): 175-187

Guilderson TP, Reimer PJ, Brown TA (2005) The boon and bane of radiocarbon dating. Science 307(5708): 362-364

Harris CD (1946) The Ruhr coal-mining district. Geogr Rev 36(2): 194-221

Haltia-Hovi E, Saarinen T, Kukkonen M (2007) A 2000-year record of solar forcing on varved lake sediment in eastern Finland. Quat Sci Rev 26(5-6): 678-689

Hegyi J, Schwartz RA, Hegyi V (2004) Pellagra: dermatitis, dementia, and diarrhea. Int J Dermatol 43(1): 1-5

Hoffmann RC (2014) An Environmental History of Medieval Europe (Cambridge Medieval Textbooks). Cambridge University Press, Cambridge

Holzhauser H, Magny M, Zumbühl HJ (2005) Glacier and lake-level variations in west-central Europe over the last 3500 years. Holocene 15(6): 789-801

Hua Q (2009) Radiocarbon: a chronological tool for the recent past. Quat Geochronol 4(5): 378-390

Hürlimann K (2008) Holzwirtschaft. In: Historisches Lexikon der Schweiz. http://www.hls-dhs-dss.ch/textes/d/D14025.php?topdf=1. Last accessed: 25.07.2018

Israel JI (2002) Radical enlightenment: Philosophy and the making of modernity 1650-1750. Oxford University Press, Oxford

Jenk TM, Szidat S, Bolius D, Sigl M, Gaeggeler HW et al. (2009) A novel radiocarbon dating technique applied to an ice core from the Alps indicating late Pleistocene ages. J Geophys Res Atmos 114 (D14)

Jordan P (2005) Großgliederung Europas nach kulturräumlichen Kriterien. Europa Regional 13(4): 162-173

Jones E (2003) The European miracle: environments, economies and geopolitics in the history of Europe and Asia. Cambridge University Press, Cambridge

Kaltenrieder P, Procacci G, Vannière B, Tinner W (2010) Vegetation and fire history of the Euganean Hills (Colli Euganei) as recorded by Lateglacial and Holocene sedimentary series from Lago della Costa (northeastern Italy). Holocene 20(5): 679-695

Kamenik C, van der Knaap WO, van Leeuwen JFN, Goslar T (2009) Pollen/climate calibration based on a near-annual peat sequence from the Swiss Alps. J Quat Sci 24(5): 529-546

Kaplan JO, Krumhardt KM, Gaillard MJ, Sugita S, Trondman AK et al. (2017) Constraining the deforestation history of Europe: Evaluation of historical land use scenarios with pollen-based land cover reconstructions. Land 6(4): 91

Krämer D (2015) Menschen grasten nun mit dem Vieh: Die letzte grosse Hungerkrise der Schweiz 1816/17 (Vol. 4). Schwabe, Basel

Lamentowicz M, Mueller M, Gałka M, Barabach J, Milecka K et al. (2015) Reconstructing human impact on peatland development during the past 200 years in CE Europe through biotic proxies and X-ray tomography. Quaternary International 357: 282-294

Lang G (1994) Quartäre Vegetationsgeschichte Europas: Methoden und Ergebnisse. Gustav Fischer, Jena

Lauber K, Wagner G (1996) Flora Helvetica. Haupt, Bern

Lotter AF (1999) Late-glacial and Holocene vegetation history and dynamics as shown by pollen and plant macrofossil analyses in annually laminated sediments from Soppensee, central Switzerland. Veg Hist Archaeobot 8(3): 165-184

Luterbacher J, Rickli R, Xoplaki E, Tinguely C, Beck C et al. (2001) The late Maunder minimum (1675–1715)–a key period forstudying decadal scale climatic change in Europe. Climatic Change 49(4): 441-462

MacDonald D, Crabtree JR, Wiesinger G, Dax T, Stamou N et al. (2000) Agricultural abandonment in mountain areas of Europe: environmental consequences and policy response. J environ manage 59(1): 47-69

MacDonald GM, Larsen CP, Szeicz JM, Moser KA (1991) The reconstruction of boreal forest fire history from lake sediments: a comparison of charcoal, pollen, sedimentological, and geochemical indices. Quat Sci Rev 10(1): 53-71

Mack RN, Lonsdale WM (2001) Humans as Global Plant Dispersers: Getting More Than We Bargained For: Current introductions of species for aesthetic purposes present the largest single challenge for predicting which plant immigrants will become future pests. Bioscience 51(2): 95-102

Malanima P (2016) Energy consumption in England and Italy, 1560–1913. Two pathways toward energy transition. Econ Hist Rev 69(1): 78-103

Masson-Delmotte V, Schulz M, Abe-Ouchi A, Beer J, Ganopolski A et al. (2013) Information from Paleoclimate Archives. In: Climate Change 2013: The Physical Science Basis. Contribution of Working Group I to the Fifth Assessment Report of the Intergovernmental Panel on Climate Change. Cambridge University Press, Cambridge, New York

Mathieu J (2015) Die Alpen: Raum – Kultur – Geschichte. Reclam, Stuttgart

Mauri A, Davis BAS, Collins PM, Kaplan JO (2015) The climate of Europe during the Holocene: a gridded pollen-based reconstruction and its multi-proxy evaluation. Quat Sci Rev 112: 109-127

McAleer J (2016) 'A young slip of botany': botanical networks, the South Atlantic, and Britain's maritime worlds, c. 1790–1810. J Global Hist 11(1): 24-43

Montanari M (1996) The Culture of Food (The Making of Europe). Blackwell, Oxford

Morales-Molino C, Colombaroli D, Tinner W, Perea R, Valbuena-Carabaña M et al. (2018) Vegetation and fire dynamics during the last 4000 years in the Cabañeros National Park (central Spain). Rev Palaeobot Palyno 253: 110-122

Pelet PL (2008) Kohle. In: Historisches Lexikon der Schweiz. http://www.hls-dhs-dss.ch/textes/d/D47174.php. Last accessed: 30.09.2018

Pérez-Díaz S, López-Sáez JA, Pontevedra-Pombal X, Souto-Souto M, Galop D (2016) 8000 years of vegetation history in the northern Iberian Peninsula inferred from the palaeoenvironmental study of the Zalama ombrotrophic bog (Basque-Cantabrian Mountains, Spain). Boreas 45(4): 658-672

Pfister C (1979) Getreide-Erntebeginn und Frühsommertemperaturen im schweizerischen Mittelland seit dem 17. Jahrhundert. Geographica Helvetica 34(1): 23-35

Pfister C (1984) Bevölkerung, Klima und Agrarmodernisierung 1525-1860: Das Klima der Schweiz von 1525-1860 und seine Bedeutung in der Geschichte von Bevölkerung und Landwirtschaft. Haupt, Bern

Pfister C, Brändli D (1999) Rodungen im Gebirge, Überschwemmungen im Vorland: Ein Deutungsmuster macht Karriere. In: Natur-Bilder. Wahrnehmungen von Natur und Umwelt in der Geschichte. Campus, Frankfurt, New York, pp. 297-324.

Pfister C, Wetter O, Brázdil R, Dobrovolný P, Glaser R et al. (2015) Tree-rings and people–different views on the 1540 Megadrought. Reply to Büntgen et al. 2015. Climatic Change 131(2): 191-198

Pini R (2002) A high-resolution late-glacial–holocene pollen diagram from Pian di Gembro (Central Alps, Northern Italy). Veg Hist Archaeobot 11(4): 251-262

Poldini L (1982) Ostrya carpinifolia-reiche Wälder und Gebüsche von Julisch-Venezien (NO-Italien) und Nachbargebieten. EUT Edizioni Università di Trieste, Trieste

Poraj-Górska AI, Żarczyński MJ, Ahrens A, Enters D, Weisbrodt D, Tylmann W (2017) Impact of historical land use changes on lacustrine sedimentation recorded in varved sediments of Lake Jaczno, northeastern Poland. Catena 153: 182-193

Poyatos R, Latron J, Llorens P (2003) Land use and land cover change after agricultural abandonment: the case of a Mediterranean mountain area (Catalan Pre-Pyrenees). Mt Res Dev 23(4): 362-368

Radkau J (2012) Wood: A History. Polity Press, Cambridge

Renner F (2013) Landschafts- und Waldgeschichte des Urserntals. Historisches Neujahrsblatt des Historischen Vereins Uri 68(1): 11-36

Rey F, Gobet E, van Leeuwen JFN, Gilli A, van Raden UJ et al. (2017) Vegetational and agricultural dynamics at Burgäschisee (Swiss Plateau) recorded for 18,700 years by multi-proxy evidence from partly varved sediments. Veg Hist Archaeobot 26(6): 571-586

Rey F, Gobet E, Szidat S, Lotter AF, Gilli A, Hafner A, Tinner W (2018) Radiocarbon wiggle matching on laminated sediments delivers high-precision chronologies. Radiocarbon 1-21

Rohr C (2011) Waldbrand. In: Enzyklopädie der Neuzeit 14. JB Metzler, Stuttgart, Weimar, pp. 573-575

Rösch M, Jacomet S, Karg S (1992) The history of cereals in the region of the former Duchy of Swabia (Herzogtum Schwaben) from the Roman to the Post-medieval period: results of archaeobotanical research. Veg Hist Archaeobot 1(4): 193-231

Rose NL (2015) Spheroidal carbonaceous fly ash particles provide a globally synchronous stratigraphic marker for the Anthropocene. Environ Sci Technol 49(7): 4155-4162

Ruddiman WF (2003) The anthropogenic greenhouse era began thousands of years ago. Climatic change 61(3): 261-293

Schneider-Orelli O (1923) Die Reblaus und unser Weinbau. Neujahrsblatt der Naturforschenden Gesellschaft in Zürich auf das Jahr 1923. Beer, Zürich

Schwörer C, Henne PD, Tinner W (2014b) A model-data comparison of Holocene timberline changes in the Swiss Alps reveals past and future drivers of mountain forest dynamics. Glob Change Biol 20(5): 1512-1526

Schwörer C, Kaltenrieder P, Glur L, Berlinger M, Elbert J et al. (2014a) Holocene climate, fire and vegetation dynamics at the treeline in the Northwestern Swiss Alps. Veg Hist Archaeobot 23(5): 479-496

Seddon AW, Mackay AW, Baker AG, Birks HJB, Breman E et al. (2014). Looking forward through the past: identification of 50 priority research questions in palaeoecology. J Ecology 102(1): 256-267

Seppä H, Birks HJB, Odland A, Poska A, Veski S (2004) A modern pollen–climate calibration set from northern Europe: developing and testing a tool for palaeoclimatological reconstructions. J Biogeograph 31(2): 251-267

Seppä H, Schurgers G, Miller PA, Bjune AE, Giesecke T, Kühl N et al. (2015) Trees tracking a warmer climate: The Holocene range shift of hazel (Corylus avellana) in northern Europe. Holocene 25(1): 53-63

Sereni E (2014) History of the Italian agricultural landscape. Princeton University Press, Princeton, New Jersey

Sigl M, Abram NJ, Gabrieli J, Jenk TM, Osmont D, Schwikowski M (2018) No role for industrial black carbon in forcing 19th century glacier retreat in the Alps. Cryosphere Discuss

Sigl M, Jenk TM, Kellerhals T, Szidat S, Gäggeler HW et al. (2009). Towards radiocarbon dating of ice cores. J Glaciol 55(194): 985-996

Simeoni U, Corbau C (2009) A review of the Delta Po evolution (Italy) related to climatic changes and human impacts. Geomorphology 107(1-2): 64-71

Sombart W (1919) Der moderne Kapitalismus. Historisch-systematische Darstellung des gesamteuropäischen Wirtschaftslebens von seinen Anfängen bis zur Gegenwart. Erster Band: Die vorkapitalistische Wirtschaft. Duncker und Humblot, Munich

Stoate C, Boatman ND, Borralho RJ, Carvalho CR, De Snoo GR, Eden P (2001) Ecological impacts of arable intensification in Europe. J Environ Manage 63(4): 337-365

Stuber M (2008) Wälder für Generationen: Konzeptionen der Nachhaltigkeit im Kanton Bern (1750-1880) (Umwelthistorische Forschungen 3). Böhlau, Köln Weimar

Summermatter S (2012) Die Prävention von Überschwemmungen durch das politische System der Schweiz von 1848 bis 1991. Doctoral dissertation, Institute of History, University of Bern, Bern

Ter Braak CJ, Prentice IC (1988) A theory of gradient analysis. Advance Ecol Ees 18: 271-317

Thevenon F, Anselmetti FS, Bernasconi SM, Schwikowski M (2009) Mineral dust and elemental black carbon records from an Alpine ice core (Colle Gnifetti glacier) over the last millennium. J Geophys Res Atmos 114(D17)

Tinner W, Ammann B, Germann P (1996) Treeline fluctuations recorded for 12,500 years by soil profiles, pollen, and plant macrofossils in the Central Swiss Alps. Arctic Alpine Res: 131-147

Tinner W, Conedera M, Ammann B, Gäggeler HW, Gedye S et al. (1998) Pollen and charcoal in lake sediments compared with historically documented forest fires in southern Switzerland since AD 1920. Holocene 8(1): 31-42

Tinner W, Conedera M, Ammann B, Lotter AF (2005) Fire ecology north and south of the Alps since the last ice age. Holocene 15(8): 1214-1226

Tinner W, Conedera M, Gobet E, Hubschmid P, Wehrli M, Ammann B (2000) A palaeoecological attempt to classify fire sensitivity of trees in the southern Alps. Holocene 10(5): 565-574

Tinner W, Theurillat JP (2003) Uppermost limit, extent, and fluctuations of the timberline and treeline ecocline in the Swiss Central Alps during the past 11,500 years. Arctic Antarctic Alpine Research 35(2): 158-169

Tinner W, Hu FS (2003) Size parameters, size-class distribution and area-number relationship of microscopic charcoal: relevance for fire reconstruction. Holocene 13(4): 499-505

Tinner W, Hubschmid P, Wehrli M, Ammann B, Conedera M (1999) Long-term forest fire ecology and dynamics in southern Switzerland. J Ecol 87(2): 273-289

Tinner W, Lotter AF, Ammann B, Conedera M, Hubschmid P et al. (2003) Climatic change and contemporaneous land-use phases north and south of the Alps 2300 BC to 800 AD. Quat Sci Rev 22(14): 1447-1460

Tinner W, van Leeuwen JFN, Colombaroli D, Vescovi E, van der Knaap WO et al. (2009) Holocene environmental and climatic changes at Gorgo Basso, a coastal lake in southern Sicily, Italy. Quat Sci Rev 28(15-16): 1498-1510

van der Knaap WO, van Leeuwen JFN, Ammann B (2001) Seven years of annual pollen influx at the forest limit in the Swiss Alps studied by pollen traps: relations to vegetation and climate. Rev Palaeobot Palynol 117(1-3): 31-52

van der Knaap WO, van Leeuwen JFN, Fankhauser A, Ammann B (2000) Palynostratigraphy of the last centuries in Switzerland based on 23 lake and mire deposits: chronostratigraphic pollen markers, regional patterns, and local histories. Rev Palaeobot Palynol 108(1-2): 85-142

Vannière B, Colombaroli D, Chapron E, Leroux A, Tinner W, Magny M (2008) Climate versus human-driven fire regimes in Mediterranean landscapes: the Holocene record of Lago dell'Accesa (Tuscany, Italy). Quat Sci Rev 27(11-12): 1181-1196

Vischer DL (1986) Schweizerische Flusskorrektionen im 18. und 19. Jahrhundert ((Mitteilungen der Versuchsanstalt für Wasserbau, Hydrologie und Glaziologie an der ETH Zürich 84). Versuchsanstalt für Wasserbau, Hydrologie und Glaziologie, Zürich

Vischer, DL (2003) Die Geschichte des Hochwasserschutzes in der Schweiz. Von den Anfängen bis ins 19. Jahrhundert (Berichte des BWG, Serie Wasser 5). Bundesamt für Wasser und Geologie BWG, Bern

Von Gunten L, Heiri O, Bigler C, van Leeuwen JFN, Casty C et al. (2008) Seasonal temperatures for the past~ 400 years reconstructed from diatom and chironomid assemblages in a high-altitude lake (Lej da la Tscheppa, Switzerland). J Paleolimnol, 39(3): 283-299

Wagenbach D, Geis K (1989) The mineral dust record in a high altitude Alpine glacier (Colle Gnifetti, Swiss Alps). In Paleoclimatology and paleometeorology: modern and past patterns of global atmospheric transport. Springer, Dordrecht, pp. 543-564

Wehrli M, Mitchell EA, van der Knaap WO, Ammann B, Tinner W (2010) Effects of climatic change and bog development on Holocene tufa formation in the Lorze Valley (central Switzerland). Holocene 20(3): 325-336

Wetter O, Pfister C, Werner JP, Zorita E, Wagner S et al. (2014) The year-long unprecedented European heat and drought of 1540–a worst case. Climatic Change 125(3-4): 349-363

Whitlock C, Colombaroli D, Conedera M, Tinner W (2018) Land-use history as a guide for forest conservation and management. Conservation Biology 32(1): 84-97

Wrigley EA (1967) A simple model of London's importance in changing English society and economy 1650-1750. Past Present (37): 44-70

Wrigley EA (2013) Energy and the English industrial revolution. Philos T R Soc A 371(1986): 20110568

Xoplaki E, Maheras P, Luterbacher J (2001) Variability of climate in meridional Balkans during the periods 1675–1715 and 1780–1830 and its impact on human life. Climatic Change 48(4): 581-615

Zoller H, Erny-Rodman C, Punchakunnel P (1996) The history of vegetation and land use in the Lower Engadine (Switzerland): pollen record of the last 13,000 years (Nationalpark-Forschung in der Schweiz 86). F. Flück-Wirth, Teufen

9 Figures

Figure 1 Map of the study site. A) Showing European biomes (= vegetation zones, following Lang 1994) and geographical regions (modified from Jordan 2005) study region (red triangle). B) Map of the Monte Rosa region in the Swiss Alps with drilling location (red triangle, topographic map: © swisstopo.ch 2018).

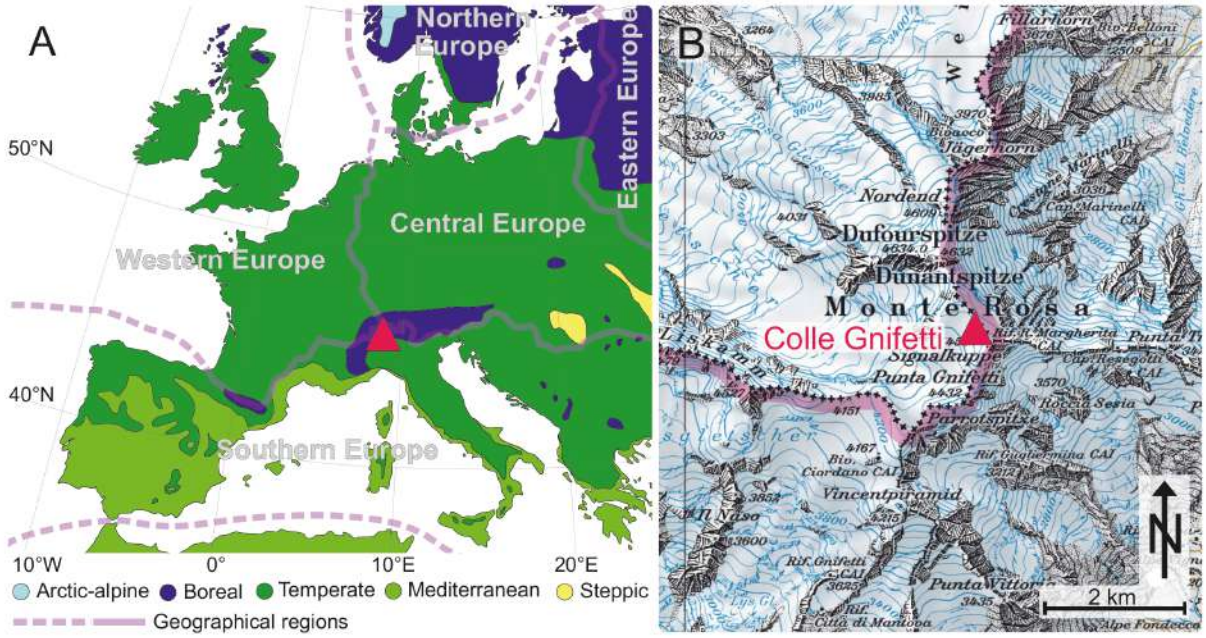

Figure 2 Chronology of the Colle Gnifetti palynological record (lilac shaded period). Chronology for the upper core (CG15 2015–2003 AD) based on annual layer counting (dashed line). For the lower core (CG03B 2003–1000AD) based on annual layer counting (2003–1763), ^{210}Pb activity (not shown), maximum Tritium peak (^{3}H maximum, orange dot), historical Sahara dust layers (SD, purple dots) and volcanic layers (VL, green dots). Below 1763 AD modeled ages as exponential equation based on ^{14}C-dates from the measured organic fraction of carbonaceous particles (yellow dots with uncertainty bars). Figure adapted from Jenk et al. (2009) and Sigl et al. (2009).

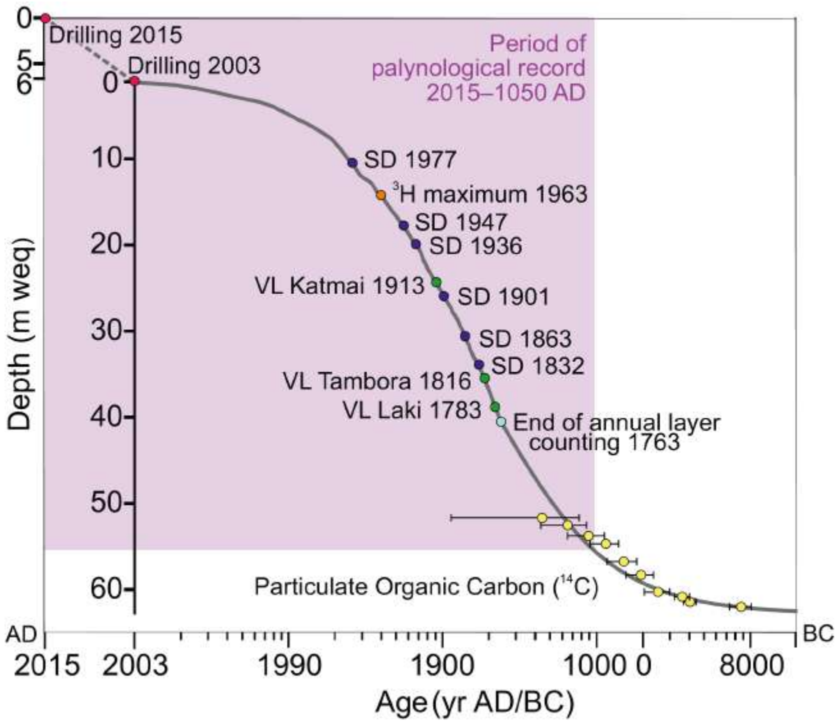

Figure 3 Modern pollen composition at Colle Gnifetti glacier shows selected pollen types and summary curves based on classification in table S1 as percentages of the terrestrial pollen sum. Colors refer to biome assignment of arboreal pollen taxa (light green = mediterranean; dark green = temperate; blue = boreal, black = other AP; red = herbaceous taxa). Pollen sum = 4729. CI = Cultural indicators, NAP = nonarboreal pollen, AP = arboreal pollen.

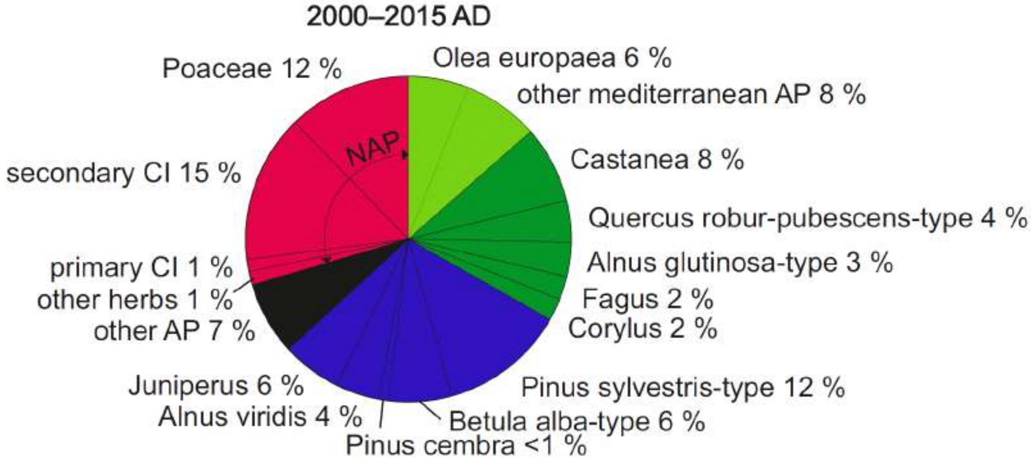

Figure 4 Percentage diagram for Colle Gnifetti for selected pollen types and the fungal dung spore *Sporormiella* based on the pollen sum. Neophyte sum includes *Eucalyptus*, *Nothofagus*, *Parthenocissus quinquefolia, Fallopia, Pterocarya,* and *Heliotropium.* Hollow curves = 10x exaggeration. Concentration curves for microscopic charcoal (including peaks exceeding 90-percentile, spheroidal carbonaceous particles (SCPs), pollen, and *Sporormiella* in particles l^{-1}. Counted pollen sums. LPAZ = local pollen assemblage zone. Depth indicates core depth in m water equivalent of core CG03B drilled in 2003. Chronology according to Jenk et al. (2009), Sigl et al. (2009) with indication of absolute reference horizons (see Fig. 2).

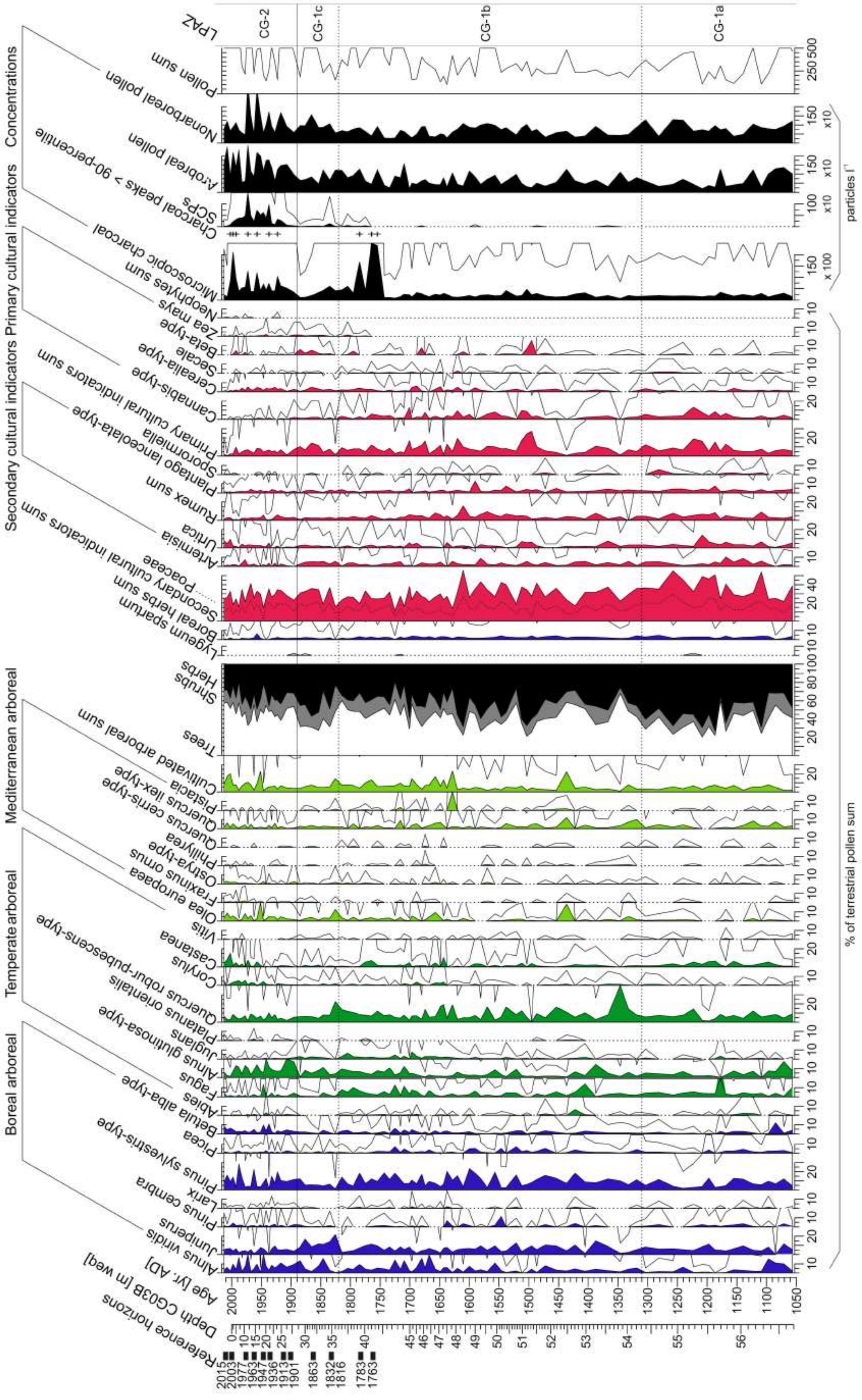

Figure 5 Principal component analysis (PCA) for the Colle Gnifetti (CG) palynological record based on percentages of the terrestrial pollen sum. A: Sample scores grouped by local pollen assemblage zones (LPAZ, marked with different colors see lilac box). B: Selected taxa scores with colors indicating assigned biome and red for primary and secondary cultural NAP (= nonarboreal pollen). Abbreviation of genera: A = *Alnus*; B = *Betula*; E = *Ephedra*; F = *Fraxinus*; Q = *Quercus*; P = *Plantago*.

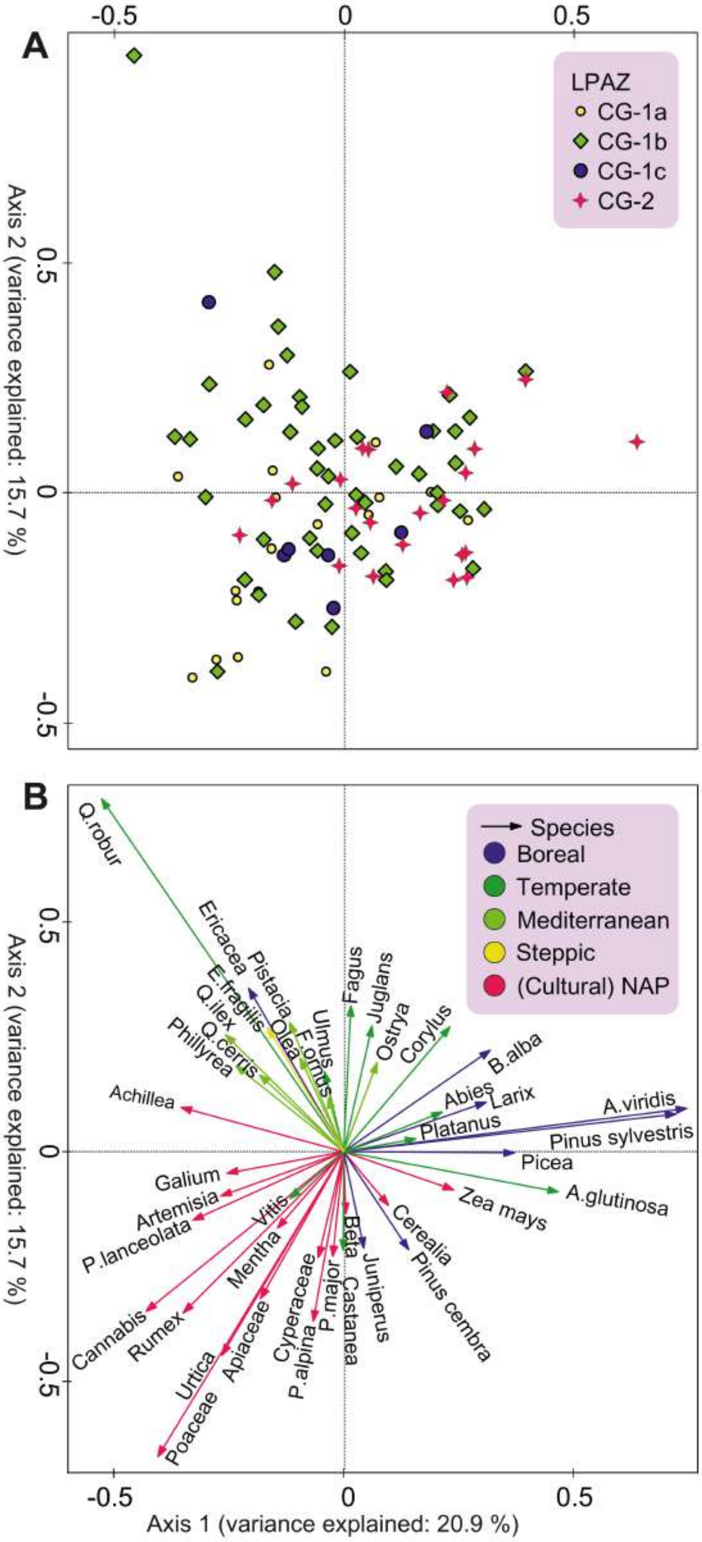

Figure 6 Scatterplot for European natural fire and industrial pollution dynamics inferred from Colle Gnifetti microscopic charcoal (x-axis) and SCP (spheroidal carbonaceous particles, y-axis) concentration records during the past millennium. Average for the period 1050–1700 AD, 50 years average for the period 1700–1900 AD, 10 year average after 1900 AD.

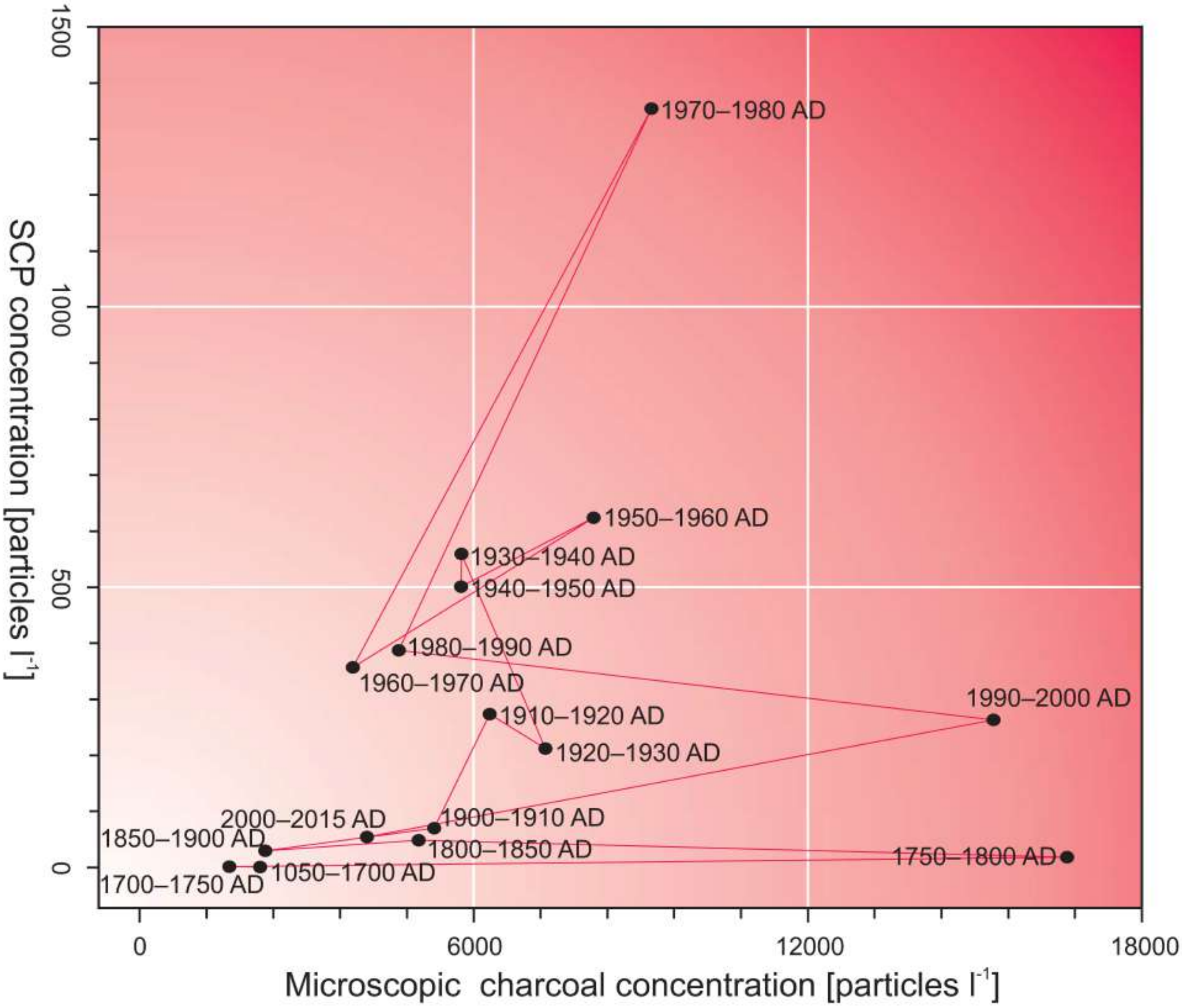

Supplementary material

Table S1 Complete pollen and NPP taxa list for the palynological record of Colle Gnifetti glacier with assignment to summary groups in the pollen diagram primary and secondary cultural indicators following Lang (1994), pollen types according to Beug (2004).

	Taxa
Mediterranean AP	• Cultivated: *Morus, Olea europaea, Pistacia* • Other: *Celtis, Fraxinus ornus, Genista*-type, *Ligustrum*-type, Mimosoideae, *Myrtus communis, Ostrya*-type, *Phillyrea, Quercus cerris*-type, *Q. ilex*-type, *Tsuga*
Temperate AP	• Cultivated: *Aesculus hippocastanum, Castanea, Juglans, Prunus*-type, *Vitis* • Other: *Abies, Acer, Alnus glutinosa*-type, , *Buxus, Carpinus betulus, Cornus mas*-type, *C. sanguinea, Corylus, Daphne, Fagus, Frangula alnus*, *Fraxinus excelsior*-type, *Hedera helix, Hippophaë rhamnoides*, *Platanus* orientalis, *Populus, Quercus robur*-pubescens-type, *Rhamnus*-type, *Salix, Sambucus*, *Sambucus nigra*-type, *Sorbus*-type, *Thymelaea passerina, Tilia, Ulmus*, *Viburnum lantana, V. opulus*-type
Boreal AP	• *A. viridis, Betula alba*-type, *Calluna vulgaris*, *Empetrum*, other Ericaceae, *Erica*, *Juniperus, Larix, Picea, Pinus cembra, P. sylvestris*-type, *Rhododendron*, *Vaccinium*-type
Steppic AP	• *Ephedra distachya*-type, *E. fragilis*-type, *Eucalyptus, Parthenocissus quinquefolia*
Neophyte AP	• *Nothofagus, Pterocarya*
Mediterranean NAP	• *Emex spinosa, Lygeum spartum*
Temperate/ steppic NAP	• Primary cultural indicators: *Cannabis*-type, Cerealia-type, *Beta*-type, *Humulus*-type, *Secale*, *Zea mays* • Secondary cultural indicators: *Allium vineale*-type, *Amaranthus*, *Ambrosia, Anagallis*-type, other Apiaceae, *Artemisia*, Asteroideae undiff., Brassicaceae, *Bupleurum*-type, other Campanulaceae, *Carduus*-type, Caryophyllaceae, other *Centaurea*, *C. scabiosa*-type, *Chaerophyllum*-type, *Chenopodium*-type, other Chenopodiaceae, Cichorioideae, *Conium*-type, *Coronilla*-type, Cyperaceae, *Daucus*-type, *Eryngium*, Fabaceae undiff., *Galium*, *Heracleum sphondylium, Lathyrus*-type, Liliaceae undiff., *Mentha*-type, *Mercurialis annua, M. perennis*-type, *Odontites*-type, *Onobrychis*, *Ononis*, *Papaver rhoeas*-type, *Peucedanum*-type, *Pimpinella*-type, *Plantago coronopus*-type, *P. lanceolata-type, P. major, P. media*, Poaceae, *Polygonum aviculare*-type, *Ranunculus, R. acris*-type, *R. arvensis*, other Ranunculaceae, Rubiaceae, *Salsola*-type, *Senecio*-type, *Trifolium repens*-type, *Urtica* • Other: *Callygonum*-type, *Cuscuta europaea*-type, *Echium*, *Filipendula*, *Hypericum*, Lamiaceae, *Parnassia palustris*-type, *Pedicularis palustris*-type, Plumbaginaceae, other Rosaceae, *Sanguisorba minor*-type, *Stachys*-type, *Thalictrum*, *Valeriana* undiff., *V. officinalis*-type, *Xanthium spinosum*-type • Neophytes: *Fallopia, Heliotropium*
Boreal NAP	• Secondary indicators: *Achillea*, *Aster*-type, *Centaurea cyanus, C. jacea*-type, *Centaurea montana*-type, *Oxyria, Plantago alpina*-type, *Rumex* undiff., *R. acetosa*-type, *R. acetosella*-type, *Rumex alpinus*-type, *R. obtusifolius* • Other: *Androsace alpina*-type, *Anthyllis montana*-type, *Bartsia*-type, *Gentiana* undiff., *Gentiana pneumonanthe*-type, *Geum*-type, *Helianthemum, Herniaria glabra*-type, *Jasione montana*-type, *Ligusticum mutellina*-type, *Lysimachia* undiff., *Lysimachia nemorum, Phyteuma*-type, *Potentilla*-type, *Ranunculus aconitifolius*-type, *Saxifraga aizoides*-type, Scrophulariaceae, *Sedum*-type, *Valeriana montana*-type
Aquatic	• *Sparganium*-type, *Utricularia*
Fern spores	• *Asplenium, Botrychium*, *Dryopteris filix-mas*, *Gymnocarpium, Isoetes,* other monolete spores, *Polypodium*, other trilete spores
Fungal spores	• *Celasinospora retispora*, *Diporotheca, Neurospora, Sporormiella, Sordaria, Ustulina*
Algae	• *Pediastrum, Tetraedron*

Manuscript 3

Ice records provide new insights into climatic vulnerability of Central Asian forest and steppe communities

Sandra O. Brugger[1,2,*], Erika Gobet[1,2], Michael Sigl[2,3], Dimitri Osmont[2,3,4], Tatyana Papina[5], Natalia Rudaya[6,7], Margit Schwikowski[2,3,4], Willy Tinner[1,2]

[1]Institute of Plant Sciences, University of Bern, Switzerland
[2]Oeschger Center for Climate Change Research, University of Bern, Switzerland
[3]Paul Scherrer Institute, Villigen, Switzerland
[4]Department for Chemistry and Biochemistry, University of Bern, Switzerland
[5]Institute for Water and Environmental Problems, SB RAS, Barnaul, Russia
[6]Institute of Archaeology and Ethnography, SB RAS, Novosibirsk, Russia
[7]University of Potsdam, Germany

[*]Corresponding author: Sandra O. Brugger

Keywords: Boreal forest diebacks – Climatic tipping points – Diversity – Ice core – Moisture change – Pollen – Microscopic charcoal – SCP

Global and Planetary Change 169, 188-201

Global and Planetary Change 169 (2018) 188–201

Contents lists available at ScienceDirect

Global and Planetary Change

journal homepage: www.elsevier.com/locate/gloplacha

Reasearh article

Ice records provide new insights into climatic vulnerability of Central Asian forest and steppe communities

Sandra O. Brugger[a,b,*], Erika Gobet[a,b], Michael Sigl[b,c], Dimitri Osmont[b,c,d], Tatyana Papina[e], Natalia Rudaya[f,g], Margit Schwikowski[b,c,d], Willy Tinner[a,b]

[a] Institute of Plant Sciences, University of Bern, Switzerland
[b] Oeschger Center for Climate Change Research, University of Bern, Switzerland
[c] Paul Scherrer Institute, Villigen, Switzerland
[d] Department for Chemistry and Biochemistry, University of Bern, Switzerland
[e] Institute for Water and Environmental Problems, SB RAS, Barnaul, Russia
[f] Institute of Archaeology and Ethnography, SB RAS, Novosibirsk, Russia
[g] University of Potsdam, Germany

ARTICLE INFO

Keywords:
Boreal forest diebacks
Climatic tipping points
Diversity
Ice core
Moisture change
Pollen
Microscopic charcoal
SCP

ABSTRACT

Forest and steppe communities in the Altai region of Central Asia are threatened by changing climate and anthropogenic pressure. Specifically, increasing drought and grazing pressure may cause collapses of moisture-demanding plant communities, particularly forests. Knowledge about past vegetation and fire responses to climate and land use changes may help anticipating future ecosystem risks, given that it has the potential to disclose mechanisms and processes that govern ecosystem vulnerability. We present a unique paleoecological record from the high-alpine Tsambagarav glacier in the Mongolian Altai that provides novel large-scale information on vegetation, fire and pollution with an exceptional temporal resolution and precision. Our palynological record identifies several late-Holocene boreal forest expansions, contractions and subsequent recoveries. Maximum forest expansions occurred at 3000–2800 BC, 2400–2100 BC, and 1900–1800 BC. After 1800 BC mixed boreal forest communities irrecoverably declined. Fires reached a maximum at 1600 BC, 200 years after the final forest collapse. Our multiproxy data suggest that burning peaked in response to dead biomass accumulation resulting from forest diebacks. Vegetation and fire regimes partly decoupled from climate after 1700 AD, when atmospheric industrial pollution began, and land use intensified. We conclude that moisture availability was more important than temperature for past vegetation dynamics, in particular for forest loss and steppe expansion. The past Mongolian Altai evidence implies that in the future forests of the Russian Altai may collapse in response to reduced moisture availability.

1. Introduction

Forest disruption has substantially increased globally in recent years (McDowell and Allen, 2015). The vast boreal forests and forest steppes in and around the Altai region in Central Asia provide an important terrestrial carbon storage but respond highly sensitive to recent global change (Sato et al., 2007; Liu et al., 2013; Chenlemuge et al., 2013; Tian et al., 2013, 2014; Hijioka et al., 2014; Dulamsuren et al., 2016; Khansaritoreh et al., 2017; Zhao et al., 2018). In the past decades, the Altai region experienced rising temperatures combined with increasing extreme events such as prolonged heatwaves, drought periods, and short-term heavy rainfall events (Lkhagvadorj et al., 2013). As boreal forest growth is not only limited by temperature but also by moisture availability, the forests progressively suffer from water constraints (Dulamsuren et al., 2010, 2014). The establishment, persistence, and decline of these boreal forests depend on soil moisture availability, which is not only constrained by precipitation, but also by the local soil development and its water-holding capacity (Henne et al., 2011) that is extremely low for the predominant soil types in the region.

The central position of the Altai Mountains between the vast Siberian Taiga forests in the north and the Gobi desert in the south results in a steep climatic and vegetation gradient with fragmented and diverse habitats including many rare and endemic species (Rudaya et al., 2008). Their natural resources such as forests, productive grasslands, and fresh water sources have attracted Central Asian nomadic groups since centuries (Rudaya et al., 2008). In recent years, these

* Corresponding author at: Institute of Plant Sciences, Altenbergrain 21, CH-3013 Bern, Switzerland.
E-mail address: sandra.bruegger@ips.unibe.ch (S.O. Brugger).

https://doi.org/10.1016/j.gloplacha.2018.07.010
Received 25 May 2018; Received in revised form 18 July 2018; Accepted 19 July 2018
Available online 21 July 2018

ecotonal mountain steppe ecosystems experienced rapid degradation through over-grazing, systematic logging, dead wood collecting, and human-set fires (Tsogtbaatar, 2004; Dulamsuren et al., 2014). Anthropogenic pressure combined with growing moisture deficiency may cause irreversible forest vegetation loss, reduce steppe pasture productivity and thus alter species composition and diversity (Lkhagvadorj et al., 2013).

Knowledge about past vegetation dynamics in the Mongolian Altai contributes to a better understanding of future ecosystem responses to climate change and human land use, and may assist forest, grassland, and fire management strategies by providing baselines of past ecosystem variability in response to strong environmental change. However, paleo records that provide information about Holocene vegetation and fire history are scarce, lack temporal resolution and/or chronological precision (Tarasov et al., 2000; Gunin et al., 1999; Rudaya et al., 2009; Umbanhowar Jr et al., 2009; Unkelbach et al., 2018). Such limitations impede a thorough assessment of ecosystem resilience and vulnerability. The snow-capped Tsambagarav Mountain provides a regional to supra-regional ice archive of ecosystem change, which is well suited to reconstruct ecosystem dynamics with high temporal resolution and precision (Herren et al., 2013). Here we address persisting knowledge gaps with the following aims: (1) for the first time, we use microscopic charcoal to reconstruct the fire dynamics in the Mongolian Altai; (2) pollen, spores, and spheroidal carbonaceous particles are used to investigate the long-term linkages between the fire regime, vegetation, land use, and pollution; (3) we use the palynological information including charcoal to assess ecosystem response variability to climate change, and (4) evidence from other studies is used to underscore the spatio-temporal relevance of our outcomes and to derive implications for ecosystem responses under global-change conditions.

2. Study site

The Altai Mountains stretch over ca. 1200 km, crossing the borders of Russia, Mongolia, Kazakhstan, and China. With 4500 m a.s.l. maximum elevation (Mount Belukha in Russia, Fig. 1A) the Altai Mountains build a continental climate barrier for air masses from northwest, resulting in a strong northwest (800 mm year^{-1}) to southeast (< 200 mm year^{-1}) precipitation gradient (Klinge et al., 2003) because the main moisture source in the region are the Westerlies. The extreme continental climate is dominated by the Siberian High with cold dry winters and precipitation prevailing in June to August (Klinge et al., 2003). The investigated ice archive on Tsambagarav Mountain is located in the Mongolian Bayan-Ölgii province (Fig. 1A), a region with very dry climatic conditions (annual precipitation ca. 200 mm at 1700 m a.s.l.).

Geologically, the Mongolian Altai consists of siliceous bedrock, including schists and granites with Leptosols as prevailing soil type that are susceptible to erosion and desiccation (Dulamsuren et al., 2014). The modern vegetation around Tsambagarav reflects the cold semi-arid continental climate characterized by huge differences in maximum and minimum daily and yearly temperatures (July average + 22.7 °C, January average − 22.6 °C at Ölgii weather station; NOAA, 2013). Gradients such as altitude and exposure lead to pronounced local differences in growth season length, heat sum, precipitation, and soil formation, which together strongly affect species distribution and productivity (Rudaya et al., 2009).

Wide areas at high elevations surrounding Tsambagarav are occupied by cryo-xerophyllic mountain steppe communities mainly composed of *Festuca sulcata* sp., *Poa botryoides*, *Carex pediformis*, but also *Artemisia frigida* and *A. tanacetifolia* (Walter, 1974). Alpine tundra communities with *Betula nana* ssp. *rotundifolia* (Spach) Malyschev (synonyms *Betula glandulosa* Michaux subsp. *rotundifolia* (Spach) Regel, and *Betula rotundifolia* Spach, see TPL, 2018; Gunin et al., 1999), *Salix glauca*, *Kobresia*, and *Potentilla sericea* become more abundant with increasing altitude and may penetrate up to 3000 m a.s.l. (Walter, 1974). High alpine *Kobresia* meadows with *Poa altaica*, *P. sibirica*, *Festuca*, *Carex* and *Thalictrum alpinum* are increasingly fragmented above 3200 m a.s.l. *Sedum algidum* is found up to the nival zone close to the eternal snow margin (Walter, 1974), which is at Tsambagarav between 3000 and 3800 m a.s.l. depending on the exposure (Herren et al., 2013). Below 1800–2000 m a.s.l. the mountain steppes are gradually replaced by dry *Stipa-Artemisia* steppe communities with *Stipa glareosa*, *S. gobica*, *Allium*, *Tanacetum*, *Artemisia* sp., and *Caragana* (Walter, 1974; Gunin et al., 1999). *Anabasis brevifolia* (Chenopodiaceae) is the most common halophilous taxon in the region. Desert-steppe communities composed of *Stipa* sp. and *Salsola* dominate in dry isolated valleys and southeast of Tsambagarav in the large mountain depression "basin of the large lakes", where precipitation is further reduced to < 200 mm year^{-1} (Gunin et al., 1999). Wet herbaceous communities and small woody stands with *Betula pendula*, *Populus tremula*, *Salix*, and *Alnus glutinosa* grow along streams (Walter, 1974; Gunin et al., 1999; Stritch et al., 2014). The closest of these parklands with dozens of km^2 sizes occur ca. 50 km northwest of Tsambagarav.

The mid-elevation forest belt in the Mongolian Altai is restricted to north facing slopes in the western (Hoton Nur area, Fig. 1A) and northwestern part of the Mongolian Altai between 1900 and 2100 m a.s.l., while on south facing slopes, mountain steppe communities directly pass over to alpine plant communities. The narrow and discontinuous forest belts are composed of *Pinus sibirica*, *Larix sibirica*, and *Betula pendula*. *Picea obovata* co-occurs where soil moisture is sufficient (Walter, 1974; Gunin et al., 1999). In these forest stands at ca. 100 km distance from Tsambagarav, the upper limit of tree growth is controlled by summer temperature and the lower limit by moisture availability and anthropogenic pressure such as logging activities (Klinge et al., 2003; Lkhagvadorj et al., 2013; Tsogtbaatar, 2013). Floristically, the Mongolian forest relicts belong to the forests in the Russian Altai (Walter, 1974), which consist of *Pinus sibirica*, *Abies sibirica*, *Larix sibirica* and *Betula pendula* that form a dense boreal forest belt between ca. 1000 and 2000 m a.s.l. in the region north of the Belukha glacier (see Fig. 1A; Walter, 1974; Eichler et al., 2011). Below 1000 m a.s.l the Russian Altai is characterized by lowland feather-grass steppes (*Stipa*, other Poaceae, *Artemisia*, and Chenopodiaceae; Walter, 1974). Modern *Pinus sylvestris* and *Abies sibirica* distribution is restricted to the Russian and Kazakh Altai, ca. 150–200 km north of Tsambagarav (Gunin et al., 1999).

3. Material and methods

3.1. Ice material and microfossil analysis

We analyzed samples from an existing ice core from Tsambagarav Mountain. The core was drilled on the eastern summit (48° 39.338′ N, 90° 50.826′ E; Fig. 1A) in July 2009 at an altitude of 4130 m a.s.l. (Herren et al., 2013). The drilling reached bedrock with a total ice core length of 72 m and a diameter of 8.2 cm. Core segments of ca. 70 cm were transported frozen to the Paul Scherrer Institute (PSI) in Switzerland.

202 continuous samples spanning the time 3500 BC to 2009 AD (55.6–0 m weq = water equivalent, corrected for varying density) from the outer part of the ice core were taken for palynological analysis. The sampling resolution was 40–90 years (3500 BC–1200 AD), 20–30 years (1200–1650 AD), 10 years (1650–1700 AD), five years (1700–1985 AD), and one year (1985–2009 AD, merged to five years after analysis) using the chronology of Herren et al. (2013). An additional ^{14}C-date from an insect remain found during palynological sampling confirmed the accuracy of the existing depth-age model (Fig. 1B; Uglietti et al., 2016). Each sample contained 200–400 g ice, except one sample with 45 g at 52.2 m weq. The microfossil extraction followed a protocol for ice sample preparation (Brugger et al., 2018). One *Lycopodium* tablet was added to each sample before lab treatment

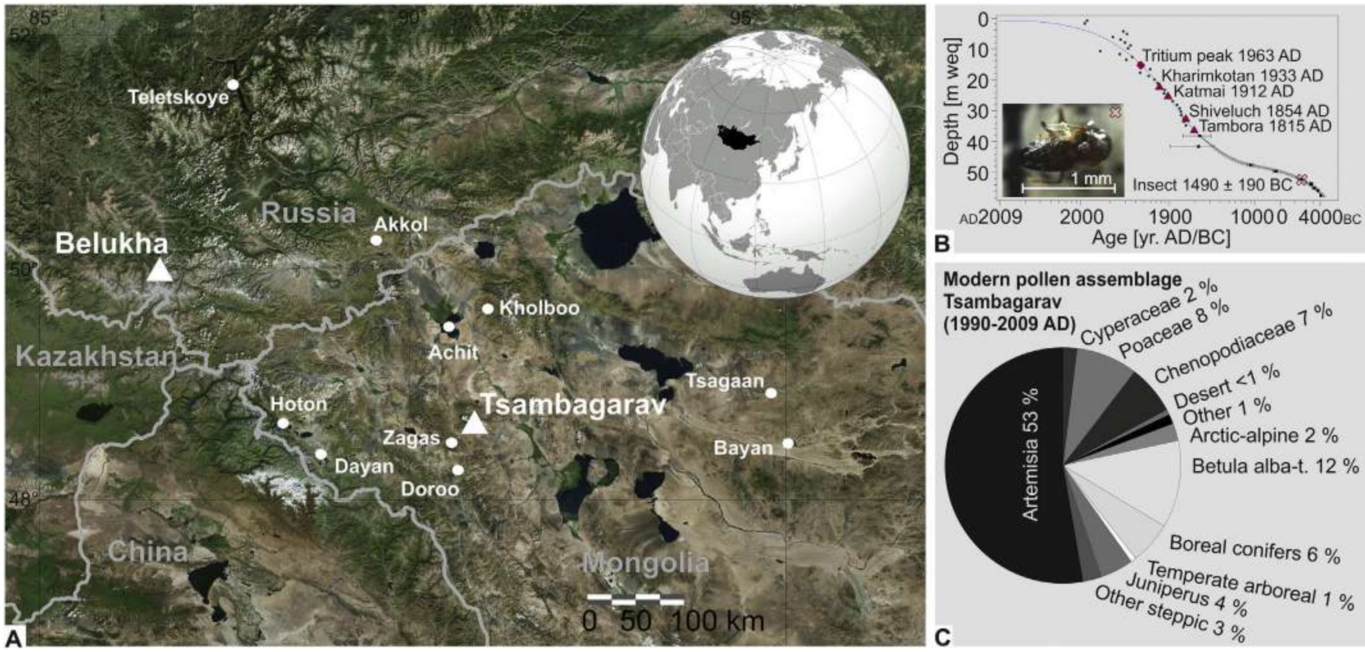

Fig. 1. Study area, chronology and modern pollen deposition at Tsambagarav glacier. Panel A: Map of the Altai region with glacier records (triangle) and selected records of fire and vegetation reconstructions (white dots), map modified (source of satellite images: U.S. Geological Survey). Panel B: Chronology of Tsambagarav record based on a glacier flow model (blue dashed line), annual layer counting (2009–1815 AD), maximum tritium peak (red diamond), volcanic layers (red triangles) and ^{210}Pb activity (green circles). Before 1815 AD modeled ages result from an exponential equation (black dashed line) with upper and lower limit of the equation (gray shaded) based on ^{14}C- dating of water-insoluble organic carbon of atmospheric origin (black squares with uncertainty bars). Insert: ^{14}C-date of an insect remain (red cross and photo, Uglietti et al., 2016). Figure adapted from Herren et al. (2013). Panel C: Modern pollen assemblage in Tsambagarav glacier ice (average over 20 years as percentages of the terrestrial pollen sum). (For interpretation of the references to colour in this figure legend, the reader is referred to the web version of this article.)

to estimate microfossil concentrations (Stockmarr, 1971). Due to strong thinning in the deeper part of the glacier caused by lateral ice flow, annual layers could not be identified before 1825 AD, preventing influx calculations with a reasonable time resolution.

We use pollen and spores to infer vegetation history and the coprophilous fungal spore *Sporormiella* as a proxy for herbivore grazing activity. A pollen sum of 500 was reached except in the samples of section 54–53 m weq (2600–2000 BC), where due to small pollen concentrations we reached 100 grains, which is above the minimum for reliable percentage calculations and environmental reconstructions (50 items; Heiri and Lotter, 2001). Pollen and spore identification under a light microscope at 400 x magnification followed palynological keys (Huang, 1972; Moore et al., 1991; Beug, 2004) and the reference collection in Bern, Switzerland. Shrub type (referred to as *Betula nana*-type) and tree type *Betula* (*Betula alba*-type) separation is based on the pore depth and the grain diameter to pore depth ratio (D/P) following Clegg et al. (2005). The palynological *Betula* distinction covers *B. pubescens*, *B. pendula* (both *B. alba*-type), *B. glandulosa* and *B. nana* (both *B. nana*-type) as well as other North American and Eurasian birch species (Birks, 1968; Clegg et al., 2005). Cerealia-type was classified according to Beug (2004). Although *Artemisia* comprises herb and shrub species, we include all *Artemisia* pollen in the herb pollen sum following Gunin et al. (1999) since pollen taxonomy allows no further discrimination. Pollen and spore data are presented as percentages of the terrestrial pollen sum.

Microscopic charcoal > 10 µm is used as a proxy for fire activity (e.g. MacDonald et al., 1991; Tinner et al., 1998; Conedera et al., 2009; Adolf et al., 2017). We counted a minimum sum of 200 items (charcoal fragments and *Lycopodium* grains, Finsinger and Tinner, 2005; Tinner and Hu, 2003). If needed (low charcoal concentrations), we continued until a minimum of 20 charcoal fragments was reached. Subsequently, the > 90th percentile (=10% upper charcoal concentration values over the entire record) was identified to infer regional fire activity peaks. SCP (=spheroidal carbonaceous particles) with a diameter > 10 µm and clear features (Rose, 2015) were counted along pollen and spores to reconstruct industrial air pollution. All microfossil concentrations were standardized to one liter.

Annual layer thickness is highest in the uppermost part of the ice core, resulting in an exponential depth-age relationship (Fig. 1B). Thus, the temporal sampling resolution in the younger part is much higher compared to the older part of the ice core where the ice had thinned substantially (i.e. one to several hundred years per m weq with increasing core depth). These archive characteristics result in varying detection limits for rare microfossil types along the record for comparable time periods. We kept the original lab sampling resolution for the interpretation of the palynological record (Fig. 2–4) while we amalgamated samples of the overview pollen and charcoal records to reach 40 to 50 years resolution in the younger part (period 1100–2009 AD; Fig. 5). This resulted in comparable time steps along the sequence.

3.2. Numerical analysis

Optimal sum-of-squares partitioning was applied for zonation of the pollen data (Birks and Gordon, 1985). Subsequently, statistically significant local pollen assemblage zones (LPAZ) were inferred with the broken stick approach (Bennett, 1996). Only LPAZ with more than two samples were accepted. We applied ordination methods to statistically summarize the pollen signal and to search for correlations with supplementary variables and similarities with external data. The short gradient length of the first axis (=1.35) of a detrended correspondence analysis (DCA, detrended by segments) justifies using linear ordination methods (Ter Braak and Prentice, 1988). Therefore, we applied principal component analysis (PCA) based on a correlation matrix. Charcoal concentrations, fern spore and *Sporormiella* percentages of the Tsambagarav data were included as supplementary variables (Fig. 4) and

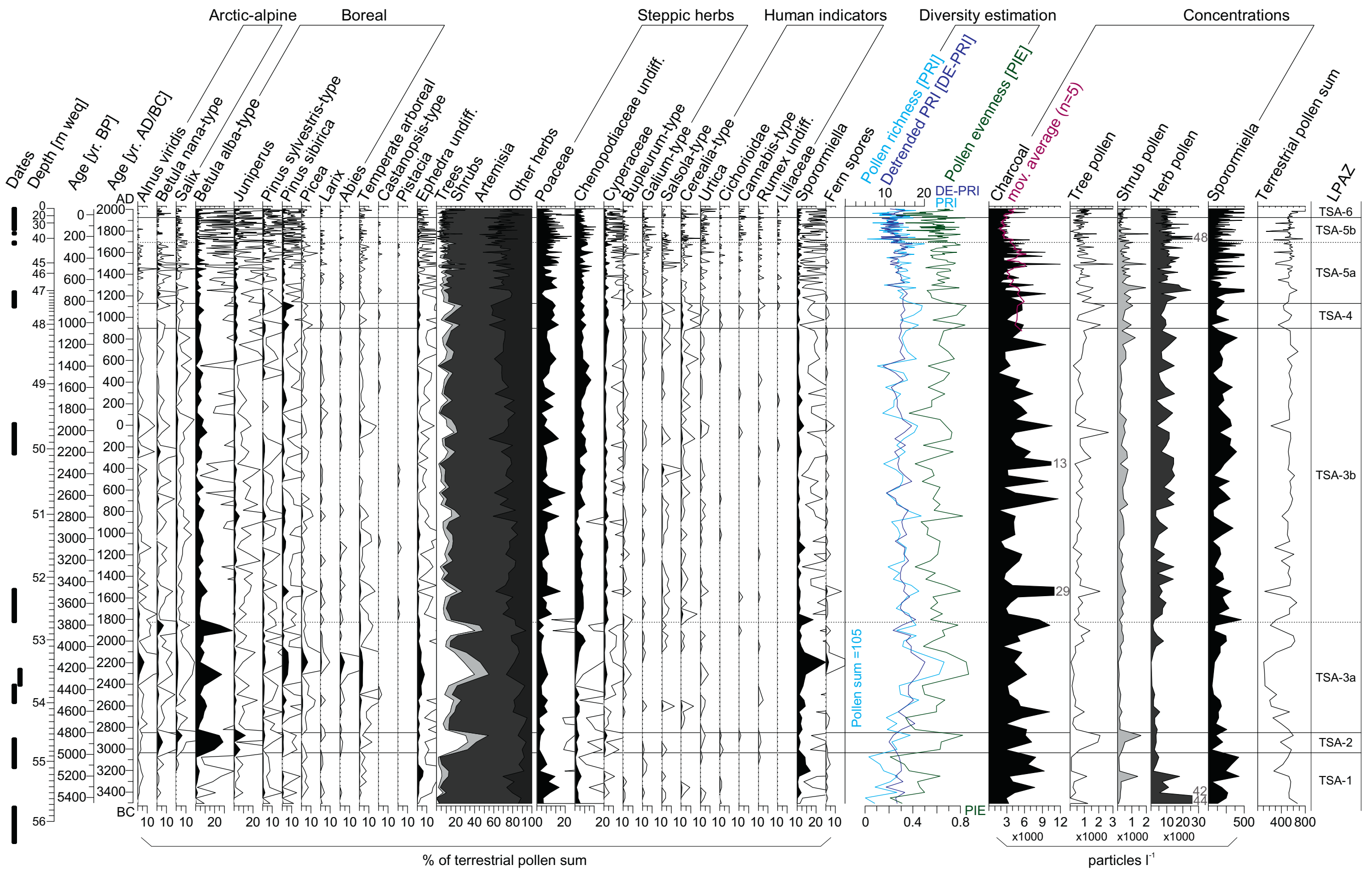

Fig. 2. Percentage diagram of Tsambagarav ice core spanning the past 5500 years. Selected pollen types, fern spores, and coprophilous fungal spores based on the terrestrial pollen sum. Temperate arboreal summary curve consists of *Fagus*, *Corylus*, *Quercus,* and other temperate arboreal pollen taxa. Hollow curves = 10 × exaggeration. Diversity estimation based on a minimum pollen sum of 105 for pollen richness (PRI; Birks and Line, 1992), evenness-detrended pollen richness (DE-PRI; Colombaroli and Tinner, 2013), and evenness index (PIE; Hurlbert, 1971). Concentration curves for charcoal, pollen and *Sporormiella* in particles l^{-1} and total terrestrial pollen sum. LPAZ = statistically significant local pollen assemblage zones, dashed lines not statistically significant. Chronology according to Herren et al. (2013), reference horizons in Fig. 1B. (For interpretation of the references to colour in this figure legend, the reader is referred to the web version of this article.)

pollen percentages from Belukha glacier (Eichler et al., 2011) were included as external samples (not influencing the ordination dataset) to search for spatio-temporal similarities between the two sites. We amalgamated *Betula* (includes *Betula nana*-type and *Betula alba*-type) and Chenopodiaceae (*Salsola* and remaining Chenopodiaceae) to homogenize the taxonomic resolution between the Tsambagarav and Belukha data.

To our knowledge palynologically-based diversity measures (e.g. palynological richness, evenness) are not available yet from the Altai region. To fill this gap we estimated palynological richness (PRI) with rarefaction analysis as a proxy for species richness and the probability of interspecific encounter (PIE) as a proxy for evenness (Birks and Line, 1992; Hurlbert, 1971). The minimum pollen sum for rarefaction analysis was 105 pollen grains. To account for evenness distortions of palynological richness we calculated PIE-detrended palynological richness (DE-PRI; Colombaroli and Tinner, 2013).

4. Results and interpretation

4.1. Modern pollen composition reflects vegetation and pollen catchment

The modern pollen concentration in the Tsambagarav record is ca. 6000 grains l^{-1} which corresponds to a total influx of 450 grains cm^{-2} $year^{-1}$. This is very low compared to sedimentary archives. The largest amount derives from the steppic taxa *Artemisia* (53%), Poaceae (8%) and Chenopodiaceae (7%), with arboreal pollen (AP) of *Betula alba*-type (12%), *Juniperus* (4%), and conifers such as *Pinus sibirica* (6%; Fig. 1C). With 25% AP and 75% non-arboreal pollen (NAP) the pollen signal reflects the patchy modern regional vegetation dominated by dry herbaceous steppes with scattered boreal trees. The presence of conifer and *Betula* pollen indicates regional sources, as the closest parklands with *Betula pendula* (*Betula alba*-type pollen) occur at ca. 50 km north-westwards and forested areas around 100 km westwards in the Hoton Nur region (Fig. 1A). Single grains of warm-loving taxa (e.g. *Castanopsis*-type and *Pistacia*; Fig. 2) along the record indicate pollen transport by southern air masses over > 1000 km, where *Pistacia* has its northern distribution limit today (Golan-Goldhirsh, 2009). Westerlies are the main moisture source for the Altai region. On the basis of the modern atmospheric pattern (Herren et al., 2013) we assume northwest as the predominant wind direction for our site during the mid and late Holocene. The historical pollen assemblages at Tsambagarav are clearly distinct from those from Belukha glacier in the Russian Altai ca. 320 km northwest (Fig. 1A; Eichler et al., 2011). This finding suggests little overlap of the two glacier pollen catchments. Based on the pollen composition in the top sample of Tsambagarav and its comparison with vegetation composition in the study area (e.g. Walter, 1974; Gunin et al., 1999) we assume that the Tsambagarav pollen signal derives from a catchment of ca. 60–200 km around the site, most likely with a strong northwest bias and with only occasional pollen grains deriving from longer distances.

4.2. Vegetation history

Six statistically significant local pollen assemblage zones (LPAZ)

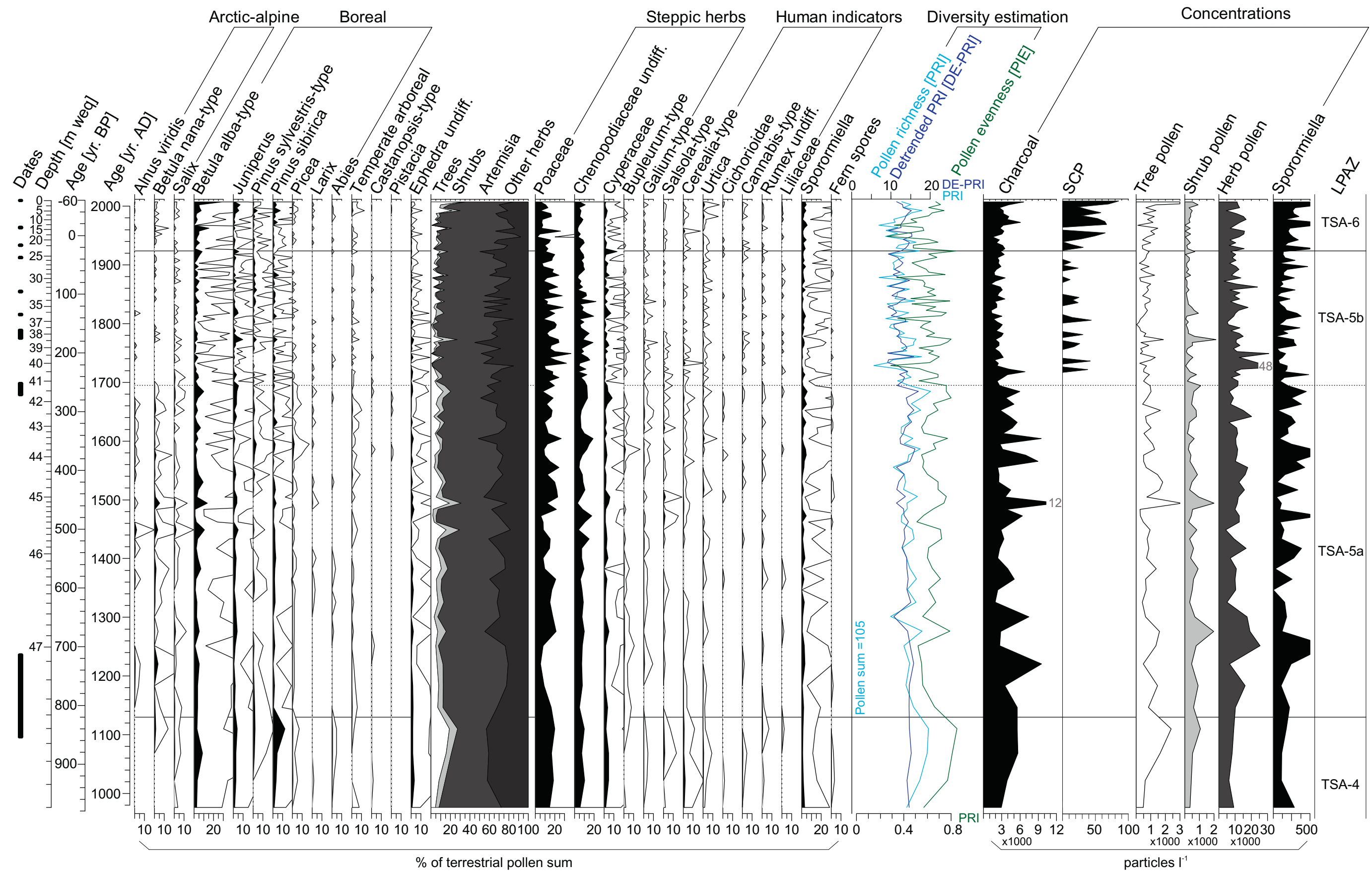

Fig. 3. Percentage diagram of Tsambagarav ice core for the past millennium. Selected pollen types, fern spores, coprophilous fungal spores based on the terrestrial pollen sum. Temperate arboreal summary curve consists of *Fagus*, *Corylus*, *Quercus,* and other temperate arboreal taxa. Hollow curves = 10 × exaggeration. Diversity estimation based on a minimum pollen sum of 105 for pollen richness (PRI; Birks and Line, 1992), evenness-detrended pollen richness (DE-PRI; Colombaroli and Tinner, 2013), and evenness index (PIE; Hurlbert, 1971). Concentrations of charcoal, SCP (spheroidal carbonaceous particles), pollen, and *Sporormiella* in particles l^{-1}. LPAZ = statistically significant local pollen assemblage zones, dashed line not statistically significant. Chronology, presented ^{14}C-dates, and reference horizons (volcanic layers, drilling year, and tritium peak) according to Herren et al. (2013). (For interpretation of the references to colour in this figure legend, the reader is referred to the web version of this article.)

were identified along the palynological record (Figs. 2–3). We additionally divided TSA-3 and TSA-5 in two non-significant subzones a and b. Results are presented as pollen percentages and pollen concentrations (around 10,000 grains l^{-1} except the period 2900–1800 BC (zone TSA-3a) with low concentrations < 2000 grains l^{-1}).

Pollen data in zone TSA-1 (3500–3100 BC) indicate that the vegetation was dominated by herbaceous steppe communities, mainly composed of *Artemisia* (80%) with Poaceae, Chenopodiaceae and other taxa growing in dry *Stipa-Artemisia* steppe communities (e.g. *Cyperaceae*, *Bupleurum*-type, *Galium*-type; Fig. 2). The pollen record indicates that *Salsola*, a key taxon of semi-desert environments occurring i.e. in sheltered valleys (Walter, 1974), was also present. AP percentages are low (0–10%) and mainly composed of *Betula alba-type* and the dry adapted taxon *Ephedra* with single pollen grains of *Pinus sylvestris*-type and *Pinus sibirica*. The conifer pollen suggests either presence of single conifers in locally favorable spots in the herbaceous steppe or long-distance pollen transport.

Tree pollen percentages reach highest peaks between 3000 and 1800 BC (up to 50%; LPAZ TSA-2–TSA-3a; Fig. 2) indicating afforestation pulses in the steppes possibly resulting from moister and/or warmer conditions. *Betula alba*-type percentages (30%) as well as tree pollen concentration peaks around 3000 and 1900 BC hint to periods with propitious environmental conditions that allowed expansion of the pioneer species. Pollen of the arctic-alpine shrub taxa *Betula nana*-type and *Salix*, as well as *Juniperus* reaches highest percentages of the entire record during this phase. This suggests an upward expansion of alpine tundra vegetation to altitudes higher than 3000 m a.s.l., which is today's upper altitudinal limit of alpine tundra shrubs such as *Salix glauca* and *Betula nana* ssp. *rotundifolia* in the area (Walter, 1974; Gunin et al., 1999). The second tree pollen peak between 2400 and 2100 BC is marked by an initial rise of *Betula alba*-type (20%) followed by a second phase where pollen percentages of *Pinus sibirica*, *Picea*, *Larix*, *Abies*, and *Alnus viridis* increase, indicating a succession from primary *Betula pendula*-dominated forests to more diverse secondary forests and green alder thickets (Fig. 2). The rise of pollen from temperate trees (mainly *Quercus*, *Corylus* and *Fagus*) to 5% may indicate a stronger influence of southern airmasses since the closest occurrence of these taxa is in China (Wu and Raven, 1999). The forest expansions coincided with a spread of ferns (maximum fern spore percentages of the record). This period is further characterized by the lowest pollen concentrations of the entire record (< 2000 grains l^{-1}) that indicate diluted microfossil concentrations possibly caused by higher ice accumulation rates due to moister environments (Fig. 2, Herren et al., 2013).

AP decreases stepwise at ca. 1800 BC, 800 BC, 1100 AD, and 1700 AD (LPAZ TSA-3b–TSA-5b), pointing to several forest or arboreal vegetation retraction phases in the areas northwest and north of Tsambagarav. Dry *Stipa-Artemisia* steppe (e.g. Poaceae, *Artemisia*) as well as desert-steppe communities (e.g. increasing Chenopodiaceae and *Salsola*-type percentage values, Figs. 2–3) expanded. The tree diebacks are defined by LPAZ boundaries indicating significant shifts in the vegetation around the glacier. A short-term *Pinus sibirica* pollen increase between 900 and 1100 AD (defined by LPAZ TSA-4) hints to a

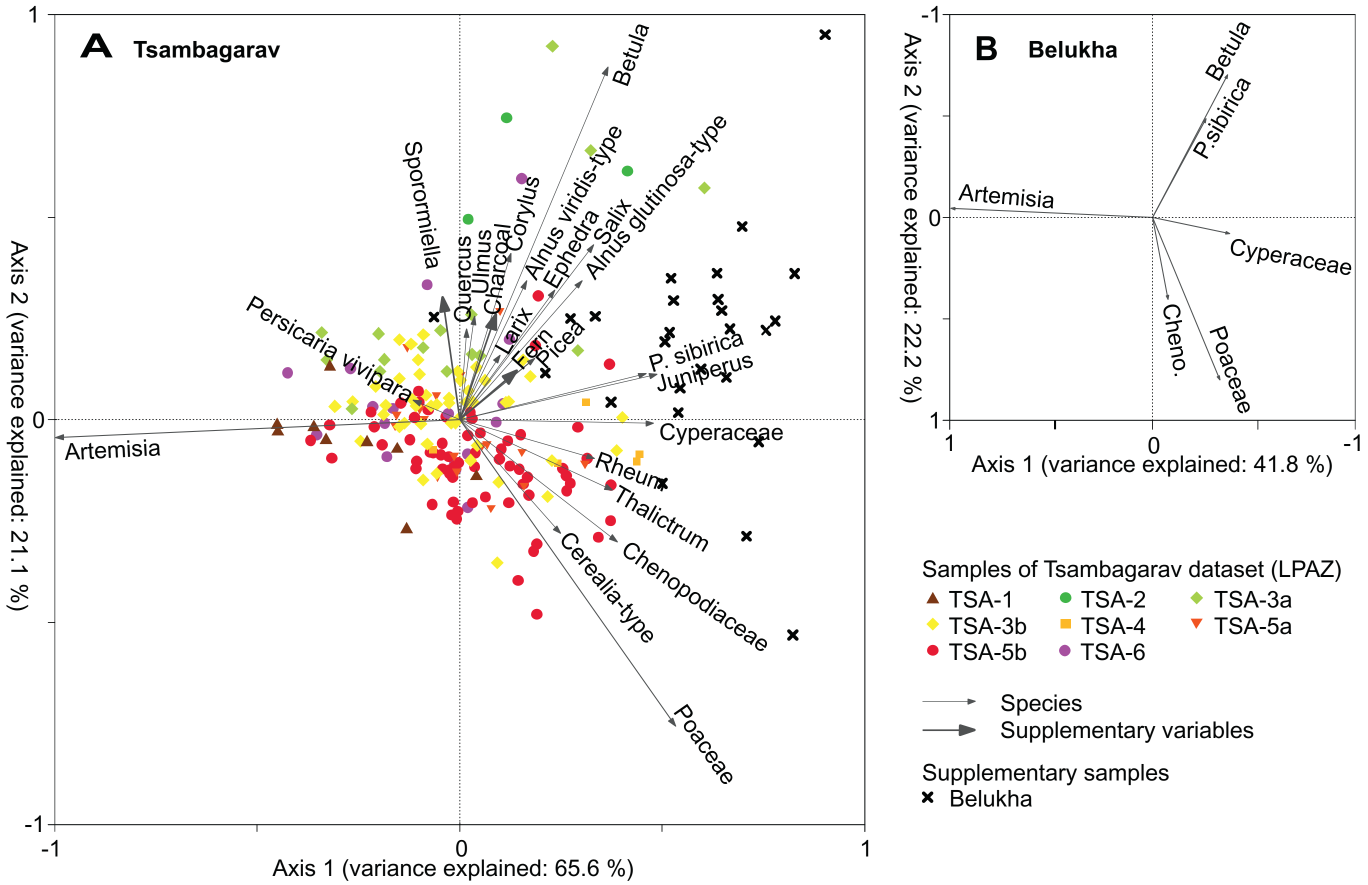

Fig. 4. Principle component analysis (PCA) for pollen percentages of Altai glacier records. Panel A: PCA for the Mongolian Altai (Tsambagarav glacier) today surrounded by open steppes with only relict forest patches, spanning 3500 BC–2009 AD. Sample scores with different symbols for the corresponding local pollen assemblage zone (LPAZ), selected species scores (black arrows corresponding to pollen types) indicate vegetation composition changes for sample scores from boreal forest (e.g. *Pinus cembra*) to less dry (e.g. *Artemisia*) and arid steppes (e.g. Chenopodiaceae). Selected supplementary variables (gray arrows, *Sporormiella* and fern spores as percentages of the terrestrial pollen sum [%], charcoal concentrations [particles l^{-1}]). Russian Altai (Belukha glacier) today with abundant boreal forests, spanning 1250–2001 AD. Sample scores of Belukha glacier (black cross symbols) are plotted as supplementary data not influencing the ordination of Tsambagarav glacier. The PCA results underline the similarity of mid-Holocene forest communities in the Mongolian Altai with historical and modern boreal forests in the Russian Altai. Panel B: Selected species scores for the Belukha dataset. Selected species scores for the Russian Altai show a close relationship with species scores from the Mongolian Altai (Panel A). Taken together this finding underscores the vulnerability of extant Central Asian forests to current and future climate change. Specifically, future vegetation dynamics in the Russian Altai may follow past climate impact trajectories in the Mongolian Altai, from forested (positive scores) to steppic communities (negative scores) along PCA axis 1. (For interpretation of the references to colour in this figure legend, the reader is referred to the web version of this article.)

temporary establishment of the species in the catchment. Maximum landscape openness was reached after 1700 AD (AP < 10%; Fig. 3). AP rises noticeably during LPAZ TSA-6 (1960–2009 AD), which is mainly due to increasing *Betula alba*-type and indicates rapid spreads of pioneer trees.

The presence of Cerealia-type is interpreted as a primary indicator for farming activities if associated with other pollen indicative of land use (e.g. *Linum usitatissimum, Plantago lanceolota*; Lang, 1994). Association with other adventive pollen (or less ideal apophytes pollen) is needed, because in entire Eurasia Cerealia-type pollen is occasionally produced by wild grass species (Beer et al., 2007; Van Zeist et al., 2016), e.g. by *Trisetum spicatum*, a common wild grass species of the Mongolian mountain steppes (Walter, 1974). Secondary anthropogenic pollen indicators such as *Rumex crispus* (*R. acetosa*-type), Cichorioideae, *Urtica,* and Liliaceae prefer nutrient enriched former campsites suggesting pastoralism activities, although they may occasionally also occur naturally on humid and nutrient-rich soils in the Mongolian Altai (Gunin et al., 1999). Thus, the presence and in particular the combined increase of these indicators (Fig. 2) might point to land use activities in the Mongolian Altai after 3500 BC. Cerealia-type pollen occurs regularly after 2000 BC and reaches a maximum around 1000 AD, often in combination with *Urtica, Rumex,* and Liliaceae. Cerealia-type pollen rises again around 1700 AD, and after 1700 AD *Urtica*, *Cannabis*-type, and *Rumex* percentages increase indicating intensified pastoralism activities (Gunin et al., 1999).

Dung fungal spores of *Sporormiella* are continuously present in large quantities along the entire record indicating continuous herbivore grazing in the steppes. The *Sporormiella* record suggests that herbivore grazing activities reached a maximum during the afforestation phase (20% around 2200 BC). Increased grazing activity was possibly released by an enhanced productivity of the steppes related to increasing moisture, or less likely, by favorable (humid) conditions for fungi growth and spore production. As observed for pollen, *Sporormiella* concentration values remain low due to increased ice accumulation rates. The *Sporormiella* concentrations rise slightly after 1600 AD, which might be related to intensified herding activities over the past centuries.

4.3. Diversity and ordination analysis

In a large pollen catchment such as Tsambagarav that includes a wide range of habitats, pollen richness is rather related to ecosystem diversity and thus the number of habitats, than to floristic diversity

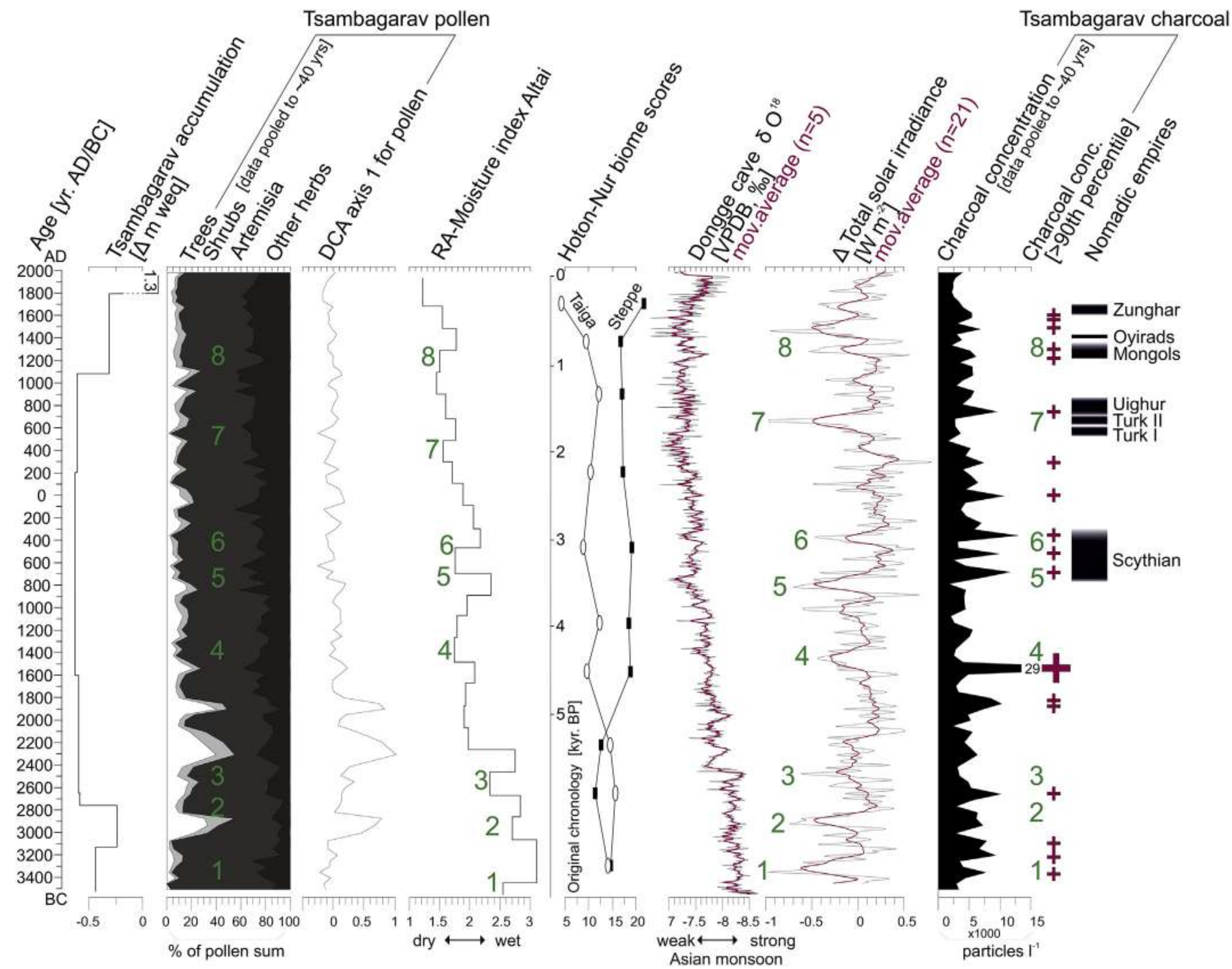

Fig. 5. Comparison of the palynological record from Tsambagarav with regional and climate records. From left: Tsambagarav ice accumulation rate (anomaly from the mean of the past 6000 years, Herren et al., 2013), Tsambagarav vegetation reconstruction (summary curve for pollen, DCA-axis 1, correlation with arboreal pollen percentages $r = 0.95$; this study), regionally-averaged moisture index for the Altai Mountains based on pollen records (Wang and Feng, 2013), biome scores from Hoton Nur with original chronology adjusted (Tarasov et al., 2000; Rudaya et al., 2009), Asian monsoon reconstruction from Dongge cave (Wang et al., 2005), solar activity fluctuation reconstruction based on ^{10}Be measurements in polar ice (Steinhilber et al., 2009), Tsambagarav fire reconstruction (charcoal concentrations, this study) and selected nomadic empires (Rogers, 2012). Green numbers indicate climatically induced forest minima phases at Tsambagarav. (For interpretation of the references to colour in this figure legend, the reader is referred to the web version of this article.)

within plant communities. Low PIE values (< 0.5) throughout the sequence follow PRI suggesting that species evenness was constantly low. However, evenness reconstructions were possibly affected by the large *Artemisia* portions, a pollen taxon that is commonly overrepresented in steppic ecosystems (Liu et al., 1999) and prevails over the entire record (Figs. 2–3). PRI and DE-PRI remain low until 3000 BC (PRI ca. 5–15, DE-PRI ca. 10), followed by an increase (PRI max. 20–30, DE-PRI 15) between 3000 and 2400 BC when AP percentages are peaking. Given that pollen richness is correlated with AP ($r = 0.64$, Figs. 2–3) it is likely that forest expansions contributed to increasing diversity. After the forest retreat at 1800 BC, diversity remained at intermediate levels (PRI ca. 10–20, DE-PRI ca. 10–15) until 1700 AD. Higher diversity in the younger steppes (pre-3000 BC vs. post-1800 BC) was possibly related to reorganizations to grassy steppe communities (e.g. Poaceae increase; Fig. 3). Palynological diversity drops to low values after 1700 AD (PRI and DE-PRI around 10) suggesting a further decline of diversity perhaps related to intensified herding (e.g. *Sporormiella* rise).

The sample distribution on the PCA axes 1 and 2 (Fig. 4A) shows a large LPAZ overlap with only minor vegetation changes over the past five millennia. Samples of LPAZ TSA-1 and TSA-6 vs. TSA-4 are separated along axis 1 and samples of LPAZ TSA-2 and TSA-3a are shifted along axis 2, reflecting variations in the vegetation composition between different steppe communities and boreal forests over time. A very high share (66%) of the variance is explained by axis 1, which splits mainly moist steppe communities (*Artemisia*, *Persicaria vivipara*) from the rest: dry steppic (Chenopodiaceae, *Rheum*, Poaceae), cryophilous alpine *Kobresia*-meadow (e.g. *Cyperaceae*) and rather mesophilous boreal forests (e.g. *Betula*, *Pinus sibirica*). Axis 2 explains another 21% of the variance and separates dry grass steppe (e.g. Poaceae, Chenopodiaceae, *Thalictrum*) from cryophilous, mesophilous and rather thermophilous communities: tundra shrublands (e.g. *Alnus viridis*), boreal (*Picea, Larix, Betula*) and nemoboreal or temperate (e.g. *Ulmus*, *Quercus*, *Corylus*) arboreal taxa. Thus, both axes may indicate aspects related to moisture availability and associated temperatures, such as steppic species composition (e.g. *Artemisia* vs. Chenopodiaceae and Poaceae for axis 1) and biomass or biome allocation (steppic vs. boreal or nemoboreal) for axis 2.

PCA for the Belukha samples (Fig. 4B) reveals that the Tsambagarav results are reproducible in the Russian Altai. Axis 1 explains 42% of the variance separating *Artemisia* from dry steppic *Stipa*-communities (e.g. Poaceae, Chenopodiaceae) and axis 2 explains 22% separating dry steppes from boreal forests (*Betula*, *Pinus sibirica*). The compositional similarities between the two PCA suggests moisture availability and less important temperature as drivers of vegetation change. If combined (Fig. 4A) Russian Altai sample scores group in one edge of Axis 1, along an axis 2 gradient. The sample score comparison suggests a high similarity of Belukha with Tsambagarav during the afforestation phase 3000–1800 BC (TSA-2–TSA-3a). The ordination clearly separates modern Tsambagarav (TSA-6) and Belukha samples probably because of moisture-related differences and different anthropogenic influence on both, Mongolian and Russian Altai plant communities.

4.4. Fire and industrial pollution history

The average charcoal concentration in the upper firn (ca. 6,000 particles l^{-1} for the period 2009–2005 AD) corresponds to a microscopic charcoal influx of ca. 200 particles $cm^{-2}\,year^{-1}$ or $0.085\,mm^2\,cm^{-2}\,year^{-1}$ (Tinner and Hu, 2003), which is extremely low if compared to sediment records (Adolf et al., 2017). Charcoal concentrations reveal no major fire activity trend between 3500 BC and 1700 AD with an average of ~5,000 particles l^{-1}. A single outstanding charcoal peak around 1540 BC (29,000 particles l^{-1}) suggests a short phase of major fire activity ca. 250 years after a major forest decline. Other charcoal-concentration inferred fire-activity peaks (> 90-percentile ≥7,300 particles l^{-1}; Figs. 2–3) also occurred following forest declines (e.g. ~2650 BC ca. 150 years after the forest decline around 2800 BC), suggesting that collapses of boreal taxa provided dead biomass and thus fuel for fire activity (De Groot et al., 2000; Eichler et al., 2011; Tinner et al., 2015; Kuuluvainen et al., 2017). Charcoal concentrations remain low after 1700 AD with an average of ~2,600 particles l^{-1} and no peaks > 90-percentile indicating minimal fire activity when herbaceous steppe ecosystems were dominant. However, microscopic charcoal hints to minor increase of fire activity after 1960 AD. Charcoal concentration as supplementary variable in the PCA (Fig. 4) groups with AP, again suggesting biomass availability as an important factor for burning.

First SCP occur around ca. 1720 AD at the beginning of zone TSA-5b (Fig. 3). Those scattered but frequent particles indicate initial atmospheric pollution, possibly deriving from early industrialization and mining activities (Naumov, 2006). Regionally, they coincide with minimum fire activity and maximum landscape openness, indicating a possible shift from solely timber-based to increasingly fossil fuel-based energy consumption, perhaps motivated by limited timber availability. SCP rise after 1920 AD, suggesting amplified industrial air pollution during the 20th century. A first concentration peak around 1960 AD with 80 particles l^{-1} and a second maximum around 2000 AD (100 particles l^{-1}) coincide with highest charcoal concentration values (6,000 particles l^{-1}) during the 20th century.

5. Discussion

5.1. Fire and fuel dynamics during the past 5000 years

Tsambagarav receives ca. 200 microscopic charcoal particles $cm^{-2}\,yr^{-1}$ today, which is in the same order of magnitude as Belukha glacier 320 km northwest in the Russian Altai (150 particles $cm^{-2}\,yr^{-1}$; Eichler et al., 2011) at a similar altitude (4062 m a.s.l.). Charcoal influx values at Belukha are ca. 40 times lower than at nearby Teletskoye Lake at 1900 m a.s.l. (8,200 particles $cm^{-2}\,yr^{-1}$; Andreev et al., 2007). The influx difference between glaciers and neighboring lake sediment archives is best explained by the remoteness of the glaciers and the limited vertical atmospheric transport to the high elevation ice core sites (Gilgen et al., 2018). To our knowledge, no microscopic charcoal records from the Mongolian Altai are available. Local fire reconstructions are based on macroscopic charcoal and cover the past millennia (Umbanhowar Jr et al., 2009; Unkelbach et al., 2018). Despite the spatio-temporal variability their reconstructed fire signal corresponds to our regional fire activity peaks from Tsambagarav (microscopic charcoal peaks > 90-percentile, Fig. A1), if dating uncertainties are considered. Recent calibration studies at the continental scale showed that micro- and macroscopic charcoal have very similar spatial proveniences spanning a radius of about 40 km around sedimentary sites (Adolf et al., 2017). Glaciers on the other hand act as a regional to subcontinental archive of biomass burning, integrating fire activity over larger spatial scales (Legrand et al., 2016). Very high concentrations > 20,000 particles l^{-1} suggest that the fire activity peak in the Tsambagarav record around 1500 BC was comparable to the maximum burning of the past 800 years that occurred around 1600 AD at Belukha glacier in the Russian Altai (Fig. A2). The 1500 BC maximum fire phase in the Tsambagarav record may chronologically correspond to the late-Holocene fire activity peak at Zagas Nur around 20 km southwest of Tsambagarav (Umbanhowar Jr et al., 2009) where it is dated to 1400 BC, while at Doroo Nur (50 km south) fire activity was only moderate around 1500 BC. As the fire peak does not occur in more distant records from western Mongolia (Fig. A1; Umbanhowar Jr et al., 2009) we assume that burning might have been localized close to the glacier (20–40 km) or located north or northwest.

Increased fire activity at Tsambagarav was related to declines of boreal tree stands or forests that likely provided fuel for burning (Fig. 5), similarly to what was found at Belukha (Eichler et al., 2011). There, a dry period inducing forest diebacks was succeeded by maximum fire activity around 1600 AD (Fig. A2), a period with increased fire activity also in the Tsambagarav area (three consecutive charcoal peaks > 90-percentile; Fig. 5) and in the Eurasian Arctic (Akademii Nauk ice record; Grieman et al., 2017). Lacking biomass availability combined with low temperatures during the Little Ice Age period may explain the fire minimum at 1700–1960 AD when maximum vegetation openness is documented in the pollen record of Tsambagarav and at adjacent sites (Fig. 5; Umbanhowar Jr et al., 2009, Unkelbach et al., 2018). Finally, the past four decades of the Tsambagarav record suggest again a slight increase of regional and local fire activity possibly caused by increased biomass availability due to pioneer birch tree expansions.

5.2. Composition, successional dynamics, and diebacks of the mid-Holocene forests

Our high-resolution record from Tsambagarav provides a unique chronological control in combination with high-temporal and continuous sampling resolution and is therefore suited to assess rapid ecosystem responses to climate change. The Tsambagarav record suggests that the Mongolian Altai experienced several prominent forest contraction and expansion phases before 1800 BC. The magnitude and fluctuation pattern of this early phase are comparable to the pattern observed for the past 800 years in the Russian Altai (Eichler et al., 2011). There, mixed *Pinus sibirica-Larix sibirica* stands form a dense forest belt between 1000 m a.s.l. and the timberline around 2000 m a.s.l., in which *Abies sibirica* and *Picea obovata* co-occur in areas where soil moisture is sufficient (Eichler et al., 2011). Below this belt *Betula pendula* and *Pinus sylvestris* form boreal forests (Walter, 1974). The forests in the Russian Altai produce a pollen signal, which is comparable to that of the Tsambagarav record during the period 3000–1800 BC (Figs. 4 and A2). The Belukha pollen assemblage is mainly composed of *Pinus sibirica* and *Betula* with only single *Larix* grains despite its importance in the vegetation (Eichler et al., 2011). Scattered *Larix* pollen in the Tsambagarav record may thus suggest that *Larix sibirica* was an important forest element during the afforestation phases in the Mongolian Altai. This similarity is striking, given that nowadays *Larix sibirica* and *Pinus sibirica* form only relict and discontinuous forest belts in the northern part of the Mongolian Altai and *Abies sibirica* has completely vanished (Walter, 1974; Gunin et al., 1999).

The multiproxy Belukha record suggests that forest diebacks in the Russian Altai were induced by severe drought decades resulting in enhanced fire risk and that forests recovered rapidly after moisture re-increased (Eichler et al., 2011). The repeated forest contractions at Tsambagarav followed by *Artemisia* steppe expansions indicate similar vegetation responses to moisture variability. Forest recoveries similar to the Russian Altai ended 1800 BC. This is in line with regional sedimentary pollen records showing consistent deforestation in the Mongolian Altai during the mid- to late-Holocene. For instance, pollen-inferred vegetation reconstructions from Hoton Nur point to taiga forest contractions between 3000 and 2000 BC (Fig. 5; Rudaya et al., 2009) to never recover again. At Bayan Nur forests contracted around 1500 BC, in the Dayan Nur region around 650 BC and in the Achit Nur area between 4000 BC and 200 AD (Gunin et al., 1999; Sun et al., 2013; Unkelbach et al., 2018). Diachronic forest diebacks suggest that moisture thresholds for forest growth were underrun in different periods in the Mongolian Altai. Specifically, local forest persistence until about 800 BC, 1200 AD, and 1700 AD indicates that decreasing moisture effects on forests endured until modern times, resulting in stepwise forest and tree stand disruptions. These late-Holocene dynamics occurred also at larger distances, e.g. at Akkol Lake (ca. 190 km) in the northern Tuva region after 1000 BC (Blyakharchuk et al., 2004; Fig. 1A) suggesting that forests contracted also far north of the Mongolian Altai in response to moisture reductions. However, chronological uncertainties as resulting from few ^{14}C-dates from bulk sediments (see Rey et al., 2018) and a general lack of ^{14}C-dates in the mid- to late-Holocene (Gunin et al., 1999; Sun et al., 2013) impede precise assessments of the deforestation timing at individual sites.

5.3. Climate-driven pulses of steppe expansions and human impact after 1800 BC

Hunter and gatherer communities inhabited the Altai region since the early-Holocene (Volkov, 1995; Hauck et al., 2012), and nomadic herders were present since at least 1000 BC (Fig. 5; Fernández-Giménez, 1999; Rogers, 2012; Rudaya et al., 2008), but their impact on the natural vegetation is supposed to be minor (Bourgeois et al., 2007; Rudaya et al., 2009). We thus assume that natural climate change, such as aridity and/or cooling, was the main forcing of repeated forest contractions and subsequent herbaceous steppes expansions during the late-Holocene (Schlütz et al., 2008). A pollen-based moisture index derived from other sites in the Mongolian Altai (Wang and Feng, 2013) was previously interpreted as a proxy for the Asian summer monsoon strength (Fig. 5). This index is driven by the same factors as our pollen data and is therefore not an independent climatic proxy and indeed its course is in line with our ecological interpretation, thus indicating similar moisture trends across sites. The vegetation-based reconstructions are in good agreement with mid-Holocene climate model simulations for Asian monsoon strength (Harrison et al., 2016) and with pollen-independent oxygen isotope records (e.g. Dongge cave record; Fig. 5; Wang et al., 2005; Wang and Feng, 2013) that suggest declining moisture availability in the Mongolian Altai in response to a weakening of monsoon activity resulting from changes of orbital forcing during the late-Holocene. Reduced monsoon sources of moisture as a possible cause for deforestation at Hoton Nur was proposed by Rudaya et al. (2009). Although our Tsambagarav vegetation and fire record begins at 3500 BC when monsoon had already started to weaken (Wang et al., 2005), we assume that the progressive late-Holocene reduction of subtropical air-masses resulted in strong moisture oscillations that may have resulted in flickering of forest ecosystems before their final collapse at ca. 1800 BC (Dakos et al., 2013).

The Tsambagarav record suggests that the long-term tree contraction in the Mongolian Altai continued stepwise after 1800 BC to reach its apex only 300–200 years ago. Contractions of forest ecosystems were possibly induced by climate variability related to e.g. solar activity changes (Eichler et al., 2009; Steinhilber et al., 2009; Roth and Joos, 2013). For instance, the forest minima around 3400 BC, 2800 BC, 2500 BC, 800–400 BC, 500 AD, and 1200 AD might have been related to dry cooling events (Fig. 5) as partly recorded regionally (e.g. the 4.2 kyr cool and dry period; Staubwasser and Weiss, 2006; Dixit et al., 2014), in other Northern Hemisphere records from the Alpine region and Alaska (Haas et al., 1998; Tinner et al., 2015) or in the reconstructed global surface air temperature (Roth and Joos, 2013).

During the past decades, climate proxies suggest reversing climate trends with warming (e.g. Eichler et al., 2009; Roth and Joos, 2013) and re-strengthening of the Asian monsoon (e.g. reconstructed from Dongge cave isotope record; Wang et al., 2005). In contrast, after the end of the Little Ice Age at ca. 1850 AD (Eichler et al., 2011) tree stands in the Mongolian Altai did not recover suggesting a decoupling of vegetation dynamics from climate, e.g. due to increasing human activities. The historical onset of larger-scale smelting in the Altai dates to 1729 AD (Naumov, 2006) coinciding with the beginning of the industrial pollution signal in our ice record as documented in SCPs (Fig. 3). The related energy requirements induced increasing human pressure not only on the Russian Altai forests but also on the remaining tree stands in the Mongolian Altai until 1960 AD (Lkhagvadorj et al., 2013), likely shifting the lower tree line upwards (Dulamsuren et al., 2014). Thus, human activities altered vegetation responses to climate. The Tsambagarav record suggests that industrial pollution remained high after 1960 AD and only pioneer *Betula pendula* may have very recently recovered, when fossil fuel-based energy consumption (e.g. coal or diesel-consuming engines for heating, transportation or water-supply) increased, relieving pressure on woody stands (Fernández-Giménez, 1999).

5.4. Altai ecosystems under future climate change

Past vegetation dynamics suggest that warmer and moister conditions during the mid-Holocene allowed boreal forest establishments in the Tsambagarav area in the Mongolian Altai. These forests collapsed around 1800 BC. Subsequently, further stepwise tree reductions and a gradual shift to more dry adapted steppe communities occurred likely in response to drying and cooling during the late-Holocene. Future climate projections for continental areas propose further warming and drying in the coming decades for the Altai Region (Sato et al., 2007; Tchebakova et al., 2009; Dai, 2011; Collins et al., 2013; Dulamsuren et al., 2014; IPCC, 2014; Lehner et al., 2017). In agreement, during the past decades, the Mongolian Altai experienced significant warming and increasing numbers of drought periods. Precipitation more often included heavy rainfall events that are only partly beneficial for vegetation (D'Arrigo et al., 2001; Dulamsuren et al., 2010; Lkhagvadorj et al., 2013). Other areas in Mongolia and southern Siberia also experienced climate warming and moisture decrease, probably affecting tree growth and hindering forest regeneration (Allen et al., 2010; Tsogtbaatar, 2013; Dulamsuren et al., 2014; Xu et al., 2017). If future climate projections are correct about declining moisture availability, the persisting forest patches and belts in the Mongolian, Russian Altai, and other dry areas of Central Asia will be strongly affected. For instance, forest boundaries might shift north of the Russian Altai releasing unprecedented forest collapses in response to increasing drought. The available fire histories from ice core records from the Russian and Mongolian Altai also suggest that fire incidence may increase where biomass is not limiting burning (Eichler et al., 2011; Hessl et al., 2016). This interpretation of the paleo record agrees with modern observations indicating a significant link between dry conditions and fire activity (Tsogtbaatar, 2013; Ponomarev and Kharuk, 2016). Thus, fire may exacerbate the effects of future climate change on vegetation, especially if associated to high grazing pressure (Tsogtbaatar, 2004; Hauck et al., 2014; Ponomarev and Kharuk, 2016).

In the past, when climate forcing was natural, warm conditions were in this region usually accompanied by increases in moisture availability, likely deriving from increased monsoonal and/or westerly wind activity that promoted forest growth. Despite many projection efforts and progresses, the magnitude of global warming and in particular of precipitation changes remains ambiguous (Braconnot et al., 2012). Future projections may underestimate moisture availability in continental areas (Berg et al., 2017), as for example, northern hemisphere monsoon simulations for the mid-Holocene underestimate its magnitude (Braconnot et al., 2012; Harrison et al., 2015). If moisture should unexpectedly increase with future warming as it did during the early and mid late-Holocene, forests may thus persist and perhaps even expand in the Mongolian Altai, as they did during the period 3000–1800 BC, at least if human pressure will not become excessive.

6. Conclusions

The Tsambagarav record demonstrates for the first time the ecological potential of ice palynology, specifically, based on its high chronological resolution and precision, it provides novel insights into past fire, vegetation, and land use dynamics in the Mongolian Altai region. Late-Holocene vegetation reorganizations in response to climate and moisture availability changes underscore the vulnerability of forest ecosystems that are still thriving in the Mongolian or Russian Altai. We conclude that precipitation regime changes were the main driver for forest diebacks ca. 4700–4000 years ago and their final collapse ca. 3800 years ago in the Tsambagarav area. The lacking resilience of forest communities (e.g. *Pinus sibirica-Larix sibirica* stands) to moisture changes emphasizes the vulnerability of forests in other dry areas of Central Asia, if global warming will be associated to moisture declines as anticipated by future scenarios (IPCC, 2014). To better assess past vegetation and forest fire dynamics, new high-resolution and -precision multiproxy studies from natural archives are urgently needed. Such studies may help to disclose the mechanisms and processes behind the vulnerability of plant species and communities. Ultimately, they are thus essential to improve our knowledge of future ecosystem responses to global change.

Data availability

All data will be deposited in the Alpine Palynological Database (ALPADABA) and the Neotoma database (www.neotomadb.org).

Declarations of interest

None.

Acknowledgments

We are grateful to Ch.E. Umbanhowar for providing macroscopic charcoal data, to J.F.N. van Leeuwen for assistance with rare pollen type analysis, to J. Unkelbach from University of Göttingen for valuable discussions, to the Russian Federation for support with the international drilling campaign, and to the ice drilling crew. We thank H. Behling and an anonymous reviewer for constructive remarks that substantially improved the manuscript. We acknowledge the Sinergia project Paleo fires from high-alpine ice cores funded by the Swiss National Science Foundation (SNF grant 154450).

Appendix A

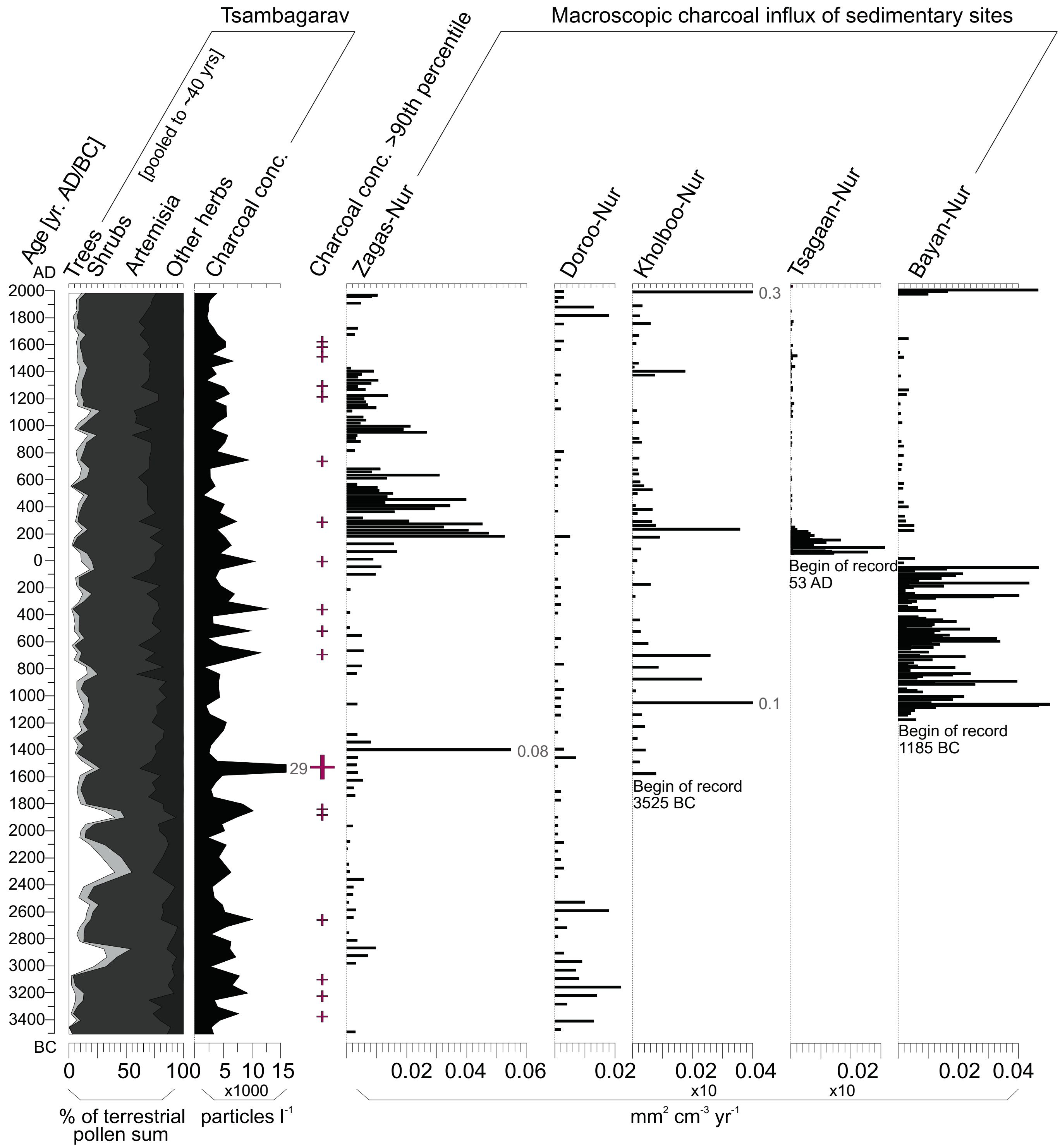

Fig. A1. Comparison of Tsambagarav vegetation and fire reconstructions (charcoal concentrations and charcoal concentrations exceeding 90-percentile of all samples) with local fire reconstructions (macroscopic charcoal influx of particles > 180 μm) from lakes in western Mongolia (Umbanhowar Jr et al., 2009) over the past 5500 years.

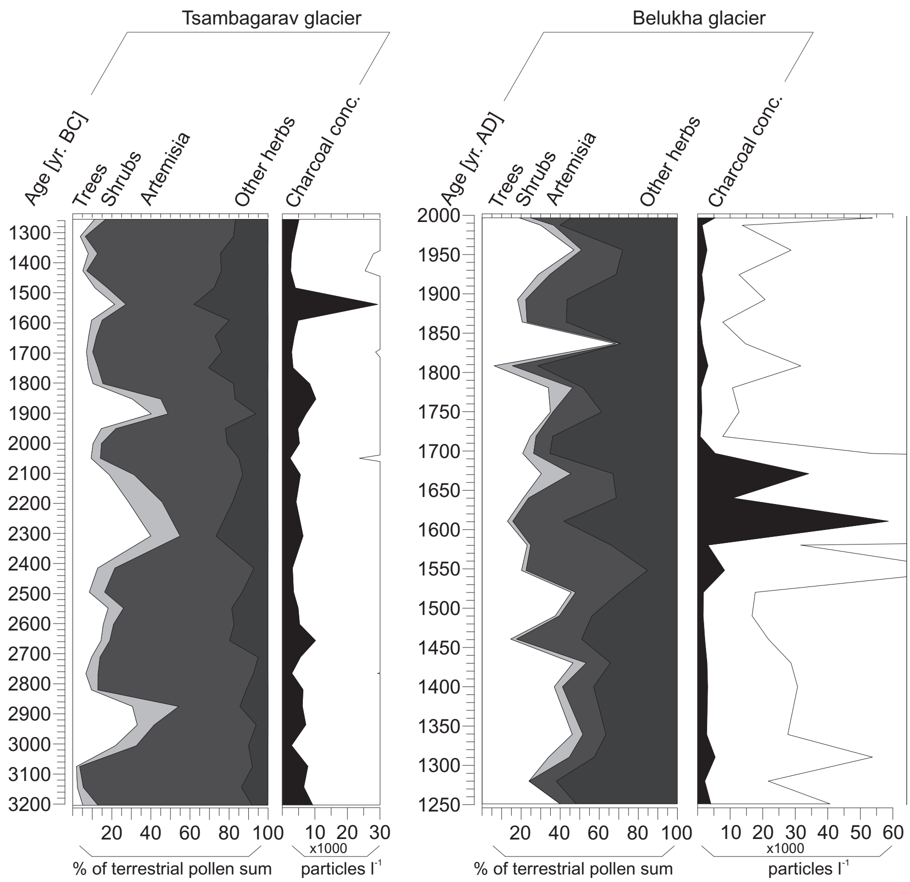

Fig. A2. Comparison of forest phases recorded in glacier archives in the Mongolian and Russian Altai. Left: Tsambagarav main pollen diagram (percentages) and charcoal concentrations (particles l^{-1}) during maximum afforestation (3000–1800 BC), right: Belukha main pollen diagram and charcoal concentrations 1250–1990 AD (Eichler et al., 2011). Hollow curves = 10× exaggeration.

References

Adolf, C., Wunderle, C., Colombaroli, C., Weber, H., Gobet, E., Heiri, O., van Leeuwen, J.F.N., Bigler, C., Connor, S.E., Gałka, M., La Mantia, T., Makhortykh, S., Svitavská-Svobodová, H., Vannière, B., Tinner, W., 2017. The sedimentary and remote-sensing reflection of biomass burning in Europe. Glob. Ecol. Biogeogr. 27, 199–212. https://doi.org/10.1111/geb.12682.

Allen, C.D., Macalady, A.K., Chenchouni, H., Bachelet, D., McDowell, N., Vennetier, M., Kitzberger, T., Rigling, A., Breshears, D.D., Hogg, E.H., Gonzalez, P., Fensham, R., Zhang, Z., Castro, J., Demidova, N., Lim, J.-H., Allard, G., Running, S.W., Semerci, A., Cobb, N., 2010. A global overview of drought and heat-induced tree mortality reveals emerging climate change risks for forests. For. Ecol. Manag. 259 (4), 660–684. https://doi.org/10.1016/j.foreco.2009.09.001.

Andreev, A.A., Pierau, R., Kalugin, I.A., Daryin, A.V., Smolyaninova, L.G., Diekmann, B., 2007. Environmental changes in the northern Altai during the last millennium documented in Lake Teletskoye pollen record. Quat. Res. 67 (3), 394–399. https://doi.org/10.1016/j.yqres.2006.11.004.

Beer, R., Heiri, O., Tinner, W., 2007. Vegetation history, fire history and lake development recorded for 6300 years by pollen, charcoal, loss on ignition and chironomids at a small lake in southern Kyrgyzstan (Alay Range, Central Asia). The Holocene 17 (7), 977–985. https://doi.org/10.1177/0959683607082413.

Bennett, K.D., 1996. Determination of the number of zones in a biostratigraphical sequence. New Phytol. 132 (1), 155–170. https://doi.org/10.1111/j.1469-8137.1996.tb04521.x.

Berg, A., Sheffield, J., Milly, P.C., 2017. Divergent surface and total soil moisture projections under global warming. Geophys. Res. Lett. 44 (1), 236–244. https://doi.org/10.1002/2016GL071921.

Beug, H.-J., 2004. 2004: Leitfaden der Pollenbestimmung für Mitteleuropa und angrenzende Gebiete. Pfeil, Munich.

Birks, H.-J., 1968. The identification of *Betula nana* pollen. New Phytol. 67 (2), 309–314. https://doi.org/10.1111/j.1469-8137.1968.tb06386.x.

Birks, H.J.B., Gordon, A., 1985. Numerical Methods in Quaternary Pollen Analysis. Academic Press, London.

Birks, H.J.B., Line, J.M., 1992. The use of rarefaction analysis for estimating palynological richness from Quaternary pollen-analytical data. The Holocene 2 (1), 1–10. https://doi.org/10.1177/095968369200200101.

Blyakharchuk, T.A., Wright, H.E., Borodavko, P.S., van der Knaap, W.O., Ammann, B., 2004. Late Glacial and Holocene vegetational changes on the Ulagan high-mountain plateau, Altai Mountains, southern Siberia. Palaeogeogr. Palaeoclimatol. Palaeoecol. 209 (1), 259–279. https://doi.org/10.1016/j.palaeo.2004.02.011.

Bourgeois, J., De Wulf, A., Goossens, R., Gheyle, W., 2007. Saving the frozen scythian tombs of the altai mountains (Central Asia). World Archaeol. 39 (3), 458–474.

Braconnot, P., Harrison, S.P., Kageyama, M., Bartlein, P.J., Masson-Delmotte, V., Abe-Ouchi, A., Otto-Bliesner, B., Zhao, Y., 2012. Evaluation of climate models using palaeoclimatic data. Nat. Clim. Chang. 2 (6), 417. https://doi.org/10.1038/nclimate1456.

Brugger, S.O., Gobet, E., Schanz, F., Heiri, O., Schwörer, C., Sigl, M., Schwikowski, M., Tinner, W., 2018. A quantitative comparison of microfossil extraction methods from ice cores. J. Glaciol. 64 (245), 432–442. https://doi.org/10.1017/jog.2018.31.

Chenlemuge, T., Hertel, D., Dulamsuren, C., Khishigjargal, M., Leuschner, C., Hauck, M., 2013. Extremely low fine root biomass in Larix sibirica forests at the southern drought limit of the boreal forest. Flora Morphol. Distrib. Funct. Ecol. Plants 208 (8-9), 488–496. https://doi.org/10.1016/j.flora.2013.08.002.

Clegg, B.F., Tinner, W., Gavin, D.G., Hu, F.S., 2005. Morphological differentiation of Betula (birch) pollen in northwest North America and its palaeoecological application. The Holocene 15 (2), 229–237. https://doi.org/10.1191/0959683605hl788rp.

Collins, M., Knutti, R., Arblaster, J., Dufresne, J.-L., Fichefet, T., Friedlingstein, P., et al., 2013. Long-term climate change: projections, commitments and irreversibility. In: Stocker, T.F., Qin, D., Plattner, G.-K., Tignor, M., Allen, S.K., Boschung, J. (Eds.), Climate Change 2013: The Physical Science Basis. Contribution of Working Group I to the Fifth Assessment Report of the Intergovernmental Panel on Climate Change. Cambridge University Press, Cambridge, United Kingdom and New York, NY, USA.

Colombaroli, D., Tinner, W., 2013. Determining the long-term changes in biodiversity and provisioning services along a transect from Central Europe to the Mediterranean. The Holocene 23 (11), 1625–1634. https://doi.org/10.1177/0959683613496290.

Conedera, M., Tinner, W., Neff, C., Meurer, M., Dickens, A.F., Krebs, P., 2009. Reconstructing past fire regimes: methods, applications, and relevance to fire management and conservation. Quat. Sci. Rev. 28 (5), 555–576. https://doi.org/10.1016/j.quascirev.2008.11.005.

Dai, A., 2011. Drought under global warming: a review. Wiley Interdiscip. Rev. Clim. Chang. 2 (1), 45–65. https://doi.org/10.1002/wcc.81.

Dakos, V., van Nes, E.H., Scheffer, M., 2013. Flickering as an early warning signal. Theor. Ecol. 6 (3), 309–317. https://doi.org/10.1007/s12080-013-0186-4.

D'Arrigo, R., Jacoby, G., Frank, D., Pederson, N., Cook, E., Buckley, B., Nachin, B., Mijiddorj, R., Dugarjav, C., 2001. 1738 years of Mongolian temperature variability inferred from a tree-ring width chronology of Siberian pine. Geophys. Res. Lett. 28 (3), 543–546. https://doi.org/10.1029/2000GL011845.
De Groot, R.C., Woodward, B., Hennon, P.E., 2000. Natural decay resistance of heartwood from dead, standing yellow-cedar trees: laboratory evaluations. For. Product J. 50, 53–59.
Dixit, Y., Hodell, D.A., Petrie, C.A., 2014. Abrupt weakening of the summer monsoon in northwest India∼ 4100 yr ago. Geology 42 (4), 339–342. https://doi.org/10.1130/G35236.1.
Dulamsuren, C., Hauck, M., Leuschner, C., 2010. Recent drought stress leads to growth reductions in *Larix sibirica* in the western Khentey, Mongolia. Glob. Chang. Biol. 16 (11), 3024–3035. https://doi.org/10.1111/j.1365-2486.2009.02147.x.
Dulamsuren, C., Khishigjargal, M., Leuschner, C., Hauck, M., 2014. Response of tree-ring width to climate warming and selective logging in larch forests of the Mongolian Altai. J. Plant Ecol. 7 (1), 24–38. https://doi.org/10.1093/jpe/rtt019.
Dulamsuren, C., Klinge, M., Degener, J., Khishigjargal, M., Chenlemuge, T., BatEnerel, B., Yeruult, Y., Saindovdon, D., Ganbaatar, K., Tsogtbaatar, J., Leuschner, C., Hauck, M., 2016. Carbon pool densities and a first estimate of the total carbon pool in the Mongolian forest-steppe. Glob. Chang. Biol. 22 (2), 830–844. https://doi.org/10.1111/gcb.13127.
Eichler, A., Olivier, S., Henderson, K., Laube, A., Beer, J., Papina, T., Gäggeler, H.W., Schwikowski, M., 2009. Temperature response in the Altai region lags solar forcing. Geophys. Res. Lett. 36 (1). https://doi.org/10.1029/2008GL035930.
Eichler, A., Tinner, W., Brütsch, S., Olivier, S., Papina, T., Schwikowski, M., 2011. An ice-core based history of Siberian forest fires since AD 1250. Quat. Sci. Rev. 30 (9), 1027–1034. https://doi.org/10.1016/j.quascirev.2011.02.007.
Fernández-Giménez, M.E., 1999. Sustaining the steppes: a geographical history of pastoral land use in Mongolia. Geogr. Rev. 89 (3), 315–342. https://doi.org/10.2307/216154.
Finsinger, W., Tinner, W., 2005. Minimum count sums for charcoal concentration estimates in pollen slides: accuracy and potential errors. The Holocene 15 (2), 293–297. https://doi.org/10.1191/0959683605hl808rr.
Gilgen, A., Adolf, C., Brugger, S.O., Ickes, L., Schwikowski, M., van Leeuwen, J.F.N., Tinner, W., Lohmann, U., 2018. Implementing Microscopic Charcoal Particles into a Global Aerosol-Climate Model. https://doi.org/10.5194/acp-2017-1116. (in press).
Golan-Goldhirsh, A., 2009. Bridging the gap between ethnobotany and biotechnology of Pistacia. Israel J. Plant Sci. 57 (1–2), 65–78.
Grieman, M.M., Aydin, M., Fritzsche, D., McConnell, J.R., Opel, T., Sigl, M., Saltzman, E.S., 2017. Aromatic acids in a Eurasian Arctic ice core: a 2600-year proxy record of biomass burning. Clim. Past 13 (4), 395. https://doi.org/10.5194/cp-13-395-2017.
Gunin, P.D., Vostokova, E.A., Dorofeyuk, N.I., Tarasov, P.E., Black, C.C. (Eds.), 1999. Vegetation Dynamics of Mongolia. Kluwer Academic Publishers, Dordrecht.
Haas, J.N., Richoz, I., Tinner, W., Wick, L., 1998. Synchronous Holocene climatic oscillations recorded on the Swiss Plateau and at timberline in the Alps. The Holocene 8 (3), 301–309. https://doi.org/10.1177/095968360708241 3.
Harrison, S.P., Bartlein, P.J., Izumi, K., Li, G., Annan, J., Hargreaves, J., Braconnot, P., Kageyama, M., 2015. Evaluation of CMIP5 palaeo-simulations to improve climate projections. Nat. Clim. Chang. 5 (8), 735. https://doi.org/10.1038/nclimate2649.
Harrison, S.P., Bartlein, P.J., Prentice, I.C., 2016. What have we learnt from palaeoclimate simulations? J. Quat. Sci. 31 (4), 363–385. https://doi.org/10.1002/jqs.2842.
Hauck, M., Javkhlan, S., Lkhagvadorj, D., Bayartogtokh, B., Dulamsuren, C., Leuschner, C., 2012. Edge and land-use effects on epiphytic lichen diversity in the forest-steppe ecotone of the Mongolian Altai. Flora-Morphol. Distribut. Funct. Ecol. Plants 207 (6), 450–458. https://doi.org/10.1016/j.flora.2012.03.008.
Hauck, M., Dulamsuren, C., Bayartogtokh, B., Ulykpan, K., Burkitbaeva, U.D., Otgonjargal, E., Titov, S.V., Enkhbayar, T., Sundetpaev, A.K., Beket, U., Leuschner, C., 2014. Relationships between the diversity patterns of vascular plants, lichens and invertebrates in the Central Asian forest-steppe ecotone. Biodivers. Conserv. 23 (5), 1105–1117. https://doi.org/10.1007/s10531-014-0648-z.
Heiri, O., Lotter, A.F., 2001. Effect of low count sums on quantitative environmental reconstructions: an example using subfossil chironomids. J. Paleolimnol. 26 (3), 343–350. https://doi.org/10.1023/A:1017568913302.
Henne, P.D., Elkin, C.M., Reineking, B., Bugmann, H., Tinner, W., 2011. Did soil development limit spruce (*Picea abies*) expansion in the Central Alps during the Holocene? Testing a palaeobotanical hypothesis with a dynamic landscape model. J. Biogeogr. 38 (5), 933–949. https://doi.org/10.1111/j.1365-2699.2010.02460.x.
Herren, P.A., Eichler, A., Machguth, H., Papina, T., Tobler, L., Zapf, A., Schwikowski, M., 2013. The onset of Neoglaciation 6000 years ago in western Mongolia revealed by an ice core from the Tsambagarav mountain range. Quat. Sci. Rev. 69, 59–68. https://doi.org/10.1016/j.quascirev.2013.02.025.
Hessl, A.E., Brown, P., Byambasuren, O., Cockrell, S., Leland, C., Cook, E., Nachin, B., Pederson, N., Saladyga, T., Suran, B., 2016. Fire and climate in Mongolia (1532–2010 Common Era). Geophys. Res. Lett. 43 (12), 6519–6527. https://doi.org/10.1002/2016GL069059.
Hijioka, Y., Lin, E., Pereira, J.J., Corlett, R.T., Cui, X., Insarov, G.E., et al., 2014. Asia. In: Barros, V.R., Field, C.B., Dokken, D.J., Mastrandrea, M.D., Mach, K.J., Bilir, T.E. (Eds.), Climate Change 2014: Impacts, Adaptation, and Vulnerability. Part B: Regional Aspects. Contribution of Working Group II to the Fifth Assessment Report of the Intergovernmental Panel on Climate Change. Cambridge University Press, Cambridge, United Kingdom and New York, NY.
Huang, T.C., 1972. Pollen Flora of Taiwan. National Taiwan University, Botany Dept. Press, Taipei.
Hurlbert, S.H., 1971. The nonconcept of species diversity: a critique and alternative parameters. Ecology 52 (4), 577–586. https://doi.org/10.2307/1934145.
IPCC, 2014. In: Core Writing Team, Pachauri, R.K., Meyer, L.A. (Eds.), Climate Change 2014: Synthesis Report. Contribution of Working Groups I, II and III to the Fifth Assessment Report of the Intergovernmental Panel on Climate Change. IPCC, Geneva, Switzerland (151 pp.).
Khansaritoreh, E., Dulamsuren, C., Klinge, M., Ariunbaatar, T., BatEnerel, B., Batsaikhan, G., Ganbaatar, K., Saindovdon, D., Yeruult, Y., Tsogtbaatar, J., Tuya, D., Leuschner, C., Markus Hauck, M., 2017. Higher climate warming sensitivity of Sibirian larch in small than large forest islands in the fragmented Mongolian forest steppe. Glob. Chang. Biol. 23, 3675–3689. https://doi.org/10.1111/gcb.13750.
Klinge, M., Böhner, J., Lehmkuhl, F., 2003. Climate Pattern, Snow-and Timberlines in the Altai Mountains, Central Asia (Klimaverhältnisse, Schnee-und Waldgrenzen im Altai Gebirge, Zentralasien). Erdkunde, Bonn.
Kuuluvainen, T., Aakala, T., Várkonyi, G., 2017. Dead standing pine trees in a boreal forest landscape in the Kalevala National Park, northern Fennoscandia: amount, population characteristics and spatial pattern. For. Ecosys. 4 (1), 12. https://doi.org/10.1186/s40663-017-0098-7.
Lang, G., 1994. Quartäre Vegetationsgeschichte Europas: Methoden und Ergebnisse. Gustav Fischer, Jena, Stuttgart, New York.
Legrand, M., McConnell, J., Fischer, H., Wolff, E.W., Preunkert, S., Arienzo, M., Chellman, N., Leuenberger, D., Maselli, O., Place, P., Sigl, M., Schüpbach, S., Flannigan, M., 2016. Boreal fire records in Northern Hemisphere ice cores: a review. Clim. Past 12 (10), 2033–2059. https://doi.org/10.5194/cp-12-2033-2016.
Lehner, F., Coats, S., Stocker, T.F., Pendergrass, A.G., Sanderson, B.M., Raible, C.C., Smerdon, J.E., 2017. Projected drought risk in 1.5 °C and 2 °C warmer climates. Geophys. Res. Lett. 44 (14), 7419–7428. https://doi.org/10.1002/2017GL074117.
Liu, H., Cui, H., Pott, R., Speier, M., 1999. The surface pollen of the woodland–steppe ecotone in southeastern Inner Mongolia, China. Rev. Palaeobot. Palynol. 105 (3), 237–250. https://doi.org/10.1016/S0034-6667(98)00074-8.
Liu, H., Park Williams, A., Allen, C.D., Guo, D., Wu, X., Anenkhonov, O.A., Liang, E., Sandanov, D.V., Yin, Y., Qi, Z., B & Badmaeva, N. K., 2013. Rapid warming accelerates tree growth decline in semi-arid forests of Inner Asia. Glob. Chang. Biol. 19 (8), 2500–2510. https://doi.org/10.1111/gcb.12217.
Lkhagvadorj, D., Hauck, M., Dulamsuren, C., Tsogtbaatar, J., 2013. Pastoral nomadism in the forest-steppe of the Mongolian Altai under a changing economy and a warming climate. J. Arid Environ. 88, 82–89. https://doi.org/10.1016/j.jaridenv.2012.07.019.
MacDonald, G.M., Larsen, C.P., Szeicz, J.M., Moser, K.A., 1991. The reconstruction of boreal forest fire history from lake sediments: a comparison of charcoal, pollen, sedimentological, and geochemical indices. Quat. Sci. Rev. 10 (1), 53–71. https://doi.org/10.1016/0277-3791(91)90030-X.
McDowell, N.G., Allen, C.D., 2015. Darcy's law predicts widespread forest mortality under climate warming. Nat. Clim. Chang. 5 (7), 669. https://doi.org/10.1038/nclimate2641.
Moore, P.D., Webb, J.A., Collison, M.E., 1991. Pollen Analysis, 2nd ed. Blackwell Scientific Publications.
Naumov, I.V., 2006. The History of Siberia. Routledge, London, New York.
NOAA, 2013. Ulgii Climate Normals 1961–1990. National Oceanic and Atmospheric Administration. Last updated 2013, accessed July 04, 2018.
Ponomarev, E.I., Kharuk, V.I., 2016. Wildfire occurrence in forests of the Altai–Sayan region under current climate changes. Contemp. Probl. Ecol. 9 (1), 29–36. https://doi.org/10.1134/S199542551601011X.
Rey, F., Gobet, E., Szidat, S., Lotter, A.F., Gilli, A., Hafner, A., Tinner, W., 2018. Radiocarbon wiggle matching on laminated sediments delivers high-precision chronologies. Radiocarbon 1–21. https://doi.org/10.1017/RDC.2018.47.
Rogers, J.D., 2012. Inner Asian States and Empires: theories and synthesis. J. Archaeol. Res. 20 (3), 205–256. https://doi.org/10.1007/s10814-011-9053-2.
Rose, N.L., 2015. Spheroidal carbonaceous fly ash particles provide a globally synchronous stratigraphic marker for the Anthropocene. Environ. Sci. Technol. 49 (7), 4155–4162. https://doi.org/10.1021/acs.est.5b00543.
Roth, R., Joos, F., 2013. A reconstruction of radiocarbon production and total solar irradiance from the Holocene ^{14}C and CO_2 records: implications of data and model uncertainties. Clim. Past 9 (4), 1879. https://doi.org/10.5194/cp-9-1879-2013.
Rudaya, N.A., Tarasov, P.E., Dorofeyuk, N.I., Kalugin, I.A., Andreev, A.A., Diekmann, B., Daryin, A.V., 2008. Environmental changes in the Mongolian Altai during the Holocene. Archaeol. Ethnol. Anthropol. Eurasia 36 (4), 2–14. https://doi.org/10.1016/j.aeae.2009.03.001.
Rudaya, N., Tarasov, P., Dorofeyuk, N., Solovieva, N., Kalugin, I., Andreev, A., Daryin, A., Diekmann, B., Riedel, F., Tserendash, N., Wagner, M., 2009. Holocene environments and climate in the Mongolian Altai reconstructed from the Hoton-Nur pollen and diatom records: a step towards better understanding climate dynamics in Central Asia. Quat. Sci. Rev. 28 (5), 540–554. https://doi.org/10.1016/j.quascirev.2008.10.013.
Sato, T., Kimura, F., Kitoh, A., 2007. Projection of global warming onto regional precipitation over Mongolia using a regional climate model. J. Hydrol. 333 (1), 144–154. https://doi.org/10.1016/j.jhydrol.2006.07.023.
Schlütz, F., Dulamsuren, C., Wieckowska, M., Mühlenberg, M., Hauck, M., 2008. Late Holocene vegetation history suggests natural origin of steppes in the northern Mongolian mountain taiga. Palaeogeogr. Palaeoclimatol. Palaeoecol. 261 (3), 203–217. https://doi.org/10.1016/j.palaeo.2007.12.012.
Staubwasser, M., Weiss, H., 2006. Holocene climate and cultural evolution in late prehistoric–early historic West Asia. Quat. Res. 66 (3), 372–387. https://doi.org/10.1016/j.yqres.2006.09.001.
Steinhilber, F., Beer, J., Fröhlich, C., 2009. Total solar irradiance during the Holocene. Geophys. Res. Lett. 36 (19). https://doi.org/10.1029/2009GL040142.
Stockmarr, J., 1971. Tablets with spores used in absolute pollen analysis. In: Pollen et spores.
Stritch, L., Shaw, K., Roy, S., Wilson, B., 2014. *Betula pendula*. The IUCN Red List of Threatened Species 2014. https://doi.org/10.2305/IUCN.UK.2014-3.RLTS.

T62535A3115662.en.
Sun, A., Feng, Z., Ran, M., Zhang, C., 2013. Pollen-recorded bioclimatic variations of the last ~22,600 years retrieved from Achit Nuur core in the western Mongolian Plateau. Quat. Int. 311, 36–43. https://doi.org/10.1016/j.quaint.2013.07.002.
Tarasov, P., Dorofeyuk, N., Tseva, E.M., 2000. Holocene vegetation and climate changes in Hoton-Nur basin, northwest Mongolia. Boreas 29 (2), 117–126. https://doi.org/10.1111/j.1502-3885.2000.tb01205.x.
Tchebakova, N.M., Blyakharchuk, T.A., Parfenova, E.I., 2009. Reconstruction and prediction of climate and vegetation change in the Holocene in the Altai–Sayan mountains, Central Asia. Environ. Res. Lett. 4 (4), 045025. https://doi.org/10.1088/1748-9326/4/4/045025.
Ter Braak, C.J., Prentice, I.C., 1988. A theory of gradient analysis. Adv. Ecol. Res. 18, 271–317. https://doi.org/10.1016/S0065-2504(03)34003-6.
Tian, F., Herzschuh, U., Dallmeyer, A., Xu, Q., Mischke, S., Biskaborn, B.K., 2013. Environmental variability in the monsoon–westerlies transition zone during the last 1200 years: lake sediment analyses from central Mongolia and supra–regional synthesis. Quat. Sci. Rev. 73, 31–47. https://doi.org/10.1016/j.quascirev.2013.05.005.
Tian, F., Herzschuh, U., Mischke, S., Schlütz, F., 2014. What drives the recent intensified vegetation degradation in Mongolia–Climate change or human activity? The Holocene 24 (10), 1206–1215. https://doi.org/10.1177/0959683614540958.
Tinner, W., Hu, F.S., 2003. Size parameters, size-class distribution and area-number relationship of microscopic charcoal: relevance for fire reconstruction. The Holocene 13 (4), 499–505. https://doi.org/10.1191/0959683603hl615rp.
Tinner, W., Conedera, M., Ammann, B., Gaggeler, H.W., Gedye, S., Jones, R., Sagesser, B., 1998. Pollen and charcoal in lake sediments compared with historically documented forest fires in southern Switzerland since AD 1920. The Holocene 8 (1), 31–42. https://doi.org/10.1191/095968398667205430.
Tinner, W., Beer, R., Bigler, C., Clegg, B.F., Jones, R.T., Kaltenrieder, P., van Raden, U.J., Gilli, A., Hu, F.S., 2015. Late-Holocene climate variability and ecosystem responses in Alaska inferred from high-resolution multiproxy sediment analyses at Grizzly Lake. Quat. Sci. Rev. 126, 41–56. https://doi.org/10.1016/j.quascirev.2015.08.019.
TPL, 2018. The Plant List. http://www.theplantlist.org/tpl1.1/record/kew-21520 Last visited 12.07.2018.
Tsogtbaatar, J., 2004. Deforestation and reforestation needs in Mongolia. For. Ecol. Manag. 201 (1), 57–63. https://doi.org/10.1016/j.foreco.2004.06.011.
Tsogtbaatar, J., 2013. Deforestation and reforestation of degraded forestland in Mongolia. In: The Mongolian Ecosystem Network. Springer, Japan.
Uglietti, C., Zapf, A., Jenk, T.M., Sigl, M., Szidat, S., Salazar Quintero, G.A., Schwikowski, M., 2016. Radiocarbon dating of glacier ice: overview, optimisation, validation and potential. Cryosphere 10 (6), 3091–3105. https://doi.org/10.5194/tc-10-3091-2016.
Umbanhowar Jr., C.E., Shinneman, A.L., Tserenkhand, G., Hammon, E.R., Lor, P., Nail, K., 2009. Regional fire history based on charcoal analysis of sediments from nine lakes in western Mongolia. The Holocene 19 (4), 611–624. https://doi.org/10.1177/0959683609104039.
Unkelbach, J., Dulamsuren, C., Punsalpaamuu, G., Saindovdon, D., Behling, H., 2018. Late Holocene vegetation, climate, human and fire history of the forest-steppe-ecosystem inferred from core G2-A in the 'Altai Tavan Bogd' conservation area in Mongolia. Veg. Hist. Archaeobotany. https://doi.org/10.1007/s00334-017-0664-5.
Van Zeist, W., Woldring, H., Stapert, D., 2016. Late Quaternary vegetation and climate of southwestern Turkey. Palaeohistoria 17, 53–143.
Volkov, V.V., 1995. Early nomads of Mongolia. In: Davis-Kimball, J., Bashilov, V.A., Yablonsky, L.T. (Eds.), Nomads of the Eurasian Steppes in the Early Iron Age. Zinat, Berkeley.
Walter, H., 1974. Die Vegetation Osteuropas, Nord-und Zentralasiens. Vegetations-Monographien der Einzelnen Grossräume, Bd 7. Gustav Fischer, Stuttgart.
Wang, W., Feng, Z., 2013. Holocene moisture evolution across the Mongolian Plateau and its surrounding areas: a synthesis of climatic records. Earth Sci. Rev. 122, 38–57. https://doi.org/10.1016/j.earscirev.2013.03.005.
Wang, Y., Cheng, H., Edwards, R.L., He, Y., Kong, X., An, Z., Wu, J., Kelly, M.J., Dykoski, C.A., Li, X., 2005. The Holocene Asian monsoon: links to solar changes and North Atlantic climate. Science 308 (5723), 854–857. https://doi.org/10.1126/science.1106296.
Wu, Z.Y., Raven, P.H., 1999. Flora of China. vol. 4 Science Press and Missouri Botanical Garden Press, Beijing and St. Louis (Cycadaceae through Fagaceae).
Xu, C., Liu, H., Anenkhonov, O.A., Korolyuk, A.Y., Sandanov, D.V., Balsanova, L.D., Naidanov, B.B., Wu, X., 2017. Long-term forest resilience to climate change indicated by mortality, regeneration, and growth in semiarid southern Siberia. Glob. Chang. Biol. 23 (6), 2370–2382.
Zhao, P., Xu, C., Zhou, M., Zhang, B., Ge, P., Zeng, N., Liu, H., 2018. Rapid regeneration offsets losses from warming-induced tree mortality in an aspen-dominated broad-leaved forest in northern China. PLoS One 13 (4), e0195630. https://doi.org/10.1371/journal.pone.0195630.

Manuscript 4

Tropical Andean glacier reveals Colonial legacy in modern montane ecosystems

Sandra O. Brugger[1,2,*], Erika Gobet[1,2], Dimitri Osmont[2,3,4], Hermann Behling[5], Sonia L. Fontana[5], Henry Hooghiemstra[6], César Morales-Molino[1,2,7], Michael Sigl[2,3], Margit Schwikowski[2,3,4], Willy Tinner[1,2]

[1]Institute of Plant Sciences, University of Bern, Switzerland
[2]Oeschger Center for Climate Change Research, University of Bern, Switzerland
[3]Paul Scherrer Institute, Villigen, Switzerland
[4]Department for Chemistry and Biochemistry, University of Bern, Switzerland
[5]Department of Palynology and Climate Dynamics, University of Göttingen, Germany
[6]Department of Ecosystem and Landscape Dynamics, University of Amsterdam, Netherlands
[7]Swiss Federal Institute for Forest, Snow and Landscape Research WSL, Cadenazzo, Switzerland

[*]Corresponding author: Sandra O. Brugger

Keywords: Illimani ice core – Microscopic charcoal – Pollen – Pre-Columbian land use– Puna – SCP (spheroidal carbonaceous particles) –Yungas (cloud forest)

Prepared for a journal with ecological focus

Abstract

The extent of pre-Columbian land use and its legacy on modern ecosystems, plant communities and species of the Americas are still hotly debated. To address this gap, we present a Holocene palynological ice record (pollen, spores, microscopic charcoal, SCP analyses) from Illimani glacier with exceptional temporal resolution and chronological control close to the center of Inca activities around Titicaca Lake in Bolivia. Our results suggest that Holocene fire activity was largely climate-driven and pre-Columbian agropastoral and agroforestry practices had moderate (large-scale) impacts on ecosystems. Unprecedented human-shaped ecosystems emerged after 1740 AD following the establishment of novel Colonial land use practices and were further reinforced in the modern era post-1950 AD with intensified coal consumption and industrial plantations. Although agroforestry practices date back to the Incas, the recent vast afforestation with exotic monocultures together with rapid climate warming and associated fire regime changes may provoke unprecedented and possibly irreversible ecological and environmental alterations.

1 Introduction

Neotropical mountain ecosystems may span broad altitudinal ranges resulting in steep environmental (e.g. temperature, precipitation) gradients. This environmental diversity results in a remarkable richness of plant communities spanning from sparse high Andean dry Puna above treeline to species-rich montane Yungas and tropical lowland forests (Mourguiart and Ledru 2003, Ibisch and Mérida 2004). These habitats are among the most threatened on Earth by human disruption and climate change (Olson and Dinerstein 2002, Bush et al. 2005), however, anticipation of future dynamics is difficult, mainly because of the high diversity which implies sensitive (e.g. species extinctions) and complex (e.g. species interactions) responses, that are co-determined by the multitude of ecological niches involved. Modern human activities include intense pastoralism, crop cultivation, and vast areas with exotic tree plantations that strongly alter these precious ecosystems and result in rapid degradation (Ibisch and Mérida 2004, Gareca et al. 2007). Climate change is expected to rise temperature by >3°C in the region by the end of the century, while precipitation may reduce by 10–30 % on the Altiplano (Minvielle and Garreaud 2011, Magrin et al. 2014).

Paleoecological studies can provide ecological baselines for naturalness prior to substantial human alterations that may be implemented into nature protection and planning measures (Mayle et al. 2004, Seddon et al. 2014, Nolan et al. 2018). In Latin America, the extent of pre-Columbian land use and its legacy on modern ecosystems, plant communities and species are still hotly debated, probably also because of the strong spatial variability in the different Neotropical regions (Levis et al. 2017, McMichael et al. 2017a, Piperno et al. 2017, Watling et al. 2017, Roberts et al. 2018). For example, studies along Northern Inca trade routes with Amazonian tribes suggest that native imperial ecosystem disturbances may have exceeded modern forest disruptions (Loughlin et al. 2018). More central areas such as the Altiplano and Titicaca Lake area in the Bolivian and Peruvian Andes are culturally important since the mid Holocene (ca. 7000 uncal BP; Lynch 1983, Aldenderfer 1999, Nunez et al. 2002, Marsh 2015). Vast archeological evidence suggests highly developed pre-Columbian cultures that successfully domesticated large herbivores (*Lamini*), cultivated crops, and had refined metallurgy skills (Burger and Gordon 1998, Abbott and Wolfe 2003, Bruno and Whitehead 2003, Eichler et al. 2017). Despite extensive research on millennial-scale climate responses of Central Andean vegetation, temporally highly resolved and accurately dated records for the past 2000 years are lacking in this central areas, where ancient cultures emerged (e.g. Baied and Wheeler 1993, Mourguiart and Ledru 2003, Bush et al. 2004, Hanselmann et al. 2005, Urrego et al. 2005, Valencia et al. 2010, Sublette Mosblech et al. 2012). This gap hampers the chronological and ecological assessment of ecosystem responses to disturbance processes by pre-Columbian and Colonial land use, ultimately hindering the estimation of natural baseline conditions for nature protection and planning measures (Olson and Dinerstein 2002, McMichael et al. 2017b).

High-Andean glaciers allow high-temporal resolution records with exceptional chronological control (e.g. Reese et al. 2013) and thus have a high potential to address such ecological knowledge gaps (Brugger et al. 2018a). The ice-capped Illimani (6300 m asl) is located above Titicaca Lake in the Bolivian Eastern cordillera (16° 39’ S, 67° 47’ N; Fig. 1A; Knüsel et al. 2003). It provides a suitable ice archive to study environmental dynamics (e.g. Eichler et al. 2015, 2017, Osmont et al. in review) with an exceptionally well-constrained chronology refined by precise reference horizons inferred from volcanic eruptions (Fig. 2; Knüsel et al. 2003, Kellerhals et al. 2010). Due to its proximity to the center of pre-Columbian activities, the ice archive is ideal to examine the resilience of mountain ecosystems to Holocene human impact, for instance the rise and fall of the Inca empire during the period 1438 to 1532 AD. We pursue the following aims: (1) to reconstruct Holocene vegetation, land use, fire, and pollution dynamics on the Altiplano and adjacent montane areas of the Central Andes during the Holocene, (2) to compare our data from the center of pre-Columbian empires with those from marginal areas (as investigated by previous studies), and (3) to assess the resilience capacity of mountain vegetation to various degrees of past human disturbance to derive baselines for nature protection under global-change conditions.

2 Material and methods

2.1 Environmental setting and vegetation

Bolivia is characterized by steep climatic and environmental gradients mainly deriving from its pronounced topography. The Eastern Cordillera divide the Amazonian lowland (100–800 m asl) from the inter-Andean Altiplano (3700 to 4400 m asl; Vuille et al. 2000, Ibisch and Mérida 2004). The climate on the Bolivian Altiplano is arid with a mean annual temperature below 18°C (Köppen class BSk for Northeastern and BWk for Southwestern Bolivian Altiplano; Peel et al. 2007). Precipitation is concentrated from November to March and originates mostly from the Amazon basin (Vuille et al. 2000), which is characterized by a tropical climate with monthly mean temperatures >18°C and high rainfall during the austral summer (Köppen class Af-Am; Peel et al. 2007).

The topographic and climatic setting results in distinct vegetation communities. The permanent snow line is around 5000 m asl and is reached by few vascular cushion plants that are adapted to the harsh climatic conditions (Ibisch and Mérida 2004). The Altiplano vegetation is composed of steppic mountain plant communities (Puna), which comprise semi-humid to humid Puna species in the Northeast of the Altiplano and increasingly dry-adapted Puna species towards the Salar Uyuni and Atacama desert (Fig. 1; Ibisch and Mérida 2004). Dry Puna is dominated by Asteroideae (e.g. *Baccharis incarum*, *B. boliviensis*, *Chaetanthera* sp., *Parastrephia lepidophylla*), Poaceae (e.g. *Deyeuxia breviaristata*, *D. crispa*, *Festuca* sp., *Stipa* sp.), various Caryophyllaceae, Apiaceae, and *Fabiana densa* (Solanaceae).

Amaranthaceae *sensu lato (s.l.)* are an important Puna family, which includes desert and salt-adapted species (*Suaeda* sp., Chenopodiaceae s.s.) that together with Cactaceae become important with reduced precipitation (Fig. 1; Ibisch and Mérida 2004).

The moister northeast and eastern areas are the most densely populated parts of the Altiplano, with vast spaces used for crop cultivation, terraces, sheep and cattle herding, and mineral exploitation (Ibisch and Mérida 2004). Semi-humid Puna communities in these areas are composed of Poaceae (e.g. *Deyeuxia* sp., *Festuca* sp., Poa buchtienii, Stipa sp.), Asteroideae (e.g. *Ageratina azangaroense*, *Baccharis* sp.), Caryophyllaceae, Gentianaceae, and Cyperaceae (Ibisch and Mérida 2004).

The montane forests on the eastern slopes of the Cordillera below the humid Puna are divided in a distinct northeastern moist montane forest belt (Yungas) and dry seasonal Tucuman forests on the southeastern slopes (Fig. 1). The humid Yungas support Páramo vegetation with *Polylepis pepei* growing up to 4200 m asl. Today these communities are widely replaced by evergreen thickets and man-made woodlands (Ibisch and Mérida 2004). *Podocarpus* sp., *Polylepis racemosa*, *Symplocos nana*, and *Weinmannia* sp. are characteristic forest components between ca. 3600–3100 m asl. Cloud forests (ca. 3100–2500 m asl) are composed of *Clusia* sp., Loranthaceae, *Myrica pubescens*, Araliaceae, Lauraceae, and *Weinmannia*. Important genera of the diverse lower montane Yungas are e.g. *Acalypha, Alchornea, Ficus, Inga, Solanum*, *Trichilia, Clethra, Hedyosmum, Miconia, Piper, Podocarpus,* and *Weinmannia* (Ibisch and Mérida 2004).

The less humid and more seasonal Tucuman forests on the southeastern slopes are composed of *Tabebuia lapacho*, Myrtaceae, *Alnus acuminata*, Lauraceae, *Weinmannia*, and above 2000 m asl *Podocarpus*, while precipitation-sheltered inter-andean valleys comprise drought-adapted forests and xerophytic shrublands with Anacardiaceae, Cactaceae, and Mimosoideae species (Fig. 1; Ibisch and Mérida 2004). The lowlands below 500 m asl are a mosaic of evergreen forests often dominated by Arecaceae (e.g. *Euterpe*, *Bactris, Mauritia, Mauritiella*), Annonaceae, and Moraceae such as *Ficus* (e.g. humid evergreen forests, riparian Várzea forests), flooded grasslands, and dry shrublands and forests (e.g. Cerrado, Gran Chaco, Chiquitano) depending on topography and edaphic conditions (Fig. 1; Ibisch and Mérida 2004, Navarro Sanchez 2011)

2.2 Ice material and chronology

In June 1999 AD an ice core (referred to as Illi'99 in this study) was drilled at 6300 m asl on the Illimani glacier saddle between Pico Sur and Pico Central (16° 39' S, 67° 47' N). The drilling reached the bedrock at 138.7 m depth (=113.2 m weq; Knüsel et al. 2003). The chronology of the Illi'99 ice core is established on annual layer counting of the electrical conductivity signal, volcanic eruptions detected as sulfate peaks, the maximum Tritium peak attributed to 1964 AD (Knüsel et al. 2003), and ^{14}C-dating of carbonaceous particles (Kellerhals et al. 2010). The depth-age model is based on a two-parameter glacier flow model fitted through the reference horizons and the ^{14}C dates. The depth-age model suggests an average accumulation rate of 0.58 m weq year^{-1} along the record (Fig. 2; Kellerhals et al. 2010). The estimated model uncertainty is ±2–5 years for 1800–1999 AD (varying with distance to reference horizons), ±20 years for 1250–1800 AD, and ±110 years at the youngest ^{14}C date (1060–1280 cal BP 1 σ range; fig. 2; Kellerhals et al. 2010).

In 2015, the shallow core Illi'15 was drilled to update Illi'99. The chronology of Illi'15 is based on annual layer counting of black carbon and has a palynological overlap of four years (years 1996–1999 AD) with Illi'99. The overlapping sequence suggests good reproducibility between the palynological results of the two ice cores (Fig. S1 and PCA in fig. 3). The tie point for the combined master core of Illi'15 and Illi'99 was set at 1998 AD (Fig. S2).

2.3 Palynological methods and numerical approaches

The palynological record covers the period ca. 10,000 BC–2015 AD and it consists of 136 continuous samples (no sampling gaps). Each sample contained 205–2300 g ice (average = 870 g). The microfossil extraction followed the evaporation-based method in Brugger et al. (2018b) with an additional HF treatment to dissolve abundant dust particles. The exponential depth-age relationship results in varying temporal sampling resolution along the record: millennial sampling intervals for 10,000 BC–1 AD, ca. 40 years for 1–1300 AD, and ca. 20 years for 1300–1700 AD. As a result of the extremely high temporal resolution related to the nature of the ice archive, the top record reached resolutions < 5 years. After analysis, we merged samples for the period 1700–2015 AD to reach a resolution of 5 years.

We use pollen and spores to infer vegetation history and land use activity. Pollen sums along the record range from 101 to 778 pollen grains per sample (average = 442 pollen grains). Pollen and spore identification was made under a light microscope at 400x magnification and followed palynological atlases of Heusser (1971), Markgraf and D'Antoni (1978), Hooghiemstra (1983), Hooghiemstra (1984), Roubik and Moreno (1991), Carreira (1996), Herrera and Urrego (1996), Colinveaux et al. (1999), Beug (2004), and the reference collection at the palynological laboratory at University of Göttingen, Germany. A complete list of all identified pollen, spores, and non-pollen palynomorphs (NPP) is provided in supplementary table S1. The assignment of pollen taxa to predominant vegetation types follows Marchant et al. (2002), with additional botanical information provided where needed (Navarro Sanchez 2011, Ibisch and Mérida 2004). We present pollen and spore percentages based on the terrestrial pollen sum. A summary curve for pollen taxa characteristic for evergreen lowland forests (Supplementary table S1) and the total pollen concentration is also shown.

We applied optimal sum-of-squares partitioning for the zonation of the pollen data (Birks and Gordon 1985) including all taxa >5 % (in at least one sample), this included the twelve taxa Asteroideae, Poaceae, *Alchornea*, Moraceae/Urticaceae, Amaranthaceae *s.l.*, *Dodonea*, Cyperaceae. *Alnus*, *Plantago major*-type, Podocarpaceae, *Polylepis*, and *Myrica*. The local pollen assemblage zones (LPAZ) were tested for significance with the broken stick approach (Bennett 1996). The short gradient length of the first axis (= 1.49) of detrended correspondence analysis (DCA, detrended by segments) justifies the application of linear ordination methods. Therefore, we used principal component analysis (PCA) to summarize square-root-transformed pollen percentage data of all taxa >1 % (in at least one sample, ter Braak and Prentice 1988).

We use microscopic charcoal >10 µm as a proxy for fire activity (e.g. Eichler et al. 2011, Brugger et al. 2016, 2018a) and counted a minimum of 200 items for each sample (sum of charcoal fragments and *Lycopodium* grains; Tinner and Hu 2003, Finsinger and Tinner 2005). If needed due to low charcoal concentrations, we continued > 200 items until we reached a minimum of 20 charcoal fragments. To check for deposition biases we calculated the correlation coefficient between pollen and microscopic charcoal concentration for the entire record. Finally, we counted SCP (= spheroidal carbonaceous particles) with a diameter >10 µm and clear features to infer industrial air pollution (Rose 2015). We standardized all microfossil concentrations to one liter.

3 Results and Interpretation

3.1 Microfossil deposition at Illimani

Pollen concentrations along the record are ca. 1000–2000 grains l^{-1} from 10,000 BC–1600 AD and increase to ca. 2500–3000 l^{-1} until present (Fig. 4). The modern pollen concentration (2000–2015 AD) is ca. 2500 grains l^{-1}, which corresponds to an influx of ca.

145 grains cm^{-2} yr^{-1}. High shares of herbaceous pollen (ca. 50 %) with abundant Asteroideae and Poaceae suggest a dominance of Puna vegetation. The most important arboreal taxa (AP = sum of trees and shrubs) are characteristic of montane Yunga forest (Fig. 4 and Supplementary table S1; Ibisch and Mérida 2004) and the record contains only marginal percentages of lowland tropical evergreen AP. The comparison with extant vegetation shows that this pollen signal must come from within a distance of max. 200-300 km (Fig. 1A), confirming previous estimations of glacier ice pollen catchments (Brugger et al. 2018a).

The modern microscopic charcoal concentration is ca. 2300 fragments l^{-1} for 2000–2015 AD (Fig. 4), which corresponds to ca. 130 particles cm^{-2} yr^{-1} or ca. 0.007 mm^2 cm^{-2} (Tinner and Hu 2003). The extremely low correlation coefficient between microscopic charcoal and pollen concentrations along the record ($R^2 = 0.002$) shows no archive bias as it could e.g. result from changing snow accumulation or single deposition events. Modern SCP concentrations (ca. 20 particle l^{-1} for 2015–2000 AD) correspond to an influx of ca. 1.1 particle cm^{-2} yr^{-1}.

3.2 Holocene vegetation dynamics

We use pollen and spores to infer past vegetation and land use dynamics presuming a catchment of max. 200–300 km around Illimani (Fig. 1). The entire pollen record contains continuously high herbaceous pollen (70–80 %) suggesting minimal shifts in landscape openness throughout the Holocene on a large regional scale (Fig. 4). Herbaceous pollen is mainly composed of Asteroideae and Poaceae, characteristic for open Puna vegetation on the Altiplano above 3700 m asl (Fig. 1B; Ibisch and Mérida 2004, Marchant et al. 2002). The most important arboreal taxa (AP = sum of trees and shrubs) are distinctive of moist montane forests (Yungas) occupying the eastern Andean slopes below Puna. The record contains only marginal percentages of characteristic lowland tropical evergreen AP (Fig. 4, Supplementary table S1).

From 10,000 BC to 7800 BC abundant Poaceae pollen (40%) suggest a grass-dominated more humid Puna vegetation (Liu et al. 2005). Tree pollen consists mainly of late-successional taxa as e.g. *Polylepis*, Podocarpaceae, and *Myrica* indicating mature upper montane forests. Around 7800 BC pollen composition changed significantly as evidenced by a statistically significant first pollen zone boundary (Illi-1–Illi-2; fig. 4), including a decrease of Poaceae to 20 % and an increase of Asteroideae to 40 %, suggesting a vegetation shift in Altiplano vegetation towards drier conditions (xerophytic Puna, Liu et al. 2005). Subsequently, the pollen record suggests relatively stable Puna communities until 500 BC. From 500 BC to 100 AD, Asteroideae pollen decreases and Amaranthaceae *s.l.* pollen (including Amaranthaceae and Chenopodiaceae) increases (5 %). This shift may have resulted from enhanced human impact on the Altiplano. Indeed, native Amaranthaceae *s.l.* includes a suite of species that are cultivated up to 3800 m asl (e.g. *Chenopodium quinoa, C. pallidicaule*, *Amaranthus* sp.; Bhargava et al. 2006, Jarvis et al. 2017) and favored by disturbance and/or halophytic conditions (Bruno and Whitehead 2003, Flantua et al. 2016). In agreement, the increase of *Sporormiella*, a coprophilous fungal spore points to increased herbivore activity (Cugny et al. 2010) and is possibly related to growing presence of *Lamini* on the Altiplano. Frequent pollen of heliophilous *Alchornea*, *Dodonea*, and Cupressaceae after 1 AD points to growing disturbance in the Yungas, possibly related to human activity (Marchant et al. 2002). First *Zea mays* pollen occurs ca. 1 AD–300 AD and reappears around 900 AD suggesting either substantial maize cultivation below 3200 m asl in the Yungas or cultivation of high-altitude-adapted varieties growing up to 4100 m asl (Staller 2016). After 1200 AD *Zea mays* reappears together with a contemporaneous increase of Amaranthaceae *s.l.* to 10 % and first presence of *Plantago sericea*-type points to intensified crop cultivation and weed expansions.

After 1360 AD (zone boundary Illi-2–Illi-3, fig. 4), Asteroideae values decrease, while Poaceae values steadily increase to reach a maximum at 1740 AD during the Little Ice Age (LIA; Apaéstegui et al. 2018). This compositional change in Puna vegetation is accompanied by a spread of upper montane forest taxa as e.g. *Polylepis*, *Alnus*, *Hedyosmum*, and Podocarpaceae that indicates slight expansions of the Yungas possibly related to a climatic shift and/or decreasing human activity (Marchant et al. 2002). Frequent *Zea mays* pollen grains after 1600 AD show growing crop production during the following centuries.

The rapid and pronounced shift in the Poaceae and Asteroideae percentages around 1740 AD (zone boundary Illi-3–Illi-4, fig. 4) suggests a drastic replacement of grass-dominated Puna by drought-adapted Asteroideae that is comparable with vegetation conditions prior to 7800 BC. The contemporaneous spread of the nutrient-loving weed taxa *Plantago sericea*-type, *P. major*-type, and *Rumex*-type together with *Sporormiella* was likely induced by expanding grazing activity. Thus, we interpret this shift in Puna vegetation after 1740 AD as a consequence of intensified European cattle herding on the Altiplano that suppressed edible grass species by advantaging xerophytic Asteroideae taxa (Baied and Wheeler 1993). The contemporaneous increase of pioneer and heliophilous tree and shrub taxa (e.g. *Trema*, *Alchornea*, *Acalypha*, *Cecropia*, *Dodonea*, Cupressaceae) between 1740 and 1950 AD illustrates the rising significance of early successional woody communities. Finally, the coeval onset of non-native tree pollen (e.g. *Pinus*, *Eucalyptus*, *Platanus*) documents the historically known and wide-spread introduction of exotic tree species for timber production or ornamental purposes (Gareca et al. 2007).

During the most recent pollen zone (1950–2015 AD), Asteroideae decrease as well, and woody taxa spread in the region pointing to afforestation. The past decades are characterized by disturbance-adapted species as e.g. Moraceae and *Dodonea* as well as further spreads of exotic *Pinus* and *Eucalyptus*. The pronounced decrease of *Polylepis* pollen is possibly related to modern anthropogenic disruption of the *Polylepis*-dominated forests at the upper treeline (Ibisch and Mérida 2004).

Principal Component Analysis (PCA) is used to summarize vegetation composition changes (in pollen samples) over time. Axis 1 and 2 explain 16 % and 10 %, respectively (Fig. 3, supplementary 2). PCA separates early-Holocene samples prior to the appearance of first cultural indicators (i.e. before 7800 BC) from the remaining mid and late Holocene record (i.e. after 7800 BC). All samples for the period between 7800 BC and 1740 AD group closely together, suggesting stable ecosystems with minor floristic changes. Samples of the period 1740–1950 AD are again clearly distinct due to their drastically different composition of herbaceous taxa possibly related to increasing grazing pressure (e.g. *Sporormiella* rise), and changing forest plants (e.g. increase of disturbance-adapted taxa and onset of exotic trees). The modern samples (1950–2015 AD) are again different, if compared to the remaining Holocene samples, likely as a consequence of excessive human impact. Overall, the PCA supports that after the first appearance of human impact around 1 AD, ecosystem and composition never returned to early Holocene conditions (i.e. natural baseline conditions prior to 8000 BC).

3.3 Fire and pollution history

We use microscopic charcoal to infer fire history (Tinner and Hu 2003, Finsinger and Tinner 2005, Eichler et al. 2011, Brugger et al. 2018a). Microscopic charcoal concentrations are low during the early Holocene around 10,000 BC (ca. 3000 particles l^{-1}) and increase markedly from around 8000 to 2000 BC (ca. 26,000 particles l^{-1}) suggesting maximum fire activity when dry-adapted Puna communities spread on the Altiplano. After 2000 BC microscopic charcoal concentrations decrease steadily to reach a minimum of <2000 particles l^{-1} during the LIA indicating decreasing fire activity during the late Holocene. Microscopic charcoal-inferred fire activity remained low until 1870 AD, when drought-adapted Puna communities expanded, likely as a consequence of human impact (e.g. cattle herding). During the past century, microscopic charcoal concentrations rise again to ca. 3000 particles l^{-1}. The long-term-trend of Holocene fire activity shows no clear correlation with phases of human land use (e.g. *Zea mays*, Amaranthaceae, or *Sporormiella* increase), suggesting natural forcing such as moisture or temperature changes of centennial-scale fire activity trends (e.g. fire activity minimum during LIA cooling 1500–1850 AD).

We use spheroidal carbonaceous particles (SCP) as a proxy for fossil fuel combustion (Rose 2015). Frequent SCPs occur after 1820 AD indicating beginning atmospheric pollution related to fossil fuel combustion (Rose 2015). SCP concentrations reach a first maximum around 1910–1930 AD with ca. 20 particles l^{-1} and a second maximum spanning 1950–2000 AD with ca. 30 particles l^{-1}suggesting two periods of amplified fossil fuel combustion that were interrupted by the second world war crisis. SCP concentrations decrease after 2000 AD in the last two horizons of the record and point to first efficient attempts to reduce atmospheric fossil fuel pollution.

4 Discussion

4.1 Holocene fire dynamics driven by precipitation

The Illimani microscopic charcoal record suggests that fire activity increased during the mid Holocene (ca. 8000–2000 BC) to subsequently steadily decline until today. Interestingly, a previous charcoal record from Sajama glacier on the Western side of the Altiplano ca. 200 km southwest from Illimani indicates only a slight increase of fire activity 4000–1000 BC followed by a massive increase during the most recent centuries (Reese et al. 2013). Especially the historical fire increase at Sajama is completely lacking in the Illimani record, which likely implies that the centennial fire activity trends in the ice records reflect different fire catchments (Reese et al. 2013). The much higher share of Puna taxa in the pollen assemblages of the Western Sajama record compared to Illimani may also be related to different microfossil catchments (Liu et al. 2005, Reese et al. 2013). Our reconstructed fire history at Illimani furthermore contrasts with sedimentary sites on the Altiplano as e.g. the Bolivian Titicaca Lake sediment record ca. 150 km northwest (Paduano et al. 2003) and Peruvian records (Hansen and Rodbell 1995). However, similar centennial-scale trends of fire records occurred in the montane cloud forest belt (e.g. Mourguiart and Ledru 2003, Valencia et al. 2010), a vegetation type which is not very flammable in absence of human impact (Bush et al. 2005). Several sites across the Bolivian lowland inferred amplified fire activity in the mid Holocene that declined towards the late Holocene (e.g. Abbott et al. 2003, Urrego et al. 2013, Brugger et al. 2016, Power et al. 2016). We thus infer a wide microscopic charcoal catchment for Illimani, a typical feature of glacier records which is supported by recent paleo-validated global modelling efforts (Gilgen et al. 2018). Large-scale fire activity may have been largely controlled by climate, as supported by independent paleoclimatic evidence from Illimani (Osmont et al. in review).

In best agreement with the Illimani record, fire activity increased across the Amazon basin ca. 8000–2000 BC, when Titicaca lake levels and speleothems suggest a pronounced dry period (Baker et al. 2001, Cruz et al. 2005). Reduced late-Holocene fire activity (Cruz et al. 2005) may be related to the subsequent precipitation increase as likely released by the strengthening of the South American summer monsoon (SASM). SASM changes may thus have controlled centennial- to millennial-scale fire activity, ultimately driven by orbital-forcing (Power et al. 2016). Holocene minimum fire activity occurred during the LIA period 1500–1850 AD (Power et al. 2013), when independent proxies for SASM strength across tropical South America inferred maximum precipitation for the past two millennia (e.g. Thompson et al. 1986, Bird et al. 2011, Vuille et al. 2012, Apaéstegui et al. 2018).

Puna vegetation rapidly expanded after 1740 AD, at the end of the LIA. Similar Puna vegetation dynamics based on the Asteroideae/Poaceae ratio were recorded at Sajama glacier and previously interpreted as a dry period starting at 1700 AD (Liu et al. 2005). Considering the pollen-independent climatic availability from the region this interpretation seems unlikely. Alternatively, on the basis of the novel evidence of increasing grazing activity from the Illimani record (as inferred from expanding *Sporormiella*), declining fire activity and vegetation-independent evidence for a wet period (Bird et al. 2011, Apaéstegui et al. 2018), we hypothesize that the shift of drought-adapted Asteroideae communities was mainly the consequence of human impact including increased erosion (Baied and Wheeler 1993).

4.2 Mountain ecosystem responses to human impact

Our Illimani record provides novel evidence of maize cultivation and increasing herbivore grazing activity after 1 AD. Such substantial agropastoral activity may have been related to the Tiwanaku culture, which was thriving in the region around Titicaca Lake (*Staller 2016*). Despite human impact, remote Puna vegetation composition remained stable during the rise and fall of several highly developed cultures in the area until 1740 AD (e.g. Eichler et al. 2017). Similarly, the Illimani record suggests no large-scale deforestation in the mountain Yungas forest belt, although a compositional shift to more heliophilous taxa occurred after 1 AD. Early succession species likely spread after deforestation or small-scaled forest openings (Marchant et al. 2002). Adjacent upper montane sites in Peru show similar vegetational trends towards heliophilous taxa as e.g. *Trema*, *Celtis*, or *Acalypha* after 1 AD (e.g. Bush et al. 2005, Valencia et al. 2010, Sublette Mosblech et al. 2012). The Illimani record suggests that mountain forest ecosystems in the surrounding Central Andes endured during the Inca Empire from 1438−1532 AD, which had its densely populated center in close proximity. Human impact likely changed forest composition as e.g. documented by the marked expansion of disturbance-adapted trees such as e.g. *Alnus* (Chepstow-Lusty et al.

2003, Valencia et al. 2010, Sublette Mosblech et al. 2012). Previous studies concluded that *Alnus acuminata* initially expanded due to climate change after ca. 800 AD and was favored by agroforestry practices of pre-Columbian societies, expanding its altitudinal range above its naturally realized climatic niche (Chepstow-Lusty and Jonsson 2000, Hastorf et al. 2005, Sublette Mosblech et al. 2012). Interestingly in the Illimani area, late-successional Yunga forest taxa (e.g. *Polylepis*, *Hedyosmum*, and Podocarpaceae) expanded together with moist Puna communities after 1360 AD. These expansions were probably climatically induced by the moisture increase of the LIA (Apaéstegui et al. 2018), providing beneficial agropastoral conditions for the rise of the Inca Empire. Rather stable forest and grassland ecosystems in the Central Andes (Chepstow-Lusty et al. 2003, Valencia et al. 2010, Sublette Mosblech et al. 2012) are in apparent contrast with contemporaneous massive forest disruptions as inferred along the Northern Inca trade routes in Ecuador (Loughlin et al. 2018). There, the Inca period was marked by rapid deforestation and a massive fire increase together suggesting ecosystem impacts exceeding the scale of modern disturbance (Loughlin et al. 2018). These differences may point to careful and long-term sustainable ecosystem management in the core region of pre-Columbian societies around Illimani while land use practices in occupied marginal areas were less sustainable.

The Inca Empire declined in 1532 AD with the arrival of the Spanish viceroyalty; during which European livestock was established on the Altiplano and silver mines around Potosi were exploited for the European market (Baied and Wheeler 1993, Preston et al. 2003, Eichler et al. 2017). The lacking response of ecosystems until 1740 AD suggests a lag of 200 years until the Spanish viceroyalty had established a novel political and economic land use system that significantly altered Bolivian and neighboring Andean environments. The sharp shift to dry Puna after 1740 AD, resulting in an Asteroideae dominance comparable to that of the mid-Holocene (Fig. 4), was accompanied by a massive spread of nutrient-loving weedy taxa. This vegetation pattern suggests that marked pastoral activities (see expansion of *Sporormiella*) overran climatic forcing on the Altiplano (Apaéstegui et al. 2018), likely generating a false dry signal (Liu et al. 2005). The large-scale Spanish Colonial land use changes after 1740 AD encompassed rapid compositional changes in mountain forest ecosystems, including new plants from the Old World, such as *Eucalyptus* and *Pinus* that are historically documented in Chile since the 17th century (Simberloff et al. 2010). Unprecedented human-shaped ecosystems shifts after 1740 AD were recorded elsewhere in the region (e.g. McMichael et al. 2017a), suggesting that not surprisingly Colonial activities played a stronger role in shaping modern ecosystems than pre-Columbian societies.

The colonial land use practices during the Spanish viceroyalty initiated a rapid transformation to humanized systems that was reinforced in the following centuries with growing industrialization. Pre-Columbian and Spanish miners exploited mainly copper and silver (Wilson and Petrov 1999, Uglietti et al. 2015, Eichler et al. 2017), despite their knowledge of black coal deposits at the Chilean coast (De Grazia 1997). The Independence from Spain (1809–1825 AD) and growing exchange with English coal-experienced mariners initiated the use of black coal around 1820 AD (De Grazia 1997). The shift to fossil fuel-based energy immediately released a large-scale atmospheric fossil fuel pollution signal, recorded as onset of SCP deposition at Illimani at ca. 1820 AD. The subsequent SCP-inferred fossil fuel pollution increase resulted in a first maximum around 1910–1930 AD. The second maximum at 1950–2000 AD lasted much longer than inferred for the Northern hemisphere, where SCPs usually decline after 1980 AD due to environmental laws and the resulting use of refined combustion technologies (e.g. Rose et al. 2015, Brugger et al. 2018a). The long-lasting fossil fuel pollution in the Andes is consistent with amplified Pb-values, suggesting steady traffic-pollution until ca. 2000 AD (Eichler et al. 2015).

The Illimani record suggests that modern ecosystem conditions were reached only recently after 1950 AD, when the Bolivian land reform of 1952 AD was implemented (Preston et al. 2003). Since the 1960s, natural mountain woodlands across the Neotropics as e.g. former *Polylepis* woodlands are increasingly replaced by monocultures dominated by few exotic species as e.g. *Eucalyptus globulus* and *Pinus radiata* (Buytaert et al. 2007, Simberloff et al. 2010). These plantations bring short-term economic value (Cubbage et al. 2007, Raga 2009) but recent observations suggest effects on soil water-nutrient balance, an invasive character of some tree species, and ecosystem erosions (Peña et al. 2007, Gareca et al. 2007). Rapid climate warming in the past decades (Vuille and Bradley 2000) and associated drought periods affected forests and climate-sensitive Puna communities on the Altiplano, reducing their carrying capacity for herding activity (Adler and Morales 1999). The Holocene fire regime suggests that such drought periods may likewise enhance future fire risks across the Neotropics (Brando et al. 2014, Power et al. 2016). Ensuing rapid ecosystem alterations may result in biodiversity losses (e.g. trough replacement by invasive exotics or extinctions) and unpredictable social costs (Gareca et al. 2007, Raga 2009, Andersson et al. 2016).

5. Conclusions

Our high-resolution record from Illimani provides novel insights into pollution history and fire as well as vegetation responses to past land use in the Central Andean Puna and Yunga vegetation belts. The millennial and centennial scale fire-activity trends were closely related to variability in moisture and the precipitation regime, in response to South American summer monsoon activity and other forcings (e.g. during the LIA), rather than human impact. Pre-Columbian societies practiced land use with moderate large-scale ecosystem alterations on the Altiplano grasslands and in adjacent mountain forest Yungas. These sustainable practices in the center of highly developed native pre-Colombian cultures such as the Incas contrast with massive ecosystem disruptions in marginal areas suggested by previous studies. Unprecedented human-shaped ecosystems emerged after 1740 AD following a wide establishment of novel land use practices by the Spanish viceroyalty. The Colonial land use played a much larger role for the emergence of modern ecosystems than pre-Columbian societies. The rapid shift to humanized ecosystems was further reinforced in the modern era post-1950 AD, with industrial plantations and coal exploitation. We conclude that sustainable agropastoral and agroforestry practices have an ancient tradition in the Central Andes, but recent vast afforestation with exotic monocultures has the potential to result in irreversible ecological and environmental modifications and risks. In combination with rapid climate change and associated fire regime changes such ecosystem modification may provoke unpredictable social and economic costs.

6 Acknowledgments

We thank the joint French-Swiss team from the Institut de Recherche pour le Développement (IRD, France) and the Paul Scherrer Institute (PSI, Switzerland) for drilling in 1999. Theo M. Jenk, Johannes Schindler, Reto Schild, Dieter Stampfli, and Felix Stampfli from PSI are acknowledged for the coring in 2015. We are grateful to Susanne Haselbeck for assistance with ice core sampling and Maria Carolina Guarinello de Oliveira Portes and colleagues at the palynological lab in Göttingen for help with the identification of rare pollen taxa. We acknowledge the Sinergia project *Paleo fires from high-alpine ice cores* funded by the Swiss National Science Foundation (SNF grant 154450).

7 References

Abbott MB, Wolfe AP (2003) Intensive pre-Incan metallurgy recorded by lake sediments from the Bolivian Andes. *Science* 301(5641) 1893-1895

Abbott MB, Wolfe BB, Wolfe AP, Seltzer GO, Aravena R et al. (2003) Holocene paleohydrology and glacial history of the central Andes using multiproxy lake sediment studies. *Palaeogeography, Palaeoclimatology, Palaeoecology* 194(1-3) 123-138

Adler PB, Morales JM (1999) Influence of environmental factors and sheep grazing on an Andean grassland. *Journal of Range Management* 471-481

Aldenderfer M (1999) The Pleistocene/Holocene transition in Peru and its effects upon human use of the landscape. *Quaternary International* 53 11-19

Andersson K, Lawrence D, Zavaleta J, Guariguata MR (2016) More trees, more poverty? The socioeconomic effects of tree plantations in Chile, 2001–2011. *Environmental management* 57(1) 123-136

Apaéstegui J, Cruz FW, Vuille M, Fohlmeister J, Espinoza JC et al. (2018) Precipitation changes over the eastern Bolivian Andes inferred from speleothem (δ 18 O) records for the last 1400 years. *Earth and Planetary Science Letters* 494 124-134

Baied CA, Wheeler JC (1993) Evolution of high Andean puna ecosystems: environment, climate, and culture change over the last 12,000 years in the Central Andes. *Mountain Research and Development* 145-156

Baker PA, Seltzer GO, Fritz SC, Dunbar RB, Grove MJ (2001) The history of South American tropical precipitation for the past 25,000 years. *Science* 291(5504) 640-643

Bennett KD (1996) Determination of the number of zones in a biostratigraphical sequence. *New Phytologist* 132(1) 155-170

Beug HJ (2004) Leitfaden der Pollenbestimmung für Mitteleuropa und angrenzende Gebiete. Pfeil, Munich

Bhargava A, Shukla S, Ohri D (2006) Chenopodium quinoa—an Indian perspective. *Industrial crops and products* 23(1) 73-87

Bird B W, Abbott MB, Vuille M, Rodbell DT, Stansell ND, Rosenmeier MF (2011) A 2,300-year-long annually resolved record of the South American summer monsoon from the Peruvian Andes. *Proceedings of the National Academy of Sciences* 108(21) 8583-8588

Birks HJB, Gordon A (1985) Numerical Methods in Quaternary Pollen Analysis. Academic Press, London

Brando PM, Balch JK, Nepstad DC, Morton DC, Putz FE. et al. (2014) Abrupt increases in Amazonian tree mortality due to drought–fire interactions. *Proceedings of the National Academy of Sciences* 201305499

Brugger SO, Gobet E, van Leeuwen JFN, Ledru MP, Colombaroli D (2016) Long-term man–environment interactions in the Bolivian Amazon: 8000 years of vegetation dynamics.

Quaternary Science Reviews 132 114-128

Brugger SO, Gobet E, Sigl M, Osmont D, Papina T et al. (2018a) Ice records provide new insights into climatic vulnerability of Central Asian forest and steppe communities. *Global and Planetary Change* 169 188-201

Brugger SO, Gobet E, Schanz FR, Heiri O, Schwörer C et al. (2018b) A quantitative comparison of microfossil extraction methods from ice cores. *Journal of Glaciology* 64(245) 432-442

Bruno MC, Whitehead WT (2003) Chenopodium cultivation and formative period agriculture at Chiripa, Bolivia. *Latin American Antiquity* 14(3) 339-355

Burger RL, Gordon RB (1998) Early central Andean metalworking from Mina Perdida, Peru. *Science* 282 1108–1111

Bush MB, Hansen BC, Rodbell DT, Seltzer GO, Young KR (2005) A 17 000-year history of Andean climate and vegetation change from Laguna de Chochos, Peru. *Journal of Quaternary Science* 20(7-8) 703-714

Bush MB, Silman MR, Urrego DH (2004) 48,000 years of climate and forest change in a biodiversity hot spot. *Science* 303(5659) 827-829

Buytaert W, Iniguez V, De Bievre B (2007) The effects of afforestation and cultivation on water yield in the Andean páramo. *Forest ecology and management* 251(1-2) 22-30

Carreira LMM (1996) Catálogo de pólen das leguminosas da Amazônia brasileira. Museu Goeldi, Belém

Chepstow-Lusty A, Jonsson P (2000) Inca agroforestry: lessons from the past. *AMBIO: A Journal of the Human Environment* 29(6) 322-328

Chepstow-Lusty A, Frogley MR, Bauer BS, Bush MB, Herrera AT (2003) A late Holocene record of arid events from the Cuzco region, Peru. *Journal of Quaternary Science* 18(6) 491-502

Colinvaux P, De Olieira PE, Moreno Patino JE (1999) Amazon pollen manual and atlas. Harwood Academic Publishers, Amsterdam

Cruz Jr FW, Burns SJ, Karmann I, Sharp WD, Vuille M et al. (2005) Insolation-driven changes in atmospheric circulation over the past 116,000 years in subtropical Brazil. *Nature* 434(7029) 63

Cubbage F, Mac Donagh P, Júnior JS, Rubilar R, Donoso Pet al. (2007) Timber investment returns for selected plantations and native forests in South America and the Southern United States. *New Forests* 33(3) 237-255

Cugny C, Mazier F, Galop D (2010) Modern and fossil non-pollen palynomorphs from the Basque mountains (western Pyrenees, France): the use of coprophilous fungi to reconstruct pastoral activity. *Vegetation history and Archaeobotany* 19(5-6) 391-408

De Grazia LM (1997) Los británicos y el carbón en Chile. *Revista Atenea* 475-1957

Eichler A, Tinner W, Brütsch S, Olivier S, Papina T, Schwikowski M (2011) An ice-core based history of Siberian forest fires since AD 1250. *Quaternary Science Reviews* 30(9-10) 1027-1034

Eichler A, Gramlich G, Kellerhals T, Tobler L, Rehren T, Schwikowski M (2017) Ice-core evidence of earliest extensive copper metallurgy in the Andes 2700 years ago. *Scientific Reports* 7 41855

Eichler A, Gramlich G, Kellerhals T, Tobler L, Schwikowski M (2015) Pb pollution from leaded gasoline in South America in the context of a 2000-year metallurgical history. *Science advances* 1(2) e1400196

Finsinger W, Tinner W (2005) Minimum count sums for charcoal concentration estimates in pollen slides: accuracy and potential errors. *The Holocene* 15(2) 293-297

Flantua S, Hooghiemstra H, Vuille M, Behling H, Carson JF et al. (2016) Climate variability and human impact in South America during the last 2000 years: synthesis and perspectives from pollen records. *Climate of the Past* 12(2) 483-523

Gareca EE, Martinez YY, Bustamante RO, Aguirre LF, Siles MM (2007) Regeneration patterns of Polylepis subtusalbida growing with the exotic trees Pinus radiata and Eucalyptus globulus at Parque Nacional Tunari, Bolivia. *Plant Ecology* 193(2) 253-263

Gilgen A, Adolf C, Brugger SO, Ickes L, Schwikowski M et al. (2018) Implementing microscopic charcoal particles into a global aerosol–climate model. *Atmospheric chemistry and physics* 18(16) 11813-11829

Hansen BC, Rodbell DT (1995) A late-glacial/Holocene pollen record from the eastern Andes of northern Peru. *Quaternary Research* 44(2) 216-227

Hanselman JA, Gosling WD, Paduano GM, Bush MB (2005) Contrasting pollen histories of MIS 5e and the Holocene from Lake Titicaca (Bolivia/Peru). *Journal of Quaternary Science* 20(7-8) 663-670

Hastorf CA, Whitehead WT, Johannessen S (2005) Late prehistoric wood use in an Andean intermontane valley. *Economic Botany* 59(4) 337-355

Herrera LF, Urrego LE (1996) Atlas de polen de plantas útiles y cultivadas de la Amazonia colombiana [Pollen Atlas of Useful and Cultivated Plants in the Colombian Amazon]. Programa Trobenbos, Bogota

Heusser CJ (1971) Pollen and Spores of Chile: Modern-types of the Pteridophyta, Gymnospermae, Angiospermae. University of Arizona Press, Tucson

Hooghiemstra H (1983) Pollen morphology of the Plantago species of the Colombian Andes and its application to fossil material. *Revista de la Academia Colombiana de Ciencias Exactas Fisicas y Naturales* 15(58) 41-65

Hooghiemstra H (1984) Vegetational and climatic history of the high plain of Bogotá, Colombia. J Cramer, Vaduz

Ibisch PL, Mérida G (2004) Biodiversity: the richness of Bolivia: state of knowledge and conservation. Editorial FAN, Santa Cruz de la Sierra

Jarvis DE, Ho YS, Lightfoot DJ, Schmöckel SM, Li B et al. (2017) The genome of Chenopodium quinoa. *Nature* 542(7641) 307

Kellerhals T, Brütsch S, Sigl M, Knüsel S, Gäggeler HW, Schwikowski M (2010) Ammonium concentration in ice cores: A new proxy for regional temperature reconstruction?. *Journal of Geophysical Research: Atmospheres* 115(D16)

Knüsel S, Ginot P, Schotterer U, Schwikowski M, Gäggeler HW et al. (2003) Dating of two nearby ice cores from the Illimani, Bolivia. *Journal of Geophysical Research: Atmospheres* 108(D6)

Levis C, Costa FR, Bongers F, Peña-Claros M, Clement CR et al. (2017) Persistent effects of pre-Columbian plant domestication on Amazonian forest composition. *Science* 355(6328) 925-931

Liu KB, Reese CA, Thompson LG (2005) Ice-core pollen record of climatic changes in the central Andes during the last 400 yr. *Quaternary Research* 64(2) 272-278

Loughlin NJ, Gosling WD, Mothes P, Montoya E (2018) Ecological consequences of post-Columbian indigenous depopulation in the Andean–Amazonian corridor. *Nature Ecology & Evolution* 2(8) 1233

Lynch TF (1983) Camelid pastoralism and the emergence of Tiwanaku civilization in the South-Central Andes. *World Archaeology* 15(1) 1-14

Magrin GO, Marengo JA, Boulanger J-P, Buckeridge MS, Castellanos E et al. (2014) Central and South America. In: Climate Change 2014: Impacts, Adaptation, and Vulnerability. Part B: Regional Aspects. Contribution of Working Group II to the Fifth Assessment Report of the Intergovernmental Panel on Climate Change. Cambridge University Press, Cambridge, New York, pp. 1499-1566

Marchant R, Almeida L, Behling H, Berrio JC, Bush M, (2002) Distribution and ecology of parent taxa of pollen lodged within the Latin American Pollen Database. *Review of Palaeobotany and Palynology* 121(1) 1-75

Markgraf V, D'Antoni HL (1978) Pollen flora of Argentina. Modern spore and pollen types of Pteridophyta, Gymnospermae, and Angiospermae. University of Arizona Press, Tucson

Marsh EJ (2015) The emergence of agropastoralism: Accelerated ecocultural change on the Andean altiplano,~ 3540–3120 cal BP. *Environmental Archaeology* 20(1) 13

Mayle FE, Beerling DJ, Gosling WD, Bush MB (2004) Responses of Amazonian ecosystems to climatic and atmospheric carbon dioxide changes since the last glacial maximum. *Philosophical Transactions of the Royal Society of London B* 359(1443) 499-514

McMichael CH, Feeley KJ, Dick CW, Piperno DR, Bush MB (2017a) Comment on "Persistent effects of pre-Columbian plant domestication on Amazonian forest composition". *Science* 358(6361)

McMichael CN, Matthews-Bird F, Farfan-Rios W, Feeley KJ (2017b) Ancient human disturbances may be skewing our understanding of Amazonian forests. *Proceedings of the National Academy of Sciences* 114(3) 522-527

Minvielle M, Garreaud RD (2011) Projecting rainfall changes over the South American Altiplano. *Journal of Climate* 24(17) 4577-4583

Mourguiart P, Ledru MP (2003) Last glacial maximum in an Andean cloud forest environment (Eastern Cordillera, Bolivia). *Geology* 31(3) 195-198

Navarro Sanchez G (2011) Clasification de la Vegetation de Bolivia. Fundation Simon I. Patino, Santa Cruz de la Sierra

Nolan C, Overpeck JT, Allen JR, Anderson PM, Betancourt JL et al. (2018) Past and future global transformation of terrestrial ecosystems under climate change. *Science* 361(6405) 920-923

Nunez L, Grosjean M, Cartajena I (2002) Human occupations and climate change in the Puna de Atacama, Chile. *Science* 298(5594) 821-824

Olson DM, Dinerstein E (2002) The Global 200: Priority ecoregions for global conservation. *Annals of the Missouri Botanical garden* 199-224

Osmont D, Sigl M, Eichler A, Jenk TM, Schwikowski M (in review) A Holocene black carbon ice-core record of biomass burning in the Amazon Basin from Illimani, Bolivia.

Paduano GM, Bush MB, Baker PA, Fritz SC, Seltzer GO (2003) A vegetation and fire history of Lake Titicaca since the Last Glacial Maximum. *Palaeogeography, Palaeoclimatology, Palaeoecology* 194(1-3) 259-279

Peel MC, Finlayson BL, McMahon TA (2007) Updated world map of the Köppen-Geiger climate classification. *Hydrology and earth system sciences discussions* 4(2) 439-473

Peña E, Hidalgo M, Langdon B, Pauchard A (2008) Patterns of spread of Pinus contorta Dougl. ex Loud. invasion in a Natural Reserve in southern South America. *Forest Ecology and Management* 256(5) 1049-1054

Piperno DR, McMichael C, Bush MB (2017). Further evidence for localized, short-term anthropogenic forest alterations across pre-Columbian Amazonia. *Proceedings of the National Academy of Sciences* 114(21) E4118-E4119

Power MJ, Whitney BS, Mayle FE, Neves DM, de Boer EJ, Maclean KS (2016) Fire, climate and vegetation linkages in the Bolivian Chiquitano seasonally dry tropical forest. *Philosophical Transactions of the Royal Society B* 371(1696) 20150165

Power MJ, Mayle FE, Bartlein PJ, Marlon JR, Anderson RS et al. (2013). Climatic control of the biomass-burning decline in the Americas after AD 1500. *The Holocene* 23(1) 3-13

Preston D, Fairbairn J, Paniagua N, Maas G, Yevara M, Beck S (2003) Grazing and environmental change on the Tarija Altiplano, Bolivia. *Mountain Research and Development* 23(2) 141-148

Raga F (2009) The Chilean forestry sector and associated risks. *Trébol* 51 10-19

Reese CA, Liu KB, Thompson LG (2013) An ice-core pollen record showing vegetation response to Late-glacial and Holocene climate changes at Nevado Sajama, Bolivia. *Annals of Glaciology* 54(63) 183-190

Roberts P, Boivin N, Kaplan JO (2018) Finding the anthropocene in tropical forests. *Anthropocene* 23 5-16

Rose NL (2015) Spheroidal carbonaceous fly ash particles provide a globally synchronous stratigraphic marker for the Anthropocene. *Environmental Science & Technology* 49(7) 4155-4162

Roubik DW, Moreno P (1991) Pollen and spores of Barro Colorado Island [Panama]. Missouri Botanical Garden, St. Louis

Seddon AW, Mackay AW, Baker AG, Birks HJB, Breman E et al. (2014) Looking forward through the past: identification of 50 priority research questions in palaeoecology. *Journal of Ecology* 102(1) 256-267

Simberloff D, Nunez MA, Ledgard NJ, Pauchard A, Richardson DM et al. (2010) Spread and impact of introduced conifers in South America: lessons from other southern hemisphere regions. *Austral Ecology* 35(5) 489-504

Staller JE (2016) High Altitude Maize (Zea Mays L.) Cultivation and Endemism in the Lake Titicaca Basin. *Journal of Botanical Research* 1(1) 8-21

Sublette Mosblech NA, Chepstow-Lusty A, Valencia BG, Bush MB (2012) Anthropogenic control of late-Holocene landscapes in the Cuzco region, Peru. *The Holocene* 22(12) 1361-1372

Ter Braak CJF, Prentice IC (1988) A theory of gradient analysis. In Begon M, Fitter AH, Ford ED, Macfadyen A. Advances in Ecological Research Volume 18. Academic Press, p. 271-317

Thompson LG, Mosley-Thompson E, Dansgaard W, Grootes PM (1986) The Little Ice Age as recorded in the stratigraphy of the tropical Quelccaya ice cap. *Science* 234(4774) 361-364

Tinner W, Hu FS (2003) Size parameters, size-class distribution and area-number relationship of microscopic charcoal: relevance for fire reconstruction. *The Holocene* 13(4) 499-505

Uglietti C, Gabrielli P, Cooke CA, Vallelonga P, Thompson LG et al. (2015) Widespread pollution of the South American atmosphere predates the industrial revolution by 240 y. *Proceedings of the National Academy of Sciences* 112(8) 2349-2354

Urrego DH, Bush MB, Silman MR, Niccum BA, De La Rosa P et al. (2013) Holocene fires, forest stability and human occupation in south-western Amazonia. *Journal of biogeography* 40(3) 521-533

Urrego DH, Silman MR, Bush MB (2005) The Last Glacial Maximum: stability and change in a western Amazonian cloud forest. *Journal of Quaternary Science* 20(7-8) 693-701

Valencia BG, Urrego DH, Silman MR, Bush MB (2010) From ice age to modern: a record of landscape change in an Andean cloud forest. *Journal of Biogeography* 37(9) 1637-1647

Vuille M, Bradley RS, Keimig F (2000) Interannual climate variability in the Central Andes and its relation to tropical Pacific and Atlantic forcing. *Journal of Geophysical Research: Atmospheres* 105(D10) 12447-12460

Vuille M, Bradley RS (2000) Mean annual temperature trends and their vertical structure in the tropical Andes. *Geophysical Research Letters* 27(23) 3885-3888

Vuille M, Burns SJ, Taylor BL, Cruz, FW, Bird BW (2012) A review of the South American monsoon history as recorded in stable isotopic proxies over the past two millennia. *Climate of the Past* 8(4) 1309-1321

Watling J, Iriarte J, Mayle FE, Schaan D, Pessenda LC (2017) Reply to Piperno et al.: It is too soon to argue for localized, short-term human impacts in interfluvial Amazonia. *Proceedings of the National Academy of Sciences* 114(21) E4120-E4121

Wilson WE, Petrov A (1999) Famous mineral localities: Cerro Rico de Potosí, Bolivia. *The Mineralogical Record* 30(1) 9-11

8 Figures

Figure 1 Vegetation map of Bolivia. A: Vegetation distribution with indication of the glacier site Illimani (red triangle), large waterbodies in blue. Red dashed circle indicates the assumed main source area for the pollen signal (a radius of ca. 200–300 km around the site, Brugger et al. 2018a). B: Altitudinal range and precipitation gradient of vegetation types. Classification adapted from Ibisch and Mérida (2004).

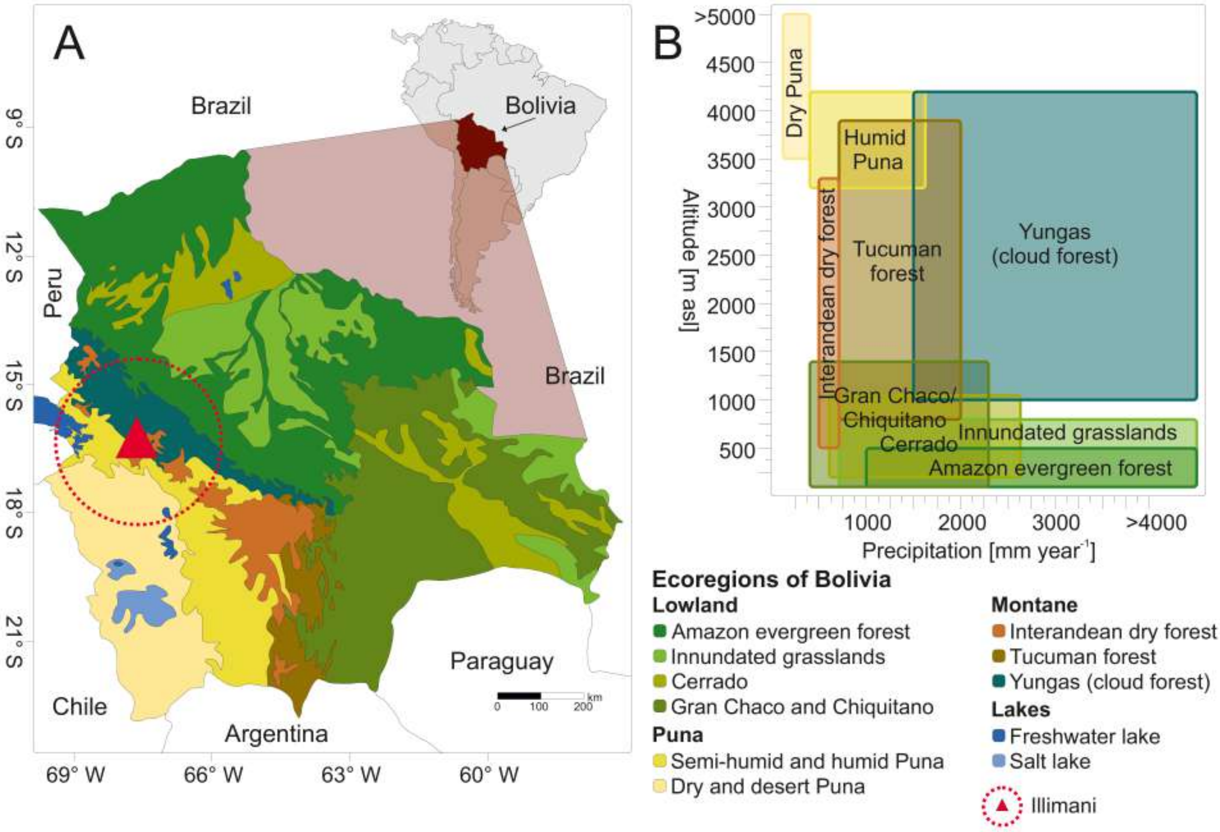

Figure 2 Chronology of the Illimani '99 ice core on a logarithmic scale. Age-depth relationship is based on the drilling year in 1999 AD. Detected volcanic ash layers (red triangles), maximum Tritium peak (green triangle) and six calibrated 14C dates (blue dots, numbers show 1σ ranges) were used for the construction of the age-depth model. The bedrock at 113.2 m weq depth is indicated by a dashed line. The Illimani '15 shallow core is not included in the original chronology as shown in this figure. Chronology adapted from Knüsel et al. 2003, Kellerhals et al. 2010).

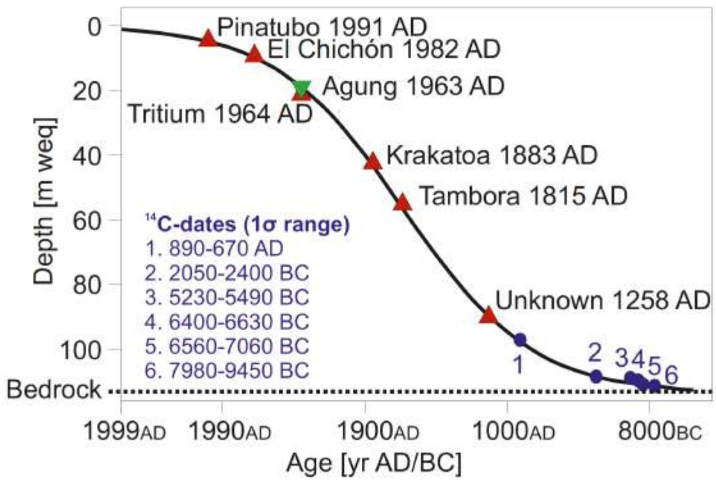

Figure 3 Principal component analysis (PCA) for the Illimani palynological ice record based on square-root-transformed pollen percentages of the terrestrial pollen sum. PCA shows vegetation shifts along an environmental gradient over time. Sample scores for axis 1 and 2 are grouped by local pollen assemblage zones (LPAZ established following Birks and Gordon (1985) and Bennett (1996), marked with different colors in lilac box). Samples of the shallow Illimani 2015 core (Illi'15) group closely together with recent samples (LPAZ Illi-5) of the Holocene Illimani 1999 ice record.

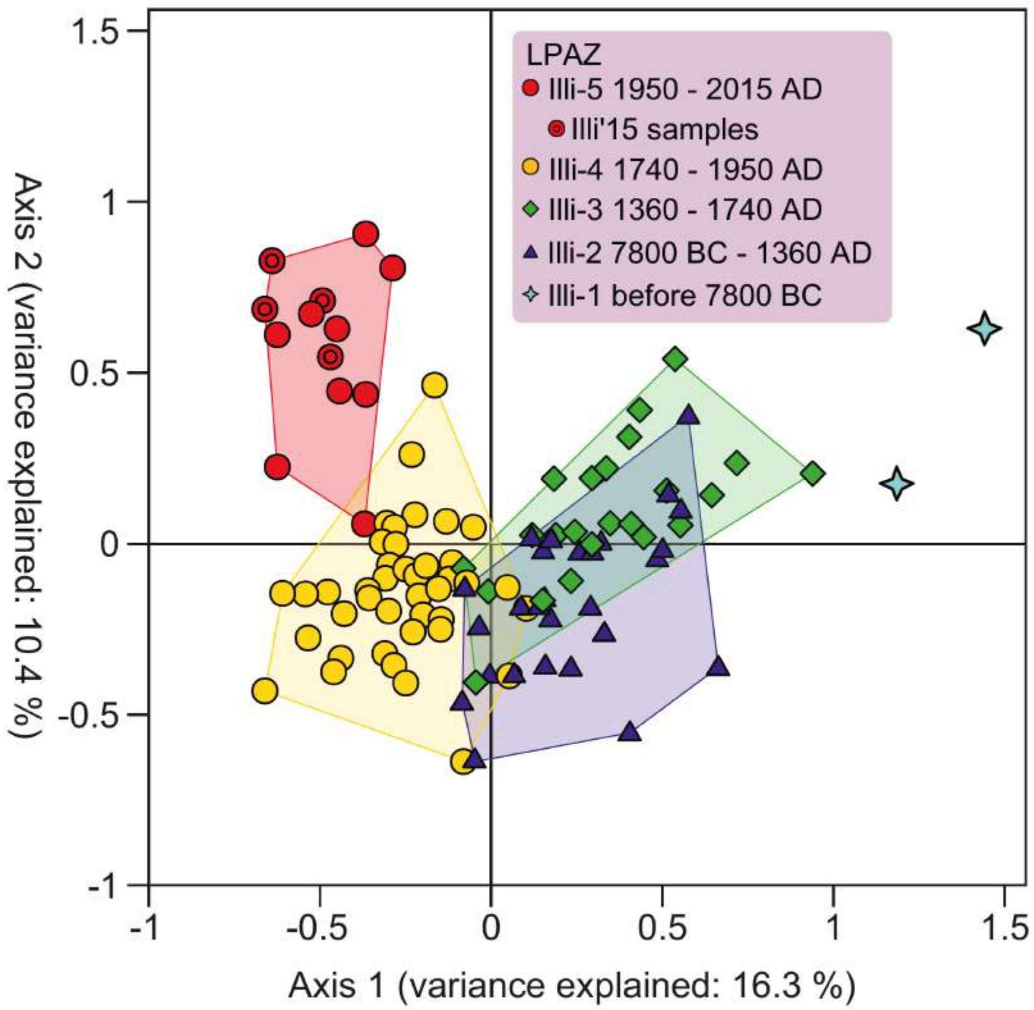

Figure 4 Percentage diagram of the Illimani ice record based on the terrestrial pollen sum with selected pollen types and the coprophilous fungal spore *Sporormiella*. See Supplementary table S1 for taxa included in the lowland evergreen sum curve. Hollow curves = 10x exaggeration. Concentration curves for microscopic charcoal, spheroidal carbonaceous particles (SCPs), and pollen. LPAZ = statistically derived local pollen assemblage zones (Birks and Gordon 1985, Bennett 1996). Depth indicates master core depth in m water equivalent of combined ice cores Illimani 2015 and Illimani 1999. Chronology is based on volcanic eruption layers (VE) and ^{14}C- dates (chronology details in Supplementary 3; Kellerhals et al. 2010). Time axis adjusted to increase visibility for the recent part (post-1 AD) due to increasing sample resolution.

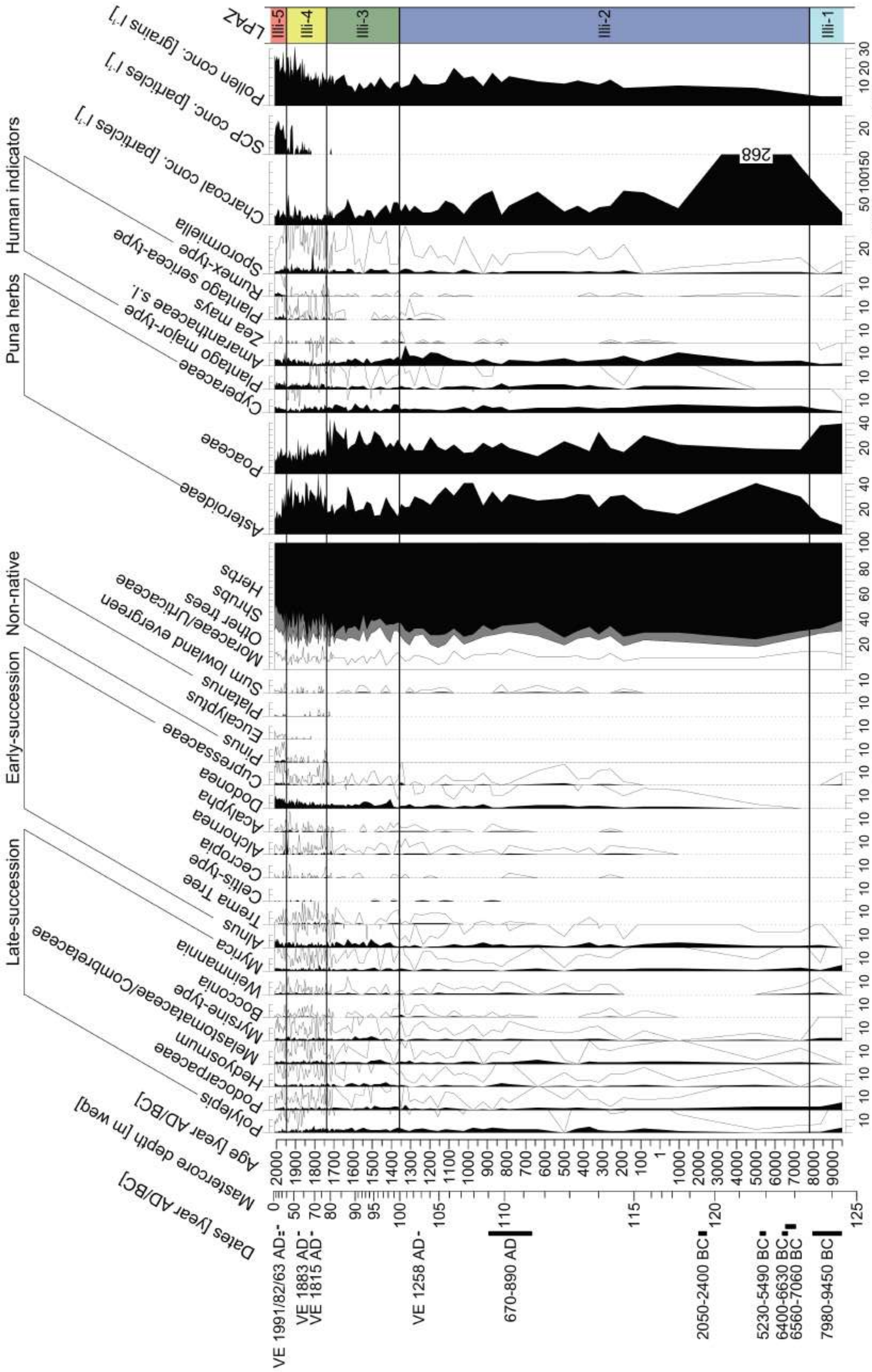

Supplementary material

Figure S1 Correlation of ice core Illi-’15 and Illi-’99. Overlapping palynological sequences (years 1996–1999 AD) from Illimani ice cores drilled in 2015 (Illi’15) and in 1999 (Illi’99). Red line indicates the tie point in 1998 AD for the two ice records based on the palynological assemblages of the overlapping sequences that suggest reproducible data.

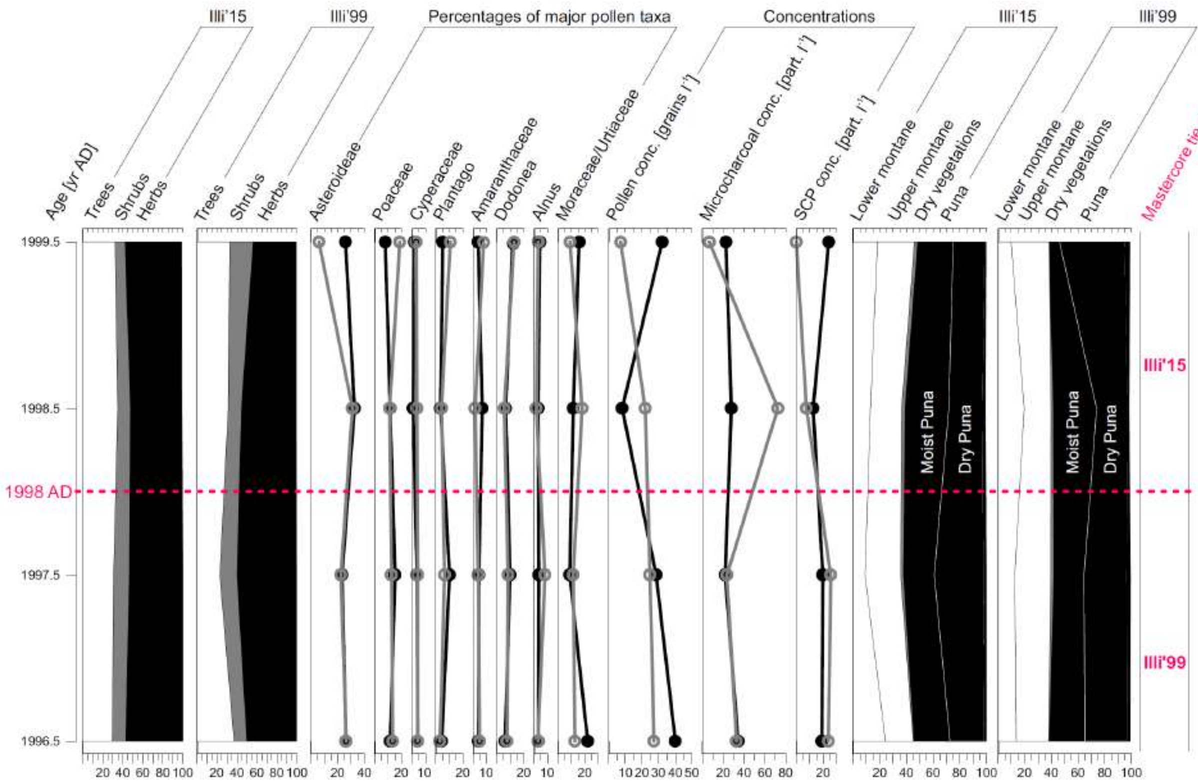

Table S1 List of pollen, spore, and other cell types found in the Illimani ice record and their attribution to summary groups in the pollen diagram. Assignment to ecosystems according to main taxa distribution following Marchant et al. (2002) and Navarro Sanchez (2011). Symbols in brackets indicate morphotype abundance in samples: taxa recorded in one sample (1), in less than 10 % of all samples (<10), in 10–50 % of all samples (+), and in >50 % of all samples (++).

Distribution	Taxa
Dry Puna	**Herbs**: *Achillea*-type (+), Amaranthaceae (++), *Ambrosia*-type (++), Apiaceae (++), other Asteroideae (++), *Baccharis*-type (++), *Artemisia* (+), Brassicaceae (<10), Bromeliaceae (++), Caryophyllaceae (+), *Cerealia*-type (++), Cichorioideae (+), Cyperaceae (++), *Fragaria*-type (<10), *Gomphrena* (+), Lamiaceae (<10), *Lathyrus*-type (+), Liliaceae (1), *Malva*-type (<10), other Malvaceae (+), other *Plantago* (++), *P. alpina*-type (<10), *P. sericea*-type (++), *P. major* -type (++),Polygalaceae (<10), other Rosaceae (++), *Potentilla*-type (<10), *Rumex acetosella*-type (++), *R. alpinus*-type (<10), *Senecio*-type (++), **Shrubs/lianas**: *Ephedra dystachya*-type (<10), *E. fragilis*-type (++)
Humid Puna	**Herbs**: *Borreria*-type (+), Geraniaceae (<10), *Hypericum* (+), *Lupinus*-type (+), Poaceae (++), other Ranunculaceae (<10), *Ranunculus acris*-type (1), *R. bonarien*sis-type (+),Valerianaceae (<10) **Shrubs/lianas**: Ericaceae (+), *Monnina* (<10)
Upper Yuncas	**Herbs**: *Cuphea* (<10), *Galium*-type (+), *Thalictrum* (++), **Shrubs/lianas**: other Cupressaceae (+), *Dodonaea* (++), *Juniperus*-type (++), Loranthaceae (+), *Muehlenbeckia*-type (<10), *Myrica* (++), *Salix humboldtiana* (+), Solanaceae (+), **Trees**: *Alnus* (++), Araliaceae (<10), *Bocconia* (++), *Clethra*-type (+), Clusiaceae (1), *Didimopanax*-type (<10), Euphorbiaceae (++), *Ficus* (<10), Flacourtiaceae (1), *Hedyosmum* (++), *Juglans* (++), other Melastomataceae/Combretaceae (++), *Miconia*-type (+), *Myrsine*-type (++), other Myrtaceae (+), Podocarpaceae (++), *Polylepis* (++), Proteaceae (1), *Prunus*-type (+), *Quercus humboldtii* (++), Rhamnaceae (<10), other Rubiaceae (+), *Sambucus*-type (1), *Sapium*-type (<10), *Styrax* (<10), Thymelaeaceae (<10), *Vallea* (++), *Weinmannia* (++)
Lower Yungas	**Herbs**: *Amaryllis*-type (1), *Begonia* (+), **Shrubs/lianas**: Cannabaceae (<10), *Croton*-type (+), Menispermaceae (+), *Paullinia* (<10), *Vitis*-type (<10), **Trees**: *Acalypha* (++), *Acer* (<10), *Alchornea* (++), other Anacardiaceae (+), other Arecaceae (+), Bignoniaceae (<10), *Cecropia* (+), *Celtis*-type (+), Elaeocarpaceae (1), *Hyeronima*-type (<10), *Luahea*-type (+), Malpighiaceae (<10), other Moraceae/Urticaceae (++), *Phyllanthus*-type (+), *Piper* (+), Sapindaceae (+), other Tiliaceae (<10), *Trema* (++), *Triumfetta*-type (+), *Vochysia*-type (<10)
Xerophytic	**Herbs**: Boraginaceae (1), Convolvulaceae (<10), *Dalechampia* (1), *Dipsacus*-type (1), *Echium* (1), Papilionoides (1), **Shrubs/lianas**: other Cactaceae (<10), *Eulychnia*-type (1), *Maihuenia*-type (1), *Opuntia* (<10), *Rhipsalis*-type(<10), **Trees**: *Acacia*-type (1), *Adenanthera*-type (+), *Albizia*-type (+), *Anadenanthera*-type (+), Apocynaceae (<10), Fabaceae (++), other *Mimosa*-type (++), *M. pteridifolia*-type (1), *M. pudica*-type (<10), *M. scabrella*-type (+), other Mimosoideae (++), *Schinus* (+)
Lowland evergreen	**Shrubs/lianas**: *Hippocratea* (<10), **Trees**: *Apeiba* (1), *Aphelandra*-type (<10), Bombacaceae (1), *Mabea*-type (<10), *Machaerium*-type (<10), *Mauritia/Muritiella* (1), *Mortoniodendron*-type (1), *Pseudobombax*-type (<10), *Tilia*-type (+)
Long-distance	**Shrubs/lianas**: *Lonicera* (1), Trees: *Abies* (<10), *Carpinus*-type (+), *Nothofagus* (+), *Ulmus* (<10)
Non-native	**Herbs**: *Impatiens* (1), *Papaver rhoeas*-type (1), **Trees**: *Aesculus hypocastanea* (<10), *Eucalyptus* (+), *Fortunaeria*-type (1), *Picea* (+), *Pinus sylvestris*-type (+), *Platanus* (+)
Other	**Cultivated herbs**: *Zea mays* (+), **Aquatic**: *Myriophyllum*-type (<10), *Typha*/*Sparganium* (+), **Varia pollen**: unknown pollen grains,
NPP	**Fern spores**: *Cyathea* (<10), *Isoetes* (++), *Lycopodium* (<10), monolete (++), trilete (++), **Fungal spores**: *Sporormiella* (++), *Ustulina* (+), other fungal spores, **Algae**: *Pediastrum* (1)

Manuscript 5

Palynological insights into global change impacts on Arctic vegetation, fire, and pollution recorded in Central Greenland ice

Sandra O. Brugger[1,2,*], Erika Gobet[1,2], Thomas Blunier[3], César Morales-Molino[1,2,4], André F. Lotter[1], Margit Schwikowski[2,5,6], Willy Tinner[1,2]

[1]Institute of Plant Sciences, University of Bern, Switzerland
[2]Oeschger Center for Climate Change Research, University of Bern, Switzerland
[3]Centre for Ice and Climate, Niels Bohr Institute, University of Copenhagen, Denmark
[4]Institute for Forest, Snow and Landscape Research, Cadenazzo, Switzerland
[5]Paul Scherrer Institute, Villigen, Switzerland
[6]Department for Chemistry and Biochemistry, University of Bern, Switzerland

[*]Corresponding author: Sandra O. Brugger

Keywords: *Betula* woodlands – Coal mining – Palaeoecology – Pollen – Microscopic charcoal – SCP (spheroidal carbonaceous particles)

Prepared for *The Holocene Research Report*

Abstract

Arctic environments may respond very sensitively to ongoing global change, as observed during the past decades for Arctic vegetation. Only little is known about the large-scale impacts of early- and mid-20th century industrialization and climate change on remote arctic environments. Palynological analyses of Central Greenland ice cores may provide invaluable insights into the long-term vegetation, fire, and pollution dynamics in the Arctic region. We present a palynological record of the Summit Eurocore ’89 ice core from Central Greenland (72°35'N, 37°38'W; the location of Greenland Ice core Project GRIP) that provides novel high-resolution microfossil data on Arctic environments spanning the past ~300 years (1730–1989 AD). Our data suggest an expansion of birch woodlands after 1850 AD that was abruptly interrupted at the onset of the 20th century despite propitious climatic conditions. We therefore attribute this *Betula* woodland decline during the 20th century to anthropogenic activities such as sheep herding and wood collection. First signs of coal burning activities around 1900 AD coincide with the onset of Arctic coal mining. The use of coal and fire activity increased steadily until 1989 AD resulting in microscopic pollution of the ice sheet. We conclude that human impact during the 20th century strongly affected (sub)-Arctic environments. Moreover, ecosystems have changed through the spread of adventive plant species (e.g. *Ranunculus acris*, *Rumex*) and the destruction of sparse native woodlands.

1 Introduction

Central Greenland ice cores are key records of past environmental change in the Northern Hemisphere (e.g. Blunier et al., 1993; Hartmann et al., in review; Rasmussen et al., 2014; Seierstad et al., 2014; Vinther et al., 2010). Palaeoecological studies from such ice cores are rare and mainly rely on molecular approaches, while microfossil-based studies are lacking (De Vernal and Hillaire-Marcel, 2008; Willerslev et al., 2007). Moreover, existing Arctic palynological ice studies are restricted to pollen source areas and the assessment of wind directions and generally do not fully exploit the potential to reconstruct large-scale ecological and environmental dynamics (Bourgeois et al., 2000; Hicks and Isaksson, 2006; McAndrews, 1984; Short and Holdsworth, 1985). Palynological studies on mire and lake deposits on the other hand focus primarily on the local impact on vegetation of Old Norse settlements (985–1500 AD) or formerly pristine Greenland environments (Barlow et al., 1997; Bryan, 1954; Gauthier et al., 2010; Schofield and Edwards, 2011; Schofield et al., 2013; Wagner et al., 2008). Consequently, little is known about the large-scale impact of recent global change in remote Greenland. Current observations of increased fires in thawing permafrost areas in Greenland and browning of vegetation raise public concern about future environmental risks in the Arctic region (Phoenix and Bjerke, 2016; Wendel, 2017). Palaeoecology may provide valuable pre-industrial base-line information and a long-term perspective on these recent observations. It may also help answering how the 20th century industrialization and rapid global change is affecting sparsely inhabited and remote Arctic environments (Petit et al., 2008). For instance, recent studies suggest that submicron particles from large-scale pollution in Europe reached the Arctic already since the Antiquity (McConnell et al., 2018) while environmental impacts of larger particle deposition may have started only with local industrialization.

Vast Greenland ice sheets cover a radius of 300 km around Summit. Hence, the area is extremely remote and exceptionally distant from local sources of biomass and industrial burning. Such a setting is ideal to investigate large-scale environmental and ecological dynamics by avoiding influences of local sources and the supra-regional impact of global change in the Arctic. To our knowledge, we present the first palynological attempt at reconstructing Greenland vegetation, fire, and pollution from fossil fuel burning history from a site in Central Greenland. Covering the past 250 years the novel data are used to compare industrial impacts to pre-industrial conditions, and to identify triggers, processes, and mechanisms of Greenland and Arctic environmental change under global change conditions.

2 Study site and the Arctic environment

Greenland is the largest island on Earth with a vast glacial area extending to 1.8 million km^2 (Pfadenhauer and Klötzli, 2015) and its apex Summit reaching 3232 m a.s.l. (72°35'N, 37°38'W). The climate is arctic to subarctic oceanic in the southern and southwestern part of Greenland exhibiting high rain- and snowfall (2200 mm weq year^{-1}; weq = water equivalent). Annual temperature amplitudes are relatively small but increase with growing continentality in the northern parts of the island, where precipitation declines (300 mm weq; Böcher et al., 1968; Mernild et al., 2015). Only a narrow ice-free band along the coast hosts Arctic tundra vegetation, with the largest stands growing in the northernmost part where snowfall is minimum (Fig. 1).

The Arctic tundra biome is characterized by a short growing season (1-3 months with a mean monthly temperature mean above 5° C) and long winters with extreme frost periods (temperatures below -30° C; Nentwig et al., 2004). Precipitation is not limiting for plant growth, as evapotranspiration is low (Nentwig et al., 2004). Due to harsh climatic conditions combined with the isolated position in the North Atlantic, the modern flora in Greenland consists only of roughly 500 vascular plants of which many are restricted to the subarctic, low-arctic, and high-arctic vegetation types (Bennike, 1999; Böcher et al., 1968).

Subarctic vegetation is constrained to the warmest valleys in the southern and southwestern part of Greenland, where summer temperatures are sufficiently high to support thickets and woodlands including *Betula glandulosa,* *Salix glauca*, *Alnus viridis*, and the only native tree species *Betula pubescens,* growing up to 4 m height (Böcher et al., 1968). This subarctic vegetation corresponds to small patches of boreal vegetation elements within the Arctic tundra biome. The potential upper tree line is at 100–200 m a.s.l. (Ødum, 1979) where average July temperatures are 9-12° C (Anderson et al., 1991; Timoney et al., 1992). Low-arctic vegetation extends up to 72° N in sheltered inland areas where July temperatures >7° C allow *Salix*-*Juniperus* shrub tundra formations (Böcher et al., 1968; Pfadenhauer and Klötzli, 2015). Finally, tall shrubs such as *B. glandulosa* and *A. viridis* are absent in the high-arctic vegetation north of ca. 69-72°N. This vegetation type is mainly composed of *Cassiope* (Ericaceae) heathlands, bogs, and grass tundra species (e.g. *Deschampsia brevifolia*, *Festuca* ssp., *Poa abbreviata*, *Taraxacum arcticum*, *T. pumilum*), and *Betula* *nana* may penetrate north to ca. 78° N (Böcher et al., 1968).

Although *B. pubescens* is the only native boreal tree, few conifer species such as *Pinus sylvestris, P. contorta, Larix sibirica, Picea glauca*, and *Abies lasiocarpa* endure in small plantations around villages in southern Greenland today (Ødum, 1979). However, the closest natural conifer forests occur in North America, where *Picea* *mariana,* *P. glauca*, *Abies balsamea,* and *Pinus banksiana* grow up to 50° N (~2000 km southwestwards from Summit; Pfadenhauer and Klötzli, 2015). American nemoboreal deciduous forests with e.g. *Acer saccharum* and *Tilia* *americana* are located about 3000 km southwest of Summit, while *Quercus* species are restricted to warmer regions further south (Pfadenhauer and Klötzli, 2015).

3 Material and Methods

The ice core was drilled during the Eurocore project in 1989 at Summit in Central Greenland (location of GRIP, Greenland Ice Core Project). Its chronology is based on electrical conductivity, chemical data, and acid layers of volcanic eruptions (accuracy ±2 years; Blunier et al., 1993; Cachier and Pertuisot, 1994). We dedicated the remaining firn ice of 2.5 x 2.5 cm thickness spanning 0–80 m of core depth (1730–1989 AD) to palynological analyses, with a gap between 58.3–61.0 m (= 11 years). The 19 samples weighed 1090–3160 g (average = 2360 g) covering ~12 years each. Microfossil extraction followed a standard protocol for ice sample preparation (Brugger et al., 2018a) with an additional 40% HF treatment to dissolve abundant dust particles.

We use pollen and spores as a proxy for vegetation and land-use. The counted pollen sums ranged between 28 and 122 (average = 56) grains which is around the absolute minimum to achieve stable percentage values for environmental reconstructions (40-50 items, Heiri and Lotter, 2001). Pollen and spore identification under a light microscope at 400 x magnification followed Beug (2004), McAndrews et al. (1973), Moore et al. (1991), and the reference collection at the Palaeoecology lab in Bern (Table S1). We separated *Betula* pollen into a tree *Betula*-type (referred to as *Betula alba*-type) and a shrub *Betula*-type (*Betula nana*-type; following Birks, 1968; Clegg et al., 2005). We present pollen and spore data as percentages of the pollen sum with summary curves (trees, shrubs) for native Greenland arboreal taxa (Böcher et al., 1968; complete taxon list and assignment to summary curves in Table S1).

We estimated palynological richness (PRI) as a proxy for plant species richness using rarefaction analysis and the probability of interspecific encounter (PIE) as a measure for palynological evenness (Birks and Line, 1992; Hurlbert, 1971). We applied Principal Component Analysis (PCA) to the pollen percentage data, only including native Greenland taxa, to investigate vegetation shifts in the subarctic and arctic vegetation types (following Böcher et al., 1968; see Table S1). The short gradient length of the first axis (= 1.57) of detrended correspondence analysis (DCA, detrended by segments) justifies using linear ordination methods (ter Braak and Prentice, 1988).

We used standard analysis for microscopic charcoal > 10 µm to infer regional fire activity (e.g. Adolf et al. 2018; Brugger et al., 2018b; Finsinger and Tinner, 2005; Tinner and Hu, 2003). Spheroidal carbonaceous particles (SCP) with a diameter > 10 µm and clear features were counted to reconstruct microscopic fossil fuel pollution (Brugger et al., 2018b; Rose, 2015). We standardized all microfossil concentrations to one liter.

4 Results and Interpretation

4.1 Pollen deposition

Pollen concentrations in the Eurocore ice record are ca. 20 grains l^{-1} in the oldest part and increase to 50 grains l^{-1} after 1790 AD, except in the uppermost sample with a relatively high pollen concentration (ca. 410 grains l^{-1}; Fig. 2). This corresponds to a pollen influx along the record of ca. 0.7 grains cm^{-2} $year^{-1}$, which increases in the top sample to ca. 7 grains cm^{-2} $year^{-1}$. Pollen influx in remote Central Greenland is extremely low compared to estimates from other ice records including Arctic sites (e.g. Hicks and Isaksson, 2006; Brugger et al. 2018b) This can be expected because of the long distance to the closest plants. In general, the taxonomic composition of the pollen assemblages is similar to that of other Arctic ice records with high shares of *Betula* (*B. alba* and *B. nana* types), Poaceae, and *Artemisia*. The large portions (average = 25 %) of long-distance airborne arboreal pollen (AP) are remarkable, e.g. up to 10 % *Pinus* subgenus *Diploxylon* that may mainly derive from the boreal zone, although it is also growing in temperate vegetation types. This finding suggests that the main pollen source includes the Arctic, with a strong influence of boreal forests (Whitmore et al., 2005), as also documented in glacier ice studies from neighboring North American Arctic islands (e.g. Agassiz and Devon ice caps, Bourgeois et al., 2000; McAndrews, 1984). Compared to these sites with much smaller ice sheets that are surrounded by Arctic shrub tundra, the Eurocore at Summit contains only few pollen grains of insect-pollinated plants such as Ericaceae, which comprise typical plants of the Arctic shrub tundra. This reduction of arctic insect-pollinated plants is likely the effect of the isolated position of the site in inland ice-covered Greenland. Pollen from plants introduced during the Old Norse settlement phase (e.g. *Ranunculus acris*-type, *Rumex*; Schofield et al., 2013) indicates large-scale persistence of these taxa until modern times. Two Cerealia-type pollen grains and one *Zea mays* grain may originate from very long-distance transport (e.g. North America). Long-distance transport over 2000-3000 km also explains the presence of pollen of temperate taxa such as *Quercus, Tilia, Ulmus, Fagus,* and *Acer* (Thompson et al., 1999) in our record.

4.2 Vegetation dynamics

Two local pollen assemblage zones (LPAZ) reflect the vegetation development. LPAZ Sum-1 (1730–1900 AD) consists of 50 to 60 % arboreal pollen (AP, sum of trees and shrubs), suggesting the prevalence of open habitats such as arctic tundra during the period 1730-1900 AD. Pollen of the only native tree (*Betula alba*-type) increases to 30 % and shrub pollen (e.g. *Alnus viridis* type, *Betula nana* type, *Salix,* and *Juniperus)* slightly raises to ca. 25 % between 1850 and 1900 AD, indicating a spread of subarctic woodlands and thickets (Fig. 2). After 1900 AD (LPAZ Sum-2, 1900–1989 AD), non-arboreal pollen (NAP, herbs) expands (e.g. *Artemisia, Ambrosia*, other Asteroideae, Poaceae), while *Betula alba*-type, *Alnus viridis*-type, and *Betula nana*-type as well as fern spores decrease, suggesting that open herb and grass tundra replaced scattered subarctic woodlands and thickets. Pollen percentages of shrubs that were probably growing in the arctic tundra remains stable (e.g. *Juniperus*) or marginally increases (e.g. *Salix*). Finally, the pollen record shows that *Betula* woodlands partly recovered around 1960 AD (supported by increasing influx values) and then decline to minimum values around 1990 AD. AP percentages and influx declined, suggesting no general increase of arboreal taxa (Fig. 2).

Pollen richness (PRI = 15–18, based on the pollen sum of 28; Fig. 2) is relatively high and remains stable over the past 250 years. The pollen spectra at Summit are markedly influenced by continuous and diverse long-distance pollen deposition from boreal and nemoboreal tree taxa such as e.g. *Quercus, Tilia, Ulmus,* and *Fagus* deriving from > 2000 km distance. This long-distance pollen hampers the regional diversity estimation, an effect, which was also recorded in calibration studies using surface soil samples (Felde et al., 2016). Pollen evenness (PIE = 0.9–0.95; Fig. 2) remains stable and relatively high due to co-occurrence of several major taxa that dominate along the record (e.g. Poaceae, *Artemisia*, *Betula alba*-type). The stable diversity estimation agrees with local richness estimations from a southern Greenland peat deposit that suggests no richness trend during the past centuries (Schofield and Edwards, 2011).

The sample distribution on PCA axes 1 and 2 (33.2 and 22.5% variance explained, respectively) separates samples from Sum-1 and Sum-2 along axis 1, supporting the LPAZ boundary. The ordination splits taxa indicative of boreal to subarctic shrub- and woodlands (e.g. *Betula alba*-type, *Alnus viridis*-type, *Cornus suecica*-type) from arctic taxa that grow on wet (e.g. *Artemisia*, *Salix,* Cyperaceae, *Anemone*-type) or dry soils (e.g. Poaceae, Chenopodiaceae; Schofield and Edwards, 2011). The co-occurrence of *Juniperus* with arctic taxa suggests that the pollen predominantly derives from the arctic subspecies *J. communis* subsp. *alpina* that grows in Greenland and not from temperate and boreal juniper species growing on continental North America. Despite the clear trends with regard to taxa and sample grouping, caution is needed when interpreting the ordination data as low pollen counts may influence PCA analyses (Heiri and Lotter, 2001).

4.3 Fire and fossil fuel combustion

Microscopic charcoal concentration (average ca. 700 particles l^{-1} along the record) and influx (average ca. 9 particles cm^{-2} $year^{-1}$) are extremely low compared to other Arctic ice records (ca. 200 particles cm^{-2} $year^{-1}$ at Lomonosovfonna; Hicks and Isaksson, 2006) or to Greenland sedimentary records (ca. 500 particles cm^{-2} $year^{-1}$; Schofield and Edwards, 2011). The microscopic charcoal influx suggests two periods of enhanced regional fire activity around 1790 AD and after 1970 AD. Considering the predominant westerly wind direction (Steffen and Box, 2001), potential sources include peatland fires on the Greenland coast and boreal forest fires in Alaska and Canada. SCP deposition at Summit starts around 1880 AD and rises steadily after 1900 AD, suggesting increased atmospheric organic pollution from regional and long-distance fossil fuel burning (e.g. coal; Rose, 2015).

5 Discussion

5.1 Fire activity and fossil fuel burning in the Arctic

Summit recorded two major peaks in fire activity during the past 300 years, around 1790 and after 1970 AD. The first peak correlates with increased fire activity documented at the boreal forest-tundra ecotone in Alaska, possibly caused by reduced precipitation during the Little Ice Age (LIA; Tinner et al., 2008) and was also recorded in the black carbon (BC) record from Eurocore (Cachier and Pertuisod, 1994). The recent fire activity peak corresponds to increases of fire severity in the Canadian and Alaskan boreal forests after 1980 AD, attributed to both man-set fires and natural ignition (Calef et al., 2017; Kelly et al., 2013; Soja et al., 2007; Veraverbeke et al., 2017). Thus, either regional fire activity trends followed similar trajectories or fire activity at Summit is reflecting distant forest fires (Thomas et al., 2017).

SCP maximum values at Summit remain about 50 times lower than in other ice records such as Lomonosovfonna on Svalbard (ca. 0.5 vs. ca. 40 particles cm^{-2} $year^{-1}$; Hicks and Isaksson, 2006). This pronounced difference is likely a consequence of the Eurocore drilling site in the center of the huge ice cap (radius 300 km) on Greenland. For instance, three coal-fired power stations are located ca. 70 km from Lomonosovfonna glacier (Hicks and Isaksson, 2006), potentially dominating its SCP record. The onset of SCP pollution at Summit at ca. 1880 AD is concurrent with the start of the SCP record in Nunatak lake in Western Greenland (Rose, 2015) and in Lomonosovfonna glacier in Svalbard (Hicks and Isaksson, 2006; Fig. 4. The synchronous onset of SCP deposition likely originated from widespread Arctic coal mining activities during the late-19th and early 20th century. Historical sources give evidence of coal mining in Greenland since ca. 1890 AD, in Svalbard since 1907 AD, whereas coal based-ore smelting started after 1911 AD in Greenland (Kosack, 1967; National Museum of Denmark). More generally, our SCP record follows the progressive fossil fuel burning of the 20th century, globally observed in many sedimentary SCP records (see Fig. 4; Rose, 2015).

The increasing long-term trends of microscopic forest fire and industrial burning proxies at Summit contrasts with black carbon (BC) and vanillic acid (VA)-based reconstructions from Greenland that suggest maximum fossil fuel pollution at the beginning of the 20th century, mainly attributed to coal burning (McConnell et al., 2007). Technical advances, which reduced pollutant emmission to the atmosphere served as an explanation for the early decline of BC (e.g. D4 record, Fig. 4; McConnell et al., 2007). In contrast to our microscopic proxies these BC records mainly capture submicron particles with a long residence time in the atmosphere and thus likely reflect a continental to northern hemispheric origin, including the industrialized countries (McConnell et al., 2007). Because of the larger size of microscopic particles (>10µm), reconstructed pollution and fires may primarily come from regional sources, as revealed by continental calibration (Adolf et al., 2018) and global modelling efforts (Gilgen et al., 2018). These contrasting trends are interesting because they suggest that despite of declining northern hemispheric trends, pollution in sensitive Arctic environments increased as late as during the 1980s. We hypothesize that in recent decades SCP may have also derived from increasing oil combustion, possibly including gasoline (Rose, 2015). This is supported by reconstructed lead (Pb)-pollution, which in the Arctic culminated in 1960-1980 AD and partly derived from gasoline consumption (Bindler et al., 2001; McConnell et al., 2007).

5.2 Anthropogenic footprint on Greenland vegetation

The Medieval Norse culture in Greenland had a strong impact on subarctic birch-willow shrublands around settlements that persisted until they were abandoned ca. 1350–1450 AD (Barlow et al., 1997; Berglund, 1986). The subsequent recovery of these shrub- and woodlands implies a resilience of Arctic vegetation to local human disturbance similar to observed vegetation recoveries after moderate anthropogenic impact of Neolithic settlements in e.g. European temperate forests (e.g. Rey et al., 2017). However, rapid colonization by alien plants (Bennike, 1999) introduced by European settlers such as *Rumex* or *Ranunculus acris* was irreversible, as documented by the supraregional palynological record at Summit three centuries later (Schofield and Edwards, 2011; Schofield et al., 2013).

Tree *Betula* may form temperature-controlled tree lines (Hoch and Körner, 2003; Wieser et al., 2014) in Greenland and other Arctic areas (Anschlag et al., 2008; Hobbie and Chapin III, 1998; Karlsson and Nordell, 1996). After the termination of the LIA at ca. 1850 AD (Fischer et al., 1998; Kaufman et al., 2009), rising temperatures increased shrub growing rates in East Greenland and the Alaskan Arctic (Büntgen et al., 2015; Myers-Smith and Hik, 2018; Sturm et al., 2001), and allowed re-expansion of forests in Alaska (Tinner et al., 2008) and elsewhere in the Arctic (Kullman and Öberg, 2009; Lescop-Sinclair and Payette, 1995; McDonald et al., 2008). In agreement, birch woodlands expanded in Greenland (Figs. 2, 4).

However, these woodland expansions ended ca. 1910 AD, when favorable climatic conditions should have promoted further expansions of subarctic birch woodlands in Southern Greenland (Fredskild, 1991; Fig. 4). This departure between temperature and vegetation dynamics coincided with the onset of Arctic coal mining activities (Hicks and Isaksson, 2006; Kosack, 1967). We therefore speculate that increasing human impact may have contributed to the reduction of woodlands in Greenland during the 20th century. *Betula pubescens* woods are currently restricted to climatically mild conditions in Southern Greenland valleys, which are attractive for human settlements (Kosack, 1967). Although substantial portions of energy consumption were covered by coal rather than timber burning, birch woodlands potentially provided an additional natural resource exploitable for various purposes. After reintroducing sheep farming in Greenland in 1905 AD, browsing may have vigorously transformed woody vegetation to grasslands (Austrheim et al., 2008; Dege, 1964; Jacobsen, 1987; Kosack, 1967; Massa et al., 2012; Ross et al., 2016). Moreover, timber was possibly harvested for constructions (e.g. fencing for cattle) since natural timber sources in Greenland are limited and apart from birch trees and several shrub species, wood is largely restricted to drift wood from the ocean (Alix, 2005). Thus, in these northernmost Greenland forest ecosystem human impact during the 20th century partly converted quasi-natural to humanized vegetation, despite the remoteness and climatically challenging natural conditions of the harsh environments (Fig. 4). Given that the birch species involved is a strong pioneer, *Betula* woodlands may re-expand rapidly in the future, e.g. through the establishment of woodland conservation areas (e.g. protection area in the Qinngua valley; Austrheim et al., 2008; Ross et al., 2016).

6 Conclusions

Our palynological record from Central Greenland reveals that increasing globalization at the beginning of the 20th century markedly affected Arctic environments. Ecosystem modification included the spread of adventive plants and subarctic deforestation as well as pollution from both, fossil fuel burning and increasing forest fires. Land use and pollution may contribute to alter even most remote Arctic ecosystems. Specifically, pollution of ice through dark microscopic particles might become of growing importance given the recent increase of fire activity in Greenland (Wendel, 2017). "Blackening" of pure Greenland snow due to deposition of black particles may accelerate climate-warming feedbacks, thus reinforcing ice melting and fire risk. This study illustrates for the first time that Central Greenland ice core records have a high potential for the reconstruction of long-term high-resolution environmental dynamics in the Arctic. Palaeoecological ice studies covering longer periods than Eurocore '89 reaching modern time may further constrain the long-term triggers, processes, and mechanisms of rapid environmental change in the Arctic.

7 Acknowledgments

We are grateful to the Eurocore '89 drilling team at Summit and to Alexander Bolland for assistance with the ice transport from Copenhagen to Bern. We acknowledge the Sinergia project *Paleo fires from high-alpine ice cores* funded by the Swiss National Science Foundation (SNF grant 154450).

8 References

Adolf C, Wunderle S, Colombaroli D, Weber H, Gobet E, Heiri O, van Leeuwen JFN, Bigler C, Connor SE, Gałka m, La Mantia T, Makhortykh S, Svitavská-Svobodová H, Vannière B, Tinner W (2018) The sedimentary and remote-sensing reflection of biomass burning in Europe. *Global Ecology and Biogeography* 27(2), 199-212.

Alix C (2005) Deciphering the impact of change on the driftwood cycle: contribution to the study of human use of wood in the Arctic. *Global and Planetary Change* 47(2-4) 83-98.

Anderson PM, Bartlein PJ, Brubaker LB et al. (1991) Vegetation-pollen-climate relationships for the arcto-boreal region of North America and Greenland. *Journal of Biogeography* 565-582.

Anschlag K, Broll G and Holtmeier FK (2008) Mountain birch seedlings in the treeline ecotone, subarctic Finland: variation in above-and below-ground growth depending on microtopography. *Arctic, Antarctic, and Alpine Research* 40(4) 609-616.

Austrheim G, Asheim LJ, Bjarnason G et al. (2008) Sheep grazing in the North-Atlantic region—A long term perspective on management, resource economy and ecology. *Rapport zoologisk serie* 3 86.

Barlow LK, Sadler JP, Ogilvie AE et al. (1997) Interdisciplinary investigations of the end of the Norse Western Settlement in Greenland. *The Holocene* 7(4) 489-499.

Bennike O (1999) Colonisation of Greenland by plants and animals after the last ice age: a review. *Polar Record* 35(195) 323-336.

Berglund J (1986) The decline of the Norse settlements in Greenland. *Arctic Anthropology* 109-135.

Beug HJ (2004) *Leitfaden der Pollenbestimmung für Mitteleuropa und angrenzende Gebiete*. Pfeil.

Bindler R, Renberg I, Anderson NJ et al. (2001) Pb isotope ratios of lake sediments in West Greenland: inference on pollution sources. *Atmospheric Environment* 35 4675-4685.

Birks HJB and Line JM (1992) The use of rarefaction analysis for estimating palynological richness from Quaternary pollen-analytical data. *The Holocene* 2(1) 1-10.

Birks HJB (1968) The identification of Betula nana pollen. *New Phytologist* 67(2), 309-314.

Blunier T, Chappellaz J, Schwander J et al. (1993) Atmospheric methane, record from a Greenland ice core over the last 1000 years. *Journal of Geophysical Research* 20 2219-2222.

Böcher TW, Holmen K and Jakobsen K (1968) *The flora of Greenland*. Haase.

Bourgeois JC, Koerner RM, Gajewski K et al. (2000) A Holocene ice-core pollen record from Ellesmere Island, Nunavut, Canada. *Quaternary Research* 54(2) 275-283.

Brugger SO, Gobet E, Schanz FR et al. (2018a) A quantitative comparison of microfossil extraction methods from ice cores. *Journal of Glaciology* 64(245) 432-442

Brugger SO, Gobet E, Sigl M et al. (2018b) Ice records provide new insights into climatic vulnerability of Central Asian forest and steppe communities. *Global and Planetary Change* 169, 188-201.

Bryan MS (1954) Interglacial pollen spectra from Greenland. Danm Geol Unders II, 80 65.

Büntgen U, Hellmann L, Tegel W et al. (2015) Temperature-induced recruitment pulses of Arctic dwarf shrub communities. *Journal of Ecology* 103(2) 489-501.

Cachier and Pertuisot (1994) Particulate carbon in Arctic ice. *Analusis Magazine* 22(7).

Calef MP, Varvak A and McGuire AD (2017) Differences in Human versus Lightning Fires between Urban and Rural Areas of the Boreal Forest in Interior Alaska. *Forests* 8(11) 422.

Clegg BF, Tinner W, Gavin DG et al. (2005) Morphological differentiation of Betula (birch) pollen in northwest North America and its palaeoecological application. *The Holocene* 15(2) 229-237.

Dege W (1964) Grönland im Strukturwandel von Wirtschaft und Siedlung: aufgezeigt am Beispiel des Raumes um Julianehåb. *Erdkunde* 285-311.

De Vernal A and Hillaire-Marcel C (2008) Natural variability of Greenland climate, vegetation, and ice volume during the past million years. *Science* 320(5883) 1622-1625.

Felde VA, Peglar SM, Bjune AE et al. (2016) Modern pollen–plant richness and diversity relationships exist along a vegetational gradient in southern Norway. *The Holocene* 26(2), 163-175.

Finsinger W and Tinner W (2005) Minimum count sums for charcoal concentration estimates in pollen slides: accuracy and potential errors. *The Holocene* 15(2) 293-297.

Fischer H, Werner M, Wagenbach D et al. (1998) Little ice age clearly recorded in northern Greenland ice cores. *Geophysical Research Letters* 25(10) 1749-1752.

Fredskild B (1991) The genus Betula in Greenland-Holocene history, present distribution and synecology. *Nordic Journal of Botany* 11(4) 393-412.

Gauthier E, Bichet V, Massa C et al. (2010) Pollen and non-pollen palynomorph evidence of medieval farming activities in southwestern Greenland. *Vegetation History and Archaeobotany* 19(5-6) 427-438.

Gilgen A, Adolf C, Brugger SO et al. (2018) Implementing microscopic charcoal particles into a global aerosol–climate model. *Atmospheric Chemistry and Physics* 18(16), 11813-11829.

Hartmann M, Blunier T, Brugger SO et al. (in review) The Variation of Ice Nucleating Particles in the Arctic over the Last Centuries.

Heiri O and Lotter AF (2001) Effect of low count sums on quantitative environmental reconstructions: an example using subfossil chironomids. *Journal of Paleolimnology* 26(3) 343-350.

Hicks S and Isaksson E (2006) Assessing source areas of pollutants from studies of fly ash, charcoal, and pollen from Svalbard snow and ice. *Journal of Geophysical Research: Atmospheres* 111(D2) 1-9.

Hobbie SE and Chapin III FS (1998) An experimental test of limits to tree establishment in Arctic tundra. *Journal of Ecology* 86(3) 449-461.

Hoch G and Körner C (2003) The carbon charging of pines at the climatic treeline: a global comparison. *Oecologia* 135(1) 10-21.

Hurlbert SH (1971) The nonconcept of species diversity: a critique and alternative parameters. *Ecology* 52(4) 577-586.

Jacobsen NK (1987) Studies on soils and potential for soil erosion in the sheep farming area of South Greenland. *Arctic and Alpine Research* 498-507.

Karlsson PS and Nordell KO (1996) Effects of soil temperature on the nitrogen economy and growth of mountain birch seedlings near its presumed low temperature distribution limit. *Ecoscience* 3(2) 183-189.

Kaufman DS, Schneider D P, McKay NP et al. (2009) Recent warming reverses long-term Arctic cooling. *Science* 325(5945), 1236-1239.

Kelly R, Chipman ML, Higuera PE et al. (2013) Recent burning of boreal forests exceeds fire regime limits of the past 10,000 years. *Proceedings of the National Academy of Sciences* 110(32) 13055-13060.

Kosack HP (1967) *Die Polarforschung*. Vieweg.

Kullman L and Öberg L (2009) Post-Little Ice Age tree line rise and climate warming in the Swedish Scandes: a landscape ecological perspective. *Journal of Ecology* 97(3), 415-429.

Lescop-Sinclair K and Payette S (1995) Recent advance of the arctic treeline along the eastern coast of Hudson Bay. *Journal of Ecology* 929-936.

Massa C, Bichet V, Gauthier É et al. (2012) A 2500 year record of natural and anthropogenic soil erosion in South Greenland. *Quaternary Science Reviews* 32 119-130.

McAndrews JH (1984) Pollen analysis of the 1973 ice core from Devon Island Glacier, Canada. *Quaternary Research* 22(1) 68-76.

McAndrews JH, Berti AA and Norris G (1973) *Key to the Quaternary pollen and spores of the Great Lakes region*. Royal Ontario Museum

McConnell JR, Edwards R, Kok GL et al. (2007) 20th-century industrial black carbon emissions altered arctic climate forcing. *Science* 317(5843) 1381-1384.

McConnell JR, Wilson AI, Stohl A et al. (2018) Lead pollution recorded in Greenland ice indicates European emissions tracked plagues, wars, and imperial expansion during antiquity. *Proceedings of the National Academy of Sciences* 201721818.

MacDonald GM, Kremenetski KV and Beilman DW (2008) Climate change and the northern Russian treeline zone. *Philosophical Transactions of the Royal Society of London B: Biological Sciences* 363(1501), 2283-2299.

Mernild SH, Hanna E, McConnell JR et al. (2015) Greenland precipitation trends in a long-term instrumental climate context (1890–2012): evaluation of coastal and ice core records. *International Journal of Climatology* 35(2) 303-320.

Moore PD, Webb JA and Collison ME (1991) *Pollen analysis*. Blackwell scientific publications.

Myers-Smith IH and Hik DS (2018) Climate warming as a driver of tundra shrubline advance. *Journal of Ecology* 106(2) 547-560.

National Museum of Denmark: *Greenland in the late 19th-early 20th century* (Th. N. Krabbe Collection)

Nentwig W, Bacher S, Beierkuhnlein C et al. (2004). *Ökologie*. Spektrum.

Ødum S (1979) Actual and potential tree-line in the North Atlantic region, especially in Greenland and the Faroes. *Ecography* 2(4) 222-227.

Petit RJ, Hu FS and Dick CW (2008) Forests of the Past: A Window to Future Changes. *Science* 1155457(1450), 320.

Pfadenhauer JS and Klötzli FA (2015) *Vegetation der Erde: Grundlagen, Ökologie, Verbreitung.* Springer.

Phoenix GK and Bjerke JW (2016) Arctic browning: extreme events and trends reversing arctic greening. *Global change biology* 22(9) 2960-2962.

Rasmussen SO, Bigler M, Blockley SP et al. (2014) A stratigraphic framework for abrupt climatic changes during the Last Glacial period based on three synchronized Greenland ice-core records: refining and extending the INTIMATE event stratigraphy. *Quaternary Science Reviews* 106 14-28.

Rey F, Gobet E, van Leeuwen JFN et al. (2017) Vegetational and agricultural dynamics at Burgäschisee (Swiss Plateau) recorded for 18,700 years by multi-proxy evidence from partly varved sediments. *Vegetation History and Archaeobotany* 26(6) 571-586.

Rose NL (2015) Spheroidal carbonaceous fly ash particles provide a globally synchronous stratigraphic marker for the Anthropocene. *Environmental science & technology* 49(7) 4155-4162.

Ross LC, Austrheim G, Asheim LJ et al. (2016). Sheep grazing in the North Atlantic region: A long-term perspective on environmental sustainability. *Ambio* 45(5) 551-566.

Schofield J E, Edwards KJ, Erlendsson E and Ledger PM (2013) Palynology supports 'Old Norse'introductions to the flora of Greenland. *Journal of Biogeography* 40(6) 1119-1130.

Schofield JE and Edwards KJ (2011) Grazing impacts and woodland management in Eriksfjord: Betula, coprophilous fungi and the Norse settlement of Greenland. *Vegetation History and Archaeobotany* 20(3) 181-197.

Seierstad IK, Abbott PM, Bigler M et al. (2014) Consistently dated records from the Greenland GRIP, GISP2 and NGRIP ice cores for the past 104 ka reveal regional millennial-scale δ18O gradients with possible Heinrich event imprint. *Quaternary Science Reviews* 106 29-46.

Short SK and Holdsworth G (1985) Pollen, Oxygen Isotope Content and Seasonally in an Ice Core from the Penny Ice Cap, Baffin Island. *Arctic* 214-218.

Soja AJ, Tchebakova NM, French NH et al. (2007) Climate-induced boreal forest change: predictions versus current observations. *Global and Planetary Change* 56(3-4) 274-296.

Steffen K and Box J (2001) Surface climatology of the Greenland ice sheet: Greenland Climate Network 1995–1999. *Journal of Geophysical Research: Atmospheres* 106(D24) 33951-33964.

Sturm M, Racine C and Tape K (2001) Climate change: increasing shrub abundance in the

Arctic. *Nature* 411(6837) 546.

Ter Braak CJ and Prentice IC (1988) A theory of gradient analysis. *Advances in ecological research* 18 271-317.

Thomas JL, Polashenski CM, Soja AJ et al. (2017) Quantifying black carbon deposition over the Greenland ice sheet from forest fires in Canada. *Geophysical Research Letters* 44(15) 7965-7974.

Thompson RS, Anderson KH and Bartlein PJ (1999) *Atlas of relations between climatic parameters and distributions of important trees and shrubs in North America*. US Department of the Interior, US Geological Survey.

Tinner W and Hu FS (2003) Size parameters, size-class distribution and area-number relationship of microscopic charcoal: relevance for fire reconstruction. *The Holocene* 13(4) 499-505.

Tinner W, Bigler C, Gedye S et al. (2008) A 700-year paleoecological record of boreal ecosystem responses to climatic variation from Alaska. *Ecology* 89(3) 729-743.

Veraverbeke S, Rogers BM, Goulden ML et al. (2017) Lightning as a major driver of recent large fire years in North American boreal forests. *Nature Climate Change* 7(7) 529.

Vinther BM, Jones PD, Briffa KR et al. (2010) Climatic signals in multiple highly resolved stable isotope records from Greenland. *Quaternary Science Reviews* 29(3) 522-538.

Wagner B, Bennike O, Bos JA et al. (2008) A multidisciplinary study of Holocene sediment records from Hjort Sø on Store Koldewey, Northeast Greenland. *Journal of Paleolimnology* 39(3) 381-398.

Wendel J (2017) Greenland fires ignite climate change fears. *Eos* 98.

Whitmore J, Gajewski K, Sawada M et al. (2005) Modern pollen data from North America and Greenland for multi-scale paleoenvironmental applications. *Quaternary Science Reviews* 24(16) 1828-1848.

Wieser G, Holtmeier, FK and Smith WK (2014) Treelines in a changing global environment. In: *Trees in a changing environment*. Springer.

Willerslev E, Cappellini E, Boomsma W et al. (2007) Ancient biomolecules from deep ice cores reveal a forested southern Greenland. *Science* 317(5834) 111-114.

9 Figures

Figure 1 Map of Greenland. Vegetation zones following Pfadenhauer and Klötzli (2015). Numbers indicate the drilling location of the Eurocore'89 at Summit and selected palynological records in the Arctic. Ice cores from 1: Agassiz ice cap (Bourgeois et al., 2000), 2: Devon island (McAndrews, 1984), 3: Baffin island (Short and Holdsworth, 1985), D4 (e.g. McConnell et al., 2007). Sedimentary palaeoecological sites from A: Eastern Norse settlement around Igaliku lake (e.g. Schofield et al., 2013), B: Western Norse settlement (e.g. Barlow et al., 1997), C: Nunatak lake (Rose, 2015). Subarctic vegetation is composed of boreal vegetation elements in arctic environments, not shown in map. The map resolution is too coarse to display smaller ice caps in the Arctic as e.g. Devon, Baffin or Agassiz.

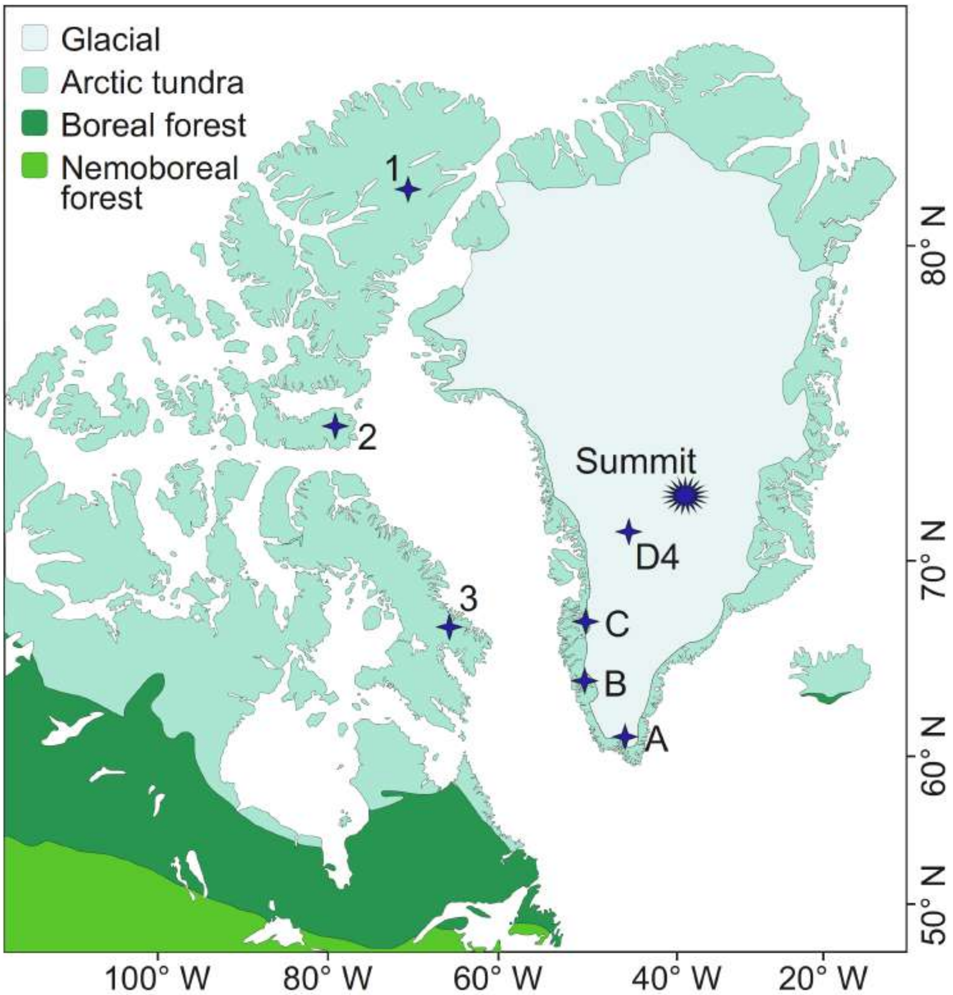

Figure 2 Pollen diagram of Summit Eurocore'89 (Greenland) shows pollen percentages of selected pollen types and fern spores based on the terrestrial pollen sum with indication of taxa growing in Greenland including introduced taxa by the Old Norse (adventive taxa) and taxa that are currently not growing in Greenland (following Böcher et al., 1968). Portion of total Greenland native trees and shrubs from all arboreal pollen in the main diagram. AP = arboreal pollen, NAP = non-arboreal pollen, t. = type. Concentration curves for pollen, microscopic charcoal, and spheroidal carbonaceous particles (SCP) in particles per liter, influx curves for microscopic charcoal and total pollen in particles cm^{-2} year^{-1}, and total terrestrial pollen sum. Hollow curves = 10x exaggeration. Diversity estimation (Hurlbert, 1971) based on a minimum pollen sum of 28 for pollen richness (PRI) and evenness index (PIE). LPAZ = optically delimited local pollen assemblage zones.

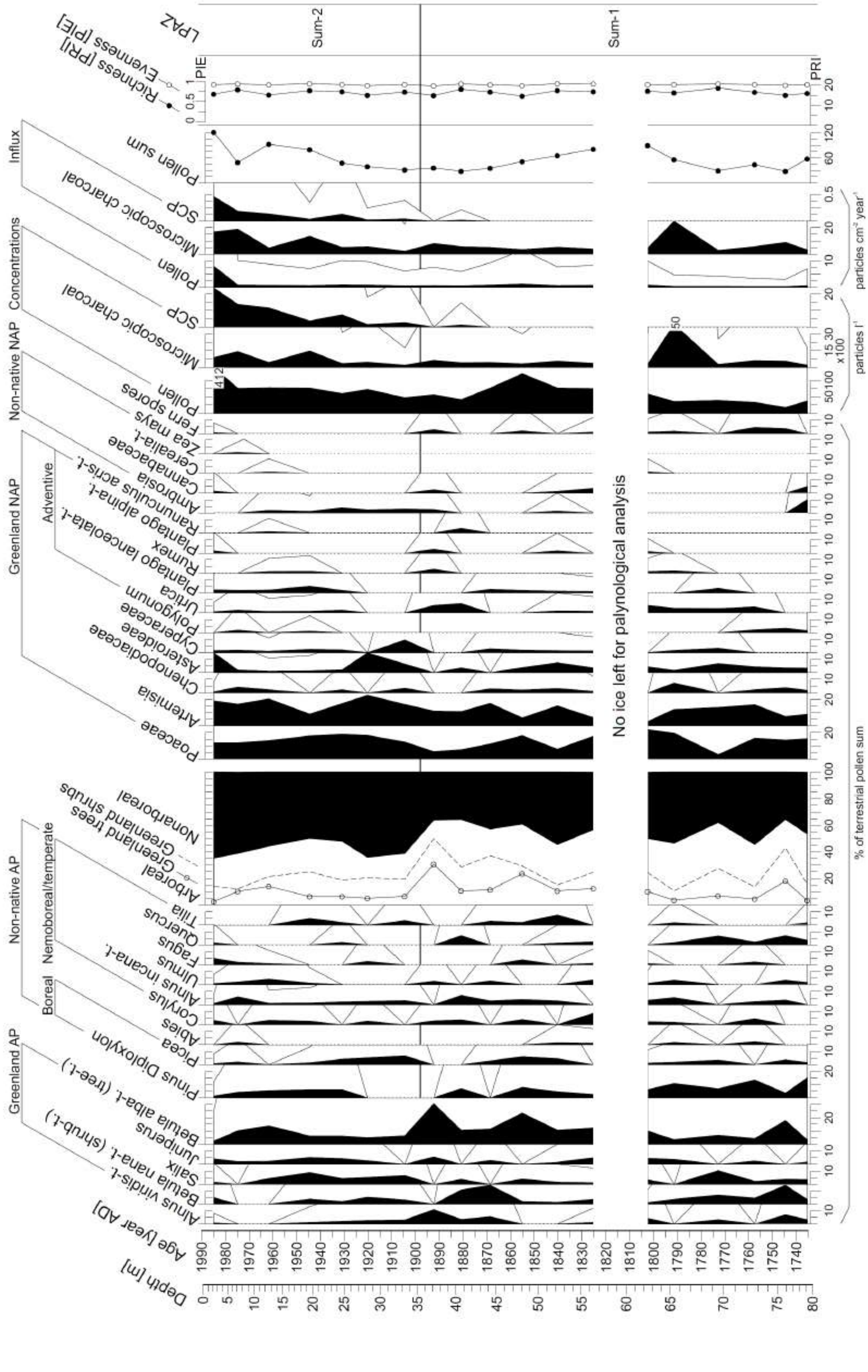

Figure 3 Principal Component Analysis (PCA) for the Summit Eurocore'89 (Greenland) pollen percentage record. Only taxa growing in Greenland (following Böcher et al., 1968) are included in the dataset. Graph shows selected pollen taxa and sample scores grouped according to the optically defined local pollen assemblage zones (Sum-1 and Sum-2). t. = pollen-type. Betula alba-type = tree-type Betula, Betula nana-t. = shrub-type Betula.

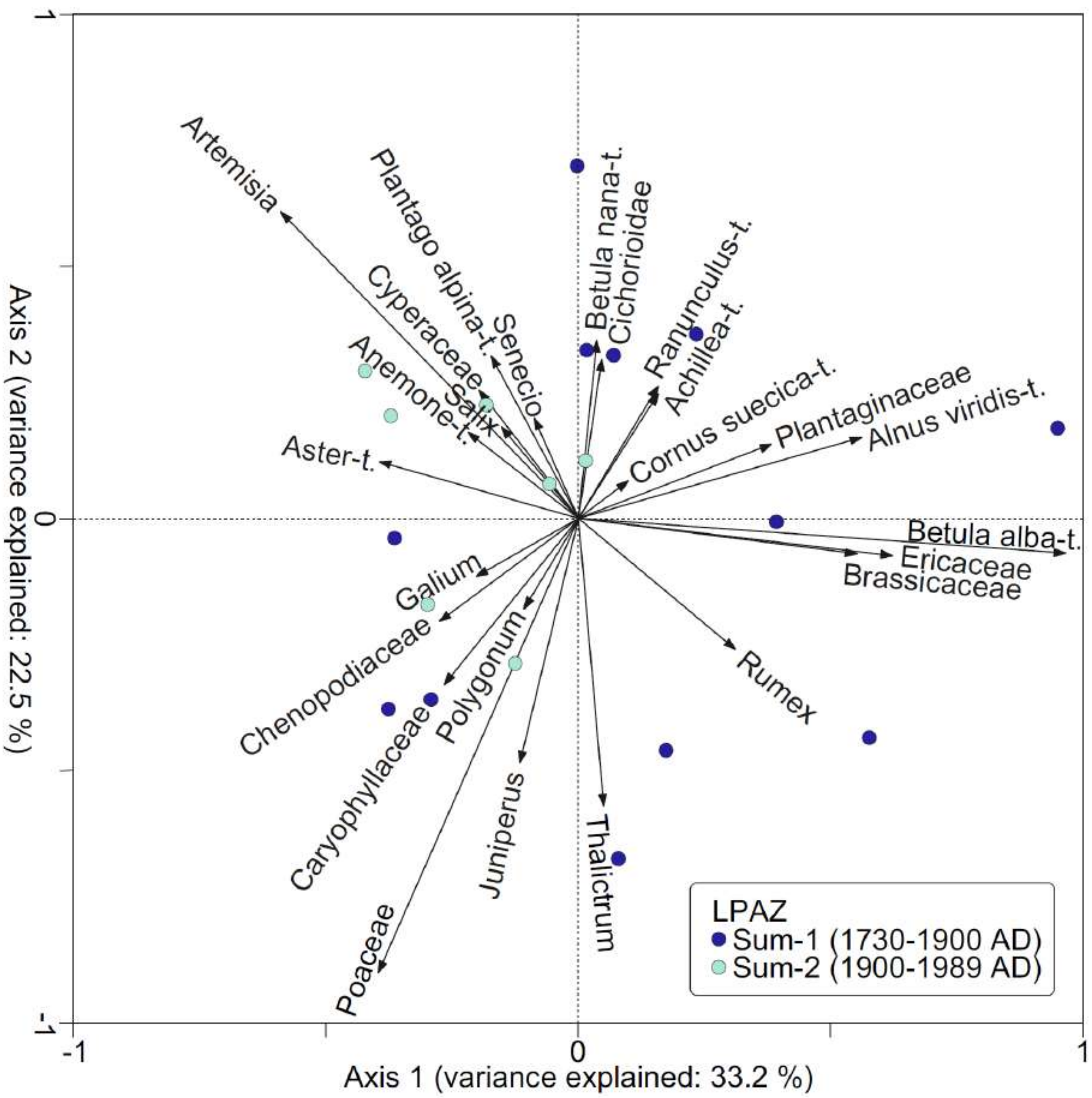

Figure 4 Comparison of Summit Eurocore '89 palynological record (pollen percentages, *Betula alba*-type concentration and influx, microscopic charcoal influx, and SCP =spheroidal carbonaceous particles influx) with independent burning, temperature and population records. Black carbon and vanillic acid records from the D4 site with the green shaded area representing the portion of black carbon attributed to industrial emissions, not boreal forest fires (pooled to resolution of the palynological record; McConnell et al., 2007), SCP record from Nunatak lake in Western Greenland (Rose, 2015), Svalbard palynological burning records (SCP and microscopic charcoal influx; Hicks and Isaksson, 2006), GRIP summer temperature ($\delta^{18}O$ in 1 year resolution and pooled to resolution of the palynological record; Vinther et al., 2010), measured summer temperature anomalies from 5 meteorological stations along the Greenland coast (Büntgen et al., 2015). Shaded in light blue after 1900 AD indicates the period of global change impact in the Arctic. *Betula alba*-type = tree-type *Betula.*

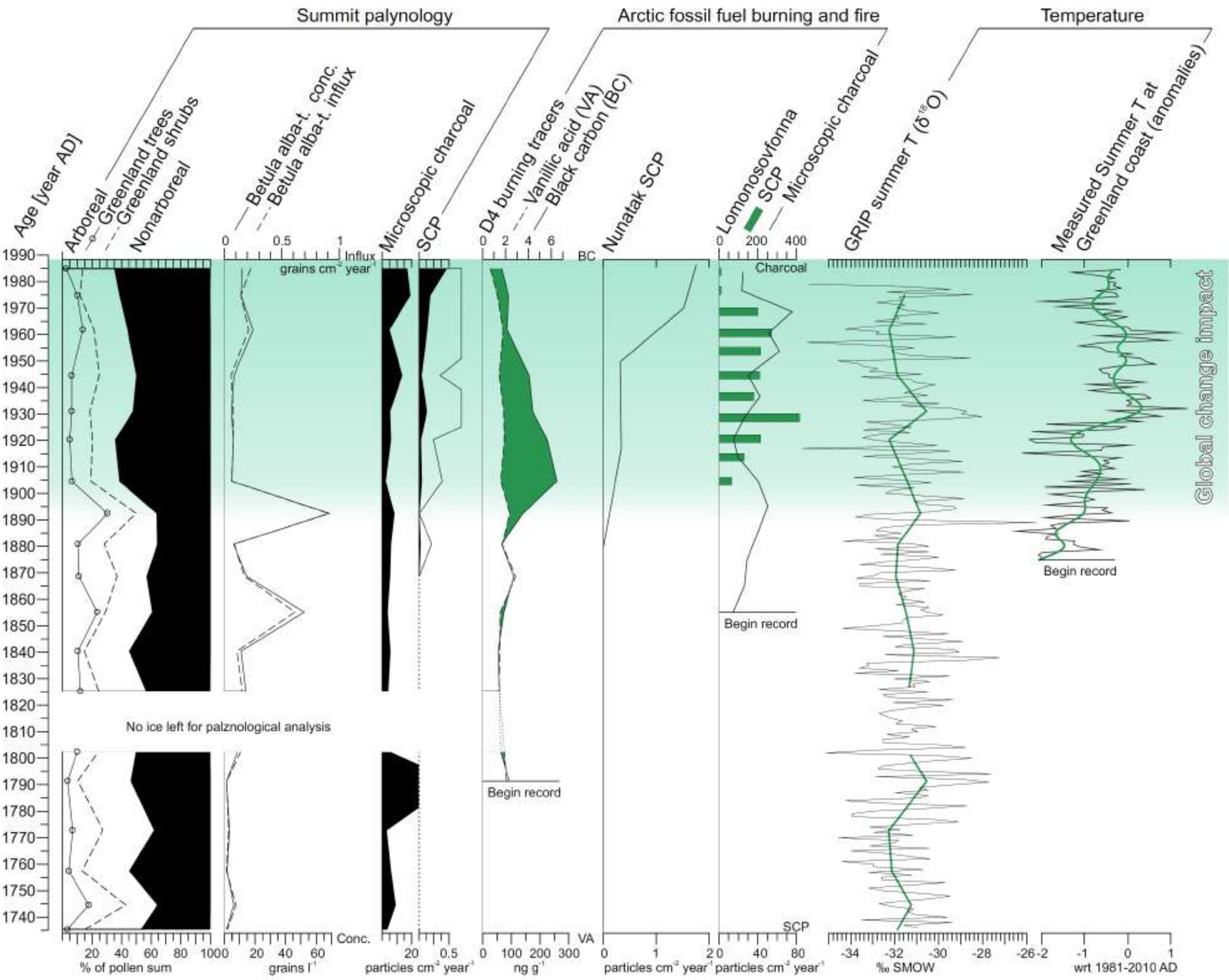

Supplementary material

Supplementary Table S1 Complete pollen taxa and non-pollen palynomorph (NPP) list for the palynological record of Summit Eurocore'89 (Greenland) with assignment to summary groups in the pollen diagram. Greenland taxa assignment including adventive taxa introduced since the Old Norse culture following Böcher et al. (1968) and Anderson et al. (1991). AP = arboreal pollen, NAP = non-arboreal pollen. Indication of occurrence in one ($^{+}$), two ($^{++}$) or more than two ($^{+++}$) samples of the record.

	Taxa
Native Greenland AP	*Alnus viridis*-type^{+++}, *Betula alba*-type^{+++}, *Betula nana*-type^{+++}, *Cornus suecica*-type^{++}, Ericaceae^{+}, *Juniperus*$^{+++}$, *Salix*$^{+++}$
Boreal AP	*Abies*$^{+++}$, *Calluna vulgaris*$^{+}$, *Picea*$^{+++}$, *Pinus* Diploxylon^{+++}, *Pinus* Haploxylon^{+++}, *Populus*$^{+++}$
Nemoboreal and temperate AP	*Acer rubrum*-type^{+}, *Acer saccharum*-type^{+}, *Acer* indet.$^{+++}$, *Aesculus hippocastanum*-type^{+}, *Alnus incana*-type^{+++}, *Carpinus*$^{+++}$, *Castanea*$^{+++}$, *Cornus sanguinea*-type^{+++}, *Corylus*$^{+++}$, *Fagus*$^{+++}$, *Fraxinus excelsior*-type^{+++}, *Juglans*$^{+++}$, Cf. *Liquidambar*$^{+}$, *Platanus*$^{+++}$, *Prunus*-type^{+++}, *Quercus*$^{+++}$, *Sambucus*$^{+++}$, *Taxus*$^{+}$, *Tilia*$^{+++}$, *Ulmus*$^{+++}$
Greenland NAP	*Achillea*$^{+}$, Apiaceae^{++}, *Artemisia*$^{+++}$, other Asteroideae^{+++}, *Aster*-type^{+++}, Brassicaceae^{+++}, *Campanula jasione*-type^{++}, Caryophyllaceae^{++}, *Centaurea*$^{+}$, Cichorioideae^{++}, Chenopodiaceae^{+++}, Cyperaceae^{+++}, other Fabaceae^{+++}, *Galium*$^{+}$, Lamiaceae^{+}, Liliaceae^{+}, *Oxyria*$^{+}$, *Parnassia*$^{+}$, *Pedicularis*$^{+}$, other *Plantago*$^{+++}$, *Plantago alpina*-type^{+++}, Poaceae^{+++}, other *Polygonum*$^{+++}$, *Polygonum aviculare*-type^{+}, Primulaceae^{+}, *Anemone*-type^{+++}, other Ranunculaceae^{+}, *Ranunculus acris*-type^{++}, other Rosaceae^{+++}, *Rumex*$^{+++}$, *Sedum*$^{+}$, *Senecio*-type^{+++}, *Thalictrum*$^{+++}$, *Trifolium pratense*-type^{++}
Other NAP	*Ambrosia*$^{+++}$, *Cannabis*$^{++}$, Cerealia-type^{++}, *Helianthemum*$^{+++}$, *Herniaria*$^{+}$, *Humulus*$^{+++}$, *Hypericum*$^{++}$, *Lupinus*-type^{+}, *Plantago major*-type^{++}, *Plantago lanceolata*-type^{+++}, *Sanguisorba minor*$^{+}$, *Trollius*-type^{++}, *Urtica dioica*-type^{+++}, *Xanthium*-type^{+}, *Zea mays*$^{+}$
Fern spores	Monolete fern spore^{+++}, trilete fern spore^{++}
Fungal spores	*Ustulina*$^{+}$

Manuscript 6

Implementing microscopic charcoal particles into a global aerosol–climate model

Anina Gilgen[1*], Carole Adolf[2,3,○], **Sandra O. Brugger[2,3,○]**, Luisa Ickes[1,4], Margit Schwikowski[3,5,6], Jacqueline F. N. van Leeuwen[2,3], Willy Tinner[2,3], Ulrike Lohmann[1]

[1]Institute for Atmospheric and Climate Science, ETH Zürich, Switzerland
[2]Institute of Plant Sciences, University of Bern, Switzerland
[3]Oeschger Centre for Climate Change Research, University of Bern, Switzerland
[4]University, Department of Meteorology, Stockholm University, Sweden
[5]Paul Scherrer Institut, Villigen, Switzerland
[6]Department of Chemistry and Biochemistry, University of Bern, Switzerland

[*]Corresponding author: Anina Gilgen
°These co-authors contributed equally to the paper and are considered joint second authors

Atmospheric Chemistry and Physics 18(16) 11813-11829

Atmos. Chem. Phys., 18, 11813–11829, 2018
https://doi.org/10.5194/acp-18-11813-2018

Atmospheric Chemistry and Physics
Open Access

Implementing microscopic charcoal particles into a global aerosol–climate model

Anina Gilgen[1], Carole Adolf[2,3,*], Sandra O. Brugger[2,3,*], Luisa Ickes[1,4], Margit Schwikowski[5,3,6], Jacqueline F. N. van Leeuwen[2,3], Willy Tinner[2,3,7], and Ulrike Lohmann[1]

[1]ETH Zürich, Institute for Atmospheric and Climate Science, Zürich, Switzerland
[2]University of Bern, Institute of Plant Sciences, Bern, Switzerland
[3]University of Bern, Oeschger Centre for Climate Change Research, Bern, Switzerland
[4]Now at Stockholm University, Department of Meteorology, Stockholm, Sweden
[5]Paul Scherrer Institut, Villigen, Switzerland
[6]University of Bern, Department of Chemistry and Biochemistry, Bern, Switzerland
[7]ETH Zürich, Institute of Terrestrial Ecosystems, Zürich, Switzerland
[*]These co-authors contributed equally to the paper and are considered joint second authors.

Correspondence: Anina Gilgen (anina.gilgen@env.ethz.ch)

Received: 1 December 2017 – Discussion started: 28 February 2018
Revised: 18 June 2018 – Accepted: 28 July 2018 – Published: 20 August 2018

Abstract. Microscopic charcoal particles are fire-specific tracers, which are ubiquitous in natural archives such as lake sediments or ice cores. Thus, charcoal records from lake sediments have become the primary source for reconstructing past fire activity. Microscopic charcoal particles are generated during forest and grassland fires and can be transported over large distances before being deposited into natural archives. In this paper, we implement microscopic charcoal particles into a global aerosol–climate model to better understand the transport of charcoal on a large scale. Atmospheric transport and interactions with other aerosol particles, clouds, and radiation are explicitly simulated.

To estimate the emissions of the microscopic charcoal particles, we use recent European charcoal observations from lake sediments as a calibration data set. We found that scaling black carbon fire emissions from the Global Fire Assimilation System (a satellite-based emission inventory) by approximately 2 orders of magnitude matches the calibration data set best. The charcoal validation data set, for which we collected charcoal observations from all over the globe, generally supports this scaling factor. In the validation data set, we included charcoal particles from lake sediments, peats, and ice cores. While only the Spearman rank correlation coefficient is significant for the calibration data set (0.67), both the Pearson and the Spearman rank correlation coefficients are positive and significantly different from zero for the validation data set (0.59 and 0.48, respectively). Overall, the model captures a significant portion of the spatial variability, but it fails to reproduce the extreme spatial variability observed in the charcoal data. This can mainly be explained by the coarse spatial resolution of the model and uncertainties concerning fire emissions. Furthermore, charcoal fluxes derived from ice core sites are much lower than the simulated fluxes, which can be explained by the location properties (high altitude and steep topography, which are not well represented in the model) of most of the investigated ice cores.

Global modelling of charcoal can improve our understanding of the representativeness of this fire proxy. Furthermore, it might allow past fire emissions provided by fire models to be quantitatively validated. This might deepen our understanding of the processes driving global fire activity.

1 Introduction

Fires are an important component of the Earth system and are closely linked to vegetation. They reduce biomass, influence the distribution of biomes, and alter biodiversity (Bond and Keeley, 2005; Secretariat of the Convention on Biological Diversity, 2001). Furthermore, fires have a large impact on the atmosphere, mainly by emitting aerosol particles and greenhouse gases (Crutzen and Andreae, 1990) and to a smaller extent by altering the surface albedo (Gatebe et al., 2014). They threaten humans not only because of infrastructure and death risks but also because of carcinogenic smoke emissions (Stefanidou et al., 2008).

The biosphere, the atmosphere, and humans not only are impacted by fires but also influence them: the occurrence and size of fires strongly depend on the vegetation properties (e.g. vegetation structure and moisture), on some climate variables (e.g. lightning frequency, precipitation, temperature), and on human behaviour (e.g. land use changes, firefighting) (Hantson et al., 2016). In recent years, global fire models have become more advanced, but open questions still remain, e.g. regarding the complexity needed for global fire models (Hantson et al., 2016). Current fire models are generally tuned to match observations from recent decades, where satellite products give valuable information on the occurrence of fires. Thus, a major goal of current research is to test the fire models against palaeo-fire data (Rabin et al., 2017), which are independent of this tuning: only if the models are able to reproduce past conditions may they capture the key processes driving fires and provide trustworthy information about the future.

A number of natural archives provide information about palaeo-fires on different spatial and temporal scales. Sedimentary charcoal records from lakes and natural wetlands are unique because of the broad temporal and spatial coverage they provide, ranging from local to global and decadal to millennial scales (Whitlock and Larsen, 2001; Schüpbach et al., 2015). Recently, charcoal particles originating from ice cores have also been analysed (Isaksson et al., 2003). Beside charcoal particles, ice cores from glaciers and ice sheets also preserve other (potential) fire indicators such as black carbon (BC) or molecular fire tracers (Rubino et al., 2016). Due to their remote locations, ice cores can provide information on regional to subcontinental scale fire activity. Especially for the last ≈ 150 years, ice cores generally have a sound chronology and a high temporal resolution, which allows recent ice core data to be linked directly to coinciding satellite observations or fire simulations. This is an advantage of ice cores compared to other charcoal fire records, which are undated in some cases and often have multi-decadal resolutions only (with some exceptions such as sediment traps or varved sediments).

Charcoal particles differ from BC (as defined in the aerosol community; see e.g. Bond et al., 2013) in terms of formation mechanism, size, density, and H : C and O : C ratios (Preston and Schmidt, 2006; Conedera et al., 2009). BC condenses as a secondary product from hot gases present in flames, thereby forming aggregates of small carbon spherules. Characteristic for BC particles are their submicron sizes and their very high carbon content, the latter resulting in pronounced absorption of visible light. In contrast, charcoal particles retain recognisable anatomic structures of their biomass source, cover the range from submicron to millimetre scale, and have considerably higher H : C and O : C ratios than BC (i.e. containing less carbon and thus absorbing less radiation). Both particles have in common that they are formed during biomass burning and are considered to be rather inert, unreactive substances.

Charcoal particles can be divided into microscopic ($D_\mathrm{M} > 10\,\mu\mathrm{m}$, where D_M is the maximum dimension of the particle) and macroscopic ($D_\mathrm{M} > 100\,\mu\mathrm{m}$) charcoal particles. In the most recent version of the Global Charcoal Database (GCDv3), more than a thousand sites with charcoal data are collected (Marlon et al., 2016). However, comparing data from the GCD with output from fire models is challenging: the collected charcoal data are only comparable to a certain degree due to differences in methods for extraction and counting, locations/environments, chronologies, particle sizes, values presented in percentages vs. concentrations or influx, etc. To circumvent the problem of inhomogeneous data, global synthesis studies such as Power et al. (2008) and Marlon et al. (2008) homogenised, rescaled, and standardised the data. The derived standardised scores (also called Z scores) enhance the comparability of the data but give only information about the relative changes of charcoal deposition. To estimate fire emissions from 1750 to 2015, van Marle et al. (2017) combined satellite retrievals, standardised scores from charcoal records, fire models, and visibility observations. The charcoal signal and the output from the fire models were scaled to match average regional GFED (Global Fire Emissions Database) carbon emissions from 1997 to 2003. However, to validate fire models and fire emission inventories, absolute values of charcoal fluxes (called influx or charcoal accumulation rate in the palaeo-science community) are still crucial.

To link the location of charcoal emissions (i.e. fires) with the fluxes derived at the observation sites (e.g. lake sediment), the transport of the particles must be taken into account. Previous studies have already investigated the transport of charcoal particles, which can take place in either air or water depending on site conditions and record type (e.g. Clark, 1988a; Peters and Higuera, 2007; Tinner et al., 2006; Lynch et al., 2004; Itter et al., 2017). Instead of explicitly modelling the transport, many of these studies chose a statistical approach.

In his pioneering study, Clark (1988a) focused on the transport of charcoal particles in air. He expected that the transport in fire plumes (which uplift particles to high altitudes) is responsible for nearly the whole long-range transport of microscopic charcoal particles. Clark (1988a) calculated that the transport of charcoal particles can be subcontinental to global: although charcoal particles are deposited relatively quickly due to their large sizes, their low density leads to considerably lower settling velocities compared to other supermicron particles (such as mineral dust).

More recently, Peters and Higuera (2007) and Higuera et al. (2007) used numerical models to simulate the major processes involved in macroscopic charcoal accumulation in lakes. Since they focused on charcoal particles from lake sediments, Higuera et al. (2007) considered not only fire conditions (size, location, and frequency) and transport but also sediment mixing and sediment sampling of macroscopic charcoal, while microscopic charcoal remained unexplored.

In the very recent study of Adolf et al. (2018), a uniform European data set of absolute charcoal fluxes is compared to satellite data of important fire regime parameters such as fire number, intensity, and burnt area at local and regional scales. Microscopic and macroscopic charcoal number fluxes are considered separately.

In this study, we explicitly simulate the aeolian transport and deposition of charcoal particles, which allows for quantitative comparison of simulated and observed charcoal fluxes. To model the transport of charcoal particles globally, we used the global aerosol–climate model ECHAM6.3-HAM2.3. We focus on microscopic charcoal particles, which primarily originate from fires in a radius of up to 100 km around the natural archive (Conedera et al., 2009) and are thus less influenced by specific site conditions (e.g. nearby burnable biomass). Part of microscopic charcoal particles can be transported over larger distances. For example, Hicks and Isaksson (2006) observed microscopic charcoal particles in Svalbard, which probably originated from the neighbouring continents and thus had been transported at least ≈ 1000 km.

Using a global aerosol–climate model allows the meteorological conditions for the transport to be calculated online. Furthermore, interactions of charcoal particles with other aerosol particles, with clouds, and with radiation can be considered. These factors might impact the removal processes of charcoal in the atmosphere and therefore where and when it is deposited.

Our main goals are to study the transport of microscopic charcoal particles on a global scale with a climate model and to test the model performance using charcoal data from different palaeo-fire records. The structure of this paper is the following: we first describe the charcoal data used for comparison with our simulations (Sect. 2). Subsequently, we describe the model, including the implementation of charcoal particles as a new aerosol species into our aerosol scheme (Sect. 3). In the "Results and discussion" section (Sect. 4), a comparison between model results and charcoal observations is shown as well as general atmospheric properties of the simulated charcoal particles such as mixing state. In the conclusions (Sect. 5), we summarise the key findings of this study.

2 Data

In this study, aerosol fire emissions (including charcoal) were prescribed using a satellite-based emission inventory. Since the emissions of microscopic charcoal are unknown, we estimated them by scaling the fire emissions of BC and comparing the model result to European charcoal observations (calibration data set, Sect. 2.1). The derived scaling factor was then tested using different charcoal observations from various regions around the globe (validation data set, Sect. 2.2).

2.1 Data used for calibration

To calibrate our emissions, we used the data from Adolf et al. (2018). This data set comprises charcoal observations from 37 lake sediments all over Europe (see Table S1 in the Supplement). Compared to other parts of the world, biomass burning emissions from Europe are small. Nevertheless, we chose this data set because of its uniqueness: (i) annual fluxes are estimated very accurately owing to the use of sediment traps; (ii) due to the recent nature of the data (spring/summer 2012 to spring/summer 2015), it coincides with satellite-based fire emissions; (iii) it includes a sufficiently large number of observation sites; (iv) it covers a region sufficiently large to compare with a global model; and (v) all charcoal samples were prepared with the same technique, and all particles counted by the same person.

For nearly all sediments considered in this study, we can assume that the transport of charcoal takes place predominantly in air, not in water. However, for one lake in southern Spain (Laguna Zóñar) and one in Switzerland (Mont d'Orge), surface run-off is expected to be important because of the bare soil around the lakes. Surface run-off can transport deposited charcoal particles from the soil to the lake and thus enhance the number of charcoal particles in the sediment traps. Therefore, data from these two sites must be interpreted with caution.

Charcoal particles were counted in pollen slides with a magnification of 200–250×. Samples for microscopic charcoal analysis were treated following palynological standard procedures (Stockmarr, 1971; Moore et al., 1991). All black, completely opaque, and angular particles (Clark, 1988b) with a minimum D_{M} of 10 µm and a maximum D_{M} of 500 µm were counted following Tinner and Hu (2003) and Finsinger and Tinner (2005).

2.2 Data used for validation

To validate the model results, we used microscopic charcoal observations covering different parts of the world, which are independent of the calibration data set. Table S2 summarises the locations and the time (period) of the observations used for validation. Overall, data from 32 lake sediments and peats were compiled using the Alpine Pollen Database of the University of Bern (ALPADABA). While many charcoal observations from lake sediments and peats exist, charcoal particles have so far only been studied in a handful of ice cores (e.g. this study; Isaksson et al., 2003; Eichler et al., 2011; Reese et al., 2013). In our analysis, we include five ice core records. Three of them were obtained in the frame of the project "Paleo fires from high-alpine ice cores" (which also includes this study), in which charcoal data from the Eurocore 89, Greenland, were also analysed. One of them is from Belukha glacier, Siberian Altai (Eichler et al., 2011).

The selected data are as homogeneous as possible: to compare the data set with our simulated results, only number fluxes of charcoal particles with a lower threshold of $D_M = 10\,\mu m$ were considered. We excluded data using a different threshold or reporting no information from which we could calculate fluxes. Since the preparation technique also influences the estimated fluxes (Tinner and Hu, 2003), we furthermore ensured that the sample preparation and charcoal identification for the validation data set are identical to that of the calibration data set. The only exception is the data from Connor (2011). Instead of counting the number of charcoal particles above $10\,\mu m$, Connor (2011) measured the charcoal area following the method from Clark (1982). To compare it with the simulated number fluxes, the linear regression from Tinner and Hu (2003) for Lago di Origlio was applied to the observed data to convert charcoal area to number.

For the lake sediments and peats, we include additional information about the dating of the records in Table S2. The sediment age was used to calculate sediment accumulation rates. Based on the original chronologies, we assumed a linear sediment accumulation between the two youngest charcoal samples to calculate a sediment accumulation rate from which we then derived the charcoal flux for the uppermost sample of the record. By assuming a linear sediment accumulation, we may underestimate true values given that surface sediments are not compacted yet. The surface of the sediment core usually reflects the time of drilling. Therefore, the older the youngest dated point of the core, the larger the uncertainty of the most recent sediment accumulation rate and, consequently, the charcoal fluxes. Furthermore, the uncertainty of the fluxes depends on the dated material and the dating method (both listed in Table S2).

The ice cores considered for validation are derived from Colle Gnifetti (Switzerland), Tsambagarav (Mongolia), Belukha (Russia), Illimani (Bolivia), and Summit (Greenland), thus spanning a wide range of the globe. An exotic *Lycopodium* spore marker was added to the melted samples, which were then evaporated to reduce the volume and afterwards treated in the same manner as the standard sediment samples (Brugger et al., 2018).

We only take into account data that are more recent than 1980 in the validation data set as we had to find a compromise between including observations reflecting the fire conditions of the simulated period (2005–2014) and observations coming from many different locations but which are older than the simulation period.

3 Methodology

3.1 Modelling charcoal particles in ECHAM6-HAM2

ECHAM6-HAM2 is a global climate model (ECHAM) coupled with an aerosol model (HAM) and a 2-moment cloud microphysical scheme. For more information about the model, we refer to Stier et al. (2005), Lohmann et al. (2007), Zhang et al. (2012), Stevens et al. (2013), and Neubauer et al. (2014). Since this is the first time that microscopic charcoal has been implemented into a global aerosol–climate model, in the following we will thoroughly describe which aspects need to be considered. First, we will describe general physical properties of microscopic charcoal and how these are represented by the model (Sect. 3.1.1). Second, we will describe how a life cycle of charcoal particles is simulated, i.e. from the emissions (Sect. 3.1.2) via atmospheric interactions (Sect. 3.1.3, 3.1.4) through to deposition (Sect. 3.1.5). In the end, some diagnostics complementary to the existing model output will be briefly mentioned (Sect. 3.1.6).

3.1.1 Size distribution, shape, and density

HAM uses the so-called M7 scheme (Vignati et al., 2004), which distinguishes seven aerosol modes classified by their size and solubility: soluble nucleation mode (number geometric mean radius $r_g < 5\,nm$), soluble Aitken mode ($5\,nm < r_g < 50\,nm$), insoluble Aitken mode, soluble accumulation mode ($50\,nm < r_g < 500\,nm$), insoluble accumulation mode, soluble coarse mode ($500\,nm < r_g$), and insoluble coarse mode. Each of these modes is log-normally distributed, and the total aerosol particle size distribution is described by a superposition of the seven modes. To implement charcoal particles, we extended the scheme by two additional modes (M9 scheme), namely by a soluble giant and an insoluble giant mode. The giant mode has the same geometric standard deviation as the coarse mode (i.e. $\sigma_g = 2$). We restricted neither the upper nor the lower bound of the giant mode, but the r_g of the emitted (i.e. initial) size distributions was set between 0.5 and $5\,\mu m$ (see Sect. 3.1.2). When a particle size distribution grows in M7, part of its mass and number is shifted to the next-larger mode, e.g. from the nucleation to the Aitken mode. To simplify diagnostics, we did not allow shifts from the coarse to the giant mode.

In HAM, all aerosol particles are assumed to be spherical. This condition is not fulfilled for charcoal particles, but at least microscopic charcoal particles seem to have a shape closer to a sphere than macroscopic charcoal particles (Crawford and Belcher, 2014). To compare our result with observations, we therefore use the volume-equivalent radius (r_{eq}) of charcoal particles. To estimate r_{eq}, the geometry of charcoal particles must be considered. Some studies analysed the shape of charcoal particles and reported their aspect ratios $R = \frac{D_M}{D_m}$, where D_m is the minimum dimension of a particle. In the Supplement (Sect. S1.1), we summarise the findings concerning R in the literature. In our model simulations, we consider a range of R between 1.33 and 2.4 (corresponding to r_{eq} of 4.9 and $3.5\,\mu m$); our initial estimate is $R = 2$ (corresponding to $r_{eq} = 3.9\,\mu m$).

A distinct characteristic of charcoal particles is their low density. Renfrew (1973) reports values of 0.3–$0.6\,g\,cm^{-3}$; Sander and Gee (1990) report similar values of 0.45–$0.75\,g\,cm^{-3}$. Hence, we chose a particle density of $0.5\,g\,cm^{-3}$ as an initial guess, which lies in the middle of these ranges. For the test simulations, we considered values where both observations overlap, i.e. from 0.45 to $0.6\,\mathrm{g\,cm^{-3}}$.

3.1.2 Charcoal emissions

Thanks to fire emission inventories based on satellite data, we have a good knowledge about where and when fires of which sizes occurred in the last 1–2 decades. Nevertheless, aerosol emissions from fires are still uncertain. This is caused to a large degree by the pronounced variability of fires: emission factors (which relate the mass of the burnt vegetation to the mass of emitted aerosol particles) vary considerably depending for instance on vegetation type, fire temperature, or fire dynamics. To our knowledge, no study has estimated the emission factors of microscopic charcoal particles so far. Clark et al. (1998) and Lynch et al. (2004) focused on macroscopic charcoal when estimating mass emission fluxes; therefore these values are not comparable.

Airborne measurements of aerosol particles from fires usually have upper cutoff sizes of a few micrometres or less (e.g. Johnson et al., 2008; May et al., 2014). The aircraft measurements by Radke et al. (1990) are exceptional since they include particles with sizes up to 3 mm, therefore covering the whole size range of charcoal. In their study, they set three fires in North America. The measured particle size distribution showed similar shapes for all of these burns. Radke et al. (1990) report that a considerable fraction of the particles measured in the plumes were larger than 45 µm in diameter. From their data, we estimate that the mass emission fluxes of supermicron particles should be of the same order of magnitude as the mass emission fluxes of submicron particles, which is usually dominated by organic carbon (OC) in fire plumes (Desservettaz et al., 2017). Thus, we assume that all of these large particles are indeed charcoal and not ash or other large particles emitted from fires.

Since both BC and charcoal particles form under conditions when oxygen is limited in the burning process, we decided to scale BC mass emissions from fires to derive charcoal mass emissions. As a starting point for the scaling factor, we assume that the mass emission fluxes of microscopic charcoal are comparable to those of submicron particles. Since BC only contributes relatively little to the total submicron particle mass, we scale the BC mass by a factor ≈ 10 (based on the ratios of BC to total submicron particles and to OC; Desservettaz et al., 2017; Akagi et al., 2011; Sinha et al., 2003). Furthermore, scaling aerosol emissions from the Global Fire Assimilation System (GFAS) by a factor of 3.4 leads to a better agreement between simulated and observed aerosol optical depth for both the global Monitoring Atmospheric Composition and Change (MACC) aerosol system and ECHAM6-HAM2 (Kaiser et al., 2012; von Hardenberg et al., 2012). Therefore, we use a factor of $10 \cdot 3.4 = 34$ as an initial estimate. Then we adjust this scaling factor until the simulated charcoal fluxes agree with the calibration data set (Sect. 2.1).

To describe the fire emissions, we use BC, OC, and SO_2 mass emissions at a 3-hourly resolution by combining the daily emissions from GFAS (GFASv1.0 until September 2014, GFASv1.2 afterwards) with the daily cycle from GFED (year 2004; Kaiser et al., 2012; Mu et al., 2011). GFAS emissions are based on fire radiative power and make use of vegetation-specific aerosol emission factors following Andreae and Merlet (2001, with annual updates by Meinrat O. Andreae). The strongest spurious signals originating from industrial activity, gas flaring, and volcanoes should be masked. However, in our simulations we found unrealistically high charcoal emissions over Iceland. These "emissions" are most likely caused by lava, which emits a signal at the same wavelength at which fires are detected. As an example, the volcano Bardarbunga caused huge eruptions over Iceland in August/September 2014, coinciding with extremely high fire emissions in GFAS ($2.32 \times 10^{-11}\,\mathrm{kg\,m^{-2}\,s^{-1}}$ averaged between 62° N, 26° W and 67° N, 11° W for September compared to global mean emissions of $1.57 \times 10^{-13}\,\mathrm{kg\,m^{-2}\,s^{-1}}$ for the same month). Therefore, we decided to mask all fire emissions over Iceland for our simulations. Furthermore, note that some fires are not detected by the satellite when clouds obscure the fire radiative power signal or when the signal is below the detection limit (which depends on the distance to sub-satellite track; Kaiser et al., 2012). Other uncertainties of biomass burning emissions include for example uncertainties in emission factors or land cover maps (Akagi et al., 2011; Fritz and See, 2008). More details about GFAS can be found in Kaiser et al. (2012).

Observations show that the larger the microscopic charcoal particles, the smaller their corresponding number concentration (e.g. Clark and Hussey, 1996). This implies that the number geometric mean radius r_g of our emitted charcoal size distribution should be smaller than the lower threshold of microscopic charcoal detection ($D_M = 10\,\mu m$); i.e. the observations rather lie on the descending branch of the emitted log-normal size distribution (see Fig. S2).

The airborne measurements by Radke et al. (1990) only show one clear maximum in the number size distribution at radius $r = 0.05\,\mu m$, which we attribute to aerosol particles other than charcoal (e.g. BC and OC). There is however a distinct flattening of the negative slope above $r \approx 0.5\,\mu m$, which could well be caused by an increase in the charcoal particle number concentration. From the study by Clark and Patterson (1997), who analysed deposited charcoal distributions, we estimate that the number geometric mean radius is $\approx 5\,\mu m$ (using $R = 2$). Based on these two studies, we roughly estimate that the number geometric mean radius at emission lies in the range between 0.5 and 5 µm.

In contrast to the studies by Clark (1988a) and Higuera et al. (2007), our fire plume heights depend on the planetary boundary layer (PBL) height (Veira et al., 2015), which is illustrated in Fig. S1. If the PBL height is lower than 4 km, 75 % of the fire emissions are distributed between the surface and the model layer below the PBL height (at a constant mass mixing ratio), 17 % are injected in the first model layer above the PBL height, and 8 % are injected in the second layer above the PBL height. In the rare cases of the PBL height being larger than 4 km, the plume height is set to the PBL height and the emissions are equally distributed from the surface to the model layer below the PBL height.

We assume that all charcoal is emitted as insoluble, non-hygroscopic particles because of their rather high carbon content and inertness (Preston and Schmidt, 2006). Observations have shown that BC, which has an even higher carbon content than charcoal, can take up soluble material and then undergo further hygroscopic growth (Shiraiwa et al., 2007; Zhang et al., 2008). Hence, we assume that the same holds for charcoal particles, i.e. that charcoal particles can become internally mixed and thus be shifted to the soluble mode. This is explained in the following section.

3.1.3 Interactions with other aerosol particles

Charcoal particles can be shifted from the insoluble giant to the soluble giant mode by two processes: (i) Brownian coagulation with soluble particles from the nucleation or Aitken mode and (ii) condensation of sulfuric acid on the particle surface. Coagulation with larger modes is not considered because the Brownian motion of these particles is very low and coagulation is therefore not effective. Schutgens and Stier (2014) reported that even coagulation between the Aitken (BC, OC, sulfate) and the coarse mode (dust) is negligible, which suggests that the same might be the case for the Aitken and the giant mode (charcoal). Since charcoal particles – in contrast to dust – are co-emitted with BC, OC, and sulfate, we decided to nevertheless implement the coagulation between the giant and the Aitken mode. By coagulation, the aerosol species BC, OC, and sulfate can be transferred to the soluble giant mode. The soluble giant mode is therefore a mixture of different aerosol species, whereas the insoluble giant mode is exclusively comprised of charcoal.

In our model, the condensation of sulfate shifts the charcoal particle to the soluble mode when at least one monolayer of sulfate covers the surface of the charcoal particle. Therefore, large charcoal particles are less likely to be transferred to the soluble mode by condensation of sulfate than small charcoal particles.

It is assumed that the soluble giant mode is *internally* mixed, i.e. that each individual aerosol particle consists of all components present in the mode. As soon as charcoal has been shifted to the soluble mode, the particles can grow further by water uptake when hygroscopic material like sulfate is present. In-cloud-produced sulfate mass can sometimes be added to the giant soluble mode when cloud droplets evaporate (see Sect. S2.1).

3.1.4 Interactions with microphysics and radiation

To our knowledge, the propensity of charcoal to act as a cloud condensation nucleus or ice-nucleating particle and the refractive index (RI) of microscopic charcoal have not been studied. In our model, mixed aerosol particles containing charcoal in the soluble giant mode can act as cloud condensation nuclei following the Abdul-Razzak and Ghan (2000) activation scheme. Charcoal itself does not dissociate. Further, we assume that charcoal particles cannot initiate freezing of cloud droplets. Concerning the interaction with radiation, we used the same RI as for dust; for explanation, see Sect. S1.2.

We do not expect these decisions to have a large impact on the atmospheric transport of charcoal particles since most charcoal particles do not reach levels where heterogeneous freezing becomes important, and the absorption of charcoal particles is likely too small to change the thermodynamic profile of the atmosphere.

3.1.5 Removal processes

Aerosol particles can be removed by three processes in HAM: wet deposition, gravitational settling, and dry deposition. Wet deposition in ECHAM6-HAM2 includes both in-cloud and below-cloud scavenging (Croft et al., 2009, 2010). Furthermore, the calculation distinguishes between liquid, mixed-phase, and ice clouds, as well as between stratiform and convective clouds. The wet-deposition calculation explicitly considers the sizes and the solubility of the aerosol particles. To prevent numerical instability, settling aerosol particles cannot fall through more than one model layer within one time step. However, this should not considerably change the spatial gravitational settling pattern (for details, see Sect. S2.2). In contrast to gravitational settling and wet deposition, dry deposition is only calculated near the surface. It accounts for the fact that a higher surface roughness leads to an increased aerosol flux to the surface because of turbulence. The surface roughness varies for different surface types, e.g. forest, water, or ice. Since gravitational settling is artificially slowed down near the surface on rare occasions (Sect. S2.2), dry deposition might take over and could therefore be somewhat overestimated.

3.1.6 Additional diagnostics

As mentioned in Sect. 3.1.2, we estimate the number geometric mean radius of the emitted charcoal size distribution to lie in the range 0.5–5 µm. This implies that a substantial portion of the simulated charcoal particles are smaller than $D_\mathrm{m} = 10\,\mu\mathrm{m}$ and are therefore not included in the counts under the microscope. When comparing the simulated number fluxes to the surface with observations, we therefore want to exclude these small particles in our diagnostics. However, in the standard set-up of ECHAM6-HAM2, only the total surface fluxes for each giant mode are calculated. To circumvent

Table 1. Exemplary results of test simulations with different parameters (emission number geometric mean radius *remi* in µm, threshold radius *rthr* in µm, and density *dens* in $\mathrm{g\,cm^{-3}}$). The scaling factor is the same for all simulations (SF = 34); the numbers hardly depend on the scaling factor. The parameters chosen for further simulations are marked in bold.

Parameters	Pearson correlation	Spearman rank correlation	Quartile coefficient of dispersion
remi2.5,rthr3.9,dens0.5	0.22	0.70	0.28
remi2.5,rthr3.9,dens0.6	0.22	0.70	0.31
remi2.5,rthr4.9,dens0.5	0.22	0.69	0.32
remi2.5,rthr4.9,dens0.6	0.22	0.68	0.37
remi4,rthr3.5,dens0.5	0.22	0.69	0.33
remi4,rthr3.9,dens0.5	0.22	0.69	0.36
remi5,rthr3.5,dens0.45	0.23	0.69	0.34
remi5,rthr3.5,dens0.5	0.23	0.68	0.36
remi5,rthr3.9,dens0.5	0.22	0.68	0.38
remi5,rthr3.9,dens0.6	0.22	0.68	0.41
remi5,rthr4.9,dens0.5	0.22	0.68	0.44
remi5,rthr4.9,dens0.6	**0.21**	**0.67**	**0.47**

this problem, we implemented additional diagnostics which calculate how many particles above a threshold radius are deposited. More information can be found in Sect. S2.3.

3.2 Model simulations

In this study, we used a model resolution of T63L31, which corresponds to a grid box size of $1.9° \times 1.9°$ ($\approx 200\,\mathrm{km} \times 200\,\mathrm{km}$ at the Equator) with 31 vertical layers. For all simulations, we used a spin-up time of 3 months. We conducted test simulations to find suitable values for charcoal emission factors and three uncertain parameters described below. As mentioned previously, we increased the BC mass emissions by a scaling factor (SF) to estimate the charcoal emissions. These test simulations were nudged towards 6-hourly ERA-Interim data from April 2012 to May 2015 to cover the same time period as the calibration data set used to evaluate the model performance. First, three charcoal parameters were varied in the test simulations at a constant scaling factor (SF = 34): the threshold radius (above which charcoal particles are counted), the emission number geometric mean radius, and the density. As an initial guess, we set the emission number geometric mean radius to $r_{\mathrm{eq}} = 2.5\,\mu\mathrm{m}$, the threshold radius to $r_{\mathrm{eq}} = 3.9\,\mu\mathrm{m}$ (corresponding to $R = 2$), and the density to $0.5\,\mathrm{g\,cm^{-3}}$. In Table 1, we refer to this simulation as *remi2.5,rthr3.9,dens0.5*. The values were varied in the ranges derived from the literature (see Sect. 3.1.2). Based on the comparison with the observations, we selected the best parameter set and then estimated which scaling factor is in best agreement with the observations.

Finally, we conducted a nudged and a free simulation of 10 years each (January 2005 to December 2014) with the derived parameter set and scaling factor and compared our results with the observations described in Sect. 2.2.

For all simulations, we used 3-hourly fire emissions based on daily GFAS emissions (see Sect. 3.1.2). The other prescribed aerosol emissions are monthly means and do not show interannual variability. For most of these aerosol particles, we used present-day emissions (year 2000) from the Atmospheric Chemistry and Climate Model Intercomparison Project (ACCMIP; Lamarque et al., 2010). Dust, sea salt, and oceanic dimethyl sulfide emissions were calculated within the model at every time step.

To compare the simulations with the observations (e.g. calculating correlation coefficients), we used the SciPy package (Jones et al., 2001–).

4 Results and discussion

4.1 Calibration of emissions

We conducted test simulations and compared the result to the European observations from Adolf et al. (2018). Three measures were used for the comparison: (i) the Pearson correlation, which is a measure for linear correlation; (ii) the Spearman rank correlation, which assesses monotonic relationships; and (iii) the quartile coefficient of dispersion, which is a normalised and robust variability measure ($\frac{Q_3-Q_1}{Q_3+Q_1}$, where Q_1 and Q_3 are the first and third quartiles, respectively). Table 1 shows some parameter combinations with positive correlation coefficients. In all test simulations, the correlation coefficients are very similar. While the Pearson correlation coefficients are low (0.21–0.23) and statistically insignificant, the Spearman rank correlation coefficients are much higher (0.67–0.69) and statistically significant. One reason for that is some observations with clearly larger charcoal fluxes than the simulated values ("outliers") since the Pearson correlation coefficients are much more sensitive to outliers than the Spearman rank correlation coefficients. These outliers can nicely be seen in Fig. S4 for the example of *remi2.5,rthr3.9,dens0.5*. Two of them (black in Fig. S4) are sites expected to be influenced by surface run-off (Laguna Zóñar and Mont d'Orge), which explains the discrepancy between observations and model results. Removing these two points from the calculation causes the Pearson correlation to increase (e.g. from 0.22 to 0.26 for simulation *remi2.5,rthr3.9,dens0.5*). The other outliers (dots in Figs. S4 and S5 above $40000\,\mathrm{no.\,cm^{-2}\,yr^{-1}}$ on the y axis) are sites located in Sicily and southern France. A minor part of the deviation might be due to the proximity of these sites to the ocean. In this case, the grid boxes contain both land and ocean, which leads to an underestimation of charcoal emission fluxes over land in the model.

In all test simulations, we found that the variability of charcoal fluxes is clearly underestimated. We think that the two following reasons are mainly responsible for the larger variability in the observations compared to the model:

- *Model resolution.* Sub-grid variability cannot be resolved by the model; i.e. the simulated emissions and depositions are an average over the whole grid box. In contrast, the observation sites can differ by a large amount, e.g. concerning the distance to burnable biomass, especially in the highly fragmented landscapes of Europe.

- *Uncertainties in fire emissions.* Some fires might not be detected by the satellite (e.g. due to dense clouds) and therefore might not be accounted for in the simulated emissions. Furthermore, charcoal particle emissions could show a different variability concerning vegetation than BC does; i.e. the charcoal emissions per mass of burnt biomass might vary more between different vegetation types than we assumed.

The quartile coefficients of dispersion (Table 1) show that the variability differs between the test simulations. The simulation with the highest variability (*remi5,rthr4.9,dens0.6*, albeit still having a lower variability than the observations) has only slightly lower correlation coefficients than the other simulations. Therefore, we choose this parameter set as the "best". However, we are aware that choosing the parameter set with the highest variability might compensate for errors not related to the parameters (e.g. the model resolution) that are responsible for an underestimated variability. Furthermore, none of the parameter sets has a statistically significant Pearson correlation. Therefore, we cannot conclude from our simulations which parameter set is the most realistic one.

For the chosen parameter set (*remi5,rthr4.9,dens0.6*), we conducted simulations with different scaling factors (see Fig. 1). The correlation coefficients and the quartile coefficients of dispersion hardly depend on the scaling factor because charcoal particles do not coagulate with each other. We did not use the root mean squared error as a measure for the best scaling factor because the charcoal observations span several orders of magnitudes and the absolute deviations would be biased by the highest absolute charcoal fluxes (including the outliers). Instead, we consider the scaling factor for which approximately the same number of observations lies above and below the 1 : 1 line to be in best accordance with the observations. This is the case for a scaling factor of the order of $SF = 250$ (see Fig. 1c), which furthermore has the smallest mean absolute error. However, note that the scaling factor depends on the chosen parameter set. Considering all parameter sets listed in Table 1, the best scaling factors range between $SF \approx 50$ and ≈ 250.

Figure 2 shows the observed and the simulated charcoal fluxes over Europe. Overall, the model is able to capture the European north–south gradient in charcoal fluxes, with lower values in the north.

In the next section, we will validate the model with observations from different regions of the world.

4.2 Comparison with observations

In this section, we compare our simulated charcoal fluxes with independent observations. Here, we show results for the nudged 10-year model simulation; those of the free 10-year simulation are very similar (for comparison, Fig. S5 shows the same as Fig. 3 but for the free simulation). For the three ice cores spanning a recent multi-annual period, we average the model output over the same time periods (2005 to summer 2009 for Tsambagarav, 2005 to 2014 for Colle Gnifetti, and 2008 to 2014 for Illimani). For all other observations, we use the mean over the whole simulation for comparison.

As for the calibration simulations described in Sect. 4.1, the high variability in the observations is not reproduced by the model (see Fig. 3). For Bhutan, Italy, Switzerland, and Georgia, several lake sediment samples were collected in a small geographical region and are therefore not further distinguished in Fig. 3 (black, yellow, green, and orange symbols, respectively; medians over these samples shown as large pentagrams). The regional medians of the observations are rather close to the simulated median charcoal fluxes, indicating that the simulated fluxes are representative for a large scale. While the simulated median over Italy agrees very well with the observations, it is overestimated for Switzerland, Georgia, and Bhutan. Note that most of the data are also shown on a linear scale (Fig. 4), where we zoom in for better visibility (red frame in Fig. 3). The data from Connor (2011) (orange crosses) are the only ones originally measured in area fluxes and afterwards converted to number fluxes (see Sect. 2.2). The converted number fluxes compare well with the other observations and the model results, which indicates that the regression from Tinner and Hu (2003) can indeed be applied in this case.

Most simulated fluxes deviate by less than 1 order of magnitude from the observations, providing evidence that the simulated results are in good agreement with observed values at the sites. However, the charcoal flux values are highly overestimated for all ice cores (triangles), for three peats in the Alpine region (Mauntschas, Rosaninsee, and Wengerkopf), and for the sediment from Lake Kharinei (northern Russia). The model probably overestimates the fluxes at the ice core sites because of their high location within complex topography. The model is not able to simulate these high locations correctly since the surface altitude is constant over the whole grid box; i.e. the topography is smoothed. The simulated grid box averages are therefore not comparable to the ice core measurements. In reality, ice cores are located above the top plume height of most fires (Rémy et al., 2017), which may prevent transport of charcoal particles to them. Furthermore, the simulated fire emission height has a bias towards higher plume heights (Veira et al., 2015), which likely also contributes to the overestimation of simulated charcoal fluxes for sites above 4000 m (Rodophu-2 and all ice cores except Greenland). In addition, we expect that this bias leads to an overestimation of the simulated transport

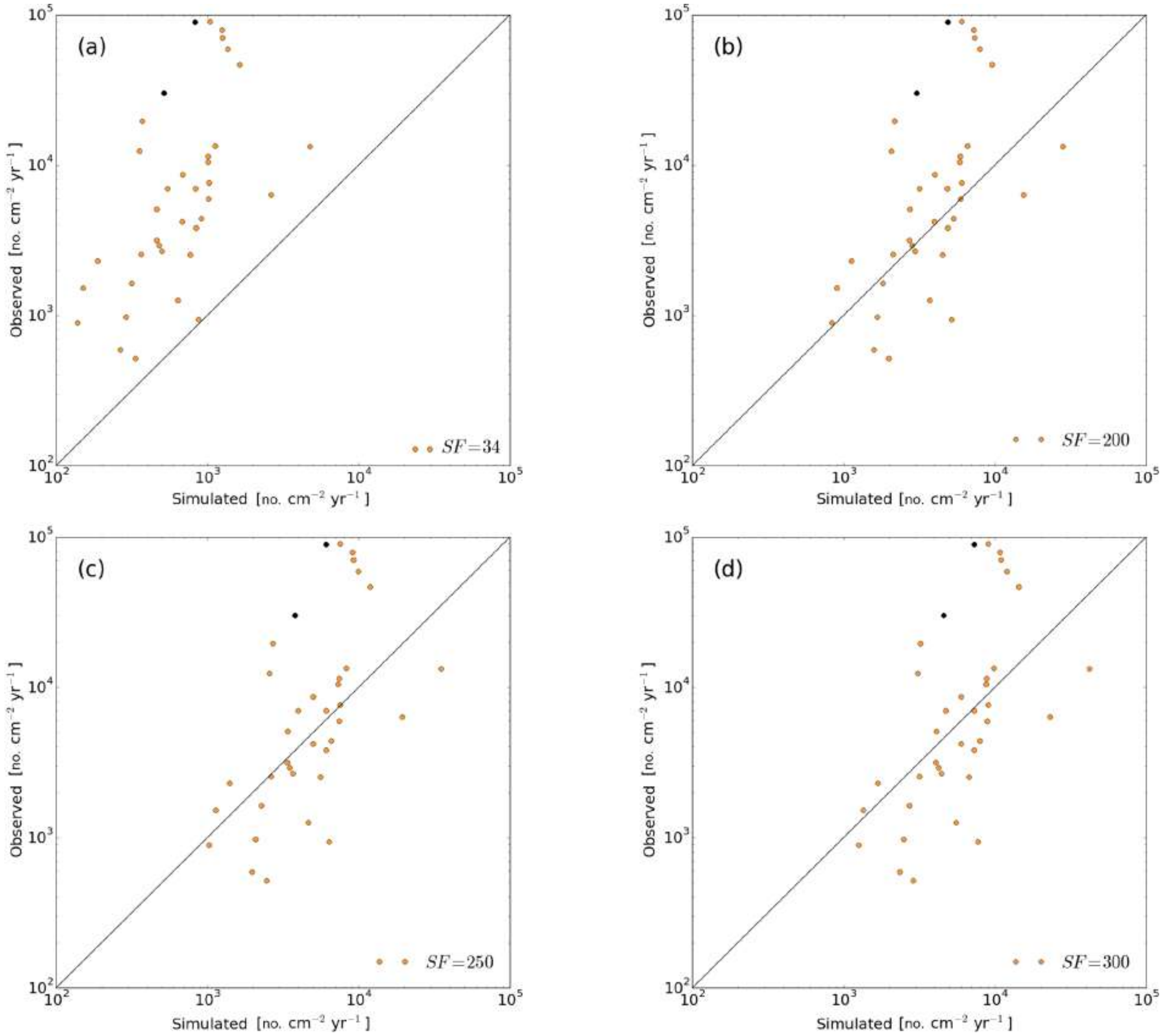

Figure 1. Simulated vs. observed number fluxes of charcoal particles above the threshold radius (in $cm^{-2}\,yr^{-1}$) using the chosen estimate of parameters (an emission number geometric mean radius of $r_{eq} = 5$ µm, a threshold radius of $r_{eq} = 4.9$ µm, and a charcoal density of $0.6\,g\,cm^{-3}$). The scaling factor increases from **(a)** to **(d)** (see legends). The two black dots show the sites likely influenced by surface run-off.

of charcoal to remote locations, which could explain the high simulated fluxes at Lake Kharinei and in Greenland. Another explanation for the overestimated simulated fluxes in Greenland is an increase in fire activity: GFAS data between 2003 and 2015 suggest that the fire emissions in Greenland might have increased in recent years. Fire activity was recorded in the years 2003, 2007, and all years from 2011 onwards, with highest aerosol emissions occurring in 2015. Therefore, it is possible that the fire activity was lower in 1989 (when the ice core was drilled) than in the simulated period (2005–2014). For the alpine sites, the observed fluxes might again not be representative for the whole grid box due to the small-scale, heterogeneous landscape around these observation sites (fire emissions and vegetation cover are constant in one model grid box).

Overall the chosen scaling factor (SF = 250) describes the data well; i.e. a *global* charcoal scaling factor seems to be justified. However, the validation data set does not cover certain regions (e.g. Africa or Australia) and is biased towards northern mid-latitudes. The correlation between observed and simulated fluxes is 0.59 and 0.48 for the Pearson and the Spearman rank correlation, respectively, and in both cases statistically significant.

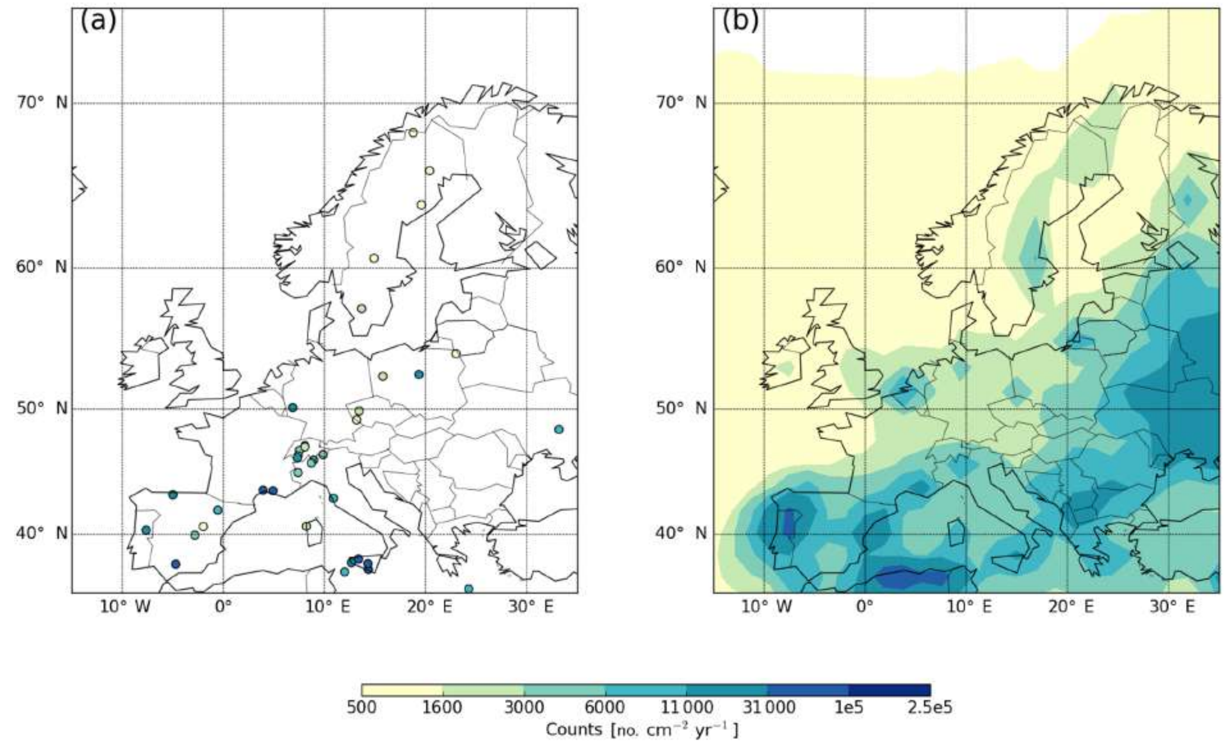

Figure 2. **(a)** Observed vs. **(b)** simulated number fluxes of charcoal particles above the threshold radius (in $cm^{-2}\,yr^{-1}$) using the chosen estimate of parameters (an emission number geometric mean radius of $r_{eq} = 5\,\mu m$, a threshold radius of $r_{eq} = 4.9\,\mu m$, and a charcoal density of $0.6\,g\,cm^{-3}$).

4.3 Global distribution considering all microscopic charcoal particles

The global microscopic charcoal burden, i.e. the vertically integrated mass of microscopic charcoal particles in the atmosphere (above the threshold radius), is shown in Fig. 5a averaged over the 10-year nudged simulation. As expected, the burden is highest where most biomass burning emissions occur, namely in the tropics followed by the northern high latitudes (mainly Siberia and North America; Kaiser et al., 2012). The simulated global mean burden above the threshold radius is $1.44 \times 10^{-6}\,kg\,m^{-2}$, i.e. approximately 6 times larger than the burden of BC, which is $2.37 \times 10^{-7}\,kg\,m^{-2}$ including all BC sources and sizes (shown in Fig. 5b). Although the largest charcoal burdens occur near the emission sources, significant fractions of charcoal mass are transported hundreds of kilometres in the model, which is for example the case near the east coast of North America or the west coast of central Africa.

Most of the charcoal above the threshold radius resides in the insoluble mode in terms of number and mass, and only a few percent is shifted to the soluble mode (see Fig. 6). The small contribution of the soluble mode can be explained by the large size of the charcoal particles (limiting amount of coating material) and the related short atmospheric lifetime. Beside charcoal, the soluble mode is predominantly comprised of sulfate (and water), while the mass contributions of BC and OC are small (not shown).

4.4 Deposition of microscopic charcoal particles

As expected, the different atmospheric removal processes for charcoal particles above the threshold radius differ in geographic distribution (see Fig. 7). While gravitational settling and dry deposition become less important the larger the distance to the emission source, this is not generally the case for wet deposition. Large wet-deposition fluxes are observed where (simulated) precipitation is high, e.g. along the Atlantic storm track. Contrary to gravitational settling, dry deposition depends on the surface properties (Stier et al., 2005). Therefore, dry-deposition fluxes are small over the ocean compared to over land.

Overall, gravitational settling is the most important removal process, followed by dry deposition and then wet deposition. Although gravitational settling and dry deposition dominate the global charcoal deposition, wet deposition is the dominant removal process in some remote regions like part of Greenland.

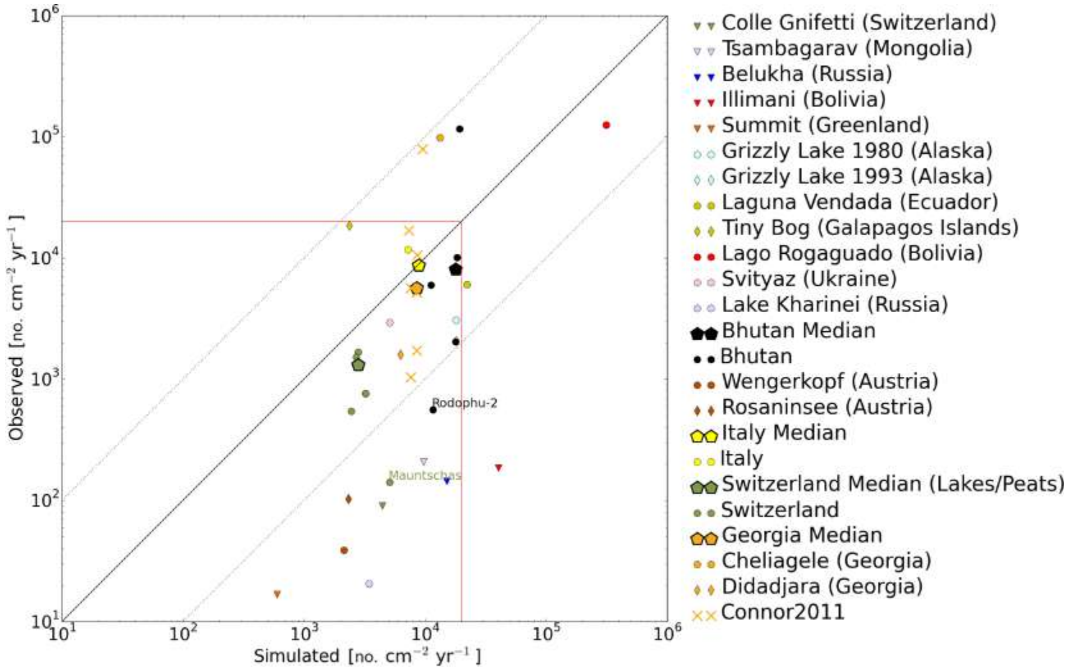

Figure 3. Simulated vs. observed number fluxes of charcoal particles above a threshold radius of $r_{eq} = 4.9\,\mu m$ (in $cm^{-2}\,yr^{-1}$) for the validation data set (with an emission number geometric mean radius of $r_{eq} = 5\,\mu m$ and a charcoal density of $0.6\,g\,cm^{-3}$). The triangles refer to observations from ice cores; all other data are from sediments. The same colours are used for samples from the same countries. The data from Connor (2011) are distinguished by symbols (X's) because a different method was used. To improve readability, the different sediment observations from Bhutan, Italy, Switzerland, and Georgia are not further distinguished in the legend since the observation sites in these countries are close together. The median over them is illustrated by the large pentagrams. The red frame shows the axis limits of Fig. 4. The black solid line is the 1 : 1 line; the lines that are 1 order of magnitude away from the 1 : 1 line are dotted.

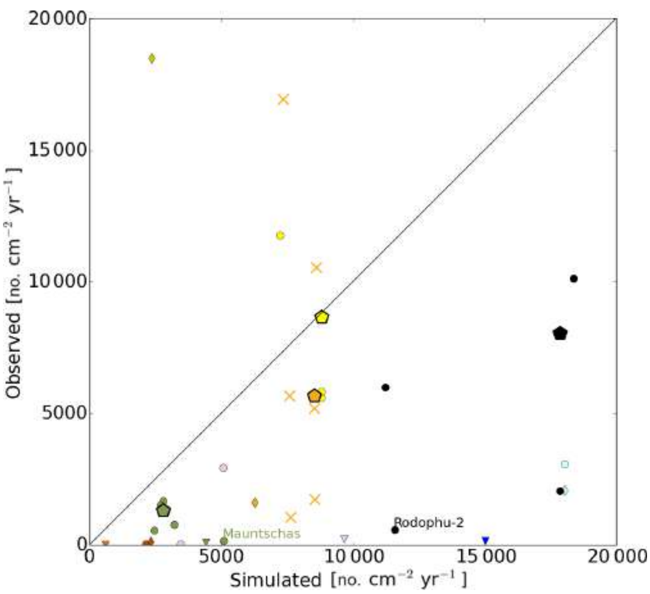

Figure 4. The same as Fig. 3 but on a linear scale with different axis limits (corresponding to the red frame in Fig. 3).

5 Conclusions

Charcoal records from lake sediments are widely used to reconstruct past fire activity. More recently, charcoal particles have also been studied in ice cores. In this paper, we implemented microscopic charcoal particles into a global aerosol–climate model. Comparing simulated with observed charcoal fluxes might help to quantitatively reconstruct past fire activity. A recent and comprehensive charcoal data set from Europe was used for calibration of model emissions. Increasing BC fire emissions by a factor of 250 resulted in the best match between the model and observations, but this scaling factor depends on the chosen parameter set (ranging from ≈ 50 to ≈ 250 for the parameter sets that we tested). Although the model is not able to reproduce the high local variability of the observations, it captures the large-scale pattern of charcoal deposition (e.g. the north–south gradient in Europe) reasonably well. The charcoal fluxes for the validation data set, which covers different locations across the globe, are well captured with the constant charcoal scaling factor derived from the European calibration data set. However, our validation data set consists mostly of samples from northern mid-latitudes. We also found an underestimation in variability for the validation data set but a positive, statistically significant correlation between modelled and observed fluxes.

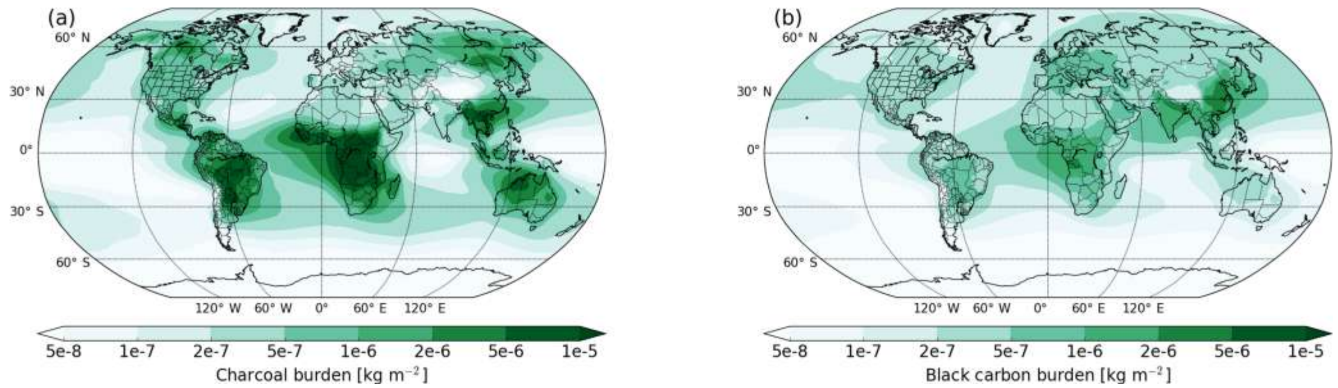

Figure 5. Simulated aerosol burden averaged over 10 years for **(a)** charcoal and **(b)** black carbon. For the charcoal burden, only particles above the threshold radius of $r_{\mathrm{eq}} = 4.9\,\mu\mathrm{m}$ are considered. A charcoal emission number geometric mean radius of $r_{\mathrm{eq}} = 5\,\mu\mathrm{m}$ and a charcoal density of $0.6\,\mathrm{g\,cm^{-3}}$ were used.

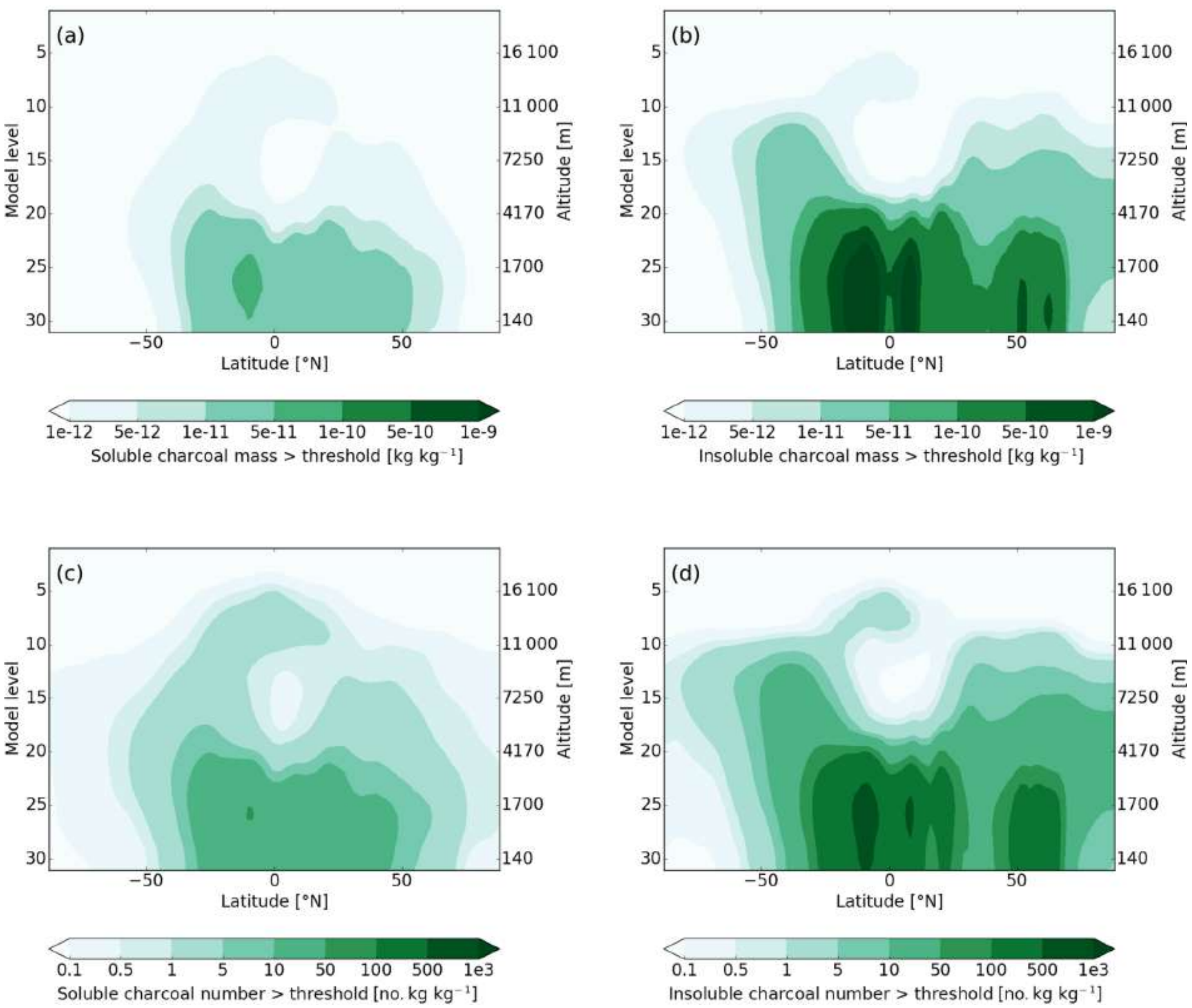

Figure 6. Ten-year zonal average of the charcoal mass concentration above the threshold radius ($r_{\mathrm{eq}} = 4.9\,\mu\mathrm{m}$) in **(a)** the soluble and **(b)** the insoluble giant mode and of the number concentration of (charcoal) particles above the threshold radius in **(c)** the soluble mode and **(d)** the insoluble giant mode (using an emission number geometric mean radius of $r_{\mathrm{eq}} = 5\,\mu\mathrm{m}$ and a charcoal density of $0.6\,\mathrm{g\,cm^{-3}}$). The right y axis shows to which altitude the model layers approximately correspond.

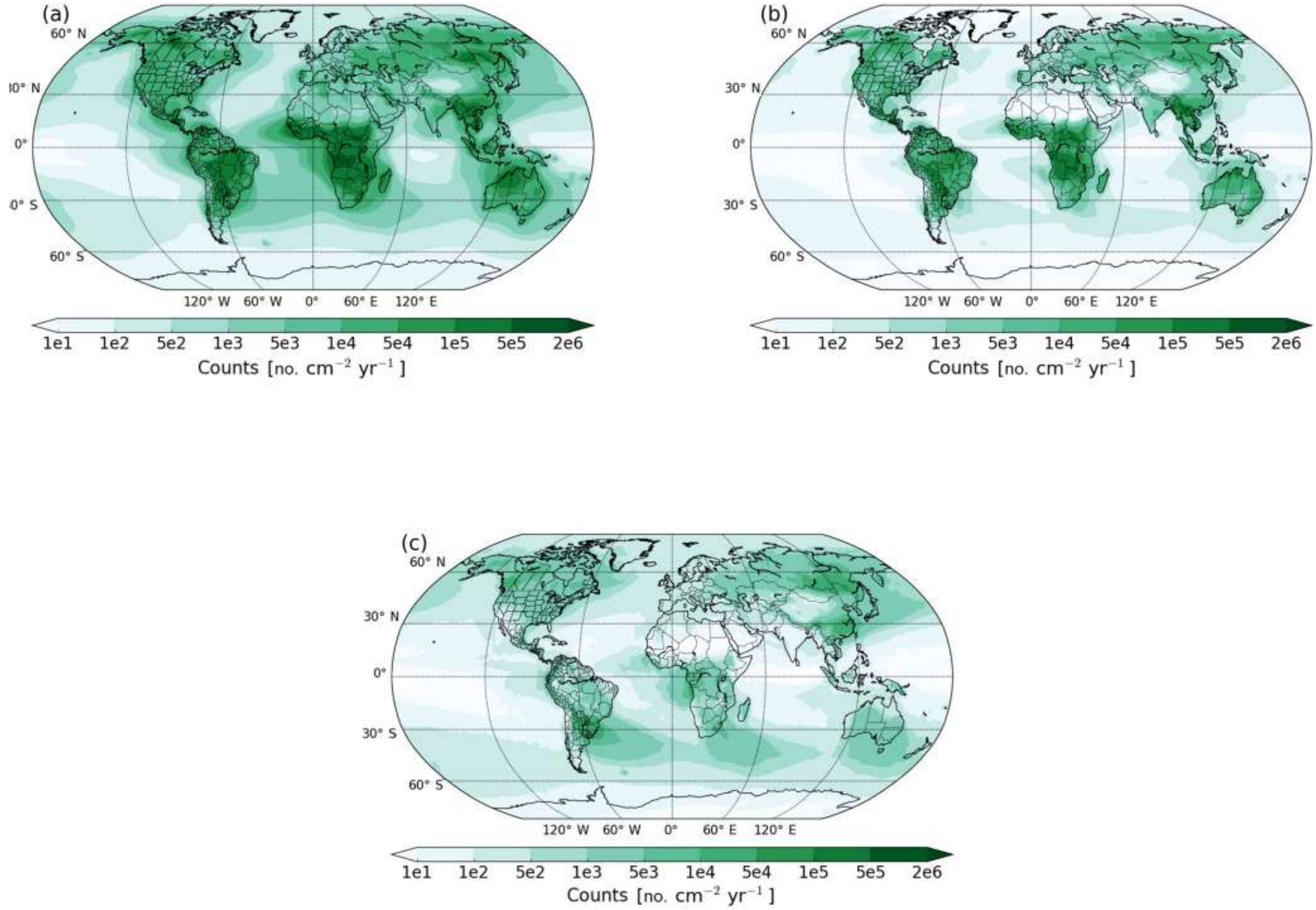

Figure 7. The number fluxes (number of particles above a threshold radius of $r_{eq} = 4.9\,\mu m$ in $cm^{-2}\,yr^{-1}$) of the three different charcoal removal processes in the model (with an emission number geometric mean radius of $r_{eq} = 5\,\mu m$ and a charcoal density of $0.6\,g\,cm^{-3}$): **(a)** gravitational settling, **(b)** dry deposition, and **(c)** wet deposition.

The model shows a systematic positive bias for the ice core observations, which is likely due to the high altitude of the ice core sites as well as the complex topography around them.

As expected, the largest simulated charcoal deposition fluxes occur near fires. However, the model suggests that a non-negligible amount of microscopic charcoal particles is transported over large distances and therefore reaches remote locations (although comparisons with observations indicate that the model might overestimate long-range transport). In the model, only a few percent of charcoal particles is mixed with soluble material in the atmosphere.

The Global Paleofire Working Group (Hawthorne et al., 2017) aims for more standardised charcoal observations that cover all relevant fire regions. Here we suggest that more systematic and standardised observations of microscopic charcoal as number fluxes (with e.g. maximum particle dimension $> 10\,\mu m$, as in Adolf et al., 2018) could help to improve data–model comparisons and to verify whether a constant scaling factor indeed describes the data well on a global scale. In future studies, our new framework allows global modelling of charcoal and other biomass-burning-relevant tracers such as black carbon, which may improve the understanding of the representativeness of individual fire proxies. In addition, simulating microscopic charcoal particles using the scaling factor found might allow us to quantitatively validate past fire emissions provided by fire models. The validation of fire models is essential to improve the understanding of the key drivers of fires and to gain confidence in projections of future fire activity.

Code availability. The ECHAM-HAMMOZ model is made freely available to the scientific community under the HAMMOZ Software Licence Agreement, which defines the conditions under which the model can be used. More information can be found at the HAMMOZ website (https://redmine.hammoz.ethz.ch/projects/hammoz, ECHAM-HAM(MOZ) developers, 2018).

Data availability. You can find the data at https://data.iac.ethz.ch/Gilgen_et_al_2018_Charcoal (Gilgen, 2018).

The Supplement related to this article is available online at https://doi.org/10.5194/acp-18-11813-2018-supplement.

Author contributions. AG did most of the programming, conducted the simulations, and wrote the main part of the manuscript, with major contributions from SOB and CA to Sect. 2 and contributions from all authors to the text. MS, WT, and UL designed the overall project, while AG, LI, and UL were responsible for the details about the charcoal implementation in the model. CA collected the data from Laguna Vendada and provided the data set used for calibration. SOB compiled and processed most of the data used for validation, contributed a great deal to the discussions about the comparison between the model and the observations, and provided unpublished ice core data. JFNvL provided unpublished data from Cheliagele, Svityaz, Tergang, Shamling, Rodophu-2, Laya, Tiny Bog, and Lake Hallwil. All authors provided valuable comments to the manuscript.

Competing interests. The authors declare that they have no conflict of interest.

Acknowledgements. We thank the Swiss National Science Foundation (SNF) for granting the Sinergia project "Paleo fires from high-alpine ice cores", which funded this research and enabled the collaboration between different research disciplines (CRSII2_154450). This work was also supported by a grant from the Swiss National Supercomputing Centre (CSCS) under project ID s652. In addition, we are grateful to Michael Sigl and Dimitri Osmont from the Paul Scherrer Institute for helping with the ice core preparation. Furthermore, we acknowledge the help of W. O. van der Knaap from the University of Bern, who extracted the raw data from ALPADAPA, and Peter Kunes, who counted the charcoal particles from Singhe Dzong. We are also thankful to Thomas Blunier from the Centre for Ice and Climate in Copenhagen; he kindly provided us ice from the Summit ice core. We generally thank the developers of ECHAM-HAM(MOZ), who continuously improve the model. The ECHAM-HAMMOZ model is developed by a consortium composed of ETH Zürich, Max Planck Institut für Meteorologie, Forschungszentrum Jülich, the University of Oxford, the Finnish Meteorological Institute, and the Leibniz Institute for Tropospheric Research, and managed by the Center for Climate Systems Modeling (C2SM) at ETH Zürich. Last but not least, we acknowledge the critical and essential comments from Brian Magi and an anonymous reviewer.

Edited by: Frank Dentener
Reviewed by: Brian Magi and one anonymous referee

References

Abdul-Razzak, H. and Ghan, S. J.: A parameterization of aerosol activation: 2. Multiple aerosol types, J. Geophys. Res.-Atmos., 105, 6837–6844, https://doi.org/10.1029/1999JD901161, 2000.

Adolf, C., Wunderle, S., Colombaroli, D., Weber, H., Gobet, E., Heiri, O., van Leeuwen, J. F. N., Bigler, C., Connor, S. E., Gałka, M., La Mantia, T., Makhortykh, S., Svitavská-Svobodová, H., Vannière, B., and Tinner, W.: The sedimentary and remote-sensing reflection of biomass burning in Europe, Global Ecol. Biogeogr., 27, 199–212, https://doi.org/10.1111/geb.12682, 2018.

Akagi, S. K., Yokelson, R. J., Wiedinmyer, C., Alvarado, M. J., Reid, J. S., Karl, T., Crounse, J. D., and Wennberg, P. O.: Emission factors for open and domestic biomass burning for use in atmospheric models, Atmos. Chem. Phys., 11, 4039–4072, https://doi.org/10.5194/acp-11-4039-2011, 2011.

Andreae, M. O. and Merlet, P.: Emission of trace gases and aerosols from biomass burning, Global Biogeochem. Cy., 15, 955–966, https://doi.org/10.1029/2000GB001382, 2001.

Bond, T. C., Doherty, S. J., Fahey, D. W., Forster, P. M., Berntsen, T., DeAngelo, B. J., Flanner, M. G., Ghan, S., Kärcher, B., Koch, D., Kinne, S., Kondo, Y., Quinn, P. K., Sarofim, M. C., Schultz, M. G., Schulz, M., Venkataraman, C., Zhang, H., Zhang, S., Bellouin, N., Guttikunda, S. K., Hopke, P. K., Jacobson, M. Z., Kaiser, J. W., Klimont, Z., Lohmann, U., Schwarz, J. P., Shindell, D., Storelvmo, T., Warren, S. G., and Zender, C. S.: Bounding the role of black carbon in the climate system: A scientific assessment, J. Geophys. Res.-Atmos., 118, 5380–5552, https://doi.org/10.1002/jgrd.50171, 2013.

Bond, W. and Keeley, J.: Fire as global "herbivore": The ecology and evolution of flammable ecosystems, Trends Ecol. Evol., 20, 387–394, 2005.

Brugger, S. O., Gobet, E., Schanz, F. R., Heiri, O., Schwörer, C., Sigl, M., Schwikowski, M., and Tinner, W.: A quantitative comparison of microfossil extraction methods from ice cores, J. Glaciol., 64, 432–442, https://doi.org/10.1017/jog.2018.31, 2018.

Clark, J. S.: Particle motion and the theory of charcoal analysis: Source area, transport, deposition, and sampling, Quaternary Res., 30, 67–80, https://doi.org/10.1016/0033-5894(88)90088-9, 1988a.

Clark, J. S.: Stratigraphic charcoal analysis on petrographic thin sections: Application to fire history in northwestern Minnesota, Quaternary Res., 30, 81–91, https://doi.org/10.1016/0033-5894(88)90089-0, 1988b.

Clark, J. S. and Hussey, T. C.: Estimating the mass flux of charcoal from sedimentary records, The Holocene, 6, 129–144, 1996.

Clark, J. S. and Patterson, W. A.: Background and Local Charcoal in Sediments: Scales of Fire Evidence in the Paleorecord, Springer Berlin Heidelberg, Berlin, Heidelberg, 23–48, https://doi.org/10.1007/978-3-642-59171-6_3, 1997.

Clark, J. S., Lynch, J., Stocks, B. J., and Goldammer, J. G.: Relationships between charcoal particles in air and sediments in west-central Siberia, The Holocene, 8, 19–29, https://doi.org/10.1191/095968398672501165, 1998.

Clark, R.: Point count estimation of charcoal in pollen preparations and thin sections of sediments, Pollen et Spores, 24, 523–535, 1982.

Conedera, M., Tinner, W., Neff, C., Meurer, M., Dickens, A. F., and Krebs, P.: Reconstructing past fire regimes: methods, applications, and relevance to fire management and conservation, Quaternary Sci. Rev., 28, 555–576, https://doi.org/10.1016/j.quascirev.2008.11.005, 2009.

Connor, S. E.: A Promethean Legacy: Late Quaternary Vegetation History of Southern Georgia, the Caucasus, Peeters, Louvain, 2011.

Crawford, A. and Belcher, C.: Charcoal Morphometry for Paleoecological Analysis: The Effects of Fuel Type and Transportation on Morphological Parameters, Appl. Plant. Sci., 2, 1–10, https://doi.org/10.3732/apps.1400004, 2014.

Croft, B., Lohmann, U., Martin, R. V., Stier, P., Wurzler, S., Feichter, J., Posselt, R., and Ferrachat, S.: Aerosol size-dependent below-cloud scavenging by rain and snow in the ECHAM5-HAM, Atmos. Chem. Phys., 9, 4653–4675, https://doi.org/10.5194/acp-9-4653-2009, 2009.

Croft, B., Lohmann, U., Martin, R. V., Stier, P., Wurzler, S., Feichter, J., Hoose, C., Heikkilä, U., van Donkelaar, A., and Ferrachat, S.: Influences of in-cloud aerosol scavenging parameterizations on aerosol concentrations and wet deposition in ECHAM5-HAM, Atmos. Chem. Phys., 10, 1511–1543, https://doi.org/10.5194/acp-10-1511-2010, 2010.

Crutzen, P. J. and Andreae, M. O.: Biomass Burning in the Tropics: Impact on Atmospheric Chemistry and Biogeochemical Cycles, Science, 250, 1669–1678, https://doi.org/10.1126/science.250.4988.1669, 1990.

Desservettaz, M., Paton-Walsh, C., Griffith, D. W. T., Kettlewell, G., Keywood, M. D., Vanderschoot, M. V., Ward, J., Mallet, M. D., Milic, A., Miljevic, B., Ristovski, Z. D., Howard, D., Edwards, G. C., and Atkinson, B.: Emission factors of trace gases and particles from tropical savanna fires in Australia, J. Geophys. Res.-Atmos., 122, 6059–6074, https://doi.org/10.1002/2016JD025925, 2016JD025925, 2017.

ECHAM-HAM(MOZ) developers: ECHAM-HAM(MOZ) code, available at: https://redmine.hammoz.ethz.ch/projects/hammoz, last access: 9 July 2018.

Eichler, A., Tinner, W., Brütsch, S., Olivier, S., Papina, T., and Schwikowski, M.: An ice-core based history of Siberian forest fires since AD 1250, Quaternary Sci. Rev., 30, 1027–1034, https://doi.org/10.1016/j.quascirev.2011.02.007, 2011.

Finsinger, W. and Tinner, W.: Minimum count sums for charcoal concentration estimates in pollen slides: accuracy and potential errors, The Holocene, 15, 293–297, https://doi.org/10.1191/0959683605hl808rr, 2005.

Fritz, S. and See, L.: Identifying and quantifying uncertainty and spatial disagreement in the comparison of Global Land Cover for different applications, Glob. Change Biol., 14, 1057–1075, https://doi.org/10.1111/j.1365-2486.2007.01519.x, 2008.

Gatebe, C. K., Ichoku, C. M., Poudyal, R., Román, M. O., and Wilcox, E.: Surface albedo darkening from wildfires in northern sub-Saharan Africa, Environ. Res. Lett., 9, 065003, available at: http://stacks.iop.org/1748-9326/9/i=6/a=065003 (last access: 16 August 2018), 2014.

Gilgen, A.: Charcoal Data, available at: https://data.iac.ethz.ch/Gilgen_et_al_2018_Charcoal, last access: 9 July 2018.

Hantson, S., Arneth, A., Harrison, S. P., Kelley, D. I., Prentice, I. C., Rabin, S. S., Archibald, S., Mouillot, F., Arnold, S. R., Artaxo, P., Bachelet, D., Ciais, P., Forrest, M., Friedlingstein, P., Hickler, T., Kaplan, J. O., Kloster, S., Knorr, W., Lasslop, G., Li, F., Mangeon, S., Melton, J. R., Meyn, A., Sitch, S., Spessa, A., van der Werf, G. R., Voulgarakis, A., and Yue, C.: The status and challenge of global fire modelling, Biogeosciences, 13, 3359–3375, https://doi.org/10.5194/bg-13-3359-2016, 2016.

Hawthorne, D., Mustaphi, C. J. C., Aleman, J. C., Blarquez, O., Colombaroli, D., Daniau, A.-L., Marlon, J. R., Power, M., Vannière, B., Han, Y., Hantson, S., Kehrwald, N., Magi, B., Yue, X., Carcaillet, C., Marchant, R., Ogunkoya, A., Githumbi, E. N., and Muriuki, R. M.: Global Modern Charcoal Dataset (GMCD): A tool for exploring proxy-fire linkages and spatial patterns of biomass burning, Quatern. Int., https://doi.org/10.1016/j.quaint.2017.03.046, 448, 3–17, 2017.

Hicks, S. and Isaksson, E.: Assessing source areas of pollutants from studies of fly ash, charcoal, and pollen from Svalbard snow and ice, J. Geophys. Res.-Atmos., 111, d02113, https://doi.org/10.1029/2005JD006167, 2006.

Higuera, P. E., Peters, M. E., Brubaker, L. B., and Gavin, D. G.: Understanding the origin and analysis of sediment-charcoal records with a simulation model, Quaternary Sci. Rev., 26, 1790–1809, https://doi.org/10.1016/j.quascirev.2007.03.010, 2007.

Isaksson, E., Hermanson, M., Hicks, S., Igarashi, M., Kamiyama, K., Moore, J., Motoyama, H., Muir, D., Pohjola, V., Vaikmäe, R., van de Wal, R. S., and Watanabe, O.: Ice cores from Svalbard – useful archives of past climate and pollution history, Phys. Chem. Earth, 28, 1217–1228, https://doi.org/10.1016/j.pce.2003.08.053, 2003.

Itter, M. S., Finley, A. O., Hooten, M. B., Higuera, P. E., Marlon, J. R., Kelly, R., and McLachlan, J. S.: A model-based approach to wildland fire reconstruction using sediment charcoal records, Environmetrics, 28, e2450, https://doi.org/10.1002/env.2450, 2017.

Johnson, B. T., Osborne, S. R., Haywood, J. M., and Harrison, M. A. J.: Aircraft measurements of biomass burning aerosol over West Africa during DABEX, J. Geophys. Res.-Atmos., 113, D00C06, https://doi.org/10.1029/2007JD009451, 2008.

Jones, E., Oliphant, T., Peterson, P., et al.: SciPy: Open source scientific tools for Python, available at: http://www.scipy.org/ (last access: 9 July 2018), 2001–.

Kaiser, J. W., Heil, A., Andreae, M. O., Benedetti, A., Chubarova, N., Jones, L., Morcrette, J.-J., Razinger, M., Schultz, M. G., Suttie, M., and van der Werf, G. R.: Biomass burning emissions estimated with a global fire assimilation system based on observed fire radiative power, Biogeosciences, 9, 527–554, https://doi.org/10.5194/bg-9-527-2012, 2012.

Lamarque, J.-F., Bond, T. C., Eyring, V., Granier, C., Heil, A., Klimont, Z., Lee, D., Liousse, C., Mieville, A., Owen, B., Schultz, M. G., Shindell, D., Smith, S. J., Stehfest, E., Van Aardenne, J., Cooper, O. R., Kainuma, M., Mahowald, N., McConnell, J. R., Naik, V., Riahi, K., and van Vuuren, D. P.: Historical (1850–2000) gridded anthropogenic and biomass burning emissions of reactive gases and aerosols: methodology and application, Atmos. Chem. Phys., 10, 7017–7039, https://doi.org/10.5194/acp-10-7017-2010, 2010.

Lohmann, U., Stier, P., Hoose, C., Ferrachat, S., Kloster, S., Roeckner, E., and Zhang, J.: Cloud microphysics and aerosol indirect effects in the global climate model ECHAM5-HAM, Atmos. Chem. Phys., 7, 3425–3446, https://doi.org/10.5194/acp-7-3425-2007, 2007.

Lynch, J. A., Clark, J. S., and Stocks, B. J.: Charcoal production, dispersal, and deposition from the Fort Providence experimental fire: interpreting fire regimes from charcoal records in boreal forests, Can. J. For. Res., 34, 1642–1656, https://doi.org/10.1139/x04-071, 2004.

Marlon, J. R., Bartlein, P. J., Carcaillet, C., Gavin, D. G., Harrison, S. P., Higuera, P. E., Joos, F., Power, M. J., and Prentice, I. C.: Climate and human influences on global biomass burning over the past two millenni, Nature Geosci., 1, 697–702, https://doi.org/10.1038/ngeo313, 2008.

Marlon, J. R., Kelly, R., Daniau, A.-L., Vannière, B., Power, M. J., Bartlein, P., Higuera, P., Blarquez, O., Brewer, S., Brücher, T., Feurdean, A., Romera, G. G., Iglesias, V., Maezumi, S. Y., Magi, B., Courtney Mustaphi, C. J., and Zhihai, T.: Reconstructions of biomass burning from sediment-charcoal records to improve data-model comparisons, Biogeosciences, 13, 3225-3244, https://doi.org/10.5194/bg-13-3225-2016, 2016.

May, A. A., McMeeking, G. R., Lee, T., Taylor, J. W., Craven, J. S., Burling, I., Sullivan, A. P., Akagi, S., Collett, J. L., Flynn, M., Coe, H., Urbanski, S. P., Seinfeld, J. H., Yokelson, R. J., and Kreidenweis, S. M.: Aerosol emissions from prescribed fires in the United States: A synthesis of laboratory and aircraft measurements, J. Geophys. Res., 119, 11826–11849, https://doi.org/10.1002/2014JD021848, 2014.

Moore, P., Webb, J., and Collinson, M.: Pollen analysis, Blackwell Scientic, Oxford, 1991.

Mu, M., Randerson, J. T., Van Der Werf, G. R., Giglio, L., Kasibhatla, P., Morton, D., Collatz, G. J., Defries, R. S., Hyer, E. J., Prins, E. M., Griffith, D. W. T., Wunch, D., Toon, G. C., Sherlock, V., and Wennberg, P. O.: Daily and 3-hourly variability in global fire emissions and consequences for atmospheric model predictions of carbon monoxide, J. Geophys. Res.-Atmos., 116, 1–9, 2011.

Neubauer, D., Lohmann, U., Hoose, C., and Frontoso, M. G.: Impact of the representation of marine stratocumulus clouds on the anthropogenic aerosol effect, Atmos. Chem. Phys., 14, 11997–12022, https://doi.org/10.5194/acp-14-11997-2014, 2014.

Peters, M. E. and Higuera, P. E.: Quantifying the source area of macroscopic charcoal with a particle dispersal model, Quaternary Res., 67, 304–310, https://doi.org/10.1016/j.yqres.2006.10.004, 2007.

Power, M. J., Marlon, J., Ortiz, N., Bartlein, P. J., Harrison, S. P., Mayle, F. E., Ballouche, A., Bradshaw, R. H. W., Carcaillet, C., Cordova, C., Mooney, S., Moreno, P. I., Prentice, I. C., Thonicke, K., Tinner, W., Whitlock, C., Zhang, Y., Zhao, Y., Ali, A. A., Anderson, R. S., Beer, R., Behling, H., Briles, C., Brown, K. J., Brunelle, A., Bush, M., Camill, P., Chu, G. Q., Clark, J., Colombaroli, D., Connor, S., Daniau, A.-L., Daniels, M., Dodson, J., Doughty, E., Edwards, M. E., Finsinger, W., Foster, D., Frechette, J., Gaillard, M.-J., Gavin, D. G., Gobet, E., Haberle, S., Hallett, D. J., Higuera, P., Hope, G., Horn, S., Inoue, J., Kaltenrieder, P., Kennedy, L., Kong, Z. C., Larsen, C., Long, C. J., Lynch, J., Lynch, E. A., McGlone, M., Meeks, S., Mensing, S., Meyer, G., Minckley, T., Mohr, J., Nelson, D. M., New, J., Newnham, R., Noti, R., Oswald, W., Pierce, J., Richard, P. J. H., Rowe, C., Sanchez Goñi, M. F., Shuman, B. N., Takahara, H., Toney, J., Turney, C., Urrego-Sanchez, D. H., Umbanhowar, C., Vandergoes, M., Vanniere, B., Vescovi, E., Walsh, M., Wang, X., Williams, N., Wilmshurst, J., and Zhang, J. H.: Changes in fire regimes since the Last Glacial Maximum: an assessment based on a global synthesis and analysis of charcoal data, Clim. Dynam., 30, 887–907, https://doi.org/10.1007/s00382-007-0334-x, 2008.

Preston, C. M. and Schmidt, M. W. I.: Black (pyrogenic) carbon: a synthesis of current knowledge and uncertainties with special consideration of boreal regions, Biogeosciences, 3, 397–420, https://doi.org/10.5194/bg-3-397-2006, 2006.

Rabin, S. S., Melton, J. R., Lasslop, G., Bachelet, D., Forrest, M., Hantson, S., Kaplan, J. O., Li, F., Mangeon, S., Ward, D. S., Yue, C., Arora, V. K., Hickler, T., Kloster, S., Knorr, W., Nieradzik, L., Spessa, A., Folberth, G. A., Sheehan, T., Voulgarakis, A., Kelley, D. I., Prentice, I. C., Sitch, S., Harrison, S., and Arneth, A.: The Fire Modeling Intercomparison Project (FireMIP), phase 1: experimental and analytical protocols with detailed model descriptions, Geosci. Model Dev., 10, 1175–1197, https://doi.org/10.5194/gmd-10-1175-2017, 2017.

Radke, L. F., Lyons, J. H., Hobbs, P. V., Hegg, D. A., Sandberg, D. V., and Ward, D. E.: Airborne monitoring and smoke characterization of prescribed fires on forest lands in western Washington and Oregon, Gen. Tech. Rep. PNW-GTR-251, Portland, OR: U.S. Department of Agriculture, Forest Service, Pacific Northwest Research Station. 81 pp., 1990.

Reese, C. A., Liu, K. B., and Thompson, L. G.: An ice-core pollen record showing vegetation response to Late-glacial and Holocene climate changes at Nevado Sajama, Bolivia, Ann. Glaciol., 54, 183–190, 2013.

Rémy, S., Veira, A., Paugam, R., Sofiev, M., Kaiser, J. W., Marenco, F., Burton, S. P., Benedetti, A., Engelen, R. J., Ferrare, R., and Hair, J. W.: Two global data sets of daily fire emission injection heights since 2003, Atmos. Chem. Phys., 17, 2921–2942, https://doi.org/10.5194/acp-17-2921-2017, 2017.

Renfrew, J. M.: Paleoethnobotany. The prehistoric food plants of the Near East and Europe, Methuen & Co Ltd, London, UK, 1973.

Rubino, M., D'Onofrio, A., Seki, O., and Bendle, J. A.: Ice-core records of biomass burning, The Anthropocene Review, 3, 140–162, https://doi.org/10.1177/2053019615605117, 2016.

Sander, P. M. and Gee, C. T.: Fossil charcoal: techniques and applications, Rev. Palaeobot. Palynol., 63, 269–279, https://doi.org/10.1016/0034-6667(90)90104-Q, 1990.

Schüpbach, S., Kirchgeorg, T., Colombaroli, D., Beffa, G., Radaelli, M., Kehrwald, N. M., and Barbante, C.: Combining charcoal sediment and molecular markers to infer a Holocene fire history in the Maya Lowlands of Petén, Guatemala, Quaternary Sci. Rev., 115, 123–131, https://doi.org/10.1016/j.quascirev.2015.03.004, 2015.

Schutgens, N. A. J. and Stier, P.: A pathway analysis of global aerosol processes, Atmos. Chem. Phys., 14, 11657–11686, https://doi.org/10.5194/acp-14-11657-2014, 2014.

Secretariat of the Convention on Biological Diversity: Impacts of human-caused fires on biodiversity and ecosystem functioning, and their causes in tropical, temperate and boreal forest biomes, Montreal, SCBD, 42 pp., CBD Technical Series no. 5, 2001.

Shiraiwa, M., Kondo, Y., Moteki, N., Takegawa, N., Miyazaki, Y., and Blake, D. R.: Evolution of mixing state of black carbon in polluted air from Tokyo, Geophys. Res. Lett., 34, l16803, https://doi.org/10.1029/2007GL029819, 2007.

Sinha, P., Hobbs, P. V., Yokelson, R. J., Bertschi, I. T., Blake, D. R., Simpson, I. J., Gao, S., Kirchstetter, T. W., and Novakov, T.: Emissions of trace gases and particles from savanna fires in southern Africa, J. Geophys. Res.-Atmos., 108, D13, 8487, https://doi.org/10.1029/2002JD002325, 2003.

Stefanidou, M., Athanaselis, S., and Spiliopoulou, C.: Health Impacts of Fire Smoke Inhalation, Inhal. Toxicol., 20, 761–766, https://doi.org/10.1080/08958370801975311, 2008.

Stevens, B., Giorgetta, M., Esch, M., Mauritsen, T., Crueger, T., Rast, S., Salzmann, M., Schmidt, H., Bader, J., Block, K., Brokopf, R., Fast, I., Kinne, S., Kornblueh, L., Lohmann, U., Pincus, R., Reichler, T., and Roeckner, E.: Atmospheric component of the MPI-M Earth System Model: ECHAM6, J. Adv. Model. Earth Sy., 5, 146–172, https://doi.org/10.1002/jame.20015, 2013.

Stier, P., Feichter, J., Kinne, S., Kloster, S., Vignati, E., Wilson, J., Ganzeveld, L., Tegen, I., Werner, M., Balkanski, Y., Schulz, M., Boucher, O., Minikin, A., and Petzold, A.: The aerosol-climate model ECHAM5-HAM, Atmos. Chem. Phys., 5, 1125–1156, https://doi.org/10.5194/acp-5-1125-2005, 2005.

Stockmarr, J.: Tablets with spores used in absolute pollen analysis, Pollen et Spores, 13, 615–621, 1971.

Tinner, W. and Hu, F. S.: Size parameters, size-class distribution and area-number relationship of microscopic charcoal: relevance for fire reconstruction, The Holocene, 13, 499–505, https://doi.org/10.1191/0959683603hl615rp, 2003.

Tinner, W., Hofstetter, S., Zeugin, F., Conedera, M., Wohlgemuth, T., Zimmermann, L., and Zweifel, R.: Long-distance transport of macroscopic charcoal by an intensive crown fire in the Swiss Alps – implications for fire history reconstruction, The Holocene, 16, 287–292, 2006.

van Marle, M. J. E., Kloster, S., Magi, B. I., Marlon, J. R., Daniau, A.-L., Field, R. D., Arneth, A., Forrest, M., Hantson, S., Kehrwald, N. M., Knorr, W., Lasslop, G., Li, F., Mangeon, S., Yue, C., Kaiser, J. W., and van der Werf, G. R.: Historic global biomass burning emissions for CMIP6 (BB4CMIP) based on merging satellite observations with proxies and fire models (1750–2015), Geosci. Model Dev., 10, 3329–3357, https://doi.org/10.5194/gmd-10-3329-2017, 2017.

Veira, A., Kloster, S., Wilkenskjeld, S., and Remy, S.: Fire emission heights in the climate system – Part 1: Global plume height patterns simulated by ECHAM6-HAM2, Atmos. Chem. Phys., 15, 7155–7171, https://doi.org/10.5194/acp-15-7155-2015, 2015.

Vignati, E., Wilson, J., and Stier, P.: M7: An efficient size-resolved aerosol microphysics module for large-scale aerosol transport models, J. Geophys. Res.-Atmos., 109, d22202, https://doi.org/10.1029/2003JD004485, 2004.

von Hardenberg, J., Vozella, L., Tomasi, C., Vitale, V., Lupi, A., Mazzola, M., van Noije, T. P. C., Strunk, A., and Provenzale, A.: Aerosol optical depth over the Arctic: a comparison of ECHAM-HAM and TM5 with ground-based, satellite and reanalysis data, Atmos. Chem. Phys., 12, 6953–6967, https://doi.org/10.5194/acp-12-6953-2012, 2012.

Whitlock, C. and Larsen, C.: Charcoal as a Fire Proxy, Springer Netherlands, Dordrecht, the Netherlands, 75–97, https://doi.org/10.1007/0-306-47668-1_5, 2001.

Zhang, K., O'Donnell, D., Kazil, J., Stier, P., Kinne, S., Lohmann, U., Ferrachat, S., Croft, B., Quaas, J., Wan, H., Rast, S., and Feichter, J.: The global aerosol-climate model ECHAM-HAM, version 2: sensitivity to improvements in process representations, Atmos. Chem. Phys., 12, 8911–8949, https://doi.org/10.5194/acp-12-8911-2012, 2012.

Zhang, R., Khalizov, A. F., Pagels, J., Zhang, D., Xue, H., and McMurry, P. H.: Variability in morphology, hygroscopicity, and optical properties of soot aerosols during atmospheric processing, P. Natl. Acad. Sci. USA, 105, 10291–10296, https://doi.org/10.1073/pnas.0804860105, 2008.

Supplement of Atmos. Chem. Phys., 18, 11813–11829, 2018
https://doi.org/10.5194/acp-18-11813-2018-supplement

Atmospheric Chemistry and Physics
Open Access
EGU

Supplement of

Implementing microscopic charcoal particles into a global aerosol–climate model

Anina Gilgen et al.

Correspondence to: Anina Gilgen (anina.gilgen@env.ethz.ch)

S1 Charcoal properties

S1.1 Aspect ratio of charcoal

In the following, we summarise findings about the aspect ratio R of microscopic charcoal particles and how we derive from those estimates for the equivalent radius r_{eq}. The measurements by Clark and Hussey (1996) show a distinct maximum for aspect ratios R = 1.5-2, and the mean aspect ratio is 2.36 ± 1.53. While Clark and Hussey (1996) used 9 sites in temperate eastern North America for their analysis, Tinner and Hu (2003) studied charcoal particles from different biomes, namely Lago di Origlio (Switzerland; warm-temperate chestnut forest), Grizzly Lake (Alaska; spruce forest), and Wien Lake (Alaska; shrub birch tundra, poplar forest, and boreal forest). For the three sites, they report aspect ratios of $R = 1.9$, $R = 1.7$, and $R = 1.6$, respectively. Crawford and Belcher (2014) measured the aspect ratios of both microscopic and macroscopic charcoal particles. For microscopic charcoal (D_{M} up to 100 µm), they found aspect ratios of 1.8 and 2.4 for charcoal from wood and grass, respectively. It is worth mentioning that they used a cross-sectional area of 315 µm^2 as the lower threshold, which corresponds to a D_M of about $11.5 - 13.4$ µm for wood and $13.2 - 15.5$ µm for grass (assuming rectangual/elliptical cross-sections), i.e. a slightly larger D_{M} than the threshold of 10 µm used in this study.

All of these measurements of R lie in the same range. For our study, we chose $R = 2$ as an initial estimate. The third, non-visible dimension of the particle is expected to be smaller or equal to D_{m} for particles detected in pollen slides since the particles may tend to lie flat on the slides (Clark and Hussey 1996). For simplicity, we describe the shape of the charcoal particles with a rectangual cuboid (see Clark and Hussey 1996). Assuming that the non-visible axis equals the minor axis D_{m} (which is rather an upper estimate), the equivalent-volume radius r_{eq} is given by:

$$V_{\text{cuboid}} = V_{\text{sphere}} \tag{1}$$

$$D_{\text{M}} \cdot \frac{D_{\text{M}}}{R} \cdot \frac{D_{\text{M}}}{R} = \frac{4}{3} \cdot \pi \cdot r_{\text{eq}}^3 \tag{2}$$

$$\rightarrow r_{\text{eq}} \approx 0.62 \cdot \frac{D_{\text{M}}}{R^{\frac{2}{3}}}, \tag{3}$$

where V stands for volume. The typical lower threshold for microscopic charcoal particles is $D_{\text{M}} = 10$ µm, which corresponds to an equivalent-volume radius of $r_{\text{eq}} \approx 3.9$ µm. However, since the aspect ratio tends to increase with charcoal size (Crawford and Belcher 2014), R of the lower threshold ($D_{\text{M}} = 10$ µm) might be smaller than the mean or median R for $D_{\text{M}} > 10$ µm. In the model, we cannot account for a size-dependent R. For this study, it is important that the lower threshold of the counted and simulated charcoal particles match well since these small particles have higher number concentrations than larger particles (Clark and Hussey 1996; Tinner et al. 1998). As a lower estimate for our test simulations, we therefore use $R = 1.33$, which corresponds to the often applied, observation-based threshold of 75 µm^2 for microscopic charcoal cross-sections (e.g. Tinner et al. 2006) and which results in $r_{\text{eq}} = 4.9$ µm. Based on the before mentioned observations from Clark and Hussey (1996) and Crawford and Belcher (2014), $R = 2.4$ is considered to be an upper bound, which corresponds to $r_{\text{eq}} = 3.5$ µm.

S1.2 Radiative index of charcoal

Many studies (e.g. Habib and Vervisch 1988) report that higher H-C ratios result in a smaller imaginary part of RI, i.e. in a smaller absorption component. However, Bond and Bergstrom (2006) reviewed the radiative properties of different carbon-containing substances with focus on light-absorbing aerosol particles and found that the number of sp^2 bonds (more precisely: the extent of sp^2-islands) matters most. More sp^2-islands result in higher absorption because sp^2-bonded carbon is arranged in planar layers, which allows the π-electrons to move freely. Although the light absorption is closely related to the imaginary part of RI, it is important to note that absorption also impacts the real part. It is therefore not possible to estimate the imaginary part independently of the real part.

In general, measured RIs of light-absorbing carbonaceous substances show a high variability caused by different burning conditions (Bond and Bergstrom 2006). In our opinion, charcoal particles should share some of the radiative properties of coal with similar H-C and O-C ratios (i.e. very low-ranked coal). If we slightly extend the "coal rank" line in Fig. 7 from Bond and Bergstrom (2006) to the H-C and O-C ratios of charcoal, we arrive at a refractive index of RI $\approx 1.75 - 0.1k$ (for a wavelength of 550 nm). Unfortunately, this approach does not give us any information about the wavelength dependence of RI. However, the imaginary part of RI should not matter as much as the particle size: the charcoal particles are large compared with the dominant wavelengths of sunlight. If the absorption is relatively high, it is expected that no light penetrates to the interior of the particle, so that only the "skin" of the particle absorbs and all light encountering the particle skin is attenuated (Tami Bond, personal communication). The aerosol absorption in our model scales with the aerosol mass and does therefore not account for this. Hence we would overestimate the absorption by charcoal when using RI $\approx 1.75-0.1k$. When we conducted 5-year test simulations with different RI for charcoal (once using RI from BC, once RI from dust), we did not detect clear differences in the atmospheric lifetime of charcoal between the model simulations. The RI of charcoal is therefore likely not important for its atmospheric transport. In the end, we decided to use the same RI as for dust (RI $\approx 1.52 - 1.1 \times 10^{-3}k$); the lower absorption component of dust compared to charcoal should counteract that only part of the charcoal mass is expected to absorb radiation.

In our simulations, we found that the vertically integrated charcoal mass in the atmosphere is approximately one order of magnitude smaller than the mass of dust (using the chosen parameter set). Therefore, charcoal only contributes little to the total aerosol absorption optical thickness in our simulations. However, our simplified approach is very uncertain and does also not consider the non-sphericity of charcoal particles. If the absorption of charcoal were larger than with our simplified estimate, the contribution to the aerosol absorption optical depth might be somewhat higher, although we do not expect it to be large.

S2 Model implementation of charcoal

S2.1 In-cloud produced sulfate

Sulfate aerosols can be produced in cloud droplets when SO_2 reacts with O_3 or H_2O_2. When cloud droplets evaporate, aerosol particles remain, the size of which depends on the mass and chemistry of the foreign material in the cloud droplets (Mitra et al. 1992). The reaction with H_2O_2 is considered to be the dominant pathway (Seinfeld and Pandis 2006). Since the H_2O_2 concentration is often the limiting factor for the reaction with SO_2, most of sulfate is added to those particles activated early in the cloud, i.e. the best cloud condensation nuclei (Harris et al. 2014). Therefore, we distribute the sulfate mass produced in-cloud among the larger soluble aerosol modes (accumulation, coarse, and giant) in case these modes exist. If none of the three modes exist, a new soluble coarse mode is created.

S2.2 Gravitational settling

To ensure numerical stability in aerosol gravitational settling, aerosol particles can only cross one model layer within one timestep. However, only size distributions with large geometric mean radii close to the surface, where the model layers are thin, are affected. We expect that this velocity restriction might delay gravitational settling for large geometric mean radii by up to

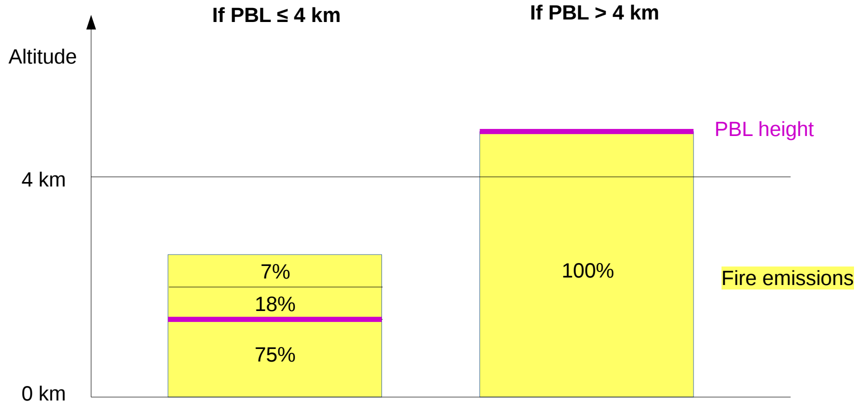

Figure S1: Illustration of fire emission heights in ECHAM6-HAM2.

a few time steps near the surface. However, this should not considerably change the spatial gravitational settling pattern since particles are not transported far horizontally within this time (as the horizontal scale of the grid is much larger than the vertical scale and horizontal wind velocities are rather low near the surface). Furthermore, only a very small number of charcoal size distributions have a sufficiently large geometric mean radius to be impacted.

S2.3 Calculation of number fluxes above threshold radius

To compare the simulated charcoal fluxes with observations, it is essential that only simulated fluxes of particles with $D_{\mathrm{M}} > 10\,\mu\mathrm{m}$ are considered. We calculated the total number of charcoal particles above this threshold directly before and after the calculation of the removal processes (gravitational settling, dry deposition, wet deposition). From the difference, we calculate the fluxes to the surface as illustrated in Supplementary Fig. S2.

Since the observations only consider pure charcoal particles, we should only take the charcoal component of the soluble giant mode into account when comparing to observations. Therefore, knowledge about the size distribution of the charcoal component is important. Our model assumes an ideal internal aerosol mixture, i.e. the total number of particles for the soluble giant mode is also representative for the number of charcoal particles in the soluble giant mode. The charcoal mass on the other hand is only a fraction of the total soluble giant mode mass (e.g. sulfate in addition). Hence, the number size distribution of the charcoal particles in the soluble giant mode is shifted to smaller radii compared to the total soluble giant mode but also follows a log-normal distribution with the same σ as the total soluble giant mode (see Supplementary Fig. S3).

Due to a small inconsistency in the code, small negative surface fluxes can occur: the radius used to calculate the removal processes is only updated once per timestep, while the number and mass tracer tendencies are updated inbetween. Since we use the tracer tendencies to calculate the radius before and after the removal process, our diagnostics do not use exactly the same radius as the calculations for the removal processes do. However, the error is negligible compared to the mean surface fluxes.

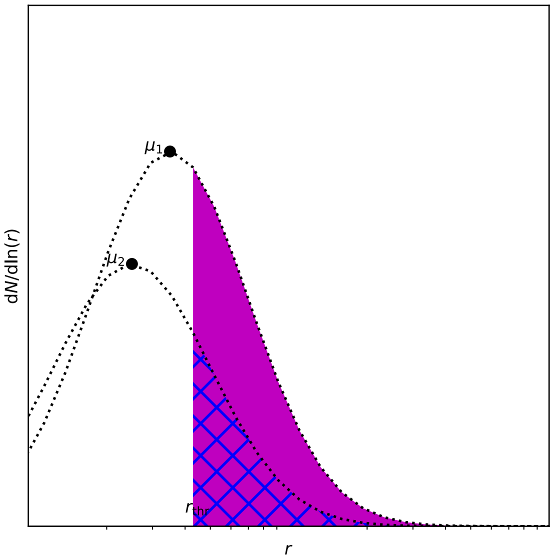

Figure S2: Illustration of how the deposition of charcoal particles above a certain threshold radius (r_{thr}) was calculated. Before the removal process (e.g. gravitational settling), the number geometric mean radius of a gridbox is μ_1. The number concentration of particles above the threshold radius is proportional to the area below the curve, i.e. the magenta area. After the removal process, both the number geometric mean radius and the total number concentration change (shift to μ_2). Now the hatched area represents the particle number concentration above the threshold radius. From the difference between the magenta and the hatched area we can calculate how many charcoal particles are removed. Number fluxes are then calculated by dividing by the time step and the area of the gridbox.

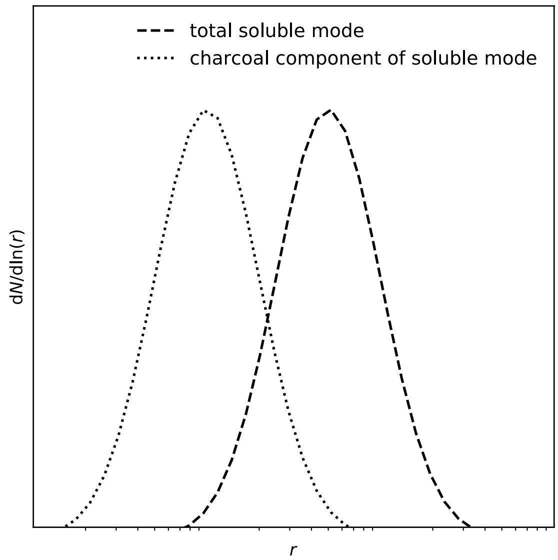

Figure S3: Schematic number size distribution of the total soluble giant mode and its charcoal component.

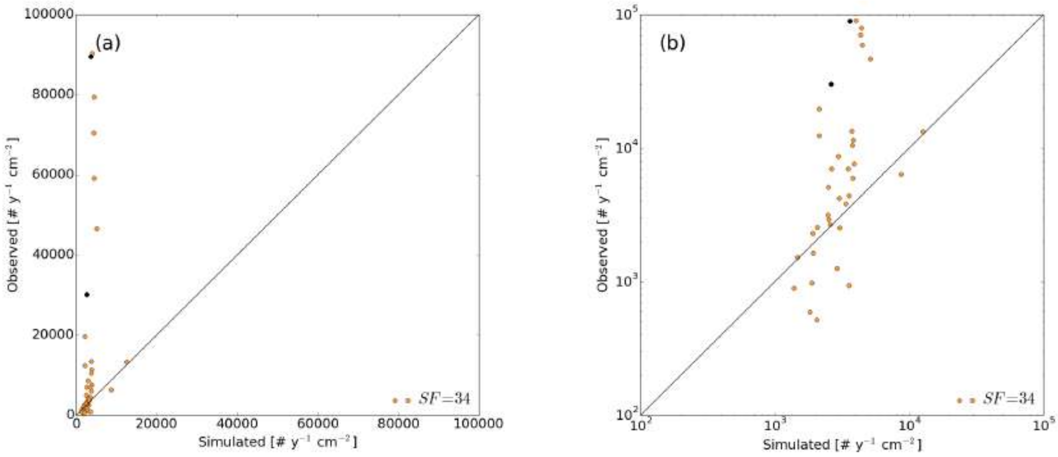

Figure S4: An example of the simulated versus observed number fluxes of charcoal particles above the threshold radius (in $cm^{-2}\,y^{-1}$) (a) on a linear scale and (b) on a logarithmic scale. The two black points show the sites likely influenced by surface runoff. The following parameters were used in this simulation: an emission number geometric mean radius of $r_{eq} = 2.5\,\mu m$, a threshold radius of $r_{eq} = 3.9\,\mu m$, and a charcoal density of $0.5\,g\,cm^{-3}$. The scaling factor is $SF = 34$.

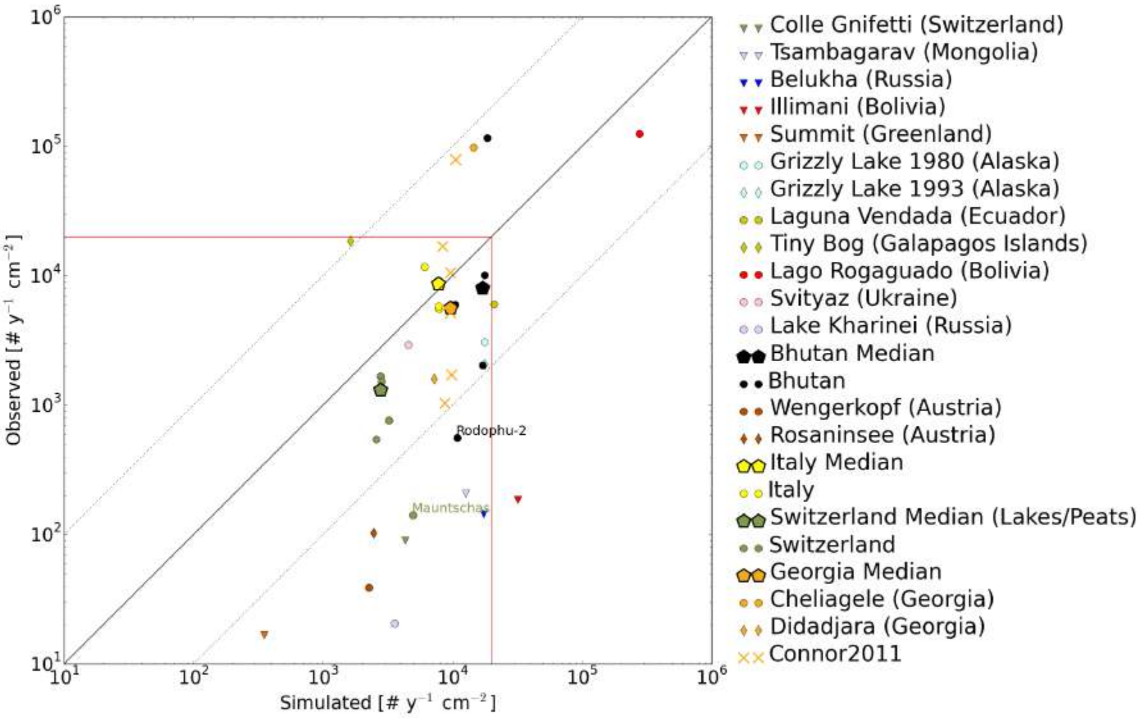

Figure S5: The same as Fig. 5 in the paper but for the free instead of the nudged model simulation.

Table S1: An overview of the observation sites from the calibration dataset (Adolf et al. 2018). The data is sorted alphabetically by country.

Site	Country	Longitude [°]	Latitude [°]	Altitude [m ASL]	Lake size [ha]
Černé jezero	Czech Republic	13.18	49.18	1007	18.4
Hromnické jezírko	Czech Republic	13.44	49.85	332	2
Étang d'Entressen	France	4.92	43.6	34	103.5
Lac du Crès	France	3.93	43.65	39	6
Holzmaar	Germany	6.88	50.12	422	20
Limni Kournas	Greece	24.27	35.33	18	42.0
Biviere di Gela	Italy	14.35	37.02	0	150
Gorgo Basso	Italy	12.66	37.61	27	3
Lago dell'Accesa	Italy	10.9	42.99	111	16
Lago dello Scanzano	Italy	13.37	37.92	547	97
Lago di Baratz	Italy	8.23	40.68	24	60
Lago di Pergusa	Italy	14.31	37.52	677	50
Lago di Varese	Italy	8.72	45.83	240	1480
Lago Piccolo d'Avigliana	Italy	7.4	45.05	288	61.1
Specchio di Venere	Italy	11.99	36.82	8	19.4
Jezioro Gołyń	Poland	15.78	52.44	26	9.5
Jezioro Gościąż	Poland	19.34	52.58	76	42
Suchar II	Poland	23.02	54.09	140	2.5
Lagoa Escura	Portugal	-7.64	40.36	1679	2
Lago Enol	Spain	-4.99	43.27	1077	12.2
Laguna Conceja	Spain	-2.81	39.93	857	29.4
Laguna de Taravilla	Spain	-1.97	40.65	1113	2.1
Laguna Grande de Estaña	Spain	-0.53	42.02	669	18.8
Laguna Zóñar	Spain	-4.69	37.48	301	37
Hagsjön	Sweden	13.69	57.26	170	22.2
Sarsjön	Sweden	19.6	64.04	274	7.78
Sisstjärnen	Sweden	14.92	60.65	216	9.6
Stora Utterträsk	Sweden	20.41	66.12	277	28.1
Vuolep Njakajaure	Sweden	18.78	68.34	408	30
Gerzensee	Switzerland	7.55	46.83	603	25.2
Iffigsee	Switzerland	7.41	46.39	2065	10
Lac du Mont d'Orge	Switzerland	7.34	46.23	595	3
Lago d'Origlio	Switzerland	8.94	46.05	423	8
Lej da San Murezzan	Switzerland	9.85	46.49	1773	78
Mauensee	Switzerland	8.07	47.17	500	51
Soppensee	Switzerland	8.08	47.09	593	24
Blue Lake	Ukraine	33.2	48.45	87	24.4

Table S2: A summary of the different observation sites used for validation. Note that the youngest date of the record is given as *calibrated* years for the ${}^{14}C$ method. Most data was taken from the Alpine Pollen Database of University of Bern (ALPADABA). The sorting follows the legend of Fig. 3.

Site	Country	Lon [°]	Lat [°]	Altitude [m ASL]	Time period	Record type	Dating method	Dated material	Youngest date	Lake size [ha]	Publication
Colle Gnifetti	Switzerland	7.88	45.93	4450	2002-2015	Ice core	Annual layer counting	-	-	-	This study
Tsambagarav	Mongolia	90.85	48.66	4130	1988-2009	Ice core	Annual layer counting	-	-	-	This study
Belukha	Russia	86.59	49.81	4062	Mean of two samples (1987, 1996/97)	Ice core	Annual layer counting	-	-	-	Eichler et al. (2011)
Illimani	Bolivia	-67.78	-16.65	6300	2008-2015	Ice core	Annual layer counting	-	-	-	This study
Summit	Greenland	-38.46	72.58	3200	1989 core	Ice core	Surface probe	-	-	-	This study
Grizzly Lake	Alaska	-144.19	62.71	720	1980, summer 1993	Lake	${}^{210}Pb$	Bulk	AD1992-1994	11	Tinner et al. (2006)
Laguna Vendada	Ecuador	-79.39	-3.61	3640	2009	Peat	${}^{14}C$	Terrestrial macrofossil	AD943 ± 35	2	This study
Tiny Bog	Galapagos Islands (Ecuador)	-90.33	0.64	819	2005	Peat	${}^{14}C$	Sphagnum	More recent than AD1950	0.01	This study

Lago Rogaguado	Bolivia	-65.93	-13.02	125	2004	Lake	^{14}C	Terrestrial macrofossil	AD1543 ±84	31500	Brugger et al. (2016)
Svityaz	Ukraine	23.84	51.50	157	2004	Lake	^{14}C	Terrestrial macrofossil	AD1139 ± 110	2519	This study
Lake Kharinei	Russia	62.75	67.37	110	Summer 1993	Lake	^{210}Pb	Bulk	AD2003	5	Salonen et al. (2011)
Tergang	Bhutan	91.07	27.83	2260	Summer 1992	Peat	^{14}C	Bulk	AD1097	Very small	This study
Shamling	Bhutan	91.12	27.77	2350	1990	Lake/peat	^{14}C	Terrestrial macrofossil	AD1807	-	This study
Rodophu-2	Bhutan	89.78	28.05	4530	2000	Lake/peat	^{14}C	Bulk	AD1189	-	This study
Laya	Bhutan	89.68	28.07	3830	2000	Lake/peat	^{14}C	Terrestrial macrofossil	AD1723	-	This study
Singhe Dzong	Bhutan	91.32	27.97	3800	2000	Peat	^{14}C	Terrestrial macrofossil	AD1248	Very small	P. Kunes
Wengerkopf	Austria	13.87	47.17	1780	Summer 2001	Peat	^{210}Pb	Bulk	AD1996	0.3	Knaap et al. (2012)
Rosaninsee	Austria	13.78	46.95	2070	Summer 2001	Peat	^{210}Pb	Bulk	AD1993	0.3	Knaap et al. (2012)
Gorgo Basso	Italy	12.65	37.62	6	2001	Lake	^{14}C	Terrestrial macrofossil	AD1772	3	Tinner et al. (2009)
Gorgo Lungo di Ficuzza	Italy	13.41	37.90	877	2003	Lake	^{14}C	Terrestrial macrofossil	AD755	0.2	Tinner et al. (2016)
Gorgo Tondo di Ficuzza	Italy	13.41	37.90	783	2006	Lake	^{14}C	Terrestrial macrofossil	AD1280	0.6	Tinner et al. (2016)
Etang de la Gruère	Switzerland	7.05	47.24	1005	1993	Peat	^{14}C	Terrestrial macrofossil	AD1809	22.5	Public data (counted by van Leeuwen)
Maumtschas	Switzerland	9.85	46.49	1819	2003	Peat	^{14}C	Sphagnum	AD1988	10	Knaap et al. (2012)

Les Amburnex	Switzerland	6.23	46.54	1375	2000	Peat	^{14}C	Terrestrial macrofossil	AD1770	0.2	Sjögren and Lamentowicz (2008)
Sèche de Gimel	Switzerland	6.23	46.54	1300	2003	Peat	^{14}C	Terrestrial macrofossil	AD1995	12	Sjögren (2005)
Le Moé	Switzerland	6.22	46.54	1310	2002	Peat	^{14}C	Sphagnum and Polytrichum stems	AD1991	12	Sjögren (2006)
Hallwilersee	Switzerland	8.21	47.28	400	Summer 1998	Lake	Annual layer counting	-	-	1030	This study
Lac de Bretaye	Switzerland	7.07	46.33	1780	2012	Lake	^{14}C	Terrestrial macrofossil	BC82	4	Thöle et al. (2016)
Cheliagele	Georgia	43.11	42.62	1100	Summer 1992	Lake/peat	^{14}C	-	AD1949	-	This study
Didadjara	Georgia	42.5	41.67	1850	2000	Lake/peat	^{14}C	-	AD859	-	Connor et al. (2017, submitted)
Sakhare	Georgia	45.32	41.58	800	2000	Lake	^{14}C	Bulk	AD500 ± 80	12	Connor (2011)
Kumisi	Georgia	44.83	41.58	469	2000	Lake	^{14}C	Bulk	AD800 ± 40	120	Connor (2011)
Tsavkisi	Georgia	44.75	41.68	1110	2000	Peat	^{14}C	Isolated pollen	AD530 ± 60	4	Connor (2011)
Imera	Georgia	44.2	41.65	1610	2000	Lake	^{14}C	Bulk	AD940 ± 40	12	Connor (2011)
Bareti	Georgia	44.17	41.65	1630	1986	Lake	^{14}C	Bulk	AD1050 ± 40	62	Connor (2011)

Jvari	Georgia	44.73	41.83	570	2000	Lake	Correlation with neighbouring sites	-	-	9.6	Connor (2011)
Aligol	Georgia	44.02	41.63	1534	2000	Lake	^{14}C	Bulk	AD1760 $\pm$ 40	9.6	Connor (2011)

References

Adolf, C., S. Wunderle, D. Colombaroli, H. Weber, E. Gobet, O. Heiri, J. F. N. van Leeuwen, C. Bigler, S. E. Connor, M. Gałka, T. La Mantia, S. Makhortykh, H. Svitavská-Svobodová, B. Vannière, and W. Tinner (2018). "The sedimentary and remote-sensing reflection of biomass burning in Europe". In: *Global Ecol. Biogeogr.* 27.2, pp. 199–212. DOI: 10.1111/geb.12682.

Bond, T. C. and R. W. Bergstrom (2006). "Light Absorption by Carbonaceous Particles: An Investigative Review". In: *Aerosol Sci. Tech.* 40.1, pp. 27–67. DOI: 10.1080/02786820500421521.

Brugger, S. O., E. Gobet, J. F. van Leeuwen, M.-P. Ledru, D. Colombaroli, W. van der Knaap, U. Lombardo, K. Escobar-Torrez, W. Finsinger, L. Rodrigues, A. Giesche, M. Zarate, H. Veit, and W. Tinner (2016). "Long-term man–environment interactions in the Bolivian Amazon: 8000 years of vegetation dynamics". In: *Quaternary Sci. Rev.* 132, pp. 114–128. ISSN: 0277-3791. DOI: 10.1016/j.quascirev.2015.11.001.

Clark, J. S. and T. C. Hussey (1996). "Estimating the mass flux of charcoal from sedimentary records". In: *The Holocene* 6.2, pp. 129–144.

Connor, S., D. Colombaroli, F. Confortini, E. Gobet, B. Ilyashuk, I. E., J. van Leeuwen, M. Lamentowicz, W. van der Knaap, E. Malysheva, A. Marchetto, N. Margalitadze, Y. Mazei, E. Mitchell, R. Payne, and B. Ammann (2017). "Long-term population dynamics – theory and reality in a peatland ecosystem". In: *J. Ecol.*

Connor, S. E. (2011). *A Promethean Legacy: Late Quaternary Vegetation History of Southern Georgia, the Caucasus.* Peeters, Louvain.

Crawford, A. and C. Belcher (2014). "Charcoal Morphometry for Paleoecological Analysis: The Effects of Fuel Type and Transportation on Morphological Parameters". In: *Appl. Plant. Sci.* 2.8, pp. 1–10. DOI: 10.3732/apps.1400004.

Eichler, A., W. Tinner, S. Brütsch, S. Olivier, T. Papina, and M. Schwikowski (2011). "An ice-core based history of Siberian forest fires since AD 1250". In: *Quaternary Sci. Rev.* 30.9–10, pp. 1027–1034. ISSN: 0277-3791. DOI: 10.1016/j.quascirev.2011.02.007.

Habib, Z. and P. Vervisch (1988). "On the refractive index of soot at flame temperature". In: *Combust. Sci. Tech.* 59, pp. 261–274.

Harris, E., B. Sinha, D. van Pinxteren, J. Schneider, L. Poulain, J. Collett, B. D'Anna, B. Fahlbusch, S. Foley, K. Fomba, C. George, T. Gnauk, S. Henning, T. Lee, S. Mertes, A. Roth, F. Stratmann, S. Borrmann, P. Hoppe, and H. Herrmann (2014). "In-cloud sulfate addition to single particles resolved with sulfur isotope analysis during HCCT-2010". In: *Atmos. Chem. Phys.* 14, pp. 4219–4235.

Knaap, W. O. van der, J. F. N. van Leeuwen, T. Goslar, R. Krisai, and W. Tinner (2012). "Human impact on vegetation at the Alpine tree-line ecotone during the last millennium: lessons from high temporal and palynological resolution". In: *Veg. Hist. Archaeobot.* 21.1, pp. 37–60. ISSN: 09396314, 16176278.

Mitra, S., J. Brinkmann, and H. Pruppacher (1992). "A wind tunnel study on the drop-to-particle conversion". In: *J. Aerosol Sci.* 23.3, pp. 245–256. ISSN: 0021-8502. DOI: 10.1016/0021-8502(92)90326-Q.

Salonen, J. S., H. Seppä, M. Väliranta, V. J. Jones, A. Self, M. Heikkilä, S. Kultti, and H. Yang (2011). "The Holocene thermal maximum and late-Holocene cooling in the tundra of NE European Russia". In: *Quaternary Res.* 75.3, pp. 501–511. ISSN: 0033-5894. DOI: 10.1016/j.yqres.2011.01.007.

Seinfeld, J. and S. Pandis (2006). *Atmospheric Chemistry and Physics: From Air pollution to Climate Change.* Hoboken, New Jersey: John Wiley & Sons, Inc. ISBN: 978-0-471-72018-8.

Sjögren, P. (2005). "Palaeoecological investigatons of pasture woodland in Combe des Amburnex, Swiss Jura Mountains". PhD thesis. Institut für Pflanzenwissenschaften, Bern.

Sjögren, P. (2006). "The development of pasture woodland in the southwest Swiss Jura Mountains over 2000 years, based on three adjacent peat profiles". In: *The Holocene* 16.2, pp. 210–223. DOI: 10.1191/0959683606hl921rp.

Sjögren, P. and M. Lamentowicz (2008). "Human and climatic impact on mires: a case study of Les Amburnex mire, Swiss Jura Mountains". In: *Veg. Hist. Archaeobot.* 17.2, pp. 185–197. ISSN: 1617-6278. DOI: 10.1007/s00334-007-0095-9.

Thöle, L., C. Schwörer, D. Colombaroli, E. Gobet, P. Kaltenrieder, J. van Leeuwen, and W. Tinner (2016). "Reconstruction of Holocene vegetation dynamics at Lac de Bretaye, a high-mountain lake in the Swiss Alps". In: *The Holocene* 26.3, pp. 380–396. DOI: 10.1177/0959683615609746.

Tinner, W., M. Conedera, B. Ammann, H. W. Gaggeler, S. Gedye, R. Jones, and B. Sagesser (1998). "Pollen and charcoal in lake sediments compared with historically documented forest fires in southern Switzerland since AD 1920". In: *The Holocene* 8.1, pp. 31–42.

Tinner, W. and F. S. Hu (2003). "Size parameters, size-class distribution and area-number relationship of microscopic charcoal: relevance for fire reconstruction". In: *The Holocene* 13.4, pp. 499–505. DOI: 10.1191/0959683603hl615rp.

Tinner, W., F. S. Hu, R. Beer, P. Kaltenrieder, B. Scheurer, and U. Krähenbühl (2006). "Postglacial vegetational and fire history: pollen, plant macrofossil and charcoal records from two Alaskan lakes". In: *Veg. Hist. Archaeobot.* 15.4, pp. 279–293. ISSN: 09396314, 16176278.

Tinner, W., J. F. van Leeuwen, D. Colombaroli, E. Vescovi, W. van der Knaap, P. D. Henne, S. Pasta, S. D'Angelo, and T. L. Mantia (2009). "Holocene environmental and climatic changes at Gorgo Basso, a coastal lake in southern Sicily, Italy". In: *Quaternary Sci. Rev.* 28.15–16, pp. 1498–1510. ISSN: 0277-3791. DOI: 10.1016/j.quascirev.2009.02.001.

Tinner, W., E. Vescovi, J. F. N. van Leeuwen, D. Colombaroli, P. D. Henne, P. Kaltenrieder, C. Morales-Molino, G. Beffa, B. Gnaegi, W. O. van der Knaap, T. La Mantia, and S. Pasta (Sept. 2016). "Holocene vegetation and fire history of the mountains of Northern Sicily (Italy)". In: *Veg. Hist. Archaeobot.* 25.5, pp. 499–519. DOI: 10.1007/s00334-016-0569-8.

Summary

Despite their potential to provide valuable information on environmental dynamics and processes, the full ecological potential of palynological ice records was hitherto neglected. The presented thesis explored for the first time the timing and different interactions between long-term fire, vegetation, land use, pollution, and climate dynamics in various biomes by generating novel, globally distributed palynological ice-core records. The presented palynological analyses rely on the same standard extraction method developed in this thesis. The ice records provide excellent chronologies, particularly for post-1800 AD. In these past 200 years occurred important climatic changes and an increasing globalization of human activities that are difficult to assess with sedimentary archives, due to often highly uncertain chronologies (Marlon et al. 2016) in the youngest period (unless varved sediments are used e.g. Rey et al. 2018). Here we aim at filling this knowledge gap about the most recent rapid environmental changes, in comparison with the long-term pre-industrial conditions, by using highly-resolved continuous ice records.

In **Manuscript 1**, we present a quantitative comparison of available microfossil extraction methods from ice samples. With an innovative, yet simple approach of adding a first exotic marker (*Lycopodium* spores) prior to the laboratory treatment and a second marker (*Eucalyptus*) afterwards, we derived quantitative estimates of microfossil behavior during the extraction process. We conclude that different extraction methods may affect estimations of pollen concentrations, pollen percentages, and ratios between pollen types, especially if vesiculate pollen is an important component of the pollen assemblage, which hampers comparison between different records. We recommend a new evaporation-based microfossil extraction method, which produced the smallest and least variable losses among the tested approaches. Since microfossil losses are inevitable, we emphasize the need of adding a marker prior to sample treatment to achieve reliable concentration estimates. The novel extraction method

builds the methodological fundament of the investigated palynological ice records presented in this thesis.

In **Manuscript 2**, we directly combined palynological ice core data with historical sources to provide novel insights into industrialized and globalized land-use impacts on fire regime and vegetation dynamics across European biomes. Preindustrial land use occurred in humanized vegetation that established millennia before the medieval climate optimum when our record begins (e.g. Rey et al. 2017). Surprisingly, our multiproxy-data suggest that the transformation to fossil fuel-based industrial land use (e.g. large-scale maize production with a contemporaneous massive fire increase) started shortly after 1750 AD, together with first signs of large-scale atmospheric pollution from fossil fuel combustion. Therefore, we propose a period prior to 1750 AD (i.e. 1650–1750 AD) to define preindustrial baseline conditions of pollution in Europe e.g. for climate modelling. Progressive globalization of economies intensified industrialized production on fertile lowland soils and heavily exploited lowland forest ecosystems, creating urban areas and industries. While this lowland temperate vegetation is still suffering, increasingly centralized land use provides novel chances for the recovery of quasi-natural plant communities in marginal land-use areas such as in the Alps. Nevertheless, globalization fosters also the spread of new invasive plants and pathogens (e.g. the introduction of the grape pest *Phylloxera* after 1860 AD), which in combination with climate change may counteract potential vegetation recoveries.

In **Manuscript 3**, we provide the first combined record of vegetation and fire dynamics from Mongolia. The temporal precision and resolution of the record enabled us to attribute the long-term environmental dynamics as well as short-term variability to independent climate records. We conclude that several maximum forest expansions before 1800 BC produced a comparable ice signal as modern forests at a similarly high-altitude glacier in the Russian Altai (Belukha, Eichler et al. 2011). After 1800 BC, precipitation regime changes were the main driver for irreversible forest diebacks and steppe expansions around Tsambagarav. Fire activity peaked in response to dead biomass availability subsequent to forest retractions. The long-term environmental dynamics suggest that vegetation and fire regimes partly decoupled from climate after 1700 AD together with land use intensification and atmospheric fossil burning pollution. The lacking resilience of past forest communities to moisture decreases in the Mongolian Altai implies that further moisture decreases associated to climate warming in the future may induce forest dieback in the Russian Altai and in other Central Asian, where tree stands currently grow at their moisture limit.

Manuscript 4 provides a Holocene record on Puna and montane forest (Yungas) vegetation dynamics in the Central Andes. We attribute the Holocene-fire maximum 8000–2000 BC and the subsequent decline towards the Little Ice Age (LIA, Apaéstegui et al. 2018) to precipitation changes, likely induced by a strengthening of the South American summer monsoon rather than fluctuating human activities. Surprisingly, according to our data pre-Columbian societies as e.g. the Incas 1438–1532 AD, altered ecosystem on the Altiplano and in adjacent Yungas only negligibly on a large scale. Unprecedented human-shaped ecosystems emerged after 1740 AD, following a wide establishment of novel land use practices by the Spanish viceroyalty (e.g. introduction of European cattle) and were further reinforced in the modern era post-1950 AD with increasing industrial *Pinus* and *Eucalyptus* plantations and coal exploitation. In combination with rapid climate change and associated fire regime shifts, we expect ecosystem modification with unpredictable ecological and societal costs in the future.

Manuscript 5 explores the potential of palynological records in Central Greenland. The Summit record reveals that 20th century globalization markedly affected Arctic environments through the spread of adventive plants, deforestation of subarctic *Betula* stands, as well as pollution from increasing fossil fuel burning and forest fires. Specifically, “Blackening” of pure Greenland snow with growing microscopic charcoal and SCP deposition increased in the 20th century and indicates that future climate-warming feedbacks may accelerate, and thereby reinforce ice melting and fire risks in thawing permafrost areas. The period with enhanced

Betula pollen concentrations ca. 1850–1900 AD correlates with higher biogenic ice nucleating particle (INP) concentrations in the same ice core (Hartmann et al. submitted), which illustrates that current changes in terrestrial biological activities may in turn affect climate by increasing highly ice-active biogenic INP concentrations in Arctic clouds, thereby changing their radiative properties (Solomon et al. 2015). This pre-study illustrates a high potential of palynology in remote Arctic environments and underscores that rapid climate change and anthropogenic impact are already strongly affecting these remote environments.

Manuscript 6 implements for the first-time microscopic charcoal particles into a global aerosol-climate model and validates simulated against observed microscopic charcoal particle influx in sediment and glacier archives. The model captures a significant portion of the spatial variability of global microscopic charcoal deposition, but it is unable to reproduce the variability between single sites due to its coarse spatial resolution. Particularly, the model overestimates charcoal deposition at the glacier sites due to the altitude of the ice archives and the surrounding complex topographies that are not well represented in the model.

Overall, the presented thesis shows that vegetation, fire, and climate interactions are complex and involve various feedback mechanisms, varying between biomes and with the degree of anthropogenic influence. If the climate is suitable (e.g. precipitation, temperature), natural forest ecosystems develop in most regions as climax vegetation. However, humans as well as climate altered these forest ecosystems since millennia. Our combined ice records (Figure 1) show that in densely populated areas with propitious climate for forest growth, humans disrupted forests and changed their floristic composition since centuries e.g. in the Bolivian Andes or the Swiss Alps during the Medieval period. On the other hand, in remote ecotone areas as the Central Asian Altai, irreversible forest diebacks were driven by precipitation reductions. During the past 100–200 years, industrialization and globalization heavily disrupted ecosystems in central and marginal areas, changing floristic compositions across biomes e.g. by introducing alien species.

The growing need of energy by increasing industrialization and globalization of economies was covered by exploitation of fossil fuel energy, documented by our ice SCP records (Figure 2). Astonishingly, atmospheric fossil fuel pollution including rather large particles (i.e. ca. 10µm) reached even the most remote areas of our planet as e.g. Central Greenland. The well-constrained chronologies of the Alpine and Altai records imply that significant fossil fuel pollution was released to the atmosphere already in the 18th century, which is corroborated by historical sources. While the implementation of new regulations and associated technical advances strongly reduced atmospheric fossil fuel pollution in Europe after the 1970s, the SCP records from Central Asia and South America rose further during the past recent decades. The spatial and temporal heterogeneities of SCP-inferred atmospheric pollution across the investigated regions have important implications for the use of SCP onset and/or maximum peaks as additional dating horizons in natural archives (Rose 2015).

Our long records from the Andes (Illimani) and Altai (Tsambagarav) suggest that Holocene fire activity in both regions was mostly driven by climate dynamics and reached a minimum during the LIA. Precipitation changes and their influence on biomass availability (Altai) and its flammability (Andes) were likely more important than temperature itself (Figure 3A). This finding confirms global sedimentary charcoal compilations suggesting that global fire activity trends during the Holocene followed climate variability and reached a minimum during the LIA (Power et al. 2008, Prentice 2010, Daniau et al. 2012). In the densely populated areas around Colle Gnifetti in Europe, pre-industrial periods with enhanced fire activity were likely connected to drought periods as e.g. the fire peak connected to the historically documented drought period in 1540 AD (e.g. Pfister et al. 2015). On the other hand, after 1750 AD, increasing fire activity was likely connected to the begin of large-scale industrial land use in Europe, suggesting that human activities overran climate as the main driver for fire dynamics.

In regard to testing the “broken fire hockey stick”-hypothesis (Marlon et al. 2008, van der Werf et al. 2013), the presented microscopic charcoal records provide important novel and continuous data from areas that are currently underrepresented in global charcoal compilations (Marlon et al. 2016). The records cover a broad range of biomes under different scales of anthropogenic land use, and provide additional vegetation and land use information, which is crucial to assess potential drivers for fire activity. Microscopic charcoal records in the tropical (Illimani), mediterranean-temperate (Colle Gnifetti), the steppic-boreal (Tsambagarav), and the arctic region (Summit) suggest continuously rising fire activity in the 20^{th} century probably induced by combined global warming and increasing anthropogenic land use (Figure 3B). These recent increases falsify the “broken fire hockey stick”-hypothesis during the 20^{th} century (i.e. declining fire activity), in best agreement with more recent global charcoal compilations that propose further increases of fire activity during the 20^{th} century, although with large uncertainties (Marlon et al. 2016).

To conclude, the thesis provides regional fire records based on microscopic charcoal combined with vegetation, land use, and fossil fuel pollution records in the four geographical areas of Central Europe, Southern Siberia, tropical Amazonia, and the Arctic. The developed data advance the understanding of the complex systemic linkages between fire, vegetation, land use, pollution, and climate, and provide regional, temporally well-constrained multiproxy-information that may contribute to refine global climate and fire models.

Figure 1 Summary diagram of palynological ice records sorted by increasing latitude of the archive: Illimani (10,000 BC–2015 AD), Colle Gnifetti (1050–2015 AD), Tsambagarav (3500 BC–2009 AD), and Summit (1730–1989 AD). Pollen percentages for sums of trees, shrubs, and herbs, as well as *Zea mays* (Illimani and Colle Gnifetti), sum of planted trees (Illimani), sum of neophytes (Colle Gnifetti) based on the terrestrial pollen sums, and microscopic charcoal and SCP concentrations (particles l^{-1}). Chronology was adjusted to increase the visibility during 1–2000 AD. Lilac shading indicates 200-year-intervals along the records. Hollow curves = 10x exaggeration.

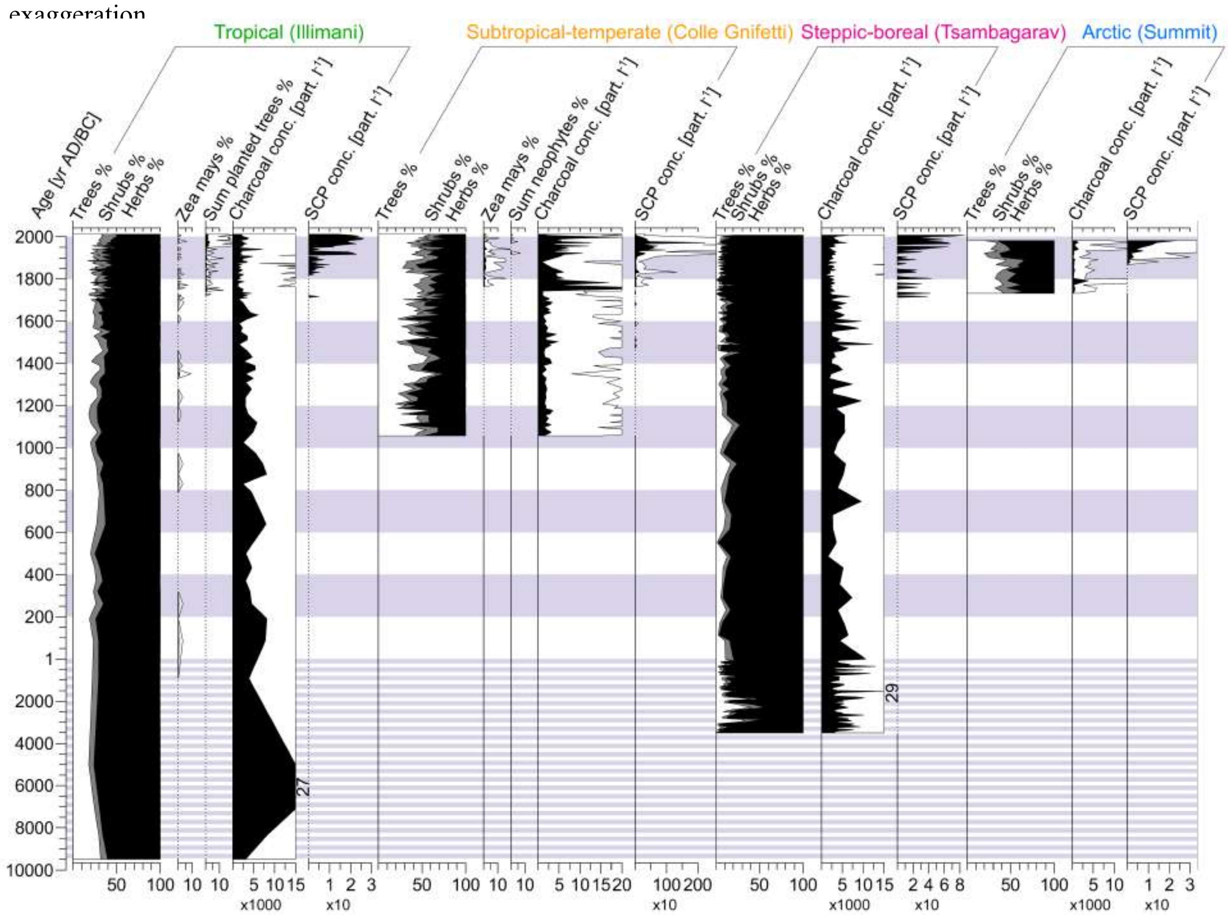

Figure 2 Summary diagram of SCP records showing 1660 AD–present show SCP concentrations (particles l^{-1}). X-axes are adjusted to the maximum SCP concentration peak in each record. Hollow curves = 10x exaggeration. Colored curve shows moving average along the records (moving average period = 5).

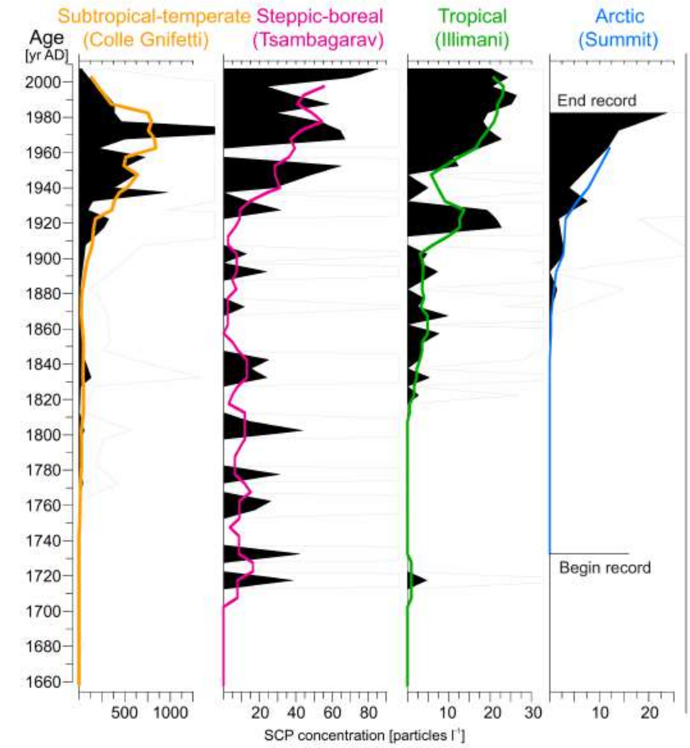

Figure 3 Summary diagram of microscopic charcoal Z-scores (fine lines) from different biomes. Charcaol concentrations (particles l^{-1}) were log transformed (log_{10}) to down-weigh extreme peaks of the original datasets before calculating Z-scores. A: Holocene records in South America (Illimani) and Central Asia (Tsambagarav). Z-scores calculated on the entire records. Bold lines show smoothed Z-Scores based on a locally weighted regression (Loess with smoothing parameter 0.1) and 95%-confidence interval (bootstrap approach with 999 iterations). B: Past millennium for records in Europe (Colle Gnifetti), Greenland (Summit), South America (Illimani), and Central Asia (Tsambagarav). Z-scores calculated on the past millennium. Bold lines show smoothed Z-Scores based on a locally weighted regression (Loess with smoothing parameter 0.1), except for Summit, where the original Z-scores were kept for comparison due to insufficient datapoints (19 samples).

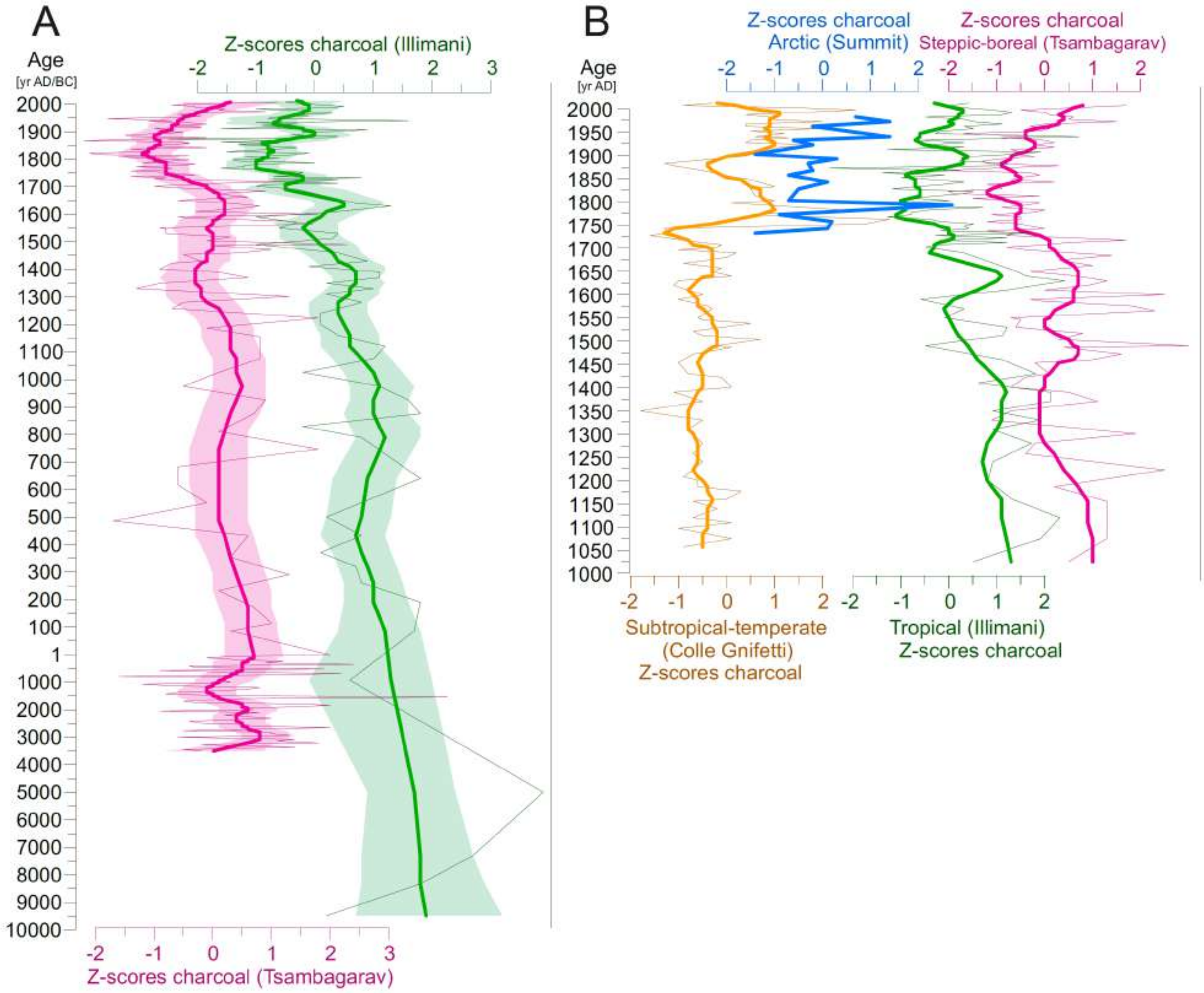

References

Apaéstegui J, Cruz FW, Vuille M, Fohlmeister J, Espinoza JC et al. (2018) Precipitation changes over the eastern Bolivian Andes inferred from speleothem (δ 18 O) records for the last 1400 years. *Earth and Planetary Science Letters* 494 124-134

Daniau AL, Bartlein PJ, Harrison SP, Prentice IC, Brewer S et al. (2012) Predictability of biomass burning in response to climate changes. *Global Biogeochemical Cycles* 26(4)

Eichler A, Tinner W, Brütsch S, Olivier S, Papina T, Schwikowski M (2011) An ice-core based history of Siberian forest fires since AD 1250. *Quaternary Science Reviews* 30(9) 1027-1034

Hartmann M, Blunier T, Brugger SO, Schmale J, Schwikowski M et al. (submitted) The Variation of Ice Nucleating Particles in the Arctic over the Last Centuries.

Marlon JR, Bartlein PJ, Carcaillet C, Gavin DG, Harrison SP et al. (2008) Climate and human influences on global biomass burning over the past two millennia. *Nature Geoscience* 1(10) 697

Marlon JR, Kelly R, Daniau AL, Vannière B, Power MJ et al. (2016) Reconstructions of biomass burning from sediment charcoal records to improve data-model comparisons. *Biogeosciences* (BG) 13 3225-3244

Pfister C, Wetter O, Brázdil R, Dobrovolný P, Glaser R et al. (2015) Tree-rings and people–different views on the 1540 Megadrought. Reply to Büntgen et al. 2015. *Climatic Change* 131(2) 191-198

Power MJ, Marlon J, Ortiz N, Bartlein PJ, Harrison SP et al. (2008) Changes in fire regimes since the Last Glacial Maximum: an assessment based on a global synthesis and analysis of charcoal data. *Climate dynamics* 30(7-8) 887-907

Prentice IC (2010) The burning issue. *Science* 330(6011) 1636-1637

Rey F, Gobet E, van Leeuwen J F, Gilli A, van Raden UJ et al. (2017) Vegetational and agricultural dynamics at Burgäschisee (Swiss Plateau) recorded for 18,700 years by multi-proxy evidence from partly varved sediments. *Vegetation History and Archaeobotany* 26(6) 571-586

Rey F, Gobet E, Szidat S, Lotter AF, Gilli A et al. (2018) Radiocarbon wiggle matching on laminated sediments delivers high-precision chronologies. *Radiocarbon* 1-21

Rose NL (2015) Spheroidal carbonaceous fly ash particles provide a globally synchronous stratigraphic marker for the Anthropocene. *Environmental science & technology* 49(7) 4155-4162

Solomon A, Feingold G, Shupe MD (2015) The role of ice nuclei recycling in the maintenance of cloud ice in Arctic mixed-phase stratocumulus, *Atmospheric Chemistry and Physics* 15(18) 631-643

Van der Werf GR, Peters W, Van Leeuwen TT, Giglio L (2013) What could have caused pre-industrial biomass burning emissions to exceed current rates?. *Climate of the Past* 9(1) 289-306

Acknowledgements

This PhD-thesis is part of the Sinergia project *Paleo fires from high-alpine ice cores* funded by the Swiss National Science Foundation (SNF grant 154450).

First, I am incredibly grateful to my PhD-supervisor **Willy Tinner**, who entrusted me with this exciting "frozen" project. Under his guidance, I developed my scientific skills and grew personally. I enjoyed our funny conversations in the kitchen, greatly appreciated that he challenged me with scientific discussions including philosophical theories as Occam's razor-concept, and I will "also" permanently remember our writing exercises during the final stage of my thesis. He gave me the freedom to explore side-projects like the Greenland study along my official PhD-project, supported my various conference and fieldwork trips but always ensured my work-life balance, sometimes with unusual methods as forcing me to listen to Müslüms song "la bambele". Finally, years have passed since an early discussion about the practicality of squared wheels. With this thesis, I gave my best to hand in a "well-rounded" scientific piece; nevertheless, I am afraid that the printing format remained "square". "Grazie mille (danke viu mau)" for being my doctoral father the past years, Willy.

It is a great honor for me and I am grateful that **John Birks** agreed to evaluate my thesis as an external co-referee. Moreover, I warmly thank him for previously reviewing our method-manuscript so positively for Journal of Glaciology.
I am grateful to **Martin Grosjean**, who kindly agreed to chair my defense.

My warmest thanks go to **Erika Gobet**, my advisor during the thesis, and most importantly, my close mentor throughout the past years. The long discussions sometimes lasting until late in the evening, the funny chats, and her continuous support were a strong pillar since the first day when she met me for my master project with my 80 cm sediment core from Bolivia. She guided me with broad scientific knowledge, critical discussions, dealt elegantly with my stubborn moments, and supported me with great creativity during our laboratory experiments. She always found "a Genghis Khan" in my wiggly pollen diagrams, when I was yet again disappointed, as another statistical approach had failed to produce reasonable results. Merci für alles, Erika.

I express my gratitude to our external Sinergia PIs, our leading PI **Margit Schwikowski**, and our co-PIs **Stefan Wunderle**, and **Ulrike Lohmann** for writing this exciting Sinergia project. Especially, I thank **Margit Schwikowski** for guiding our project with great enthusiasm, for always having an open door, and for finding time to personally discuss our data and method approaches. Moreover, we shared unforgettable moments during our lovely travels to conferences in Krasnojarsk and Kyoto and I appreciate extremely that she introduced me to so many great scientists and lovely friends. Most importantly, I experienced her as a warm and caring mentor during the past four years and I always felt extremely welcome at the PSI. I am grateful to **Michi Sigl** for all his support during our project and for his courage to guide this interdisciplinary PhD quartet. I will never forget our funny and endless ice material negotiations in the ice room at minus 17°C. I thank **Dimitri Osmont**, **Anina Gilgen**, and **Helga Weber** for sharing the Paleo fire-PhD experience with me. I could not have wished for a better team to tackle this interdisciplinary challenge. Especially, I thank **Dimitri Osmont** for our cold days in the ice room and for a warm and efficient exchange of our ice record data and knowledge during the past years. I thank **Anina Gilgen** for our joint efforts with the charcoal database. We mastered interdisciplinary understanding, sometimes only by sending each other emails with drawn sketches to bridge the disciplinary differences. I am extremely grateful that she patiently explained me important details on how the model work (spatial resolution, assumptions about particles, etc) so we could interpret the results together.

I am deeply indebted to the **drilling crews** at Tsambagarav in 2009, at Colle Gnifetti in 2003 and 2015, at Illimani in 1999 and 2015, and at Summit in 1989 who made this project possible with their incredible work in harsh glacial environments. I am grateful to **Susi Haselbeck** from PSI for substantial assistance with our sampling in the ice room.

Apart from the Sinergia project, a number of **co-authors** shared their scientific knowledge on different environments, supported the project, and motivated me. I thank **Hermann Behling** for hosting me in Göttingen for analyzing the Illimani record and for his help with all the rare tropical taxa. I am grateful that he reviewed our Tsambagarav manuscript. I will never forget the “Pollen Parties”, and moreover, I will remember the warm welcome in the laboratory and the after-work visits to the “Weihnachtsmarkt” with Luda, Caro and the other laboratory members. I am grateful to **Sonia Fontana** for helping me with pollen identification. I express my gratitude to **Thomas Blunier** from Copenhagen for entrusting me the precious ice leftovers of the famous Eurocore ’89 and for giving me the opportunity to extend my PhD to the Arctic. I am grateful to **Oliver Heiri** for statistical and scientific career advices. I thank **Henry Hooghiemstra** for going through all Illimani pollen taxa with me during the Moorexcursion in Poland and for giving me advice on the interpretation of the Bolivian record. I thank **Andy Lotter** for the critical discussions on the Summit record, and most importantly for sensing my mood in stressful times. I warmly remember our Greek sediment core descriptions together in the lab, when we chatted and correlated “dead frogs”. I thank **César Morales del Molino** for supplying me in the right moments with important literature about Greenland and South America and for our enthusiastic discussions. I am grateful to **Tanja Papina** and her team at the IWEP, who welcomed us warmly in Barnaul and helped to organize the Tsambagarav drilling campaign. I thank **Christian Rohr** for sharing his historical knowledge about Europe. I especially thank **Federica Schanz**, my Bachelor student for building the foundation of our methodical paper. A warm thank you to **Natalia Rudaya** for sharing her Altai knowledge with me and for visiting our laboratory in Bern. I am grateful to **Christoph Schwörer** for statistical inputs, his help with the Colle Gnifetti record, and his sunny personality during coffee breaks. I warmly thank **Fabian Rey** for sharing unforgettable office years: For our funny and lovely moments, our “PhD sibling”-fights, our friendly competition (that was extremely beneficial for my PhD-project), and our exchange of scientific knowledge as well as personal life matters on a daily basis.

I warmly thank all the **Palaeoecology lab members** in Bern, who became my second family during the past years. I am extremely grateful for all the joyful hours, the funny and sometimes silly chats in the kitchen, and the great scientific experiences we shared in the seminars, during various fieldwork campaigns and in coffee breaks. Especially, I thank **Jacqueline van Leeuwen** for her endless enthusiasm about pollen identification and for introducing me to pollen counting during my Msc. She continued to be an extremely important support during my PhD for the identification of rare taxa in the Colle Gnifetti and Tsambagarav record and I missed her cheerful personality tremendously after she retired. I am grateful to **Florencia “Flor” Oberli** who introduced me to laboratory methods with “empty jam jars” and shared her knowledge on previous attempts to extract microfossils from ice. I extremely enjoyed her bubbly personality and her jolly visits in our laboratory during the past years. I thank **Alex Bolland** for joining me on a crazy trip to the coldest place we ever encountered (-50°C in the Copenhagen freezer) shortly after we met the first time and for all the cheerful and funny chats that followed. I warmly thank **Carole Adolf** and **Tiziana Pedrotta**, who shared their experiences as “older PhDs” with me and supported me in the PhD jungle. I will never forget the funny fieldwork adventures with Carole in Spain, Portugal, Poland, and Czech Republic that included also hilarious moments as the fish pedicure in Prague. Many thanks to Tiziana for giving me cooking advice, and especially for our walks in the Botanical gardens. I thank **Daniele Colombaroli, Mara Deza Araujo**, **Sebastian Eggenberger**, **Sylvie Gassner**, **Ieva Grudzinska**, **Petra Kaltenrieder**, **Kasia Marcisz**, **Nina Perret-Gentil-dit-Maillard**, **Patrick Schläfli**, **Pim van der Knaap**, and **Lieveke van Vugt**.

I am grateful to everyone at the **Institute of Plant Sciences** for providing a lovely working environment and I thank all the incredible people I met at conferences, on the yearly Moorexcursions, and during fieldwork campaigns. Especially, I thank **Willi Tanner** with whom I shared many precious fieldwork trips in Switzerland, Austria, Greece, and hopefully soon in Tansania. He gave me private trailer driving lessons and finally, he teached me the difference between “äiwäg” und “diesewäg”. “Danke viu mau”, Willi.

I thank **Hannah Hoag**, a freelance journalist from Canada. She provided us with tremendous publicity for our project with a New York Times Article after we met at the Polar2018 conference in Davos. I am grateful to Christian von Burg for the radio interview in SRF Wissensmagazin.

Finally, I thank **my parents, Santos Quinteiro**, the rest of **my family**, and **my friends** outside Academia for supporting me during the entire project.

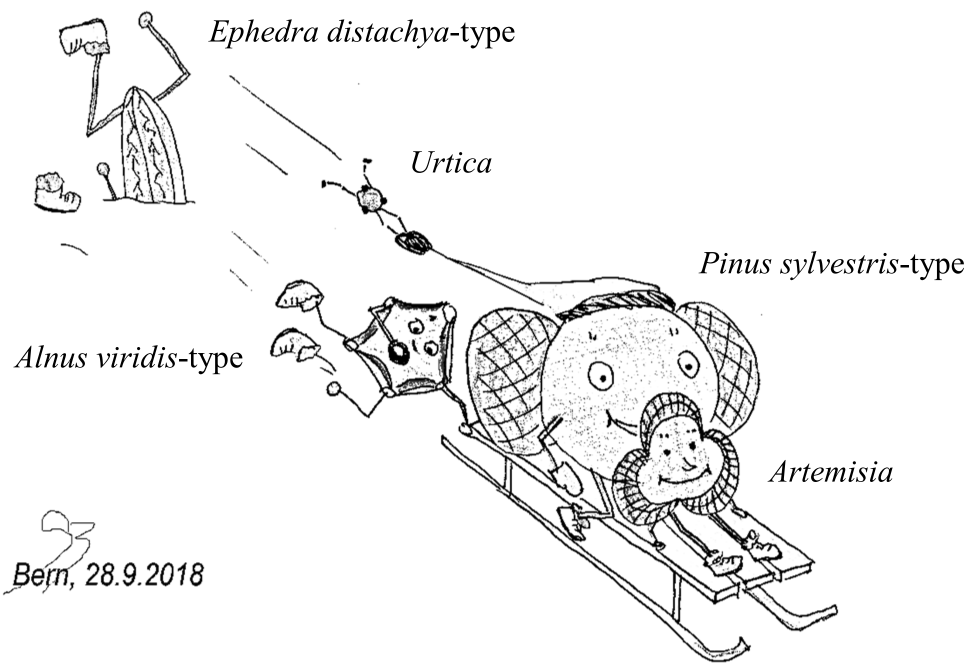

Figure 1 Pollen deposition in glacial environments and the reason why microfossil concentrations are so humble in high-alpine ice cores.

Declaration

under Art. 28 Para. 2 RSL 05

Last, first name: Brügger Sandra Olivia

Matriculation number: 07-101-298

Programme: Graduate School of Climate Sciences

Bachelor ☐ Master ☐ Dissertation X

Thesis title: FrozenNature – The palynological contribution to reconstruct paleo fire, vegetation, land use, and pollution dynamics from high-alpine ice cores

Thesis supervisor: Prof. Dr. Willy Tinner,
Institut für Pflanzenwissenschaften, Universität Bern
Altenbergrain 21, 3013 Bern

I hereby declare that this submission is my own work and that, to the best of my knowledge and belief, it contains no material previously published or written by another person, except where due acknowledgement has been made in the text. In accordance with academic rules and ethical conduct, I have fully cited and referenced all material and results that are not original to this work. I am well aware of the fact that, on the basis of Article 36 Paragraph 1 Letter o of the University Law of 5 September 1996, the Senate is entitled to deny the title awarded on the basis of this work if proven otherwise.

Bern, 10.10.2018
Place, date

SB.
....
Signature

Curriculum Vitae Sandra Olivia Brügger

Contact: Institute of Plant Sciences & Oeschger Centre for Climate Change Research, University of Bern, Altenbergrain 21, CH-3013 Bern
email: sandra.bruegger@ips.unibe.ch
Birth date 29.08.1987
Place of origin Kandergrund BE, Switzerland
Languages German (mother language), English (fluent), French (advanced)

ACADEMIC CAREER

Feb 15–to date	PhD candidate Graduate School of Climate Sciences, University of Bern
Sep 12–Dez 14	Master of Science in Geography, University of Bern
Sep 08 –Sep 12	Bachelor of Science in Geography, University of Bern

PUBLICATIONS

Brugger SO, Gobet E, Sigl M, Osmont D, Papina T et al. (2018) Ice records provide new insights into climatic vulnerability of Central Asian forest and steppe communities. *Global Planet Change* 169 188-201

Gilgen A, Adolf C, **Brugger SO**, Ickes L, Schwikowski M et al. (2018) Implementing Microscopic Charcoal Particles into a Global Aerosol-Climate Model. *Atmos Chemistry Physics* 18 (16) 11813-11829

Brugger SO, Gobet E, Schanz FR, Heiri O, Schwörer C et al. (2018) A quantitative comparison of microfossil extraction methods from ice cores. *J Glaciol* 64(245) 432–442

Brugger SO, Gobet E, van Leeuwen JFN, Ledru MP, Colombaroli D et al. (2016) Long-term man–environment interactions in the Bolivian Amazon: 8000 years of vegetation dynamics. *Quat Sci Revi* 132 114-128

PRESENTATIONS AND CONFERENCES

Ecological Society of America, Annual meeting, New Orleans, Louisiana. Poster and session moderator, Aug 18
Polar 2018 - SCAR & IASC Conference, Davos, Switzerland. Oral presentation and poster, Jun 18
Biology day, Faculty of Biology, Bern. Oral presentation, May 18
19th Swiss Global Change Day, Bern. Poster, Apr 18
Symposium on Cryosphere and Biosphere, IGS, Kyoto, Japan. Oral presentation, Mar 18
LUC seminar, Laboratory of Environmental Chemistry, PSI, Villigen, Switzerland. Oral presentation, Apr 17
Institute of Water and Environmental Problems, SB RAS, Barnaul, Russia. Oral presentation, Apr 17
PAGES workshop Altai region, Siberian Federal University, Krasnoyarsk, Russia. Oral presentation, Apr 17
Center for Ice and Climate group seminar, Copenhagen, Denmark. Oral presentation, Feb 17
Biology'17 conference, Bern, Switzerland. Oral presentation, Jan 17
Swiss Geoscience Meeting, Geneva, Switzerland. Poster, Nov 16
Biology'16 conference, Lausanne, Switzerland. Poster, Jan 16

FURTHER COURSES AND QUALIFICATIONS

Workshop Networking for Nerds, New Orleans, organized by A. Levine, ESA, New Orleans, Aug 18
Session presider training, organized by ESA, New Orleans, Aug 18
16th Young Researchers Meeting "Career planning for Climate Scientists", OCCR, Aeschi, Switzerland, Jun 17
Ice core analysis techniques (ICAT) PhD school, CIC, University of Copenhagen, Denmark, Nov 16
Multivariate Data analysis in Palaeoecology, organized by Th. Giesecke, University of Göttingen, Jul 16
15th Young Researchers Meeting "How to read and publish research articles", OCCR, Aeschi, Jun 16
International Moorexcursion: Austria, Switzerland, France, Poland, years 15–18
14th Swiss Climate Summer School, organized by ETH Zürich, Ascona, Switzerland, Aug 15

FIELDWORK EXPERIENCE

Livingston/Niederreiter UVITEC/Gravity piston coring: Lake Mondsee (Austria), Moossee, Burgäschisee, Hurden (Switzerland), Lake Viktoria (Tansania), Lago Rogaguado (Bolivia), Makedonia region (Greece). Archeological excavations: Ukraine. Pollen traps: France, Germany, Poland, Spain.

PUBLIC OUTREACH AND MEDIA

Science in Siberia Newspaper: Scientists have investigated ice of a Mongolian Altai glacier. 26 Sep 2018
New York Times, Science: Europe's Triumphs and Troubles Are Written in Swiss Ice. 17 Sep 2018
Swiss national radio SRF2, Wissenschaftsmagazin: Eiskalte Geschichten. 23 Jun 2018
Research Night – Nacht der Forschung, scientific speed-dating with public, University of Bern, Sep 17
Outreach event "Rendez-vous Forschung: a scientist-public speed-dating", Biology day, Bern, Feb 27

OTHER ENGAGEMENTS

Sep 16–to date	PhD and postdoc representative in the Institutes of Plant Sciences steering committee, Uni Bern
Sep 14–to date	Voluntary supervisory of the nature reserves of the Bernese Cantons (FNA)
Jan 09–Dez 13	Commitee Umwelt, Ver- und Entsorgung (UVEK) at the community Laupen BE, chair for Environment and Waters

AWARDS

Winner of Early Career Poster Award at Polar 2018 conference, Jun 18
Best Poster Price in the category Geosphere/Biosphere. 19th Swiss Global Change day, Apr 18
SEP-NGB-Prize for young scientists for the best poster. Swiss Geoscience Meeting, Nov '16
Best Poster Price in the category Biogeography. Biology'16 conference, Jan '16